Polysaccharide Derived Mesoporous Carbonaceous Materials for Bulky Dyes and Metals Adsorption from Wastewater

(Green Chemical Technology for The Production of Polysaccharide Derived Mesoporous Carbonaceous Materials for Wastewater Treatment)

Hayman Jalal Abdoul

PhD

University of York

Chemistry

February 2015

Abstract

The current world crisis in the demand for water is a real problem for all forms of life on our planet. For years, scientists have tried to propose various technologies which might be able to clean and reuse contaminated water. It is crucial to develop a sustainable low cost form of technology. This is especially important for Third World countries, where the ability to get high level technology is difficult and ideally, the form of technology should be cheap, simple and based on the local resources. One of the most available local resources is a polysaccharide such as starch, pectin, cellulose or alginic acid. The major goal of this dissertation is to develop a green form of technology to capture potentially harmful, toxic or valuable compounds from waste water using mesoporous carbonaceous materials based on the local polysaccharide resources.

To achieve this target, a novel and improved method of synthesis of mesoporous carbonaceous materials from starch (hereafter referred to as Starbon®) and alginic acid (hereafter referred to as Algibon) was established at the beginning of the project. Based on this method, a number of mesoporous materials with different textural and surface properties have been generated and characterised by various techniques including nitrogen porosimetry, solid state NMR, DRIFT spectroscopy, electron microscopy, elemental analysis and ash content tests.

Some of the major water pollutants in industrial wastes are dyes from textile industry and heavy metals from mining, steel industry, welding, batteries, refinery, fertiliser and other processes. Therefore, the produced materials were systematically tested as dye adsorbers. Bulky azo-dyes, which represent 75% of the current cotton industry market, were selected as model absorbates. A wide range of Algibons and Starbons materials with different properties (from the completely hydrophilic to completely hydrophobic and with different micro/mesopore volumes and ratios) enabled the optimum material to be found for certain types of adsorption process. It was found that in this type of adsorption, Starbons materials cannot compete with commercially available adsorbents. In contrast, Algibon has demonstrated great potential and significantly outperformed the commercially available adsorbents such as activated carbon (up to 6 times more) for the uptake of a range of bulky dyes.

The adsorption data reveals that the BET specific surface area (N_2-adsorption) was not the only governing factor and that the dominant mesoporous character of these materials, the accessibility of the pores versus the bulkiness of the dyes and the nature of the surface functionality (hydrophobic versus hydrophilic) also played key roles.

The maximum adsorption capacity of Algibon prepared at $800^{\circ}C$ (A800) is markedly higher than the one recorded for A450 and outperforms Norit as a commercially available activated carbon (AC) adsorbent. It was found that the higher adsorption capacity of A800 relates to a higher surface area in the mesoporous region. Moreover, it was found that the energy of adsorption is smaller for A800 than for AC. This shows that A800 is not only the preferred adsorbent but will also enable a more effective and easier recovery of the dyes.

In addition, the project involved the use of the developed Starbon materials to recover metals. This application is crucial not only for the cleaning of waste waters but also for recovering the valuable and critical metals from solid wastes. Some of these metals are in the EU critical list of elements due to their significant demand in modern economy technologies or are substantial components of industrial waste. These elements are in short supply because of their large demand in growing economy and their scarce abundance in the world. Therefore, a variety of Starbons were screened to test the selectivity of the polysaccharide derived carbonaceous materials towards the high value metals from digested solid wastes consisting of Pulverised fly ash (PFA), Red Mud (RM), Bottom ash (BA), Titano gypsum (TiG), Red Titano gypsum (RTiG) and Phospho Gypsum (PG).

Further investigation of metals adsorption based on Algibon was systematically conducted. A800 which demonstrated the most promising results early on and was found to be the most stable material, and was used as the adsorber. A solution containing four high value metal ions (i.e. Co, Cu, Ag and Cd) were selected for the adsorption experiment. Investigation focused on the nature of the metal ions and how they affect the kinetic parameters of adsorption in a detailed experimental analysis of the model system. Different types of adsorption isotherms were applied. The maximum adsorption capacity for each metal was found from the fit isotherm type. Kinetic adsorption was tested and kinetic order model study was carried out.

Table of Content

List of Figures

14

CHAPTER FOUR Algibons Generated Application in Bulky Azo Dye Adsorption

CHAPTER SIX Experimental Section.

Appendices

Appendix two

retrogradation was carried out at 5 ^{o}C for (A) 12 h (adsorption pore size distribution (Apsd)), (A-) 12 h (desorption pore size distribution (Dpsd)); (B) 24 h (Apsd), (B-) 24 h (Dpsd); (C) 48 h (Apsd), (C-) 48 h (Dpsd); (D) 72 h (Apsd), (D-) 48 h (Dpsd); (E) 96 h (Apsd), (E-) 96 h (Dpsd).

Appendix three

distribution (Apsd)), (A-) A300 (desorption pore size distribution (Dpsd)); (B) A450 (Apsd), (B-) A450 (Dpsd); (C) A600 (Apsd), (C-) A600 (Dpsd); (D) A800 (Apsd), (D-) A800 (Dpsd).

Appendix four

List of Tables

CHAPTER FIVE Starbon Technology Used in Recovery of Metals From Waste Water

CHAPTER SIX Experimental Section

Acknowledgements

Declaration

I declare that I am the sole author of this thesis. The work presented in it are my own and was generated by me as the result of my own research and it has not been submitted for examination at this or any other institution for another award.

CHAPTER ONE

Literature Review

1.1 Introduction

Water resources are of critical importance for both the natural ecosystem and for human development. Increasing environmental pollution from industrial wastewater, particularly in developing countries, is of major concern. There are two major types of industrial water contaminations: metals and dyes.

Metals contamination exists in the aqueous waste streams of many industries, such as metal plating facilities, mining operations, tanneries, etc. Some of the metals associated with these activities are cadmium, chromium, iron, nickel, lead, mercury and so on, which tend to accumulate in living organisms causing diseases and disorders.[1]

Many industries, such as textiles, paper and plastics, use dyes to colour their products, however they also consume substantial volumes of water. As a result, they generate a considerable amount of coloured wastewater. The presence of small amounts of dyes (less than 1 ppm) is highly visible and undesirable.[2] Many of these dyes are also toxic and even carcinogenic, posing a serious threat to living organisms.[3] Therefore, there is a need to treat the wastewaters containing toxic dyes and metals before they are discharged into the main water bodies. Many physico-chemical methods like coagulation, flocculation, ion exchange, membrane separation, oxidation, etc., are available for the treatment of heavy metals and dyes.[4] However, the methods which are involved produce sludge which itself has handling and disposal problems, along with high costs and technical constraints. Therefore, attention focusing on the environment has motivated research for new and sustainable forms of technology that would be able to treat the waste water polluted by metals and dyes efficiently.[5] Such pollution has substantially increased over the last few decades.[5,6]

1.1.1 Project objectives

Adsorption technologies used to deal with contaminants in industrial wastewater are relatively easy to operate and have several advantages, including low costs, operations over a wide range of conditions and the possible reuse and regeneration of the adsorbents.[7] Trapping contaminantes through the physical adsorption process is a commonly known method which has been applied by scientists for years due to its low cost, its possibility for regeneration and its environmentally-friendly impact.[8] However, current adsorbers, such as activated carbons and silica gels, are inefficient for the adsorption of large dye

molecules. Furthermore, the adsorption process is usually very slow and has a recovery period of days. One of the possibilities in overcoming these problems is to use mesoporous materials.[9] The existing method of mesoporous carbonaceous materials is very complex, costly and unsustainable since it uses a petroleum-based precursor, hazardous chemicals and it requires a significant number of technological steps.[10,11] Recently, novel types of bio-derived mesoporous materials, known as Starbon$^{®}$, have been developed.[12] They have demonstrated extraordinary properties in the adsorption of small organic molecules but have never been used for large, bulky dyes and metals adsorption.[13] As such, it would be very interesting to apply the Starbon technology to industrial wastewater treatment.

- The aim of this research is to manufacture polysaccharide derived porous Starbon materials and develop them for application to wastewater treatment, focusing on the removal of the coloured compounds and metals contaminants. This approach has to help industrial factories remove the pollutants from their wastewater before discharging them into the environment.[14]
- Another target of the project comprises of examination of a traditional adsorber, such as activated carbon (AC) and the Starbon$^{®}$ materials, as a comparison of efficiency for the treatment process.

To achieve the major goals of the project, the following tasks have been prioritised:

- To optimise Algibon production in order to obtain materials with maximum pore volume.
- To develop large scale Algibon production (on a scale greater than 1 Kg).
- To find which Algibon properties are critical for optimal adsorption capacity of organic dyes and which could be useful in metal adsorption.
- To develop a procedure for the removal of bulky organic dye molecules and, later, removal of metals from the contaminated water sample using the Algibons.
- To reduce the costly method of water treatment by lowering the energy consumption and increase the efficiency of preparation processes used with Algibon.

- To develop methods linked to the reuse of Algibon and recovery of adsorbates.

1.1.2 Current challenges of wastewater treatment

The levels of organic contaminants and metal pollutants are regulated by the World Health Organisation standards.[15] To reach these targets, the purification of both industrial and municipal wastewater requires many complex steps which could not be considered as an ideal clean technology.[16] Of the different types of impurities found in contaminated water such as suspended, colloidal[17,18], metals and soluble organic molecules, the latter is the most problematic and expensive to remove.[19,20]

This study focuses on the removal of bulky and complex organic molecule dyes which have a very strong colour due to their large aromatic system.[21] Although it may not pose a major risk to human health, coloured wastewater causes public concern about the water quality.[22] Another aspect of this study is the development of new adsorption technologies for carcinogenic and toxic heavy metals which cause a significant risk to human health.

1.1.3 Green aspects of the Project

During the project, major attention was paid to meet the green chemistry principles,[23,24] shown in Table.1.1.

Table.1.1: Connection between the project strategy and the green chemistry principles.

	Green Chemistry Principles (GCP)	Project Application Strategy
1	Prevention of waste	Produced mesoporous materials have to be reusable and derived from polysaccharide bio-waste.
2	Atom economy	Recovery of the solvents for the expansion of polysaccharides.
3	Less hazardous chemical synthesis	The synthesis of carbonaceous porous material such as Algibon preparation does not require templating, avoiding such harmful compounds as hydrogen fluoride (HF) and caustic soda used in the preparation of traditional mesoporous carbonaceous materials.
4	Designing safer	Starbons produced are environmentally friendly

	chemicals	and no toxic aspects have been found.
5	Safer solvents and auxiliaries	Only solvents from the "green solvents" list such as ethanol, acetone and $scCO_2$ will be used during the project.
6	Design for energy efficiency	Minimal/reduced temperatures used for adsorption and desorption. Ideally these processes should be optimised to an ambient temperature.
7	Use of renewable feedstock	All materials prepared have been produced from renewable polysaccharide sources.
8	Reduce derivatives	Reduce the number of intermediate mesoporous materials by reducing a number of carbonisation steps in the process.
9	Catalysis	Avoid using additional catalyst for the carbonisation process. Only the internal ability of acid functionalised polysaccharides (e.g. Alginic acid) should be used for self-carbonisation.
10	Design for degradation	The polysaccharide derived mesoporous materials are benign and do not persist/accumulate in the environment.
11	Real-time analysis for Pollution Prevention	To use such analytical method as TG-FTIR for step by step analysis of carbonisation process.
12	Inherently safer chemistry for accident prevention	In contrast to the traditional technologies, Starbon does not require hazardous chemicals.

1.2 Wastewater review

Fresh water is a vital natural resource that can only be renewable as long as it is well managed. To meet local requirements for sustainable pure water resources, the prevention of pollution from domestic, industrial, and agro-industrial activities is important.[25] Undoubtedly, current water pollution control policies have already achieved significant success. However, the continual increase in demand for water in development countries raises the complexity and intensity of water treatment, demanding new innovation technologies based on local resources. It is estimated that millions of people in the world in developing countries have no access to sustainable safe water,[26] and this situation forces the development of new approaches which help to substitute the old inadequate sewage, industrial and municipal wastewaters.[27]

Municipal water waste combines both water or liquid carried wastes which originate from commercial facilities, government institutions and any of the

sources of the groundwater; also storm and surface water.[28] The untreated water wastes usually contains increased levels of the organic material, various pathogenic microorganisms and toxic compounds, i.e, heavy metals.[29] Thus, health issues and environmental hazards can be a direct consequence of these contaminations and should immediately be controlled from the source, with appropriate treatment before final disposal. The key reason for managing the waste water is in order to protect the environment in such a way that maintains good public health and fits with the socio-economic concerns.[30] There is a significant difference in municipal and industrial water waste. Most of the pollutants in the industrial waste water range from trace amounts to ten thousand parts per million (ppm),[31] whereas those of the municipal waste water occurs within narrower limits of hundred to thousand ppm.[32] Industrial sewages containing wastewater have almost twice as much degradable organic matter as all of the municipal waste water combined. [31-33].

Wastewater Types[34]

| Human and Animal Wastewater | Household Wastewater | Storm Wastewater | Industrial Wastewater |
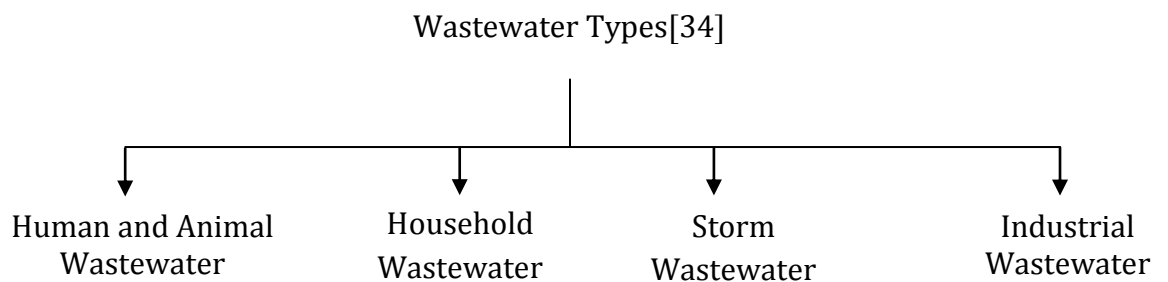
1.2.1 Domestic wastewater

It typically comprises of inorganic and organic matter in colloidal, dissolved and suspended forms. The term in its most common use refers to the municipal waste water, comprising of a broad spectrum of contaminants; This is often a result of mixing water wastes from varied sources. Alternatively, the term is reference to the sewage which comes from a households' waste water which includes cesspit leakage, septic tank discharge and lavatories.[35]

1.2.2 Industrial wastewater

The industrial wastewaters contains certain kinds of inorganic and organic matter in colloidal, suspended and dissolved states, or it also might contain dangerous materials and compounds that are toxic or carcinogenic in nature including phenols, cyanides, dyes, metals, alkalis and acids, flammable sources

from the industry operations; such examples include paper mills, chemical industries, tanneries, steel plants, fruit and vegetable refineries.[36] As such, there are potentially many sources of industrial wastewater discharge.

Table.1.2: Typical industrial wastewater contaminants[37-39]

Waste generator	Characteristic of waste
Chemical manufacturer	Acids and bases, spent solvents Waste water containing organic constituents and heavy metals such as Hg, Pb, Cd, Fe etc.
Printing industry	Heavy metal solution Waste ink and solvents
Textile industry	Dyes, suspended solids and alkaline
Petroleum refining industry	Waste water containing benzene and other hydrocarbons such as phenolics, free and emulsified oils and other dissolved organics
Leather products manufacturing	Toluene and benzene
Paper industry	Paint Waste Containing heavy Metals Ignitable Solvents
Construction industry	Ignitable Paint Waste Spent Solvents Strong Acids and Bases
Metal manufacturing	Sludges containing heavy Metals, cyanide Waste Paint Waste
Pharmaceuticals	High in dissolved and suspended organic
Plastics and resins	Dissolved organics, including acids, aldehydes, phenolics, cellulose, alcohols, surfactants and oils
Explosive manufacturing	Organic acids and alcohols, soaps and oils
Food processing	High mainly in protein, fat and polysaccharide
Rubber and textile manufacturing	Dissolved and suspended organics, fats and oil

1.2.3 The monitoring of wastewater properties

Wastewater characterisation and understanding of the properties of wastewater is important because the selection and design of treatment facilities depends on the study of the physical (e.g. colour, odour, taste, turbidity, temperature and solids)[40], chemical (e.g. total dissolved solid, metals, pH, chloride, organics and nutrient, alkalinity)[41] and biological characteristics (e.g. BOD and COD)[41-43]. As well as the quality that must be maintained in the environment to which the wastewater has is to be discharged, the fact that it is reused also

means that it must meet the discharge requirement standard[44]. Monitoring of these physical-chemical and biological parameters in the waste water before releasing it is crucial to ensure that there is not a chance of harm or damage to the environment.

1.2.4 Dyes and metals in wastewaters

Dyes are a key pollutant group which are causing some of the greatest pollution in the bodies of fresh water. These chemical compounds have an ability to attach themselves to the surfaces or fabrics and impart colour. These complex molecules are mostly resistant to biodegradation or photodegradation. The synthetic dyes are used in various technologies fields, for instance, in most branches of the textiles[45], leather and tanning sector[46,47]; in production of paper[47], in technology of food [48], in research of agriculture[49], in arrays of light harvesting[50], in photo-chemical cells[51] and in the hair colourings.[52] Dyes can also be classified as per their chemical structure and usage. Therefore, classifications vary from one country to another even though there are certain basic categories which are common for all.

Table.1.3: Types of dyes depending on their applications[53]

Type of dye	Applications
Acid dyes	Wool, silk and nylon
Reactive azo dyes	Cotton
Basic dyes	Acrylic
Direct dyes	Cotton, leather, paper and synthetics, cotton silk
Disperse dyes	Polyester
Food dyes	Food, cosmetics
Metal	Cotton
Whitening	Plastics, paper, soap
Pigment dyes	Paints and plastics
Reactive dyes	Wool and cotton
Sulphur dyes	Cotton and synthetics

Due to this, the relative amounts of dyes that are produced across the globe are not known until now; it is estimated to be more than ten thousand tonnes each year. Data on dye quantities that are discharged in environment is not available. It can be assumed that there is a loss of approximately one or two percent in

the production of the dye and one to ten percent in the usage of the dye. These are the rough estimates for general dyes, but for the reactive dyes, these estimates can be more accurate at four percent loss. [54] The large scale production of synthetic dyes along with their general applications causes considerable pollution in the environment. Major health risk factors tend to result in reduced freshwater consumption. Additionally, these dyes tend to give poor wastewater treatment results.[55,56] They also increase public concern and create problems in the legislation that pose a challenge for the environmental scientist.

Metals in wastewater are of a greater concern and are counted as an important category for pollutants that are present across the world. There are many examples of metal elements that have been extracted from the earth and have been used in many products and industries. Currently, heavy metals can be abundant in drinking water because of the greater usage of heavy metals containing compounds in each area of industry and science. For instance, from medicine to the pharmaceuticals[57], tanneries, plastics, pesticides, haulage and others[58], large quantities of toxic metals effluence are generated. This creates an environmental situation of higher risk which puts ecosystems at a higher toxic risk as a direct consequence of the persistent and non-degradable nature of the metals.[59]

1.2.5 Toxicological effects of dyes

Sewage waste waters produced by the dying companies are highly problematic and are treated not just for their great chemical oxygen demand, increased of biological oxygen demand, turbidity, suspended solids and toxic constituents, but for the coloured contaminants that can be seen by the human eye.[60] Dyes can have an effect on photosynthetic water life because of the decreased penetration of light into the water. Often, these dyes are toxic for some marine life because of the presence of the metals and aromatics in them,[61] also potentially putting human health at great risk. Past research has shown that textile waste water sewage can cause mutagenesis, teratogenicity, respiratory issues and chromosomal fractures.[62] Hence, sewage of dye textile has been ranked second in the toxicity, between certain other industrial sectors.[63]

1.2.6 Toxicology of heavy metals

38

Heavy metals are a particularly important category of inorganic contaminants in environment because of their mobility in aquatic ecosystems and their toxicity to the greater life forms.[64] The industrial waste water is a key transporter of the heavy metals, which are well known for acting as carcinogens with high toxicity, causing problems for the human population and other life forms. It is very important to note that these chemicals are dangerous even in dilute quantities because they are mobile and persistent in water systems promoting processes such as bio-magnification.[65] These metals are typically detected in the ionic or elemental state meaning that they are not subjected to biodegradable processes or bound in salt complexes. As a consequence, heavy metal pollution has become one of the most serious environmental problems today.[66]

1.2.6.1 Toxicity of heavy metals on humans

Many heavy metals are hazardous to humans. Table 1.4 shown below, provides the information on certain metals which are a dangerous and pose health problems.

Table.1.4: Type of metals and their effect on human health

Heavy metal	Major sources	Effect on human health	Permissible level (ppm)
Cr(VI)	Stainless steel, in chrome plating and in metal ceramics, dyes and paints, tanning of leather, catalysts[67]	Carcinogenic, Weakened immune systems, Kidney and liver damage, Skin rashes, Respiratory problems[68]	0.05 ppm[69]
Hg	Pesticides, batteries, paper, industry[70]	Damage to nervous system, protoplasm, poisoning[70]	0.01 ppm[71]
Ni	Stainless steel industry, welding, electroplating, pesticide, fertilizer CdNi batteries, catalysts and alloy[72]	Decreased body weight, heat and liver damage and skin irritation, Birth defects, Asthma and chronic bronchitis, Heart disorders[73]	0.02 ppm[67]
As	Pesticides, fungicides, metals smelter [74]	Neurological disorder, Bronchitis, dermatitis, kindle cancer, muscular weakness[75]	0.01 ppm[76]
Cd	Welding, electroplating, pesticide fertilizers, CdNi batteries and nuclear fission plant[77]	Kidney damage, bronchitis, gastrointestinal, disorder, bone marrow, cancer[78]	0.003 ppm[67]
Pb	Paint, pesticides, smoking, automobile, emission, mining and burning of coal[79]	Liver, kidney, gastrointestinal damage, mental retardation in children[80]	0.1 ppm[67]
Zn	Refineries, brass manufacture, metal plating, plumbing[81]	Zinc fumes have corrosive effect on skin, cause damage	15 ppm[67]

		to nervous membrane[82]	
Cu	Metal cleaning, plating baths, pulp, paper board mills, wood pulp production, and the fertilizer industry, electrical equipment, industrial machinery[83]	It causes headaches, stomach aches, dizziness, vomiting and diarrhoea, liver disease and neurological defects[84]	0.05-0.1 ppm[67]

1.2.6.2 Marine aqua toxicity of heavy metals

Heavy metal toxicity has an effect on marine organisms in the environment. After metals have been mineralized by microorganisms, they can bio-accumulate in marine ecosystems which can be taken up by plankton and transferred into different sea animals. Ultimately, the metals that are bio-magnified many times, for instance, highly toxic metals that have been magnified in fish, might be a serious threat to the health of humans , particularly where people tend to consume fish from the tainted water.[85] It is believed that increased levels of metals in natural water may cause problems for aquatic organisms including, for instance, changes in reproduction or in biochemistry, such as enzyme activity and blood chemistry.[86]

1.2.6.3 Heavy metal transport via irrigation

Contaminated waste water containing heavy metals has been supplied to many different areas around the world for the purpose of irrigation.[87-89] Providing water contaminated with sewage and industrial wastes for the purpose for agriculture could transport dangerous quantities of dissolved heavy metals to the agricultural fields. This could cause problems for agricultural production.

Excessive accumulation of the heavy metals in the irrigation waste water can increase the risk of contaminantes in agricultural soils. This might lead to the elevated heavy metals incorporation by the crops, and therefore, have an effect on the safety and quality of the food.[90] Unfortunately, this is one of the key methods for entry of the toxic pollutants into the human body, giving rise to potential risks to human health.[91]

Therefore, it is necessary to set up wastewater treatment plants (WWTP) to minimise the amount of pollutants in discharge wastewater effluence to reduce the risks on human health, and to protect other forms of life and the environment.

1.2.7 Importance of wastewater treatment plant (WWTP)

WWTP technology is a multi-stage process (see fig.1.1) designed to clean water and preserve life, as well as to protect natural water bodies. The primary aims of the treatment plant are not only to clean the wastewater, but also reuse it to meet the demand requirements of crops.

Treatment plants perform this by reducing the concentrations of solids, organic matter, nutrients, pathogens, and other soluble pollutants such as dyes and metals in wastewater.[92] Additionally, in order to meet the permit requirements for treatment plants, it is important that the assessing governor must take in to consideration certain points that are fundamental to the minimum legal requirements. These include, preventing nuisances, preventing diseases, providing protection to the supplies of drinking water, maintaining navigable waters, conserving waters, protecting the water for recreational usage and swimming, maintenance of the health habitat for fishes and other marine animals and preserving the waters that are clean for the purpose of protecting the ecosystems.[93] These wastewater treatment procedures are combined into a variety of systems, classified as primary, secondary, and tertiary wastewater treatment.[94]

Sludge, resulting in the end of wastewater treatment operations, is another significant problem, which has to be reduced to a minimal quantity to ensure that it is suitable for final disposal and can be reused with less expense.[95]
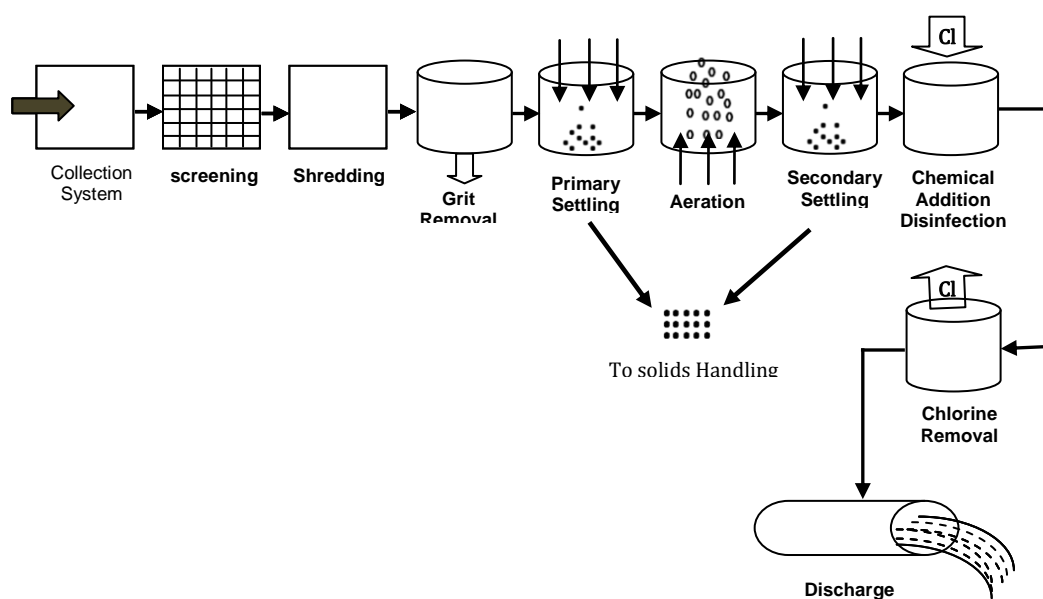
Fig.1.1: Multi-stage process in wastewater treatment plant (WWTP)[92]

Table.1.5: Wastewater Treatment Plant (WWTP) unites[96]

Process/Steps	Purpose
Primary Treatment	**Removes 90-95% settle able solids, 40 to 60% total suspended solids, and 25 to 35% BOD5**
Collection	Conveys wastewater from source to treatment plant
Screening	Removes debris that could foul or damage plant equipment
Shredding	Screening alternative that reduces solids to a size the plant equipment can handle
Grit removal	Removes gravel, sand, silt, and other gritty materials
Flow measurement	Provides compliance report data and treatment process information for hydraulic and organic loading calculations
Pre-aeration	Freshens septic wastes, reduces odors and corrosion, and improves solids separation and settling
Chemical addition	Reduces odors, neutralizes acids or bases, reduces corrosion, reduces BOD5, improves solids and grease removal, reduces loading on the plant, and aids subsequent processes
Flow equalization	Reduces or removes the wide swings in flow rates for plant loadings
Primary sedimentation	Concentrates and removes settleable organic and floatable solids from wastewater
Secondary Treatment	**Produces effluent with not more than 30 mg/L BOD5 and 30 mg/L suspended solids. It includes biological, chemical and physical treatments**
Biological treatment	Provides BOD removal beyond that achievable by primary treatment, using biological processes to convert dissolved, suspended and colloidal organic wastes to more stable solids
Secondary sedimentation	Removes the accumulated biomass that remains after secondary treatment
Tertiary or Advanced Treatment	**Removes pollutants, including nitrogen, phosphorus, soluble COD, and heavy metals to meet discharge or reuse criteria with respect to specific parameters**
Effluent polishing	Filtration or microstraining to remove additional BOD or TSS
Nitrogen removal	Removes nutrients to help control algal blooms in the receiving body
Phosphorus removal	Removes limiting nutrients that could affect the receiving body
Land application	Controlled land application used as an effective alternative to tertiary treatment methods. Reduces TSS, BOD, phosphorus and nitrogen compounds, as well as refractory organics
Disinfection	Destroys any pathogens in the effluent that survived treatment
Dechlorination	Protects aquatic life from high chlorine concentrations, needed to comply with various regulations
Discharge	Releases treated effluent back to the environment through evaporation, direct discharge, or beneficial reuse.
Solids treatment	Transforms sludge to biosolids for use as soil conditioners or amendments

In addition to this, at the final unit of wastewater treatment plant, before the effluent is discharged into a receiving body, the water stream must be disinfected because fumigation has certain objectives that are highly important. A major objective is to protect the health of the public by reducing the population of the organisms in the waste waters to a lower level that makes sure that the pathogenic organisms are not present in significant quantities to cause disease. Chlorine is a common disinfectant used, for both water and wastewater treatment, with alternatives to chlorine including chlorine dioxide, ozonation, potassium permanganate, ultraviolet (UV), and membrane processes.[97]

Depending on the reviewed recent topics in this chapter, the treatment of wastewater effluents has become a required step before discharged into freshwater bodies.

1.2.8 Technologies of dye removal in wastewater

The global annual production of pigments and dyes is more than $7x10^7$ tonnes and is utilized extensively in the cosmetics, food, paper mills and textile industries, which cover greater than seventy percent of the total quantity manufactured.[98] Cotton and fibres are ranked highest based on dyed textiles and more than fifty percent of their products are items that are dyed with a reactive dye.[99] Approximately 16 percent of the entire amount of dyes made are lost during these procedures[100] and water colourisation can be observed in a concentration of less than one ppm.[101]

All these processes of production are not just heavy water consumers, but they are also great generators of pollutants that potentially cause danger to both environment and humans. Most of these dyes are carcinogenic as well as toxic; they have properties that are persistent to the environment as none of them are naturally degradable.[102] Therefore, dye effluence has attracted great attention from the scientific community. The following methods are mainly used for dye removal in wastewater.

1.2.8.1 Traditional treatment

➢ *Biological treatments*

These treatments reproduce a phenomena known as self-purification which prevails in the nature. This concept of self-purification comprises of a complete process with which a marine environment achieves the good quality water after it is polluted. The biological treatments are different depending on the absence or presence of the oxygen and are often applied, hence a treatment which is used most commonly.[103,104] As a result of the low biodegradability of most of the dyes and chemicals used in the textile industry, biological treatment of these would not always meet with great success. Therefore, biological treatment must be combined with other methods of treatment as most of the dyes produced within the textile sector are resistant to aerobic biological treatment and are non-biodegradable or the organic substance can poison microorganisms.[105-107] It is noticed that the combination of biological treatment with other methods of treatment or vice versa are very costly.[103]

> ➢ *Dye removal using coagulation-flocculation*

In general, these treatments are utilized for eliminating substances that are organic. Normally, these products do not have an effect on the eradication of the soluble dyestuffs, but they are used widely in order to effectively eliminate the dyes that are insoluble.[108] Disposing of sludge which is produced from this method of treatment is a great concern and very costly.[109]

1.2.8.2 Electrochemical technology

In this process, the dye found in the household water waste is circulated in a electrolytic cell that contains the iron electrode. A key advantage with this kind of a process is its capacity to adapt to different pollution and volumes loads. The formation of iron hydroxide sludge is the main disadvantage of this method which limits its use.[110,111]

1.2.8.3 Dye treatment using Ozone

This treatment is mostly used either alone or in alliance with the different treatments, for instance, O_3-UV or O_3-H_2O_2 in treatment of industrial sewage.[112] Ozone attacks double bonds that are responsible for the colouration. For this reason, de-colourisation of wastewater by ozone alone does not always come with a significant reduction in the amount of the dyes.[113] Moreover, the installation of the ozonation process requires additional costs.[114]

44

1.2.8.4 Membrane techniques

The process of membrane filtration provides possible application that can offer interesting possibilities in the separation of dyestuffs that are hydrolysed and their auxiliaries. Therefore, they simultaneously reduce colouration and biological oxygen demand as well as chemical oxygen demand of the wastewater.[86,115] There are a few particular membrane processes (MF, UF, NF and RO) as follows:

➢ *Reverse osmosis (RO)*

In this process the membranes have greater rate of retention for varied kinds of ionic compounds and produce a higher quality of treated effluent.[116,117] The elimination and discolouration of the chemical auxiliaries in the waste water dye might be carried out in a singular step which allows removal of the hydrolysed dyes that are reactive and the auxiliaries of chemical[116]. The problem involved is the higher concentration of salt, leading to an increase in the osmotic pressure and therefore greater energy is required.[118]

➢ *Nanofiltration (NF)*

These membranes keep the organic compounds that have lower molecular weight such as the dyes which are hydrolysed and the auxiliaries used for dyeing.[119,120] The sewages are polluted normally with a single dye and the volume studied is normally low.[121]. Waste water treatment using nano-filtration represents the potential treating solutions of greater complexity.[122,123]

➢ *Ultrafiltration (UF)*

This technique enables eradication of the particles and macromolecules, but eradication of all the substances that pollute, including colour, is never completed. Hence, in the best cases, the treated water containing colour cannot be reused directly for processes that are sensitive to colour contamination, for instance dyeing textiles.[122] The fact that ultrafiltration could only be used as a pre-treatment for reverse osmosis or biological treatment has been studied.[123,124]

➢ *Microfiltration (MF)*

This is suitable for providing treatment to the dye baths and later washing baths that contain pigment dyes; this keeps dye auxiliaries.[125] This process might

also be utilized as a Nano filtration pre-treatment or for the reverse osmosis.[116,117]

1.2.8.5 Dye adsorption treatment technology

The techniques of adsorption are applied extensively in order to remove different classes of the pollutants from the streams of water, depending on their efficiency in removal of pollutants. This technique offers a higher quality product and additionally it is economically feasible.[126-128] This class of pollution is dyes that are of a particularly problematic group. As a result decolourisation using the adsorption treatment is dependent on certain factors which includes dye size and shape, interaction between dye and adsorbent, surface area adsorbent and the size of the adsorbent particle, contact time, temperature and the waste water characteristics.[129,130]

Activated carbon is used as the most common method for the removal of the dyes such as a pigment, mordant, acid dyes, reactive and cationic dyes in the waste waters that makes use of adsorption techniques.[131,132] Activated carbon has been prepared from many precursors, but the most common one is coal.[133]

Starbons®, is a derived polysaccharide mesoporous material[134] that has been developed and produced at the University of York in the Green Chemistry Centre of Excellence. It is proposed that this technology is applied to a four dye treatment in a stream of water as an absorption technique.

The proposed four dyes are Procion Crimson H-XEL(PC), Procion Navy H-XEL (PN), Procion Yellow H-XEL (PY), and Remazol Black (RB). They are reactive azo dyes and represent twenty to thirty percent of the entire market[135] and greater than fifty percent of the cotton industry.[135] Their structure contains two types of functional groups, one of those is a reactive group that reacts with the fibre and the other one is a chromophore group which causes its colour. The group of chromophore azo (-N=N-) shows almost sixty percent of the global production of dye in the industry.[136-138]

The chemical structures of the four reactive dyes selected are listed in Figure 1.2 and their reactive groups are listed in Table 1.6.[139] Further information about these dyes[140] such as colour, odour, chemical characterisation, acute

oral and dermal toxicity, mutagenicity, and degree of hazard are given in the Appendix.

Table.1.6: Reactive bulky azo dyes proposed for this research work[139]

Dyebath	Concentration in dyebath effluent (mg/L)	Reactive group	λ_{max} (nm)	Effect
Procion yellow H-EXL (PY)	33.3	Monochlorotriazine	416	
Remazol Black (RB)	72	Monochlorotriazine	595	Harmful for the environment, having a significant threat to the public concern's with safety
Procion crimson H-EXL(PC)	40.6	Monochlorotriazine	545	
Procion navy H-EXL(PN)	86.3	Monochlorotriazine	606	
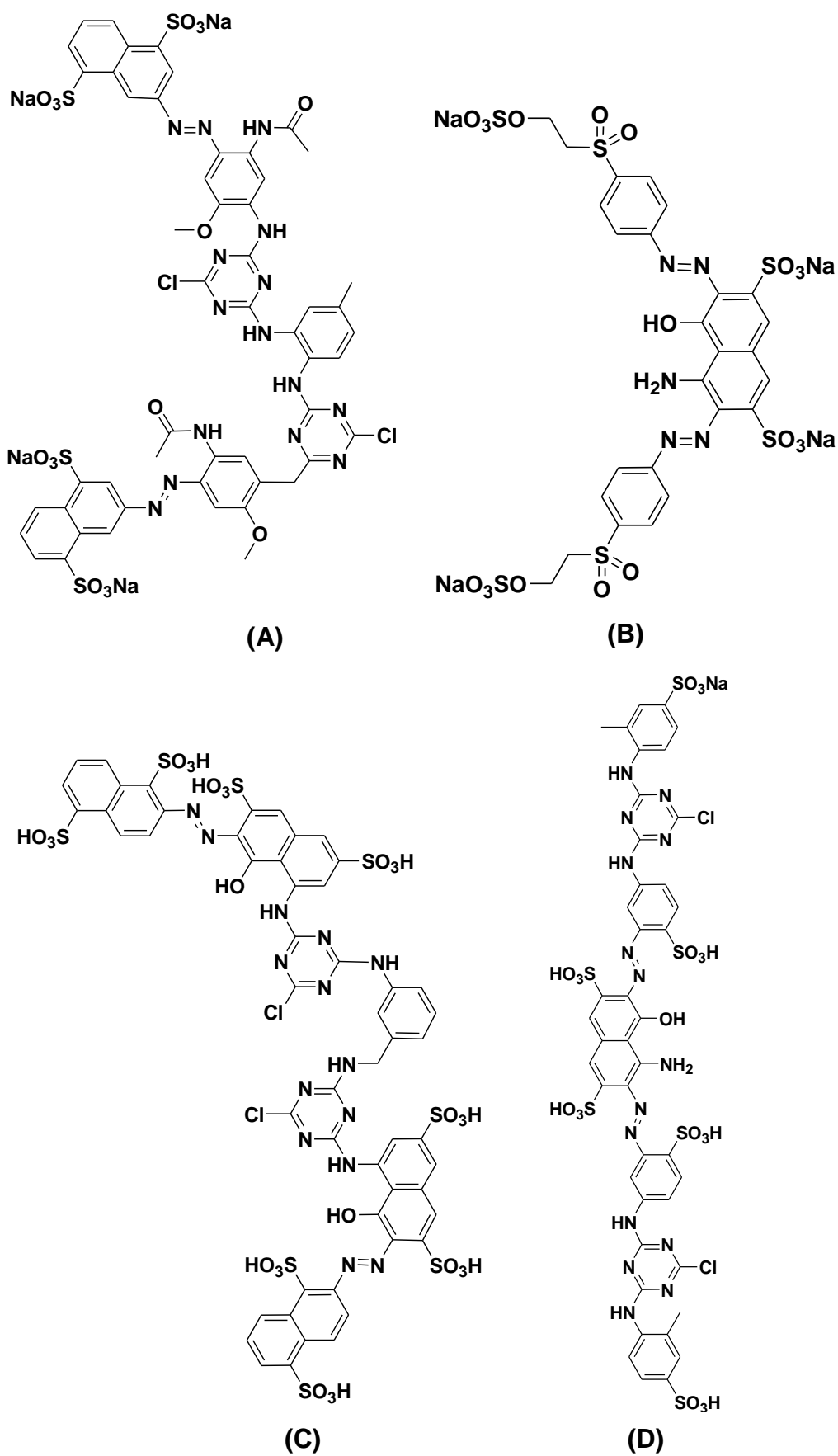
Fig.1.2: Chemical structures of (A) Procion Yellow (PY), (B) Remazol Black (RB), (C) Procion Crimson (PC) and (D) Procion Navy (PN) dyes[139]

At the end of dye treatment technologies section, generally, the relative advantages and disadvantages of the methods of dye removal in water stream are listed. Therefore, the information is listed in Table 1.7 below.

Table.1.7: Advantages and disadvantages of current methods of dye treatment[141]

Methods	Advantages	Disadvantages
1. Biological Treatment	Low costs	Low biodegradability of dyes
2. Membrane Process	Removal of all types of dyes, all mineral salts and chemical auxiliaries	Concentrated sludge production
- Reverse Osmosis	Good removal of hydrolyzed reactive dyes and mineral salts	High pressure
- Nanofiltration	Separation of organic compounds of low molecular weight and divalent ions from monovalent ones	Very expensive
- Ultrafiltration-microfiltration	Low pressure	Insufficient quality of the treated wastewater
3. Adsorption	Effective removal of a wide range of dyes	Adsorbents requires regeneration or disposal
- Activated carbon	Good elimination of suspended solids and organic substances	High costs, blocking filter, limited pore diameter
- Low cost sorbents	Low costs of preparation and usage	Poor capacity
- Ion exchangers	High capacity for dyes	Difficult regeneration
4. Oxidation	Rapid process	High energy costs and formation of by- products
- Ozonation	Good decolorization	No reduction of the COD, additional costs
- Fenton reagent	Effective decolorization of soluble and insoluble dyes	Sludge generation
5. Coagulation/flocculation	Economically feasible	High sludge production, costs

1.2.9 Treatment technologies of wastewater containing heavy metals

Many methods of metal removal have been found to capture metals in wastewater, with each method having its own advantages and disadvantages. The techniques discussed below have been used.

1.2.9.1 Chemical precipitation technique

The precipitation of chemicals is an important way and can be used widely as a process in the sector as it is relatively simple and is inexpensive for operations. In the processes of precipitation, the chemicals react with ions of heavy metals in order to create precipitates that are stable. These precipitates can be separated from water with filtration or sedimentation. After this the water that has been treated is decanted and discharged in an appropriate manner or it is reused.[142]

Commonly, the conventional process for chemical precipitation is the addition of sulphide and hydroxide. The hydroxide precipitation is used widely as a technique for removing the metals with its simplicity, ease and lower cost of the pH control in which solubility of numerous metal hydroxides might be reduced in the basic pH range. The hydroxides of metals produced can be eliminated with the use of sedimentation and flocculation.[143] Employing the types of hydroxides for the precipitation of the metals in the waste waters is dependent on the lower cost and ease of handling. For example, lime is a favoured base and it has been utilized in the industrial companies that specialise in the process of hydroxide precipitation.[143,144] This method of metal treatment has some disadvantages which include the fact that a huge amount of sludge is generated and there is the problem of disposing of it.[145]

The precipitation of sulphide is a process which is highly effective for treating the sewage ions of heavy metals. A basic benefit of sulphide is its ability to precipitate metals which is substantially lesser than for metal hydroxides. Therefore, sulphide can approach greater extent of metal removal in a wide pH range when compared with hydroxide.[146] The limitation of this method is due to certain dangers in the application of the sulphide precipitation process. The acidic conditions that produce the precipitants of sulphide create toxic fumes of H_2S and yields greater amounts of extensive sludge, making it expensive to dispose of.[147] Precipitation of chemicals in combination with the other

methods has been suggested in order to achieve successful removal of metal from the waste waters. For instance, it has been noticed that the precipitation of sulphide when combined with the nano filtration as a second step for removing the metal might work well, but generating sludge and disposing of it is expensive.[148]

1.2.9.2 Ion exchange

The process of ion exchange has widely been used for displacing metals that are heavy from the waste water because of various advantages, such as greater capacity of treatment and faster removing efficiencies.[149] Natural or synthetic solid resin ion exchange in particular has an ability to replace the cations with metals that exists in the waste waters. Among the materials that are used in the processes of ion exchange, the synthetic resins are often applied as they are highly effective at removing the heavy metals from solution.[150] The extremely common cation exchanges are strong resins of acids with sulfonic acid group ($-SO_3H$) and also the resins of weak acids with the groups of carboxylic acid($-COOH$). The following equations represent the ion exchanges:

$$n\ R\text{-}SO3H\ +\ M^{n+}\ \longrightarrow\ (R\text{-}SO_3^-)_nM\ +\ n\ H^+$$

$$n\ R\text{-}COOH\ +\ M^{n+}\ \longrightarrow\ (R\text{-}COO^-)_nM\ +\ n\ H^+$$
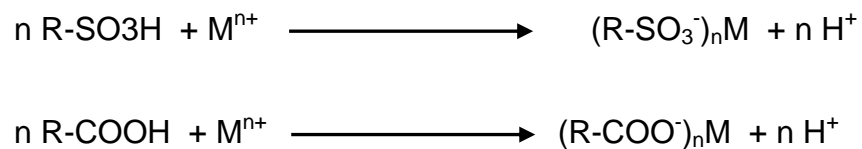
The disadvantage of this method is that the ion exchange material needs to be regenerated or disposed of and its disposal is costly.[151]

1.2.9.3 Membrane filtration technology

This method has generated the possibility for the elimination of heavy metals from waste water as it has high efficiency, ease of use and is space saving. Metal retention by the membrane is based on the contaminants size.[152] This process is used for removing the metals from waste waters with ultrafiltration[153], reverse osmosis[154], nanofiltration[155] and electrodialysis[156]. They perform the removal of several heavy metals well, but they are remarkably expensive, with the amount of sludge yield being massive and disposal of it being costly.

1.2.9.4 Coagulation and flocculation methods for metals removal

A method known as coagulation is very important for treatment of waste waters and it destabilises colloids by neutralising forces that keep them away from one another. In the conventional methods of waste water treatments, most of the coagulants are utilized including ferric chloride, aluminium and ferrous sulphate that can precipitate the metals, followed by filtration and sedimentation.[157] This might result in elimination of the waste water metals in an effective manner.[158]

Another method known as flocculation is used for removing metals from waste water through the use of polymers, for instance, macromolecular flocculants heavy metals are adopted. One example of this kind of flocculant is mercaptoacetyl chitosan[159,160] and can eradicate waste water metals. Besides the fact that both flocculants as well as coagulants are being used, they tend to be highly expensive and are not environmentally friendly.[161]

1.2.9.5 Metal elimination using electrochemical treatment

This kind of technology of metal eradication has gained importance due to stringent environmental regulations in the treatment of waste water.[162] It has also been reported that by adopting aluminium electrodes in the system of electrochemical treatment these will perform in an excellent manner for removing certain heavy metals. However, the process is intensive in terms of consuming the energy and yields greater amounts of contaminated mud (or sludge).[163]

1.2.9.6 Adsorption treatment

The technology of adsorption is an economical and an effective method for the adsorption of heavy metals in the waste waters that brings higher quality of the discharge water after treatment. Activated carbon is used widely for removing the pollutants of heavy metals and it has been shown that it can perform well.[164] It is useful for eliminating the metals which relates to larger micropore properties and results in an area of higher surface.[165]

It has also be said that CNTs (carbon nanotubes) that have been discovered years ago, have been studied for suitable properties and corresponding applications.[166] They have demonstrated a great potential for the eradication of several heavy metals in the waste waters.[167,168] The limitations for

52

making use of the activated carbon are the higher cost with the disposal and regeneration being too expensive.

A summary of the advantages and disadvantages of various methods of metal treatment in wastewater is demonstrated in Table 1.8 below.

Table.1.8: Current methods of heavy metal treatment in wastewater[169,170]

Physical or chemical methods	Advantages	Disadvantages
Chemical precipitation	Simple, easy in operation and cheap	Massive chemical sludge production, expensive disposal
Oxidation	Rapid process	High energy costs and formation of by-products
Ion exchange	Good removal wide range of heavy metals	Regeneration or extra cost for disposal
Membrane filtration technologies	Good removal of heavy metals	Concentrated sludge production, costly
Coagulation/Flocculation	Economically feasible	High sludge production, additional cost for sludge disposal
Electrochemical treatment	Economically feasible	High energy consumption, high sludge production
Adsorption using AC	Effective, economic	Regeneration is required, causes changing texture property of AC, disposal is expensive
Biological treatment	Feasible in removing some heavy metals	Expensive in commercialising it, sometimes heavy metals toxic for microbes

1.3 Adsorption concept

Adsorption is defined as the adhesion of the ions, molecules or atoms from liquid, gas or dissolved solids to a surface.[171] A process which is similar to adsorption is when a substance in a gas or liquid gets bound to the surface of the other phase. Adsorption is a phenomenon in which the substance gets stuck to the surface of another phase.[172] Therefore, porous materials (example shown in Figure 1.3) with high surface area typically are the most efficient adsorbents. It can be a pollutant which might be a heavy metal ion or a dye molecule, which is also known as the adsorbate, while material that is adsorbing

is called as an adsorbent that could be liquid or solid.[173] The process of adsorption takes place usually by the adsorbate getting adsorbed on the adsorbent. The forces that prevail between the adsorbent and adsorbate are attraction. As these forces of attraction are built, heat energy is released during this process. So most adsorption processes are exothermic.[174]
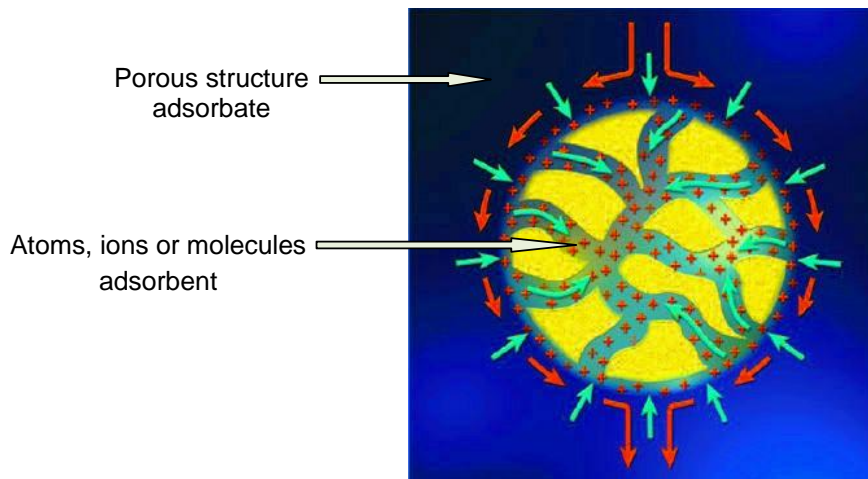
Fig.1.3: Adsorbent and adsorbate example[173]

Porous structure adsorbate

Atoms, ions or molecules adsorbent

1.3.1 Porosity

It refers to pore volume and pore diameter. Pore volume is taken from the quantity of the adsorbate, for example nitrogen, at a relative temperature close to unity and at the boiling temperature of the adsorbate. It assumes the pores are filled up with liquid adsorbate. It can be demonstrated mathematically as follows[175]:

$$V_{liq} = \frac{P_a \cdot V_{ads} \cdot V_m}{RT}$$

V_{ads} is volume of gas adsorbed, V_{liq} is volume of liquid N_2 in pores, V_m presents molar volume of liquid adsorbate ($N_2=34.7 cm^3/mol$), P_a = ambient pressure and T= ambient temperature. Pore diameter can be calculated from the pore volume. Assuming it as a cylindrical pore geometry which has average pore radius (r_p) can be mathematically expressed as:

$$r_p = \frac{2v_{liq}}{S}$$

V_{liq}= volume of liquid adsorbate, S= BET surface area

1.3.2 Adsorption mechanisms

The adsorption is a process which is competitive where the equilibrium is identified which most of the parameters including Van der Waals interaction between adsorbates and adsorbents, adsorption temperature, and polarity, solubility, mass, structure including the molecules size.[176] The steps of the overall processes generally can be divided into three main stages[177]:

Step 1: Adsorbate diffuses to adsorbent surface.

Step 2: The absorbate migrates into pores of adsorbent.

Step 3: Monolayer or mutilayer build-up of adsorbate.

The explanation of why these materials gather at the interface which is based on the excessive energy associated with interfaces of particles.[178] For example, in the case of pure water and air, the water molecules at the air-water interface have higher energy than water molecules in the interior of the water phase. This is the reason that energy of the water molecule is reduced after adsorption on the surface.[179]

1.3.3 Types of adsorption

Generally, the adsorption types can be classified into two depending on the nature of forces which exist between adsorbent and adsorbate molecules[180]:

One is a physical adsorption is also known physisorption. If forces of attraction prevail between adsorbent and adsorbate is forces of Van der Waal, adsorption is called as the physical adsorption or Van der Waal's adsorption. In physical adsorption the force of attraction between the adsorbate and adsorbent is very weak, therefore this type of adsorption can be easily reversed by heating or by decreasing the pressure. It has generally low enthalpy of adsorption, (ΔH=20 to40 KJ/mol), it can take place at low temperature below boiling point of adsorbate. While the temperature increases, the process of physisorption decreases. Also, it usually requires very low activation energy.[181]

One more kind of adsorption is also called chemisorption. In general, it is a process which is exothermic and (ΔH=80 to 240 kJ/mol). In chemisorption force of the chemical bonds is much stronger than force of Van der Waal. Therefore, adsorption might not be reversed easily as an outcome of that fact

Chemisorption is not appreciably affected by small changes in adsorption conditions, in addition, it generally forms monomolecular layers and requires higher activation energy.[182]

1.3.4 Adsorption isotherm

Adsorption is usually analysed through isotherms, that is, functions which connect the amount of adsorbate on the adsorbent, with its pressure. If the substrate is gas or liquid, there are several different models for predicting the equilibrium distribution in literature describing these processes of adsorption. They are named Linear isotherm[183], Langmuir isotherm[184], Freundlich isotherm[185], BET isotherm[186], etc. These four models which are most commonly observed will be discussed in more details as following:

1.3.4.1 Linear isotherm model

This model is one of the simplest models of adsorption isotherm that is also known as adsorption isotherm of Henry. This model might be used for describing the basic part of most of the isotherms that are practical. Typically, it is useful for low surface coverage, and the adsorption energy being independent of the coverage. The equation is written as:

$$X = K_H\ P \quad or \quad X = K_H\ C$$

Where X is the surface coverage, P is the partial pressure, K_H is Henry's adsorption constant. For solutions, concentration is used instead of the partial pressures.[183]

1.3.4.2 Langmuir isotherm model

In the year 1916, Irving Langmuir suggested an isothermal model for the adsorption of gases rather than adsorbed gases. It is an isotherm which is semi-empirical and is derived from the proposed mechanism of kinetics. This model was dependent on the various assumptions of which one is the dynamic equilibrium which prevails between the adsorbed gaseous molecules and free gaseous molecules. It is based on three assumptions[184]:

1. The surface of the adsorbent is uniform, that is, all the adsorption sites are equivalent.

2. Adsorbed molecules do not interact themselves.

3. At the maximum adsorption, only a monolayer is formed to the surface.

Langmuir proposed an equation to determine the monolayer adsorption capacity of a solid. The Langmuir adsorption isotherm has been successfully applied to many adsorption processes. The linear form of the isotherm is represented by the following equation[184]:

$$\text{Non-linear equation:} \quad Q_e = \frac{K\,Q_m C_e}{1 + K\,C_e}$$

$$\text{Linear equation:} \quad \frac{C_e}{Q_e} = \frac{1}{Q_m K} + \frac{C_e}{Q_m}$$

Where C_e is the adsorbate concentration at equilibrium (mg/L), Q_e the adsorption load at equilibrium and and K is constant of equilibrium. Q_m is the maximum monolayer adsorption capacity of the solid adsorbent (mg/g).

This model assumes monolayer coverage of adsorbate on the homogeneous surface of the adsorbent. This isotherm makes the simple assumption that adsorption is occurring at specific homogeneous sites within the adsorbent and once an adsorbate molecule is occupying this site no further adsorption can take place on it.[184]

1.3.4.3 Freundlich adsorption isotherm model

In the year 1909, Freundlich suggested an empirical model for the representation of the variation in the isotherm of adsorption of a gas quantity which is uptaken by the unit mass of the solid adsorbent in the presence of pressure. This empirical equation is called the Freundlich adsorption isotherm or equation. This equation is used for describing multilayer adsorption on heterogeneous surfaces, which is characterised by the heterogeneity factor n. The equation is following as[185]:

$$\text{Non-linear equation:} \quad q_e = K_F C_e^{\frac{1}{n}}$$

$$\text{Linear equation:} \quad \ln q_e = \ln K_F + \frac{1}{n} \ln C_e$$

Where K_F is the Freundlich constant (L/g) and is linked to adsorbance capacity of the solid. The heterogeneity factor (n), and signifies the intensity of adsorption. An n of close to or greater than unity indicates favourable adsorption of the adsorbate molecule. The Freundlich equation is related to the Langmuir equation, however, it models for adsorption on an amorphous or heterogeneous surface where the amount of adsorbed material is the summation of adsorption on all sites. This isotherm describes multilayer adsorption.[185]

1.3.4.4 BET adsorption isotherm model

In the year 1938, Edward Teller, Stephen Brunauer and Paul Emmett formulated a model that modified the mechanism provided by Langmuir. This theory is known as the BET isotherm. The model describes certain molecules which are adsorbed on a layer which is already adsorbed, which in the mechanism of Langmuir did not fit in the condition. Therefore, this is a more general and a multiple layer model. It assumes that a Langmuir isotherm applies to each layer and that no transmigration occurs between layers. It also supposes that there is equal energy of adsorption for each layer except for the first layer. The equation is written as following:

$$\frac{P}{V(P_o - P)} = \frac{1}{V_m\,c} + \frac{C-1}{v_m\,c}\frac{p}{P_o}$$

V is adsorbed gas volume (cm^3/g), V_m is the volume of gas adsorbed when the entire adsorbent surface is covered with a complete unimolecular layer(cm^3/g), P is pressure (M Pa), P_o is liquid adsorbed saturated vapour pressure of same temperature (M Pa), C is constant related with the heat of adsorption. The Langmuir isotherm is generally used for chemisorption; however, the BET isotherm is better employed for physisorprion for non micoporous surfaces.[186]

1.3.5 Solid surface area and pore size determination

Characterising the pore volume, distribution of pore size and surface area are considered as important characteristics of materials that are sold as they are manufactured in different applications, for instance, the production of adsorbents, pharmaceutical products and catalysts, chromatographic and

filters.[187] There are three classes of porous material according to their pore diameter which are micropore, mesopore and macropore.[188] Solid characteristic is monitored by gas sorption analysis as an integral part of quality control programme for conformity. For years several definition and terminology have been used for characterisation of porous material such as physisorption, sorption, desorption, monolayer adsorption, multilayer adsorption and capillary adsorption.[189]

1.3.6 Choice of adsorptive

Nitrogen gas is the best convenient adsorptive to measure the surface area and pore volume of a solid material. Because it is chemically inert and it is cheaper compared to other gases.[190]

1.4 Porous adsorbent materials used in adsorption applications

The material which is porous is shown as a solid matrix which comprises of interconnected system of networking of the pores that are filled with fluids which are either gas or liquid, based on the IUPAC (The International Union of Pure and Applied Chemistry) there are three classes of porous materials that includes mesoporous, macroporous and microporous[188] each type relates to a specific pore size system (see Table 1.9).

Each pore size range has its own characteristic mechanisms of nitrogen adsorption and desorption. The mircoporous materials have three dimensional condensation of nitrogen adsorbate inside a strong electromagnetic field made by the narrow pore dimension. In the system of mircopore the inter phase system properties is near to a single phase, while in the system of mesopores, adsorption process carries on by one after other formations of the adsorbate layers which is completed by the capillary condensation mechanism and the surface properties of macropore materials have similar characters to the conventional flat surface, which cannot be described by capillary condensation mechanism.[191]

Variety in the adsorption characters of these different pore materials attract them to be employed in many different applications. For example, because of strong Van der Waals interaction, mircopore materials are basically suitable for liquid and gas adsorption, conversely, mesopores are suited to liquid phase application such like its uses in heterogeneous catalysis and separation science

in which the pores allow better loading and, interestingly, offering sufficient diffusion and mass transfer of liquid phase analyte or substrate.[192] In general, it is crucial to mention that the real porous material contains all these kinds of pore regime as shown in Figure 1.4.[193]

Table.1.9: porous material classification according to IUPAC[188]

Pore size	Size regime	Condensation mechanism
Micropore	< 2nm	Three dimensional
Mesopore	≥ 2 ≤ 50 mn	Capillary
Macropore	>50 nm	Non condensation
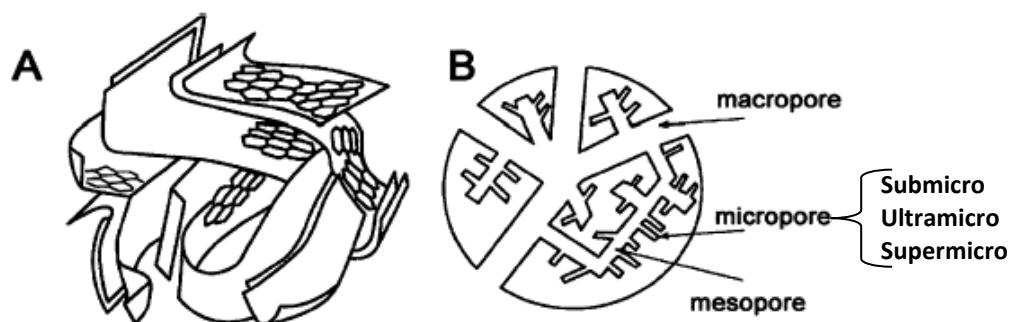
Fig .1.4: Schematic drawing (A) three dimensional and (B) two dimensional structure of porous material (activated carbon).[193]

Usually porous adsorbent materials are used in the form of spherical pellets, rods, mouldings, or monoliths with hydrodynamic diameters between 0.5 and 50mm.[194] They must have high scratch resistance, excellent heat stability and suitable pore diameters, which results in higher exposed surface area and therefore a high surface capacity for adsorption. The adsorbents must also have a distinct pore structure which enables fast transport of target absorbate which need to be adsorbed.[193, 194]

There are generally three classes of adsorbents which are widely used in industry as following[195, 196]:

1.Oxygen-containing compounds which are typically hydrophilic and polar such as silica gel and zeolites.

2. Carbon based compounds which are typically hydrophobic and non polar like activated carbon and graphite.

3. Polymer based compounds in which are polar or non polar functional groups in a porous polymer matrix.

Generally, a range of adsorbent materials are available for adsorption applications which are classified into two main categories which are inorganic such as aluminas, bauxite and silica gel; and organic such as activated carbon (AC), polymers and a new family of polysaccharide mesoporous carbonaceous materials generated in Green Chemistry Centre of Excellence at The University of York in the UK. Briefly some of these adsorbents are described in the following sections.

1.4.1 Alumina and bauxite materials

These adsorbents are effective for the removal of heavy metals from aqueous waste streams.[197] Bauxite is an alumina containing mineral and can be used as it is, alternatively, the alumina can be extracted and is also an effective adsorbent. This material was very popular recent decades, thus it is not used as much currently. The main reason for this fall in its popularity is the significant rising price of alumina.[198,199]

1.4.2 Silica gel materials

Silica gels are useful adsorbents because of their porous structure, high surface area and mechanical stability.[200] However, these materials have some limitations that restrict their appeal as adsorbents, siliceous materials have lower resistant to alkali media, therefore they are only able to be used in acidic solutions.[201] But mainly silicas are heterogeneous materials also tends to be in the microporous size range, which has limited their use for large molecules for instance, dyes.

1.4.3 Activated carbon

These are the most popular materials used for adsorption. Activated carbon has appointed as one of the best environmental control technologies available according to the US Environment Protection Agency.[201] Coal is the most common material for activated carbons, although theoretically any carbonaceous starting material could be used.[202] Activated carbon offers very high surface areas and porosities which are essential for good adsorptive

performance. Their adsorption is non-specific and so can be applied to a variety of different types of contaminations, as well as their microporosity makes them less effective for large molecules. As with other materials studied there is a barrier to large scale use of this materials.[201-203]

Activated carbon is also called activated charcoal, activated coal, or carbon activates, which is considered as the most popular and remarkable porous materials for adsorption, due to its high surface area that can reach in excess of (500 m^2/g).[204] According to other studies, the pore volume and structure are the most important factors for their applications in adsorption processes.[205,206] Activated carbon has wide range of pore sizes, from micropores to macropores. However, most of them are micropores, therefore, due to this limitation, activated carbon performance in large molecules is not very effective.[207,208] In addition, the commercially available activated carbon is expensive, due to several problems of these adsorbents.[209]

1.4.4 New family of adsorbents (polysaccharide mesoporous carbonaceous materials)

Porous materials are of interest to the scientific community due to their ability to interact with atoms, ions and molecules not only at their surface, but also throughout the bulk of the materials.[210] As a result of this, they are technically useful for a variety of applications including adsorption.[211] Traditionally, microporous materials such as zeolites and activated carbons (AC) were employed for chemical applications. However, their applications limited by the relatively small pore size which restricts diffusion of adsorbates or reagents in and out of the pore network.[212] In response to this problem the focus of materials chemistry became the enlargement of pores and development of the ability to control pore size during the fabrication of new porous solids.[210,211] A few decades ago the synthesis of novel ordered mesoporous silica materials called MCM-41 was found by Mobile Research and Development Corporation.[213] That group employed an organic template that was coated with silica, the template was then removed, leaving behind a highly structured silica solid (see Fig.1.5 micellar rod). By altering the template these mesoporous materials could be made with varying structures and pore diameters that can be controlled over a wide range of 2-30 nm.[214] Aim of manufacturing these materials was to offer the opportunity for size or shape

62

selectivity purpose for adsorption or catalysis of large components which had been in previous time difficult to achieve it with microporous materials. Further work was conducted to produce highly mesoporous carbon materials in which the MCM-type silica material was employed as template themselves.[214-217]
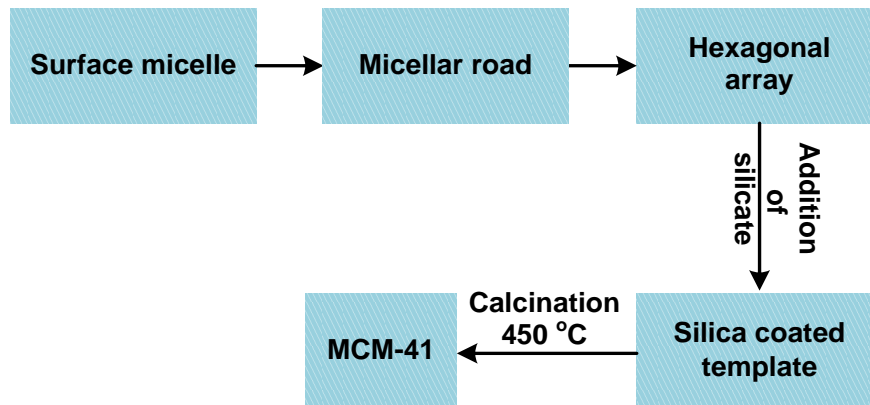
Fig.1.5 : Steps of synthesis of MCM-41.[213]

The advantages of these solid is that they offer different physicochemical properties compared with silica materials while offering a similarly ordered, mesoporous structure.
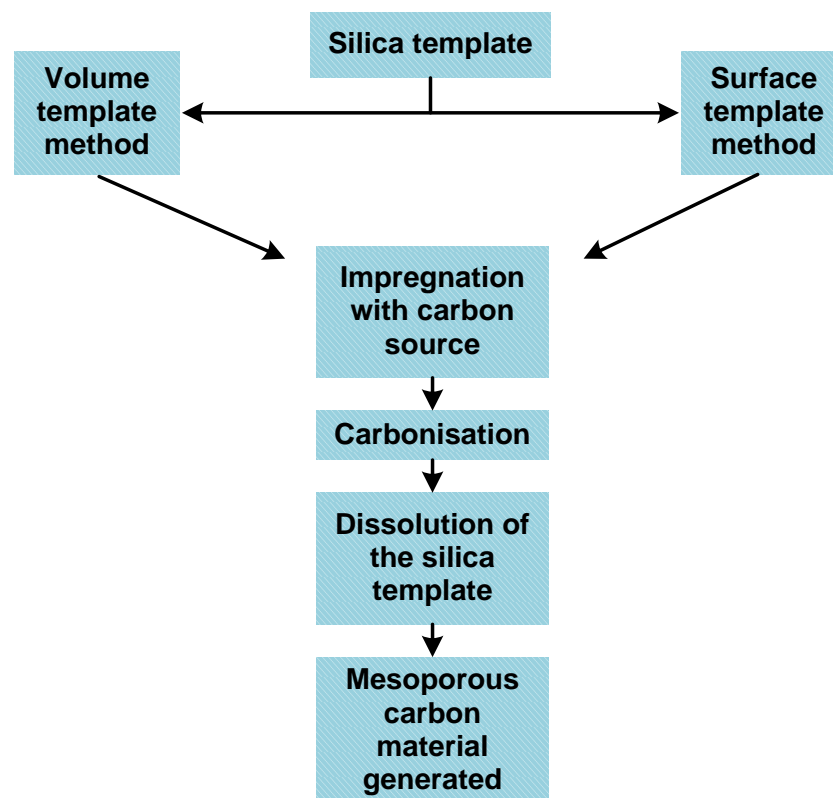
Fig.1.6: Synthesis of mesoporous carbon materials using silica template. Using either volume template or surface template.[215-217]

63

Unfortunately, from a green chemistry perspective the use of these mesoporous material which were prepared by the templating methods (Fig.1.6) for production is highly not attractive and unsuitable, because, this synthesis method engages with considerable numbers of complex steps, especially for carbon materials, there is also a large level of waste generation which is mainly caused by the removal of the template. These all together add additional cost, resource and the process is insufficient.[218]

Researchers at the Green Chemistry Centre of Excellence at The University of York have discovered an approach to generate mesoporous carbonaceous materials from polysaccharides precursors such as starch and alginic acid by carbonisation without the use of templating methods and agents. This new family of mesoporous carbon based materials discovered has been defined under the trademarked name, Starbon®.[219]

A typical method of preparation of polysaccharides derived mesoporous materials consists of three main stages as following[218-220]:

1. Gelation
2. Retrogradation and solvent exchange
3. Drying and carbonisation

Gelation is defined as a simultaneous loss of crystal structure of the polysaccharides and expansion of the polysaccharide granule to produce porosity.[221] To achieve this the polysaccharides including starch or alginic acid is mixed with water (1 g: 20 mL) and heated for certain time. The gelation stage in expansion of alginic acid is conducted at 90 ^{o}C and atmospheric pressure whereas starch required slightly stronger gelation temperature of 120 ^{o}C and under pressure (80 kPa) due to the more complex structure of the polymer caused by the mixture of amylose and amylopectine. Step one is complete a sol-like suspension is achieved and this is allowed to cool to room temperature. The mixture is then left to retrograde for 24 hours at 5 ^{o}C, this retrogradation lets the expanded polysaccharides to slightly recrystalise which brings stability to the pores structure created. The next step is solvent exchange of water with a lower surface tension organic solvent such as ethanol to prevent the porous networking system from collapsing when drying is carried out.
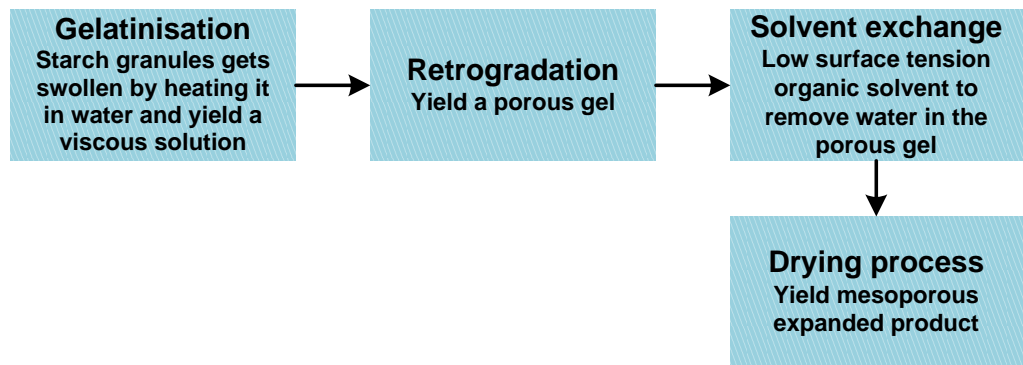
Fig.1.7: Stages of starch expansion formation.

The method of drying of expanded materials differs depends on the starting material. The starch derived material can be dried in a vacuum oven, however, this is not suitable for the alginic acid derived materials in which vacuum drying results in losing of textural properties of the materials.[222] Supercritical carbon dioxide (scCO$_2$) was used to successfully dry the alginic acid material providing maintaining a high textural property.
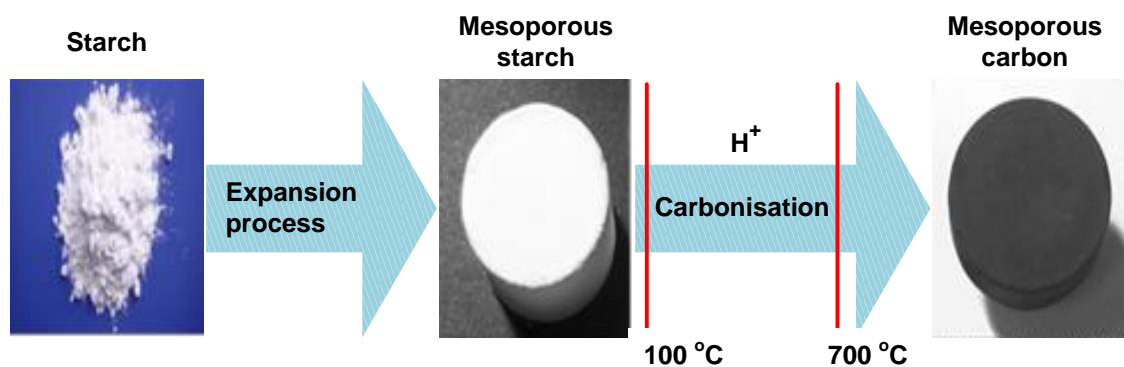
Fig.1.8: Thermal carbonisation of mesoporous starch to Starbon material.

This is followed by the carbonisation of the materials under nitrogen to increase the stability of the materials and preserve the pore structure. As a result of the acidic nature and occurrence of sodium and calcium in alginic acid, carbonisation can be performed directly.[223,224] Expanded starch cannot be directly carbonised unless it is doped with 5% w/w para toluene sulphonic acid (PTSA) which allows carbonisation to take place without collapsing the porous system whilst expanded alginic acid can be directly carbonised without doping

with any additional chemical. Heating of the materials creates changes in physical and chemical characteristics of the materials.

1.4.4.1 Starbon

Starbon is a mesoporous carbonaceous structured material based on polysaccharide starch. Starch occurs naturally on large scale on our planet and has many uses domestically as source of food and industrially when it is modified.[225] Starch is a polymer built of amylose and amylopectin. Amylose is a linear polymer with α(1,4) glycosidic bond of D-glycopyranose units.

Amylopectin has a similar structure to amylose but is cross linked by α(1,6)-glycosidic linkage to form a branched structure which presents a helical structure.[226] Starch surface area is around (1 m^2/g), this porosity property of the starch makes it very attractive for manufacturing Starbons.[227] This polysaccharide can be physically modified by expansion process (see Fig.1.7) which produce remarkably a mesoporous starch precursor with excellent surface area about 180 m^2/g.[228,229]
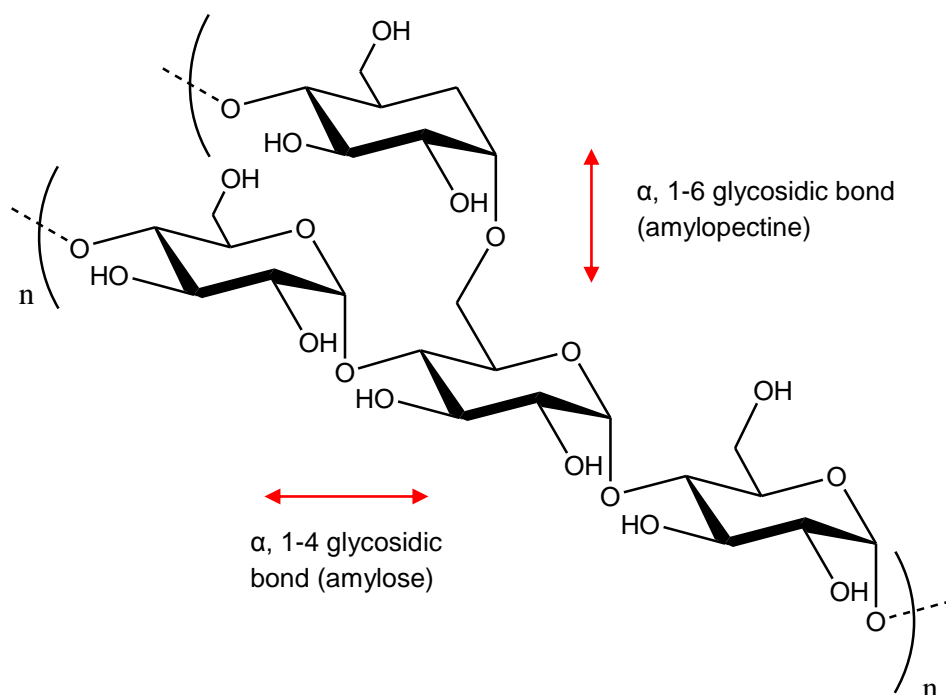
Fig.1.9: Structure of starch.

This is followed by mixing the mesoporous starch precursor with an organic acid PTSA as a catalyst. The mesoporous starch is carbonised at certain

66

temperature to generate different Starbons. The Starbon's porous structure, including surface area and pore volume, is highly dispersed in characters and also their physical and chemical properties make them very interesting in numbers of application in applied science and industry.[230]

It was recently reported that there are three known chemical changes throughout the conversion of starch to Starbons. The first thermal decomposition step is between (150 and 200 ^{o}C) and causes changes of the -CH$_2$OH groups to form ether groups, the second carbonisation temperature between (200-300 ^{o}C) can condense the residual CH$_2$OH groups and couple it with the glycosidic ring opening to form carbonyl groups which can conjugate with olefinic groups generating aliphatic and alkene/aromatic system. At last step, once the carbonisation temperature approached over 300 ^{o}C, the aliphatic groups are step by step converted to the extended aromatic π system.[231]
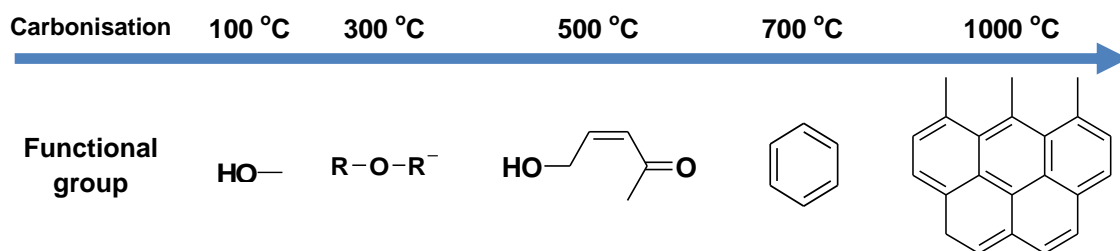
Fig.1.10: Temperature increased caused changes of surface functionality of Starbon produced.[192]

The porous structure of the mesoporous starch precursor is maintained throughout the carbonisation process. This is significantly vital in the process of Starbon production. Because it neglects the problem of pore collapsing which was noticed in previous methods of producing mesoporous carbons and removes the steps required for the mesoporous templates like silica to define the structure.

Furthermore, both scanning electron microscopy (SEM) image (see Fig.1.11) and porosimetry analysis (see Table.1.16) deliver information on the maintenance of the pores of the mesoporous starch and Starbon. Scanning electron microscopy (SEM) images introduces that the composed morphology of mesoporous starch can remain constant during pyrolysis with only small

changes due to shrinkage.[192,232] These porous materials are predominantly mesoporous. The total surface area is increased due to a growth in microporous region, but it is still smaller compared to the total mesoporous size. Starbon materials have many unique properties such as tuneable functionality, high mesoporosity (up to 2.0 cm^3/g), high surface area (up to 500 m^2/g), controllable electrical conductivity, excellent solvent stability, and good chemical and heat resistance which make it at present time hot topics.[192] The pore size distribution of the Starbon derived starch are shown in Table 1.10 which are measured by nitrogen adsorption.
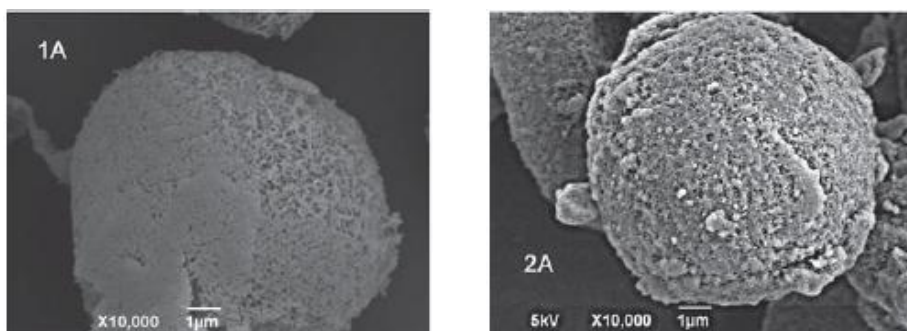
Fig.1.11: SEM images of yielded mesoporous starch (1A) and Starbon (2A), presenting the morphology and textural properties are remain constant.[192]

Table.1.10: Porosity analysis for starch and starch-derived starbon materials[192]

Material	Surface area S_{BET} (m^2/g)	Pore volume (cm^3/g)	Average pore diameter (nm)
Mesoporous starch	184	0.61	7.6
Acid/ doped mesoporous starch	230	0.66	8.6
Starbon300 (S300)	293	0.37	17.2
Starbon350 (S350)	332	0.38	16.8
Starbon450 (S450)	475	0.32	14.5
Starbon600 (S600)	528	0.43	12.1
Starbon700 (S700)	538	0.55	10.6
Starbon800 (S800)	600	0.43	7.0

Fortunately, it was confirmed in recent years that a few members of starch derived mesoporous carbonaceous materials were successfully employed as adsorbents in small dye adsorption application due to their excellent textural properties.[233]

1.4.4.2 Algibon

Algibon is a mesoporous carbonaceous material derived from alginic acid which is sourced from seaweed. Alginic acid is a linear biopolymer consisting of two blocks polyuronide with blocks of β-(1,4) linked D-mannuronic and α-(1,4) guluronic acid residues.[234] It is synthesised either as a homo polymeric units or heteropolymer of D-mannuronic or gluronic acid.[235-237] Native alginic acid has a small surface area about (5 m^2/g) and a very small pore volume which is almost zero. Interestingly, expansion of alginic acid is conducted which yields a mesoporous precursor.
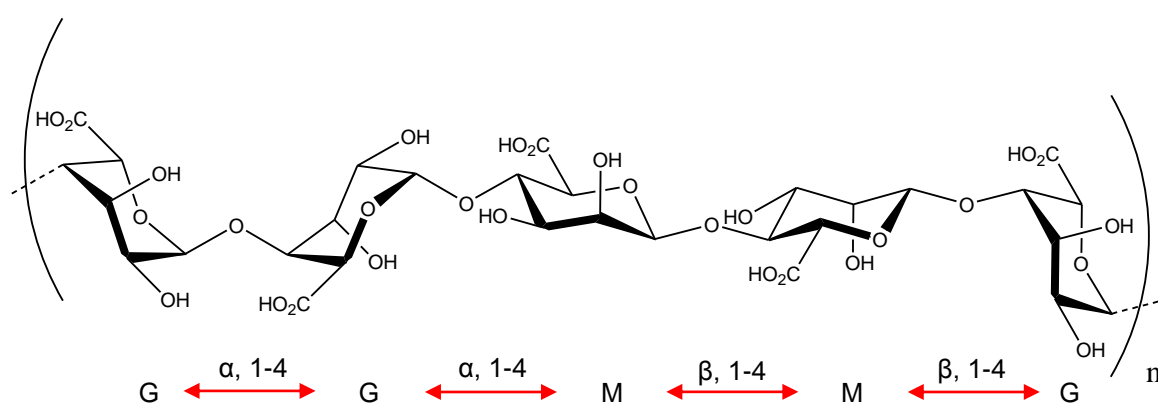
Fig.1.12: Structure of alginic acid.

This precursor is directly decomposed to certain temperatures to obtain different textural temperature Algibons. Throughout the carbonisation process no extra chemical is added. There are two main changes throughout the direct conversion of the mesoporous precursor to the Algibon. The first one occurs at 250 ^{o}C in which the percentage of mass loss is about 50%. This is noticed as a result of surface carboxylic groups are decomposed. And the second decomposition occurs between 300 and 600 ^{o}C around 32% of mass loss again observed because of the decomposition of the bulk catalysed OH group takes place.[220] This means the degree of polysaccharide character in the

mesoporous precursor is gradually changed to aliphatic and then aromatic character in response to the increased temperature throughout the carbonisation process.[220]

In addition, the mesoporosity can change while, the preparation temperature is increased. Decomposition at 250 ^{o}C which removed the carboxylic groups does not affect the mesoporous structure of the Algibon produced.[220] However, preparation temperatures greater than 300 ^{o}C, which cause the loss of OH groups, could result in a small loss in mesoporosity. Furthermore, we refer the reader to read an article which gives information on using TG IR technique in green chemistry centre at York to detect the volatile compounds throughout pyrolysis of expanded alginic acid for Algibons production.[220] On the one hand, Algibon prepared at 500 ^{o}C gave a massive increase in surface area due to a minor growth in microporosity content. On the other hand, Algibon produced at temperatures greater than 600 ^{o}C gave a reduction in pore size distribution, but the mesoporosity was still remarkably large (99%).[220] This means the pore size and diameter of the carbonised materials produced are preserved throughout the carbonisation process that indicates the mesoporosity is predominant.
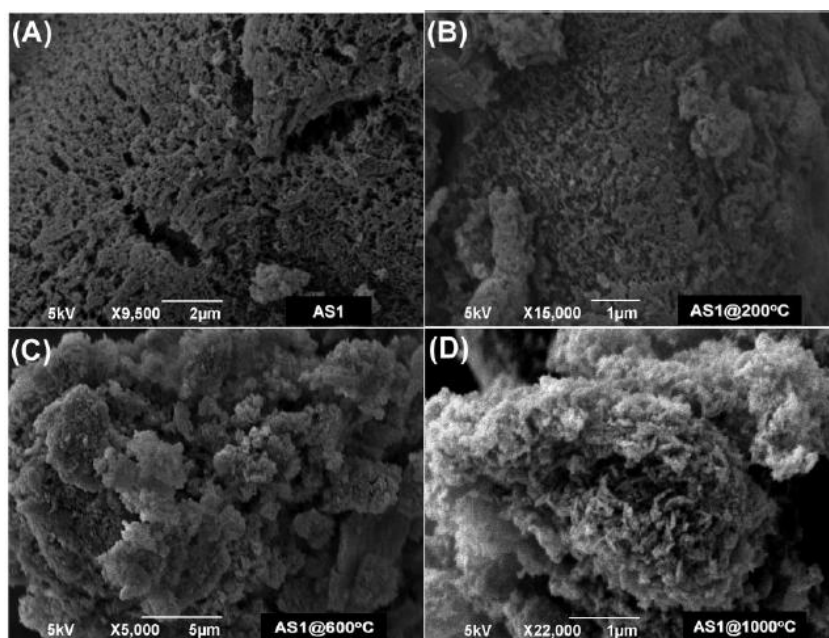
Fig.1.13: SEM image of (A) AS1: expanded alginic acid Supercritical CO_2 (scCO$_2$) dried, and (B)-(D) carbonaceous materials (Algibons) obtained at preparation temperature 200, 600 and 1000 ^{o}C.[220]

70

An article was published a few years ago which demonstrated the Algibon materials were successfully employed as adsorbers in small dye adsorption application.[233]
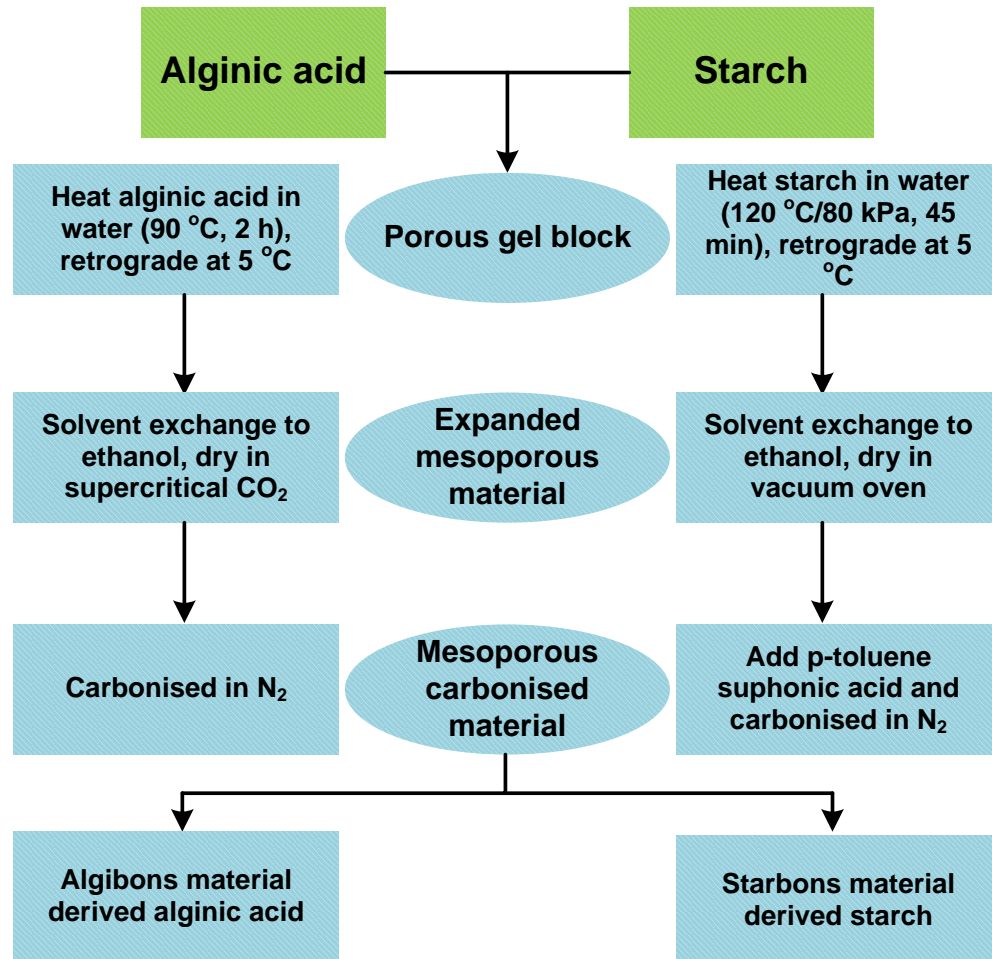
Fig.1.14: Preparation procedure for starch and alginic acid derived Starbon and Algibon respectively.

1.5 Introduction to work in this thesis

This section is devoted to give short information about the works was carried out in this thesis. In the second chapter a method for expanding alginic acid is developed. Stages of the expansion process, including temperature and time of gelation process, retrogradation time, and solvents have effects on the expansion process as well as the drying technique and are investigated. The aim of that chapter is to generate a mesoporous alginic acid precursor with large pore size and diameter.

In the third chapter, temperature programming will be applied to carbonise the mesoporous alginic acid precursor. This temperature programme and controlling preserve the pore volume and diameter of the product. Different carbonisation temperatures of the mesoporous alginic acid precursor generate different textural properties of Algibon materials. The Algibons produced are characterised by N_2 adsorption porosimetry to test their pore size distribution. DRIFT IR and Solid State NMR are applied to characterise the surface functionalities of different Algibons produced. Ash content tests are conducted to determine the amount of ash that exists, which corresponds to the degree of hydrophobicity, aromatisation and graphitic content present in each product. The aim of this chapter is to generate a predominantly mesoporous carbonaceous materials (Algibons) with large pore volume and diameter for bulky dye adsorption in water stream and metals removal in aqueous phase.

In the fourth chapter, the Algibons produced will be applied for bulky dye adsorption in wastewater. The dyes chosen represent more than 50% of the cotton market. It is estimated there is about 4% loss throughout their applications in dying process. Due to large-scale production and extensive application these dyes can cause considerable problems for the environment. In addition, they increase public concern and reduce the consumption of freshwater. This lowers the output of wastewater and poses a challenge to environmental scientists.

Commercially available activated carbons can less effectively remove these large molecules in wastewater, due to their predominantly microporous character. This microporosity has limited the efficiency of AC to uptake the large dyes. Therefore, the Algibon produced can replace the AC are applied for bulky dye adsorption in contaminated water. Its adsorption efficiency will be compared to that of AC.

In chapter five, the Algibon generated will be employed in metals adsorption. These metals are mainly used in research and industries such as in generation and application of low carbon technologies like wind turbines, electric cars, energy saving light bulbs, fuel cells and catalytic converters, photovoltaic and many other areas. Such elements are running out because of their many technologically dispersed applications and their geographically limited locations on our planet. Therefore, recovering them form resulting solid wastes is vital. By

developing efficient methods for adsorbing these metals it might be possible to recycle and reuse them in the industry and for research.

In this chapter, several rich high value metals containing solid waste ores namely: Pulverised fly ash (PFA), Red Mud (RM), Bottom ash (BA), Titano gypsum (TiG), Red Titano gypsum (RTiG) and Phospho Gypsum (PG) will be digested and Starbon materials will be screened as adsorbers. This will be carried out to recover the high value metals including Ag, Cd, Li, Au, Cu, Sc, Be, Co, W, V, Ni and etc which are extracted into the water stream after the solid ore materials are digested.

Finally, further systematic work on metal adsorption on Starbon based on A800 will be conducted in a concentrated water sample solution containing (Co, Cu, Ag and Cd). This is to determine types of adsorption, kinetic adsorption and evaluation of kinetic parameters of the process.

CHAPTER TWO

Developing Method of Expanding Alginic Acid

2.1 Introduction

This section deals with the optimisation of alginic acid expansion procedure based on a method developed in Green Chemistry Centre of Excellence at The University of York in the UK to produce an expanded alginic acid precursor with the best textural properties such as optimum pore volume and average pore diameter as well as optimum degree of mesoporosity.[238]

At the beginning of the chapter a small scale expansion technique is described. The developed method includes four most important preparation steps (see table 2.1).

Table 2.1: Parameters of alginic acid expansion procedure

Stage of expansion		Optimised parameter
1	Gelation	Time, temperature
2	Retrogradation	Time
3	Solvent Exchange	Solvent, number of solvent exchange steps
4	Drying	Vacuum oven vs scCO$_2$

It has been proved that the developed procedure of expanding alginic acid production could also be applied for large scale (up to 5kg). The expanded alginic acid's textural property (surface area, pore volume and pore diameter) was determined by nitrogen adsorption analysis (porosimeter). Expanded materials produced according the method described in this chapter was used as a precursor to manufacture Algibons (see chapter three).

2.2 Experimental section

A mixture of one gram of alginic acid with 20 mL of distilled water (D.W) was stirred in a closed 35 ml vessel at certain temperature and time. It was left to cool down to room temperature, retrogradation was then done by keeping it in fridge for 24 hours at 5 $^{\circ}$C. The gel was then firstly solvent exchanged with three individual portions of ethanol, secondly it was solvent exchanged with three individual amounts of acetone. The precipitate was either vacuum oven dried or supercritical (scCO$_2$) dried. The same procedure was applied for large scale to produce the expanded alginic acid scCO$_2$ dried. Thereafter the mesoporous precursor yielded was characterised by testing it in nitrogen

adsorption analysis (porosimetry) as a key point to examine the texture property of the product including surface area, pore volume and pore diameter.

2.3 Results and discussion

2.3.1 Investigation of temperature and applied time influence onto the gelation process

Gelatinisation of the native alginic acid is one of the key steps that control the whole expansion process. During previous investigations in the Green Chemistry Centre of Excellence at York it has been found that most important parameters which influence this stage are temperature and time. Therefore during the current project the gelation process have been investigated at different temperatures (80, 90, 100 and 110 ^{o}C) and time (40, 80, 120, and 160 minutes). For consistency the rest of the steps of alginic acid expansion including retrogradation, solvent exchanging and drying were applied under the same conditions: i) retrogradation step (5 ^{o}C, 24h); ii) solvent exchanging (three times ethanol followed by three times acetone) and iii) drying (vacuum oven). Conditions of the experiments together with textural properties of the final materials (S_{BET}, pore volume and pore diameter) are shown in Table 2.2 and Figure 2.1. It can be seen that expanded materials with the best textural properties were produced under gelation temperature 100 ^{o}C and 160 min. It is important to note that samples generated at lower and higher temperature than 100 ^{o}C show lower pore volume. It is important to note that samples prepared at 100 ^{o}C after 200 minutes slightly carbonised and the solid materials obtained was completely non-porous. The time of gelation critically influences on pore volume of the product: at high temperature (110°C) pore volume is reduced with increased time whereas at temperatures lower than 110°C pore volume grows with time. This can be partly explained by a significant reduction of molecular weight of polysaccharides at elevated temperatures.[239]

Table.2.2: Obtained results for four studies in which different gelation temperature applied over varying time period

sn	CAa in DW	Gn Cn		Rt Cn (T °C/time h)	S_{BET} (m²/g)	Pore volume (cm³/g)		Pore diameter (nm)		Meso-porosity %
		T (°C)	Time (min)			Apv	Dpv	Apd	Dpd	
Experiment one										
Sa1	5%	80	40	+5/24	80	0.198	0.21	11	7.7	20
Sa2	5%	80	80	+5/24	76	0.22	0.22	12.6	8.8	24
Sa3	5%	80	120	+5/24	50	0.17	0.17	15.4	9.6	18
Sa4	5%	80	160	+5/24	95	0.30	0.31	13.2	10	30
Experiment two										
Sb1	5%	90	40	+5/24	49	0.17	0.18	16	10.2	19
Sb2	5%	90	80	+5/24	80	0.27	0.273	14.2	10.3	29
Sb3	5%	90	120	+5/24	139	0.55	0.54	19.3	17	43
Sb4	5%	90	160	+5/24	167	0.58	0.57	13	12.4	47
Experiment three										
Sc1	5%	100	40	+5/24	40	0.17	0.20	20.7	17	19
Sc2	5%	100	80	+5/24	127	0.47	0.51	14.5	13.3	35
Sc3	5%	100	120	+5/24	110	0.516	0.518	18.7	15	39
Sc4	**5%**	**100**	**160**	**+5/24**	**195**	**1.021**	**1.019**	**16.4**	**14.8**	**83**
Experiment four										
Sd1	5%	110	40	+5/24	190	0.55	0.58	12	10.6	46
Sd2	5%	110	80	+5/24	109	0.49	0.54	17.8	16	36
Sd3	5%	110	120	+5/24	87	0.31	0.32	16.5	13.5	32
Sd4	5%	110	160	+5/24	81	0.275	0.281	16	13.2	29

sn: Sample name, CAa in DW: Concentration of alginic acid in distilled water, GnCn: Gelatinisation condition, Rt Cn: Retrogradation condition (T °C/time in hour), S_{BET}: Surface area BET, Apv: BJH adsorption pore volume, Dpv: BJH desorption pore volume, Apd: BJH adsorption pore diameter, Dpd: BJH desorption pore diameter. pore volume, Apd: Adsorption pore diameter, Dpd: Desorption pore diameter.

Note: Gelation condition (at temperature 100 °C for 160 min.), retrogradation for 24 hours at 5 °C, washing by ethanol and then acetone followed by vacuum oven drying generated sample (Sc4) in Table 2.2. That sample (Sc4) gave the best pore structure and it was predominantly mesoporous. This gelation condition was taken as the best condition to make alginic acid gel. Further work was carried out to optimise the rertrogradation time (see 2.3.2), type of solvents used in solvent exchange stage (see 2.3.3). Level of water left in the gel in each stage (see 2.3.4). As well as repeatability of generating expanded alginic acid vacuum oven or scCO$_2$ dried was studied (see 2.3.5).

Reproducibility of expanded alginic acid production (Sc4) is excellent as many time as it is repeated.
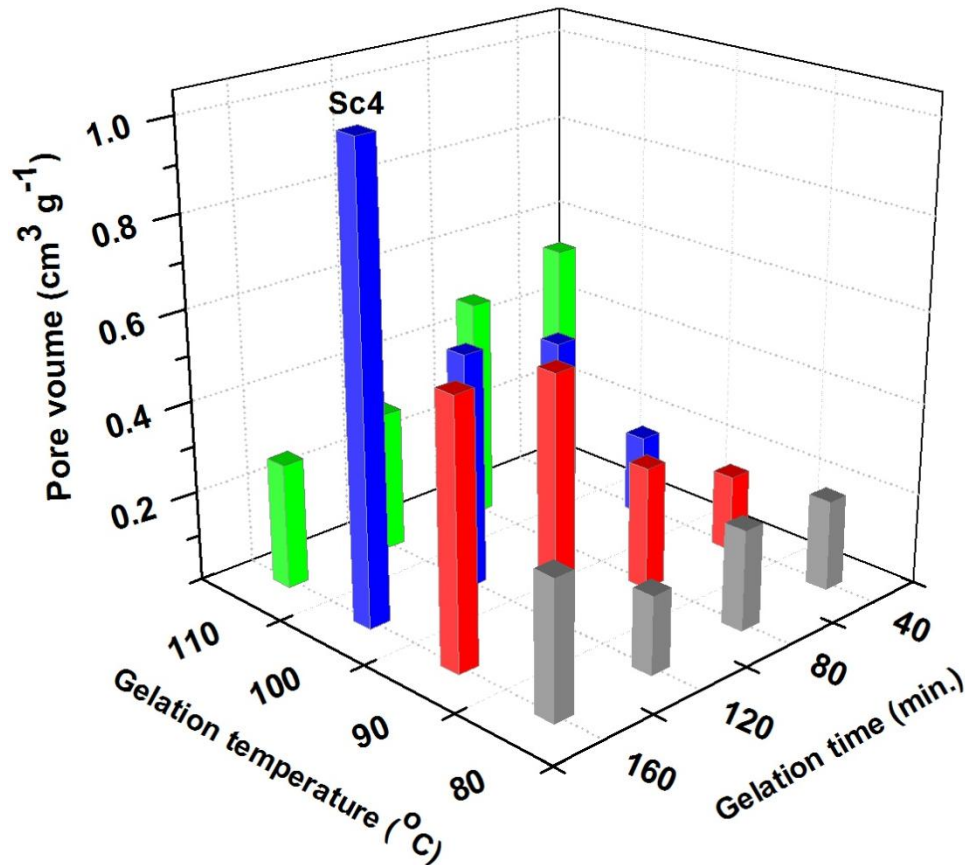
Fig.2.1: Pore volume of the expanded alginic acid produced at certain gelation temperatures (^{o}C) including 80, 90, 100 and 110 ^{o}C and hold it for certain of period of times including 40, 80, 120 and 160 minutes.

According to the data reported in this section, low gelation temperature cannot disrupt the inner or intercellular forces between the alginic acid molecules. Beside this, applying excessive temperature or over-heating in the gelation stage does not bring good results because of the influence on the molecular weight of this polysaccharide polymer.[240- 242]

The gelation parameters influence on pore volume and diameter are shown in Figures 2.2 and 2.3. This demonstrates that pores within expanded alginic acid samples have a bottle like shape.[243-245] The adsorption pore size distribution, which is wider represents the bottom area of that bottle and the desorption, which is narrower, presents the neck part of that bottle.
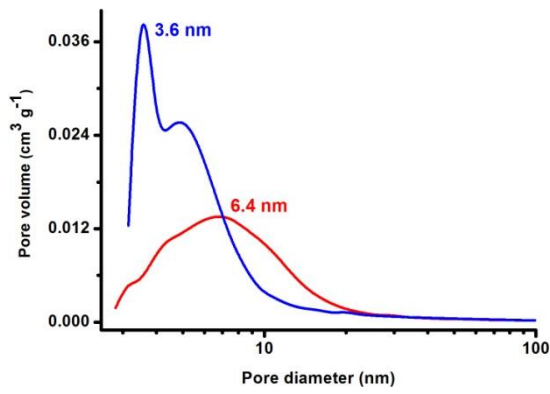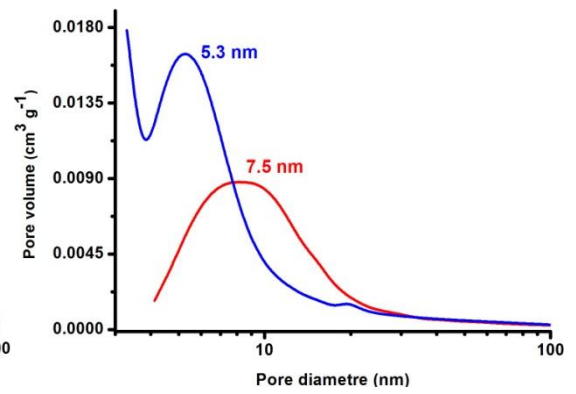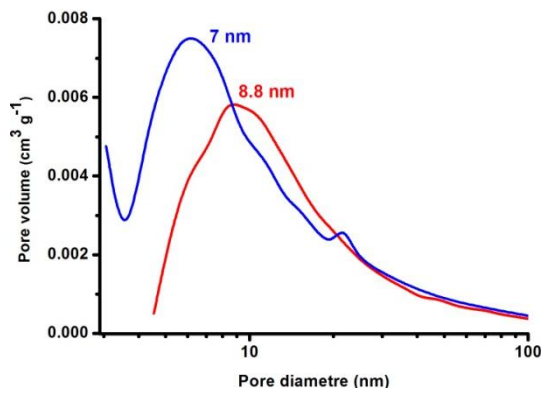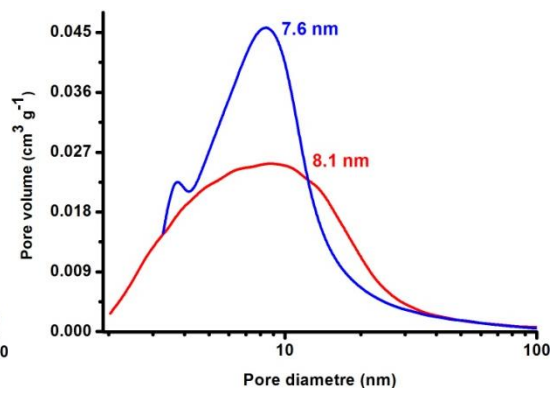
Fig.2.2: dv/dD pore size distribution (cm^3/g) of the expanded alginic acid produced at certain gelation temperature including (A) gelation at 80 ^{o}C, (B) gelation at 90 ^{o}C, (C) gelation at 100 ^{o}C and (D) gelation at 110 ^{o}C. They were all held for 40 minutes. Red line colour presents adsorption pore size distribution, blue line colour presents desorption pore size distribution.
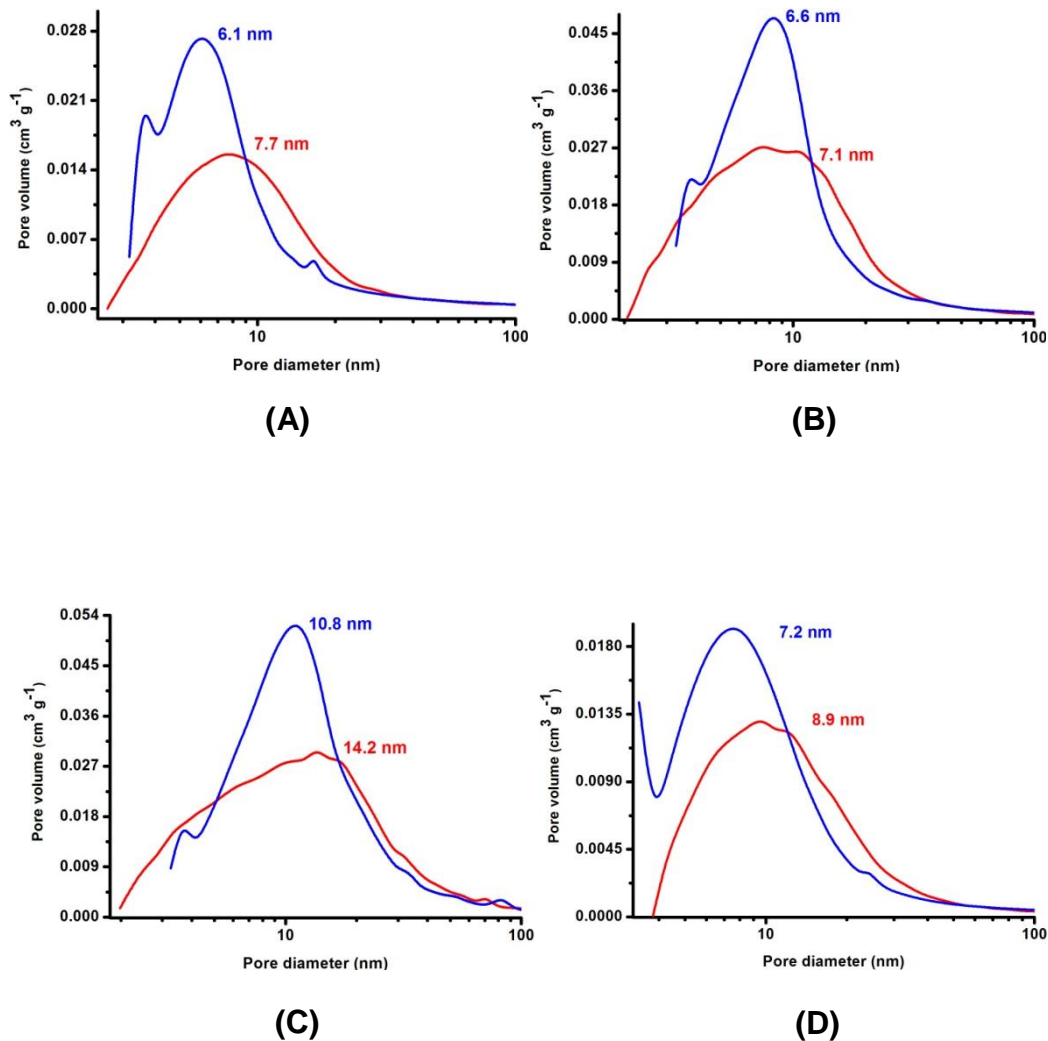
Fig.2.3: dv/dD pore size distribution (cm^3/g) of the expanded alginic acid produced at certain gelation temperature including (A) gelation at 80 $^{\circ}$C, (B) gelation at 90 $^{\circ}$C, (C) gelation at 100 $^{\circ}$C and (D) gelation at 110 $^{\circ}$C. They were all held for 160 minutes. Red line colour presents adsorption pore size distribution, blue line colour presents desorption pore size distribution.

2.3.2 Investigating of applied time influence on retrogradation process

Retrogradation of the alginic acid which had been gelatinised at 100 $^{\circ}$C for 160 minutes is of great concern and regarded also as a vital stage in the expansion process. It is believed the most important parameter which influences this stage is time. Therefore to optimise the final materials, retrogradation was investigated at different times: 0, 0.5, 1, 2, 3, 4 and 5 days. For consistency the rest of the procedure of alginic acid expansion including gelation process, solvent exchanging and drying steps were the same for all samples [i) gelation step (100 $^{\circ}$C, 160 minutes); ii) solvent exchanging (three times ethanol following three times acetone) and iii) drying (vacuum oven)]. Textural

properties (S_{BET}, pore volume and pore diameter) as well as conditions of experiments are shown in Table 2.3, Figures 2.4 and 2.5.

Table.2.3: Porosity analysis for expanded alginic acid in experiment five in which retrogradation time was studied. Gelation T= 100 ^{o}C, time : 160min.; ethanol and acetone was used for solvent exchange, vacuum oven drying was applied

sn	CAa in DW	Gn Cn		Rt Cn (T ^{o}C/time day)	porosity measurement					Meso-porosity%
		T (^{o}C)	Time (min)		S_{BET} (m^2/g)	Pore volume (cm^3/g)		Pore diameter (nm)		
						Apv	Dpv	Apd	Dpd	
Se1	5%	100	160	zero	< 2	--	--	--	--	--
Se2	5%	100	160	+5/0.5	57.2	0.62	0.63	73	52	49
Se3	**5%**	**100**	**160**	**+5/1**	**203**	**0.98**	**0.99**	**16.7**	**15**	**82**
Se4	5%	100	160	+5/2	151	0.71	0.71	17.4	14.4	61
Se5	5%	100	160	+5/3	196	0.61	0.61	12.8	11.4	48
Se6	5%	100	160	+5/4	53	0.37	0.38	79	53	34
Se7	5%	100	160	+5/ 5	80	0.31	0.32	16.5	12	30

sn: Sample name, CAa in DW: Concentration of alginic acid in distilled water, GnCn: Gelatinisation condition, Rt Cn: Retrogradation condition (T ^{o}C/time in day), S_{BET}: Surface area BET, Apv: BJH adsorption pore volume, Dpv: BJH desorption pore volume, Apd: BJH adsorption pore diameter, Dpd: BJH desorption pore diameter.

It can be seen from the data that expanded materials with the most interesting textural properties were produced at gelation temperature of 100 ^{o}C and held for 160 min, retrogradation for one day at 5 ^{o}C.

It was noted that the sample generated with no retrogradation was a nonporous material whereas retrogradation for 0.5, 1 and 2 days gave better results in comparison to the samples produced by retrogradation for 3, 4 and 5 days and in particular sample generated within 1 day of retrogradation provided the best textural properties. Retrogradation for less than a day is not sufficient time to let the gel to undergo thermo reversible crystallisation[246,247].
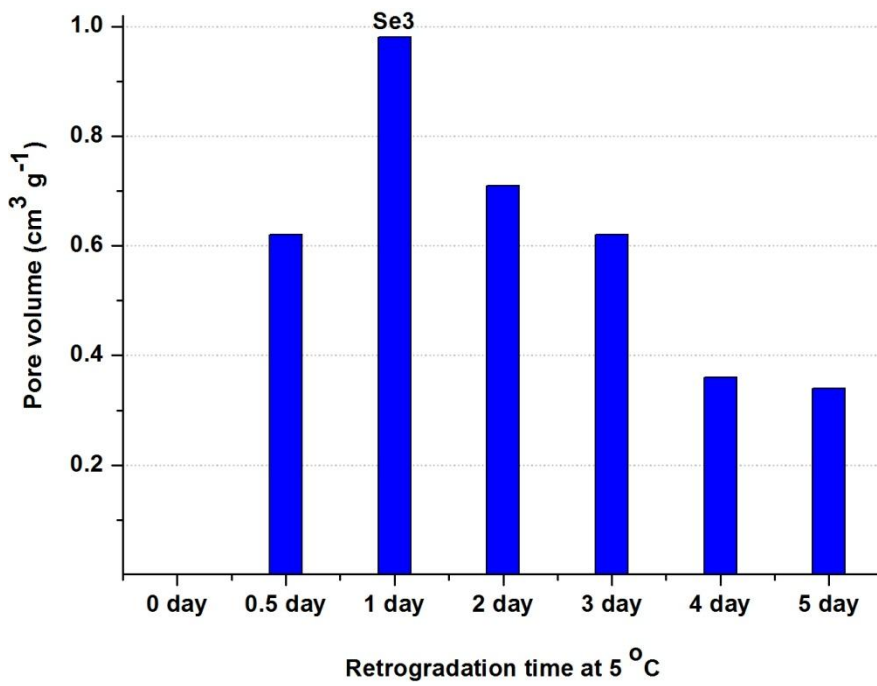
Fig.2.4: Pore size of the expanded products in experiment five drawn in Table 2.3 reveals different pore size as a result of different retrogradation period of time.

(A)

(B)

(C)

(D)
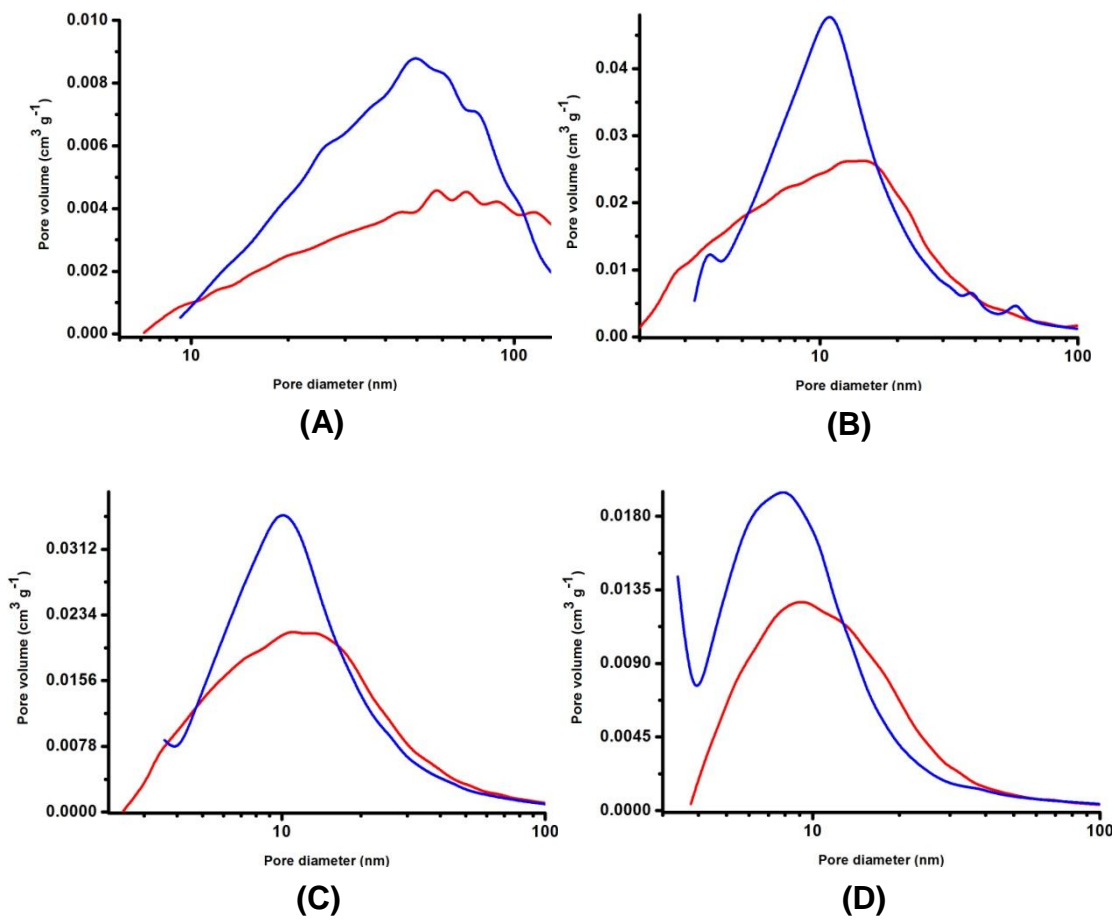
Fig.2.5: dv/dD pore size distribution (cm^3/g) of the expanded alginic acid produced at certain retrogradation time including (A) retrogradation for 0.5 day, (B) retrogradation for 1 day, (C) retrogradation for 2 days and (D) retrogradation for 5 days at 5 ^{o}C. Red line colour presents adsorption pore size distribution, blue line colour presents desorption pore size distribution.

82

On the other hand retrograding it for more than a day would cause the collapse of the porous system, could be, due to long contact with water left in the pores of the alginic acid gel. Therefore, retrogradation for one day at 5 ^{o}C was chosen as the best condition to retrograde the gel. This is less expensive and less time consuming as well as more practically realistic for manufacture.

2.3.3 Investigating the influence of solvents manure on the textural properties of the expanded materials produced

Solvent exchanging of the alginic acid retrograded (for one day at 5 ^{o}C) is a crucial stage in the expansion process. Throughout previous investigations in the Green Chemistry Centre it was found that washing the retrograded gel with ethanol solution six times was an important process to remove the remaining water in the retrograded porous networking gel.[248] Therefore to investigate this further, three more organic solvents including methanol, hexane and acetone were employed instead of ethanol. For consistency the other parameters used in expanding alginic acid including gelation process, solvent exchanging and drying steps were the same for all samples generated:[i) gelation step (100 ^{o}C, 160 minutes); ii) solvent exchanging conducted three times with ethanol. Three times ethanol followed by again three other times ethanol. Three times ethanol followed by three times methanol. Three times ethanol followed by three times hexane. Three times ethanol following by three times acetone and iii) drying in a vacuum oven. The material washed using acetone was either vacuum oven dried or scCO$_2$ dried.

Textural properties (S$_{BET}$, pore volume and pore diameter) as well as conditions of experiments are shown in Table 2.4 and Figure 2.6. It can be observed from these data that expanded materials with the promising textural properties was produced by washing with ethanol then acetone followed by vacuum oven drying.

It was noticed that among the samples (Sf1, Sf2, Sf3, Sf4, Sf5), Sf5 showed the optimum textural properties in which pore size is around 1 cm^3/g. Therefore, the same procedure of solvent exchange of sample (Sf5) was carried out, but scCO$_2$ dried was applied to produce the sample (Sf6). It was found that the sample generated by solvent exchange with ethanol plus acetone followed by vacuum oven or scCO$_2$ techniques gave the greatest pore volume. Obtaining the optimum results of Sf5 may be due to the systematic gradual decrease of

using low surface tension solvents. Ethanol surface tension is lower than water and is miscible with water; on the other hand, acetone has a close surface tension to ethanol, but lower surface tension than of water as well as being miscible with both of them which helped reduce water in the pores during the solvent exchange process.[249] Also acetone has the lowest boiling point[250] could be then evaporated with no resistance in the pores of the alginic acid precipitate in vacuum oven. Therefore washing the gel with ethanol and then acetone provided better pore volume.

Hexane did not give a good pore volume and this may be due to the immiscible nature of hexane[251] with the remaining water left in the pores. In case of applying ethanol and then methanol (Sf2), the methanol is miscible with ethanol and water, but it has a higher boiling point than of acetone.[250] Also hexane is a cancer suspect compound which should not be applied for the sake of health and environment.[252-254] Acetone might be safer than hexane because it is polar.

Sf6 was solvent exchanged with ethanol and then acetone as was done for Sf5, but the technique of drying used was in $scCO_2$. It was noticed that supercritical drying had an effect on the textural properties of the expanded material. The pore size and diameter of product is almost twice greater as Sf5.

Vacuum oven drying for samples reduced organic solvent, but allowing the air to evacuate too quickly which could crack and collapse some pores yielding a poor quality expanded alginic acid.

In contrast, $scCO_2$ drying technique is a gradual technique in which the pressure in increased from the atmospheric pressure to the highest level and CO_2 diffuses through the system constantly for few hours at 50 $^{\circ}$C pushing the solvents in the pores of the expanded alginic acid precipitate to outside of the pores. This process of drying the alginic acid precipitate could preserve the porous alginic acid networking system since CO_2 has higher diffusivity, zero surface tension and lower solvent residue and is chemically stable.[255, 256] Therefore, $scCO_2$ can ensure the preservation of the porous nature of the final materials.

Table.2.4: Porosity measurement for expanded alginic acid in experiment six in which different organic solvents was used to wash the retrograded alginic acid gel

		Gn Cn		Rt Cn (T °C/time h)	porosity measurement						Meso-porosity %
sn	CAa in DW	T (°C)	Time (min)		S_{BET} (m²/g)	Pore volume (cm³/g)		Pore diameter (nm)			
						Apv	Dpv	Apd	Dpd		
Sf1	5%	100	160	+5/24	93	0.22	0.23	11.2	7.8		23
Sf2	5%	100	160	+5/24	130	0.48	0.5	15	12		36
Sf3	5%	100	160	+5/24	79	0.31	0.34	16.5	13.3		31
Sf4	5%	100	160	+5/24	111	0.56	0.54	20.7	16		49
Sf5	**5%**	**100**	**160**	**+5/24**	**235**	**0.98**	**1.02**	**16.5**	**15.2**		**82**
Sf6	**5%**	**100**	**160**	**+5/24**	**299**	**1.99**	**2.01**	**33**	**27**		**95**

sn: Sample name, CAa in DW: Concentration of alginic acid in distilled water, GnCn: Gelatinisation condition, Rt Cn: Retrogradation condition (T °C/time in hour), S_{BET}: Surface area BET, Apv: Adsorption pore volume, Dpv: Desorption pore volume, Apd: Adsorption pore diameter, Dpd: Desorption pore diameter.
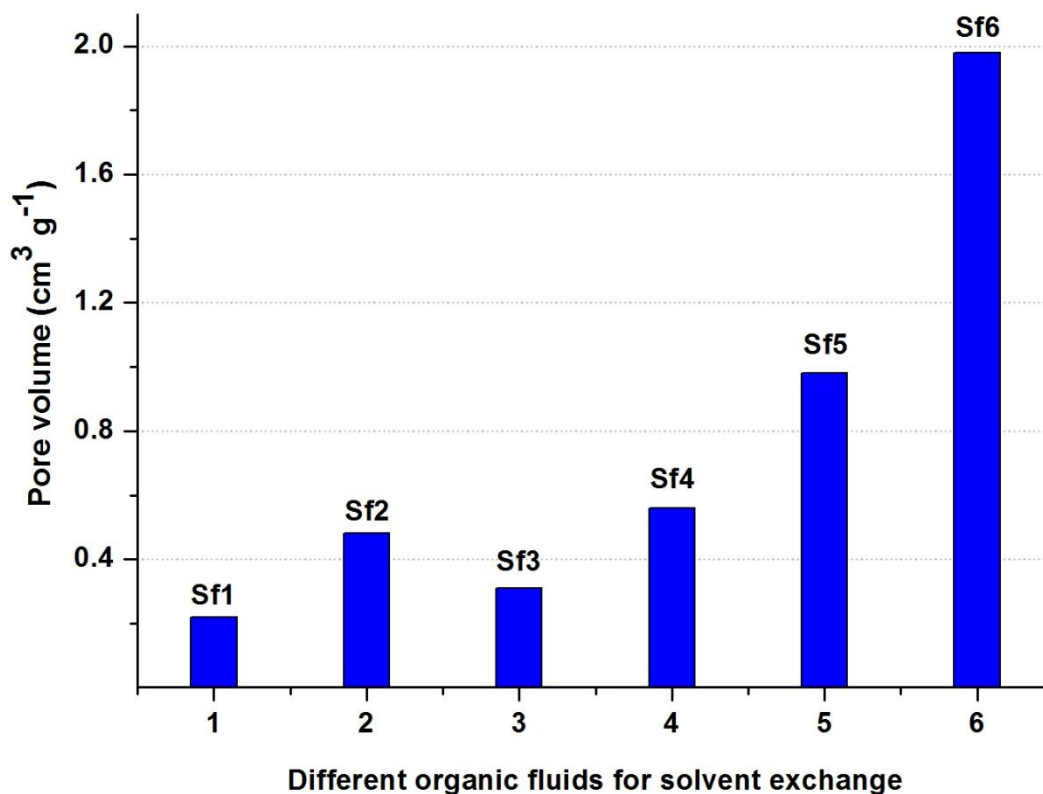
Fig.2.6: Washing the alginic acid retrograded with different organic solvents, thereafter, it was dried either in vacuum oven or scCO$_2$.
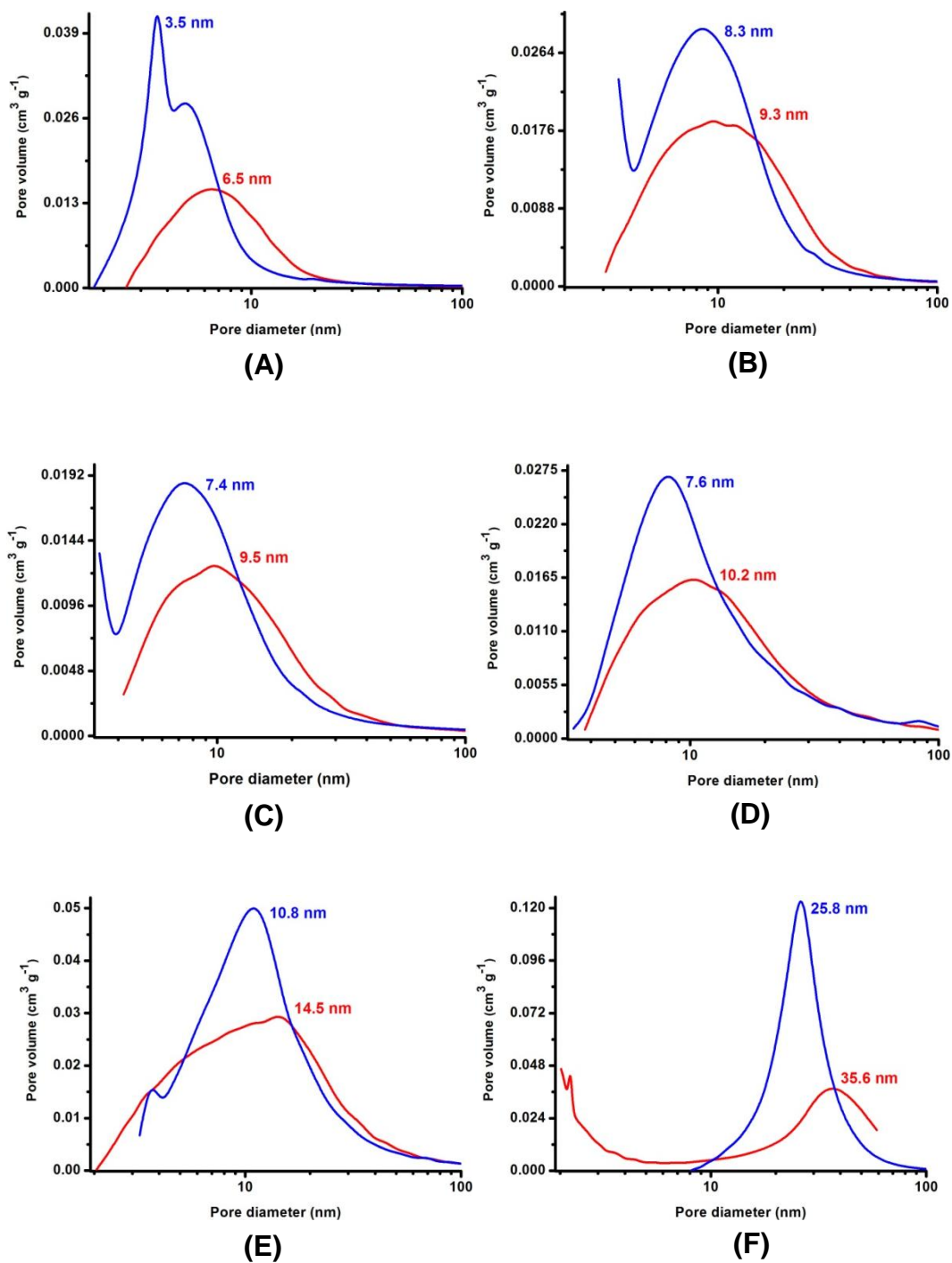
Fig.2.7: dv/dD pore size distribution (cm^3/g) of the expanded alginic acid produced by applying the conditions placed in Table 2.4 where the retrograded gel was (A) 3 times washed with ethanol following by vacuum oven dried, (B) 3 times washed with ethanol plus 3 times more again ethanol following by vacuum oven dried, (C) 3 times with ethanol plus 3 times with methanol following by vacuum oven dried, (D) 3 times with ethanol plus 3 times with hexane following by vacuum oven dried, (E) 3 times ethanol plus 3 times with acetone following by vacuum oven dried, (F) 3 times with ethanol plus 3 times with acetone following by scCO$_2$ dried. Red line colour presents adsorption pore size distribution, blue line colour presents desorption pore size distribution.

86

Table.2.5: Performing solvent exchange of the retrograged gel with ethanol following by either methanol, hexane or acetone generated different pore sizes

I: Pore volume of the vacuum oven dried EAA products
(1) Sf1: 3X ethanol, Pore volume: 0.25 cm^3 g^{-1}
(2) Sf2: 3X ethanol+3X ethanol, Pore volume: 0.35 cm^3 g^{-1}
(3) Sf3: 3X ethanol+3X methanol, Pore volume: 0.29 cm^3 g^{-1}
(4) Sf4: 3X ethanol+3X hexane, Pore volume: 0.6 cm^3 g^{-1}
(5) Sf5: 3X ethanol+3X acetone, Pore volume: 1 cm^3 g^{-1}
II: Pore volume of the scCO$_2$ dried EAA product
(6) Sf6: 3X ethanol+3X acetone, Pore volume: 1.92 cm^3 g^{-1}

3X: means three individual wash of the retrograded gel with the organic fluids employed sized the same amount of water had been employed in gelation of native alginic acid.

2.3.4 Investigating the level of water in the pores of the gel washed

The aim of this section is to show the level of water dropped on washing the retrograded gel with ethanol and then acetone followed by either vacuum oven or scCO$_2$ drying.

Water reduction to the minimum level in the porous networking system is of importance in order to ensure the water level is the lowest level in the pores before drying the gel to protect the pores from collapsing.

At temperature between room temperature and 100 ^{o}C there is a mass loss due to the organics fluids (ethanol and acetone) and water. Figure 2.8 shows that the number of washes reduces the level of water in the pores. The line number one gives the level of water present in the material directly after retrogradation finished (24 hours at 5 ^{o}C). Lines 2 to 4 show the gel after washing with ethanol 1-3 times. Lines 5 to 7show the gel after further washing with acetone 1-3 times.

Line number 8 is the expanded alginic acid after complete solvent exchange with ethanol and then acetone following by vacuum oven drying. Line number 9 is the expanded alginic acid after solvent exchange with ethanol and then acetone following by supercritical CO$_2$ drying.
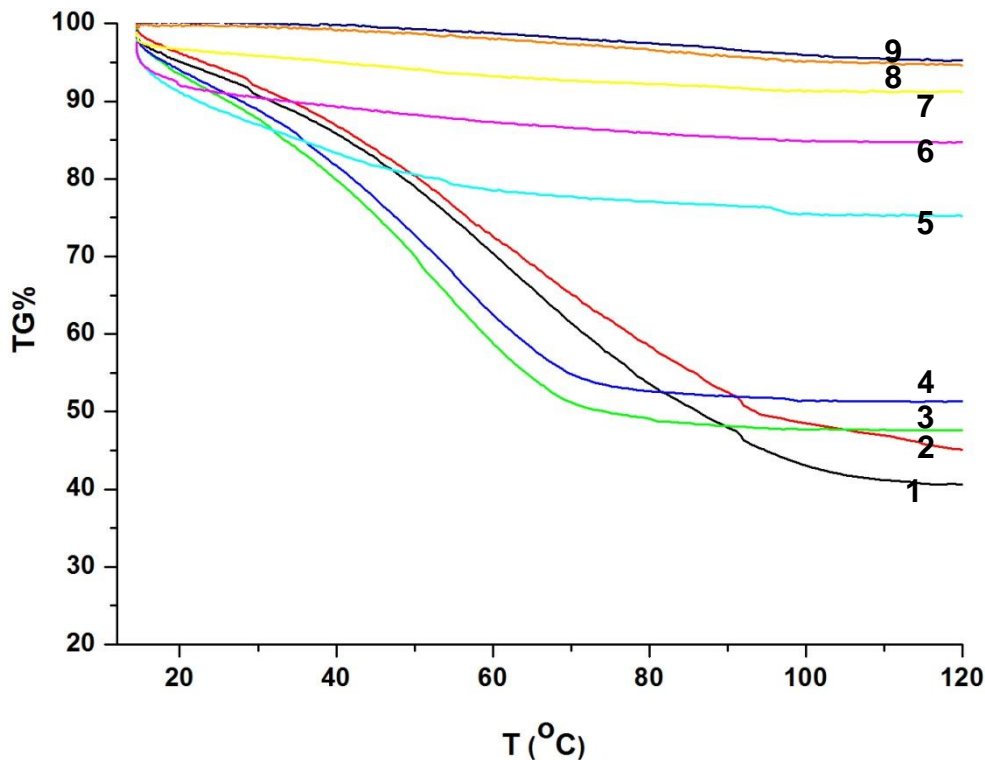
Fig.2.8: Plot of TG versus temperature increased for the retrograded alginic acid washed with ethanol and acetone which dropped the level of water in the in the porous alginic gel.

Plot 2.8 shows that when the temperature reached 120 ^{o}C all organic fluids and the small level of water left in the pores had been removed. Interestingly, for samples washed with ethanol and then acetone, all solvents (and water) appeared to have been removed at a temperature as low as 60 ^{o}C. This could be as a result of massive increase in the concentration of organic solvents which cause greatly decrease the surface tension of the final solvents mixture left in the pores of the expanded alginic acid.[257]

2.3.5 Reproducibility of generating mesoporous precursor

The conditions of the stages of expanding alginic acid: i) gelation at 100 ^{o}C for 160 min., ii) retrogradation for 24 hours at 5 ^{o}C, iii) solvent exchange with ethanol three times and then acetone three times followed either by vacuum oven or scCO$_2$ drying was repeated successfully. This current method produced a high mesoporous precursor with excellent texture property.

Fortunately, this procedure of expansion process to generate a mesoporous material has been reproducible. Repeatability of expanded alginic acid either vacuum oven dried or scCO$_2$ dried is excellent as many time as is repeated.

Throughout repeatition it was noticed that the percentage of difference in surface area was 4%, pore volume 3%, average pore diameter 6% as well as change of mesoporosity% was 4% for expanded alginic acid vacuum oven dried products. It was also found that the percentage of change in surface area was 1%, pore volume 2% , average pore diameter 2.5% as well as the change of mesoporosity% is approximately 2% for expanded alginic acid scCO$_2$ dried products.

In addition, further work will be done in next chapter (chapter three) in which this mesoporous precursor (expanded alginic acid scCO$_2$ dried) will be employed to generate mesoporous Algibons. Porosity analysis (Figures 2.9 and 2.10) presents that the expanded alginic acid generated was predominantly mesoporous precursor. The isotherm plots for the products are isotherm type four[258] for the expanded alginic acid either vacuum oven dried or scCO$_2$ dried. This means the majority of the product is mesoporous. Figure 2.10 which shows the pore diameter against pore volume (dv/dD) indicates the material has a large pore, but the expanded alginic acid scCO$_2$ dried material has a larger pore which is almost twice greater than the pore of the material produced by vacuum oven drying (see Table.2.6).

Table.2.6 : Porosity analysis results for the expanded alginic acid achieved by the current method developed for generating mesoporous alginic acid

New expanded alginic acid generated	S_{BET} (m^2/g)	Pore volume (cm^3/g)$_{BJH}$	Maximum pore diameter (nm)$_{Ads}$	Maximum pore diameter (nm)$_{des}$	Meso-prosity %	Micro-porosity %
Expanded alginic acid vacuum oven dried (A1)	105	1	12	8	85	7%
Expanded alginic acid scCO$_2$ dried (A2)	183	2	21	14	96	3%

A1: Alginic acid precipitate, after it was gelated at 100 ^{o}C for 160 minutes and retrograded for 24 hours at 5 ^{o}C, was solvent exchanged with three times ethanol and three times acetone followed by vacuum oven drying.

A2: Alginic acid precipitate, after it was gelated at 100 ^{o}C for 160 minutes and retrograded for 24 hours at 5 ^{o}C, thereafter, it was solvent exchanged three times with ethanol and three times with acetone respectively following by scCO$_2$ drying.
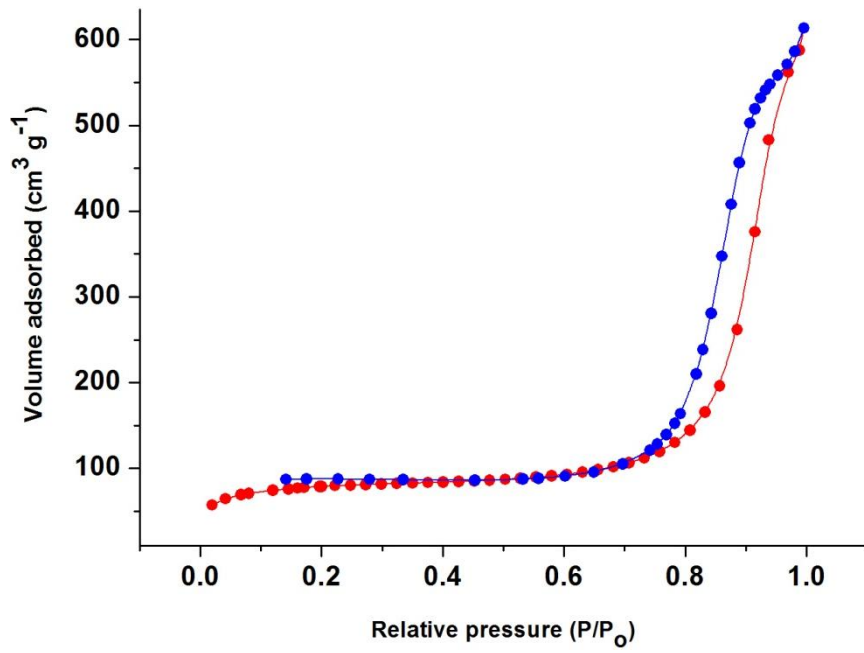
(A) A1
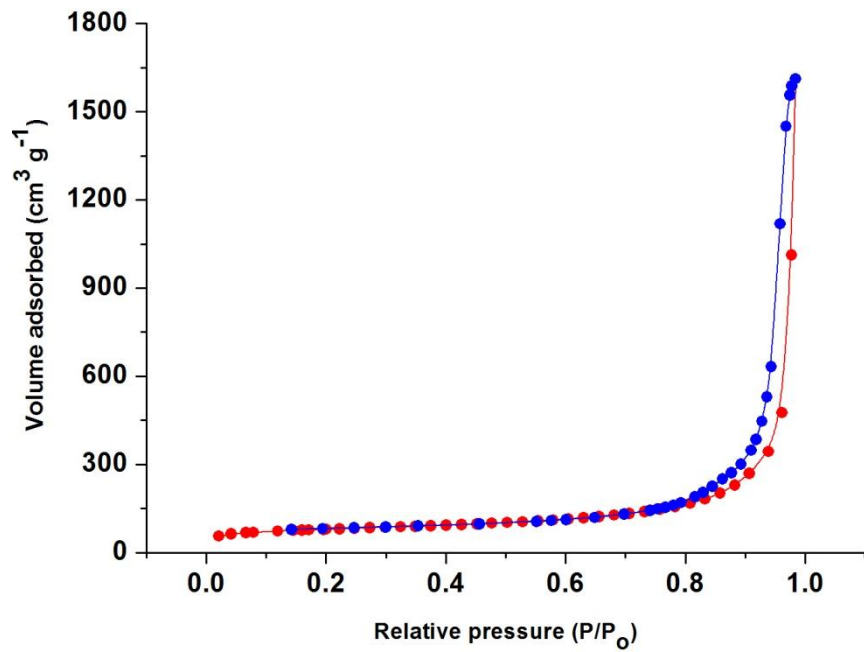
(B) A2

Fig.2.9: Isotherm plot for (A) A1: expanded alginic acid vacuum oven dried and (B) A2: expanded alginic acid $scCO_2$ dried achieved from the current method, the red line is adsorption isotherm and the blue line is desorption isotherm.
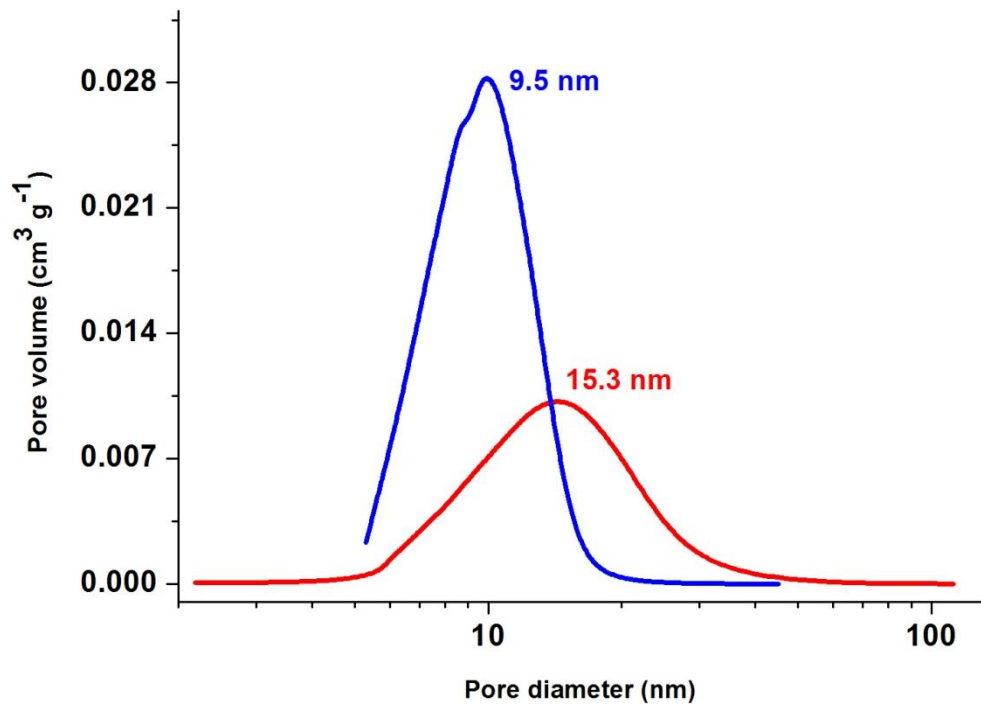
(A) A1
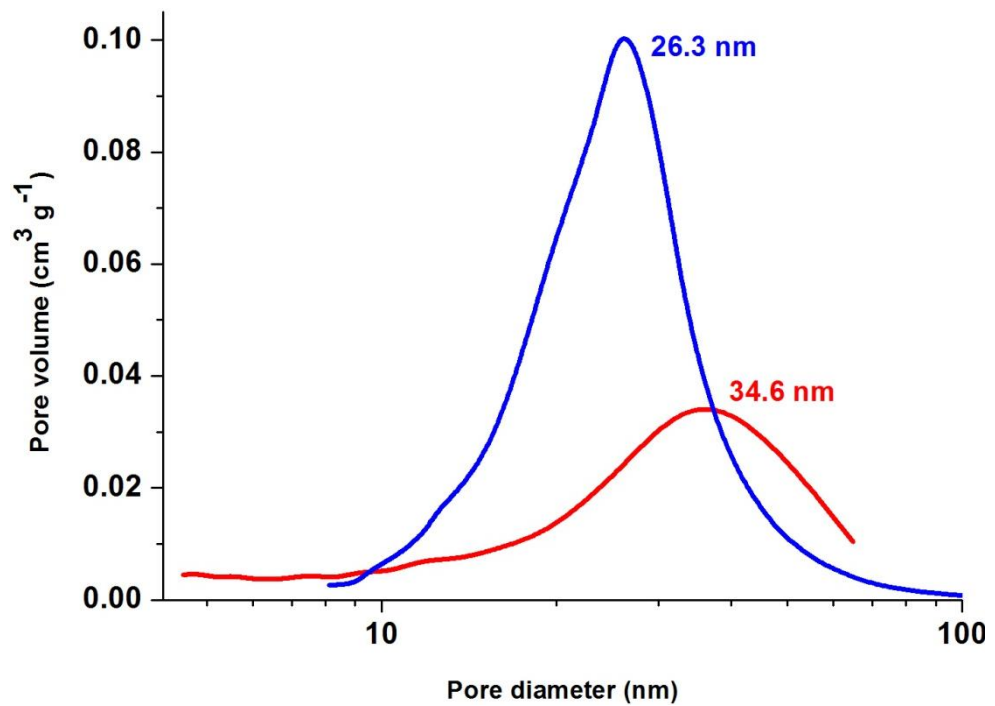
(B) A2

Fig.2.10: dV/dD pore volume (cm^3/g) against pore diameter (nm) for (A) A1: expanded alginic acid vacuum oven dried and (B) A2: expanded alginic acid $scCO_2$ dried from the current method. Red line colour presents adsorption pore size distribution (dV/dD), blue line colour presents desorption pore size distribution (dV/dD) .

Based on the results repeated in this chapter and the two plots of pore volume distribution dV/dD versus pore diameter of the expanded alginic acid generated (see Fig.2.10), it is assumed that the pores shape are a bottle flask like.[243-245] The adsorption pore size distribution represents the bottom of the flask which is greater in size compared to the desorption pore size distribution which presents the neck of the pore.

(A) A1   (B) A2
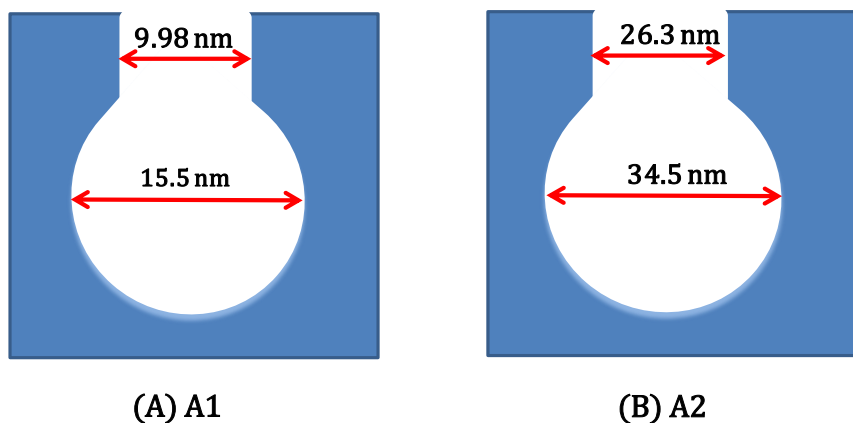
Fig.2.11: Pore shape of expanded alginic acid (A) A1: vacuum oven dried and (B) A2: scCO$_2$ dried.

2.4 Conclusion

The stages of the expansion process for alginic acid were investigated. Gelation of the native alginic acid was done at 100 $^{\circ}$C for 160 minutes and retrogradation of the gel was taken place in fridge at 5 $^{\circ}$C for 24 hours. Solvent exchange of the retrograded alginic acid was carried out by washing it three times with ethanol plus three times with acetone followed either by vacuum or scCO$_2$ drying. Materials either vacum oven dried (A1) or scCO$_2$ dried followed isotherm type four indicating that the materials produced were predominately mesoporous. The shape of pores in mesoporous region is the bottle flask like.

It was noticed the current method of preparing expanded alginic acid gives a very promising result of a pore volume ca 1 cm^3/g (for vacuum oven dried) and ca 2 cm^3/g (for scCO$_2$ dried). Fortunately, this procedure of expansion process to generate a mesoporous material has been reproducible. Repeatability of production of expanded materials is excellent as many time as is repeated.

In the next chapter this mesoporous alginic acid precursor generated (scCO$_2$ dried product known as A2) will be employed to produce Algibons at certain

temperatures to provide different textural properties of the carbonised mesoporous materials.

```
┌────────────────────┐     ┌────────────────────┐     ┌────────────────────┐
│ 200 g alginic acid │     │ Retrograde at 5 °C │     │ Add 4 L ethanol and│
│ in 4 L D.W  stir at│ ──► │ for 24 h  in fridge│ ──► │ stir: 1st wash (1 h)│
│ 100 °C for 160 min.│     │                    │     │ 2nd wash (30 min.) │
└────────────────────┘     └────────────────────┘     │ 3rd wash (30 min.) │
                                                       └────────────────────┘
                                              3 times           │
                                                                ▼
                                                       ┌────────────────────┐
                                                       │  Filtration using  │
                                                       │    sinter filter   │
                                                       └────────────────────┘
┌────────────────────┐                                          │
│ Test the textural  │                                          ▼
│   property of      │                                 ┌────────────────────┐
│ mesoporous product │                                 │  Add 4 L acetone   │
│ applying N2 sorption│                                │  and stir for 30 min.│
│     analysis       │                                 └────────────────────┘
└────────────────────┘                         3 times          │
         ▲                                                       ▼
┌────────────────────┐  ┌────────────────────┐  ┌────────────────────┐
│ Mesoporous alginic │  │ Dry the precipitate│  │  Filtration using  │
│       acid         │◄─│ in scCO2 at 50 °C/ │◄─│    sinter filter   │
│    generated       │  │ 100 bar/3h,        │  └────────────────────┘
└────────────────────┘  │ depressurise       │
                        │ slowly overnight   │
                        └────────────────────┘
```

Fig.2.12: Practical steps of the current method developed to generate mesoporous alginic acid in the laboratory of Green Chemistry Centre of Excellence at The University of York, UK.

CHAPTER THREE

Generating and Characterising of The Algibons Derived from The Mesoporous Alginic Acid Precursor Produced

3.1 Introduction

This section deals with the preparation of Algibon formed from the mesoporous alginic acid precursor (A2) produced in chapter two. Thermal hydrolysis of the mesoporous precursor at different carbonisation temperatures can generate polysaccharide carbonaceous mesoporous materials with different textural properties and surface functionalities.[259] This family of mesoporous carbonaceous materials obtained are called Algibons.[260] The mesoporous precursor material produced can be either carbonised in small scale (200 mg) in Netzsch under nitrogen gas or in large scale (200 g) in vacuum furnace.

Programming and controlling a carbonisation process to certain temperatures can specify the surface functionality of the Algibons produced. Steps of preparing Algibons from the mesoporous precursor require shorter time and is simpler. Therefore technology of generating Algibons has been recommended.

The Algibons generated were characterised using techniques such as nitrogen adsorption analysis (porosimetry) in particular to find out more about porosity structure, Diffuse Reflectance Infrared Fourier Transform (DRIFT IR) and Solid state NMR (^{13}C cross polarization magic angle spinning NMR) to learn the surface functionalities of the Algibons. CHN Elemental analysis was done to determine the carbon and hydrogen percent. Ash content test was conducted to determine the amount of carbon residue exist in each type of Algibon when they were burned in the presence of 50% Oxygen and 50% Nitrogen. Our goal was to develop a method of producing the less expensive materials with excellent pore volume which can then be applied in trapping organic bulky dyes and might be useful in metals adsorption technology.

3.2 Experimental section

Algibon was generated from thermal carbonisation of the mesoporous alginic acid precursor (A2) achieved in chapter two. 200 mg of the expanded precursor was employed into the Netzsch ceramic cup pan. The Carbonisation temperature was programmed and controlled from room temperature to the desired temperature required to produce a certain type of Algibon.

For example, Algibon300 (A300) was produced by programming (0.2 to 0.5 ^{o}C per minute) and controlling the carbonisation temperature to 300 ^{o}C. Then A450, A600 and A800 were respectively prepared by programming and

controlling their carbonisation temperatures to the required top temperature. Ultimately, the different texture Algibons received were tested applying numbers of techniques to characterise their pore structure and surface functionalities.

3.3 Results and discussion

3.3.1 Detecting thermal decomposition of the mesoporous alginic acid

Simultaneous thermal analysis (STA) was applied to learn how mass loss varied with temperature increased. This thermolysis process was carried out between room temperature and 625 ^{o}C. This test was an important tool which clearly revealed information where the main decomposition which took place when the mesoporous precursor was carbonised to the required temperature. It could produce information help us to propose a proper programming and controlling of carbonisation temperature which would preserve the mesoporous structure of the Algibon materials. STA demonstrates the large mass loss from expanded alginic acid between 170 and 300 ^{o}C. This could be a consequence of losing functional groups (carboxylic and hydroxyl groups rich in polysaccharide alginic acid).[261,262] Before 100 ^{o}C traces were lost due to either remaining water or moisture absorbed by the expanded alginic acid. Both TG and DSC confirm the greater mass loss occurs over 170 ^{o}C (Figure 3.1 A and B).
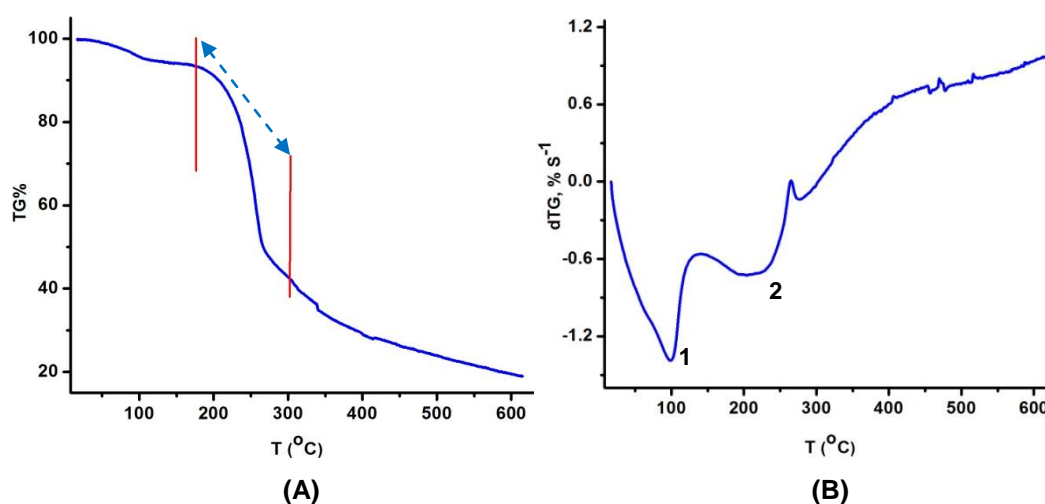
Fig.3.1: Plots of (A) thermal gravimeteric (TG) against temperature (^{o}C) increased and (B) dTG versus temperature (^{o}C) increased for expanded alginic acid scCO$_2$ dried (A2).

Interestingly, further investigation was done to learn what was the reason for that massive mass loss between that temperature range of thermal hydrolysing

96

of the expanded alginic acid in STA. Thermal gravimetric infrared spectroscopy (TG IR) was used.

3.3.2 Conducting TG IR throughout carbonisation of the mesoporous precursor

Thermal gravimetric infrared spectroscopy (TG IR) was conducted, based on the Figure 3.1 in which a massive mass loss was observed, especially, between 170 to 300 ^oC.
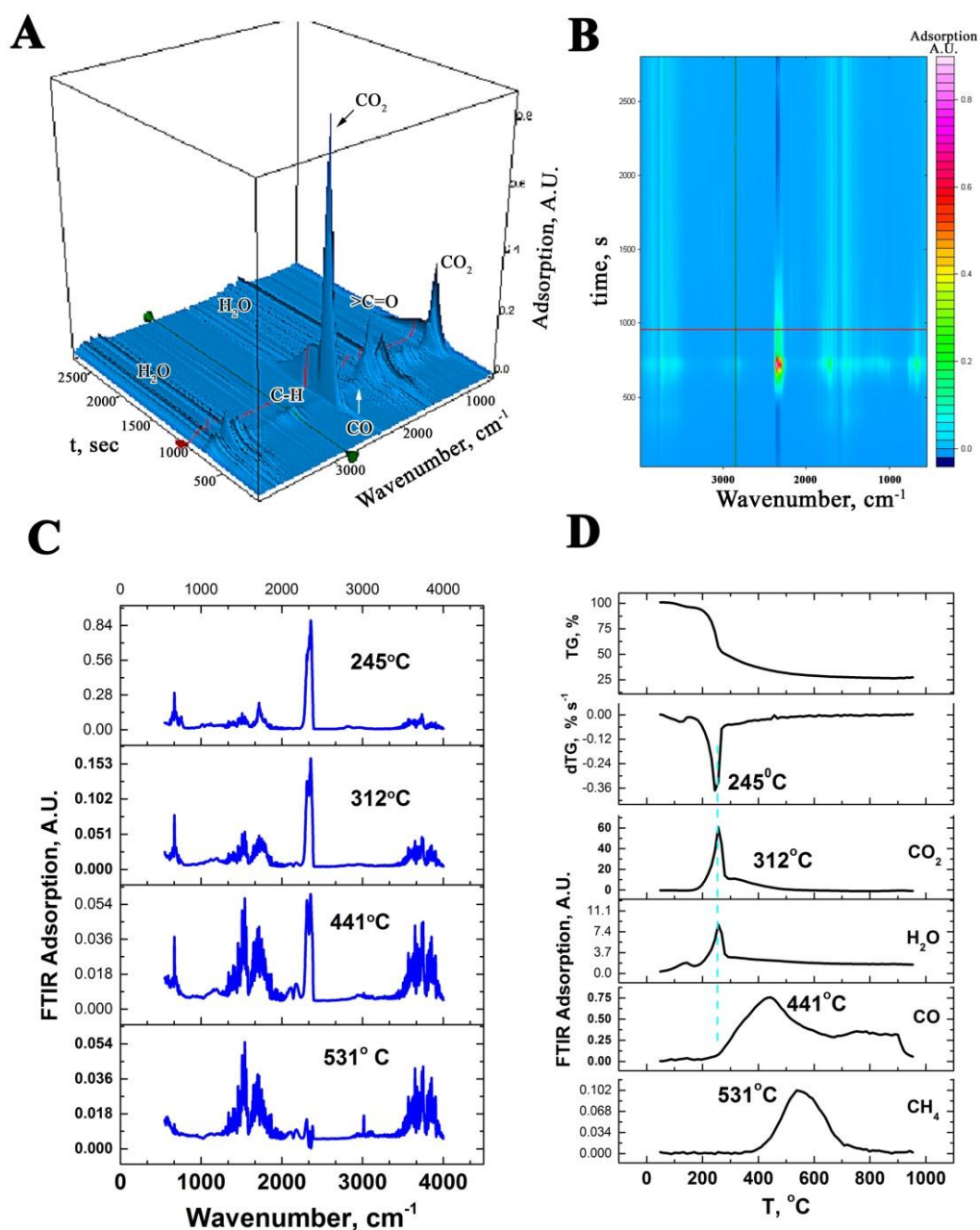
Fig.3.2: TG IR spectrum of expanded alginic acid (A2) thermally hydrolysed at temperature rate (20 ^oC/min.) up to 900 ^oC under N_2. A: Intensity of three dimensional band spectrum of the components released throughout the carbonisation of expanded alginic acid, B: Two dimentional band spectrum, C: FT IR spectrum of the components observed as the carbonisation temperature increased. D: Trace spectra of the components released during the pyrolysis process.

Aim of TG IR experiment in this section was to identify the main components released between room temperature and 900 $^\circ$C throughout the thermal pyrolysis of the expanded alginic acid (A2).

The TG IR spectrum reveals that the majority of the mass lost is water and carbon dioxide (Fig.3.2). Over 170 $^\circ$C the material underwent dehydration and after that decarboxylation; then thermal gravimetric infra red continuously measured up to the maximum temperature. TG plot (Fig.3.3) shows the mass residue was approximately a fifth of the expanded alginic acid precursor employed for TG IR.

In Figure 3.2 (A) the intensity of the spectrum at a temperature around 200 $^\circ$C is due to CO_2 released at (2350 cm^{-1} refers to O=C=O asymmetric bond stretching and 680 cm^{-1} is O=C=O bending bond) and 1730 cm^{-1} is C=O asymmetric bond stretching belongs to CO gas.[263, 264]

Water vapour is noticed at 1550 cm^{-1} is H-O-H scissor bending, 3630 cm^{-1} is H-O-H symmetric bond stretching and 3760 cm^{-1} is H-O-H asymmetric bond stretching.[265,266] When temperature increased to 270 $^\circ$C and over the same spectrum was observed but at lower intensity because the majority of the mass lost had been completed.
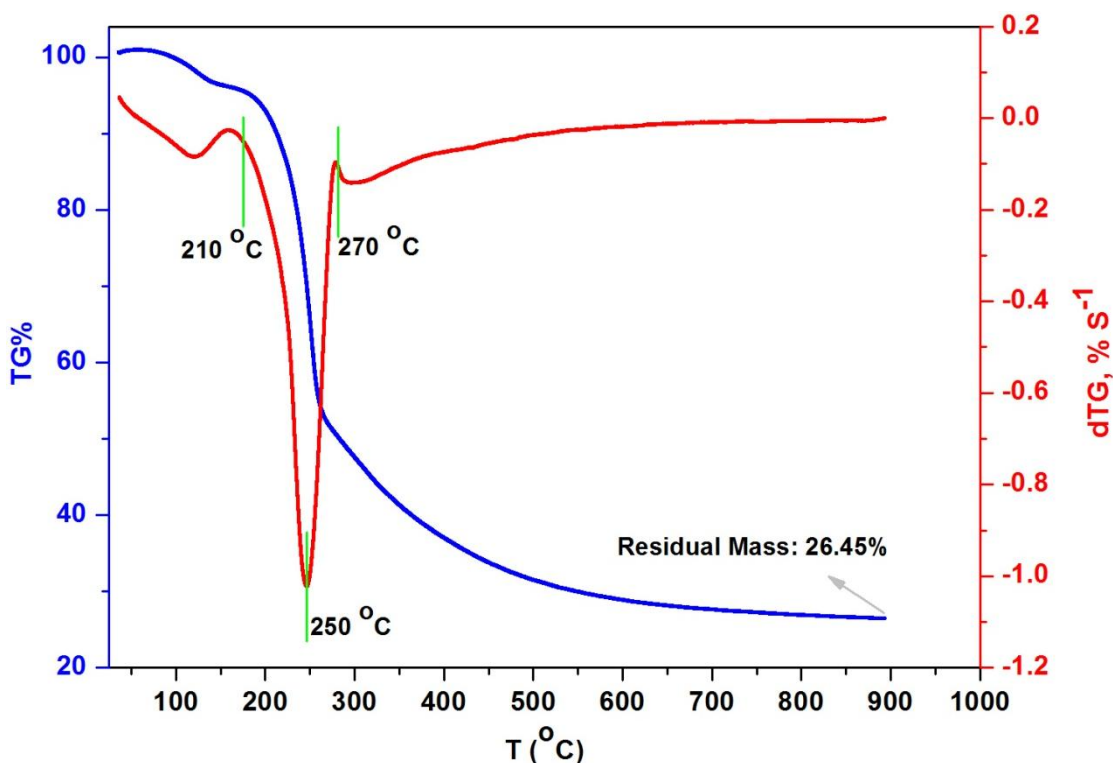
Fig.3.3: TG and dTG plots for thermally hydrolysed expanded alginic acid (A2) at (20 $^\circ$C/min.) up to 900 $^\circ$C combined with IR spectroscopy.
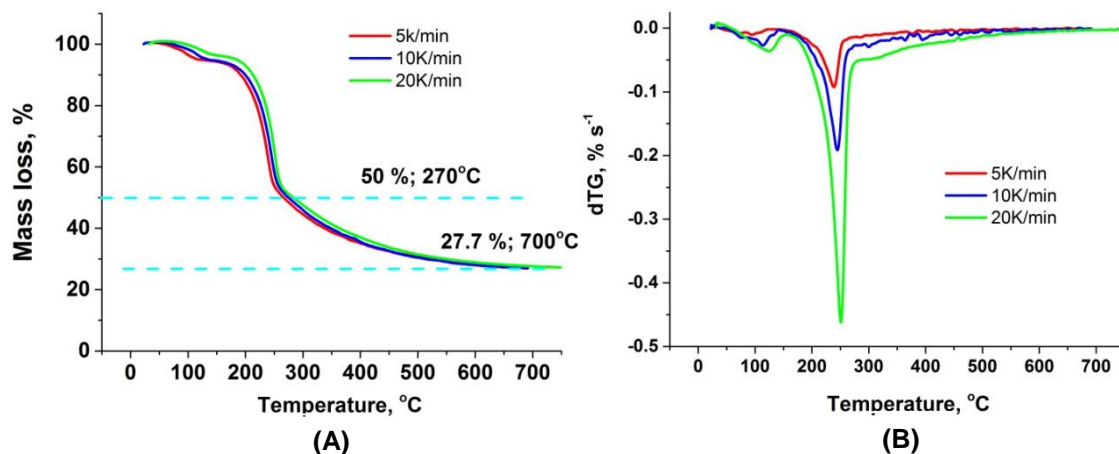
Fig.3.4: TG and dTG plots for thermally hydrolysed expanded alginic acid (A2) at various rate of carbonisation temperatures applied (5, 10 and 20 ^{o}C/min) up to 700 ^{o}C combined with IR spectroscopy. A: Mass loss (TG)% versus temperature, B: dTG% versus temperature.

Figure 3.4 gives information on pyrolysis of expanded alginic acid precursor at different rate of carbonisation temperatures including 5, 10 and 20 ^{o}C per minute. TG plot (A) in Figure 3.4 implies that different rate of temperature programme applied did not change the percentage of mass loss observed. The main mass loss, which is between 200 to 300 ^{o}C, is observed for each rate of heating indicating expanded alginic acid has the same response to the dissimilar rates of carbonisation. It implies the carbonisation process is reproducible. On the other hand dTG plot (B) in Figure 3.4 presents versatile response to the different carbonisation temperatures used.
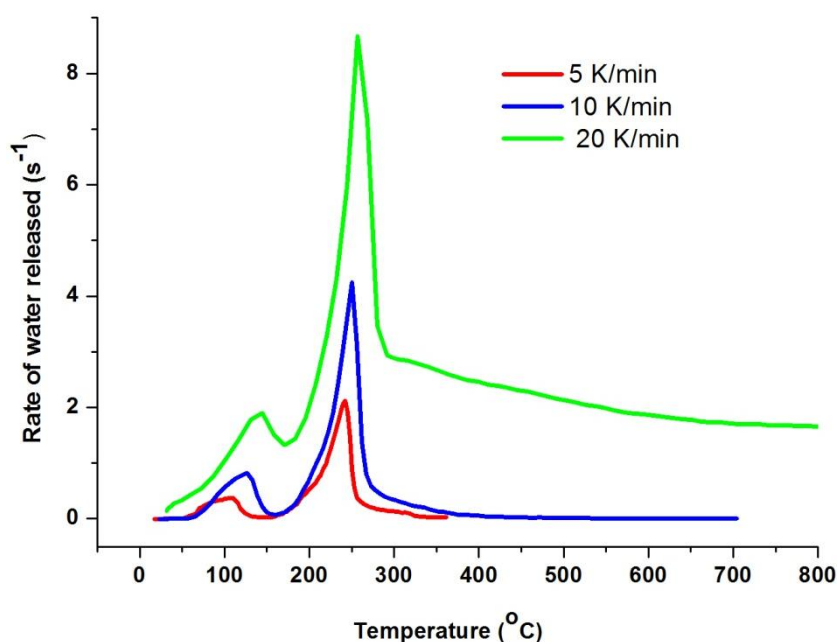
Fig.3.5: Rate of water released throughout the dehydration of the expanded alginic acid as it was carbonised to 700 ^{o}C at various rate of temperatures (5, 10 and 20 ^{o}C/min).

This indicates that the lowest pyrolysis heating rate applied (5 ^{o}C/min) could gradually dehydrate the precursor and convert it to the top wanted temperature. This can be noticed in Figure 3.5. This diagram demonstrates the consequence of high rate carbonisation temperature on the speed of water released from the expanded precursor during the process. It proposes that within a shorter range of time a greater rate of water seems to have been liberated into the system.

In addition, TG and dTG plots of thermal pyrolysis of native and expanded alginic acid are drawn in Figure 3.6. These two materials were carbonised at the same conditions up to 800 ^{o}C at temperature rate 10 ^{o}C/min. under N_2 gas. This was carried out to examine and compare the range of mass loss and decomposition in both compounds.
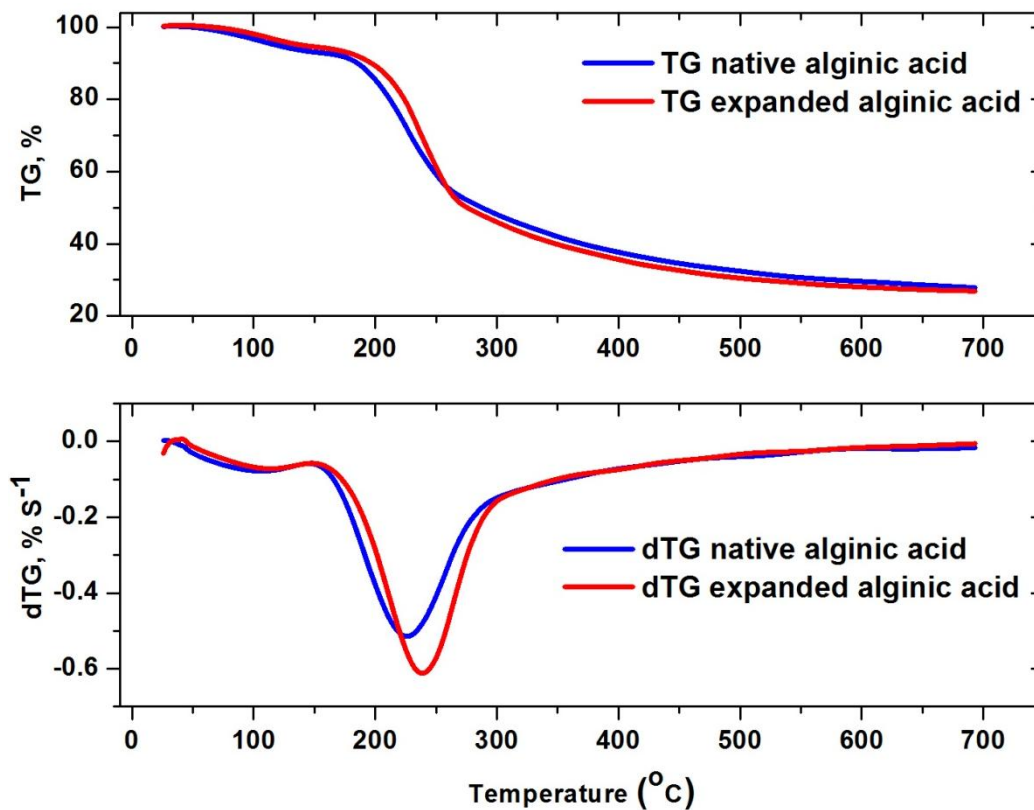
Fig.3.6: Comparing TG and dTG plots of native and expanded alginic acid carbonised at temperature rate (10 ^{o}C/min.) up to 800 ^{o}C.

It is noticed that there is a small difference between both materials carbonised this is possibly due to the influence of expansion stages on the alginic acid biopolymer. The stages of expansion process, which consists of gelation at 100 ^{o}C/160 min., retrogradation at 5 ^{o}C/24 hours, solvent exchange with ethanol

followed by acetone and finally scCO$_2$ drying step, transformed some physical properties of this polysaccharide. Porosity as a key example can be illustrated in here. Unexpanded alginic acid is nonporous material, whereas the expanded alginic acid is completely a mesoporous material. This extreme difference in degree of mesoporosity between the expanded product and the native precursor may have been the cause of the changes in TG and dTG diagrams of the two materials.

3.3.3 Proposing a thermal pyrolysis temperature programme on mesoporous alginic acid to produce Algibon materials

A slow heating rate for carbonisation has been recognised to be important ever since Starbons materials have been found in Green Chemistry Centre. This necessity is paid attention in order to generate Algibons with high quality and texture properties which its porosity is preserved compared to the precursor.

Algibon was prepared from expanded alginic acid (A2) on a small scale. Expanded alginic acid was carbonised according to the temperature programme shown in Table 3.1. To obtain different texture properties of Algibon including Algibon 300, 450, 600 and 800. TG plots in Figure 3.7 shows that the mass lost up to 100 ^{o}C is around ca 2% this is may be because of some water vapor that expanded alginic acid adsorbed in the storage. Massive mass loss occurred around between 170 to 250 ^{o}C which is about 45% of the total mass. Finally, only about 37% of the yield remain in is Algibon300. So, this means a gram of expanded alginic acid could yield approximately 600 mg of Algibon300.
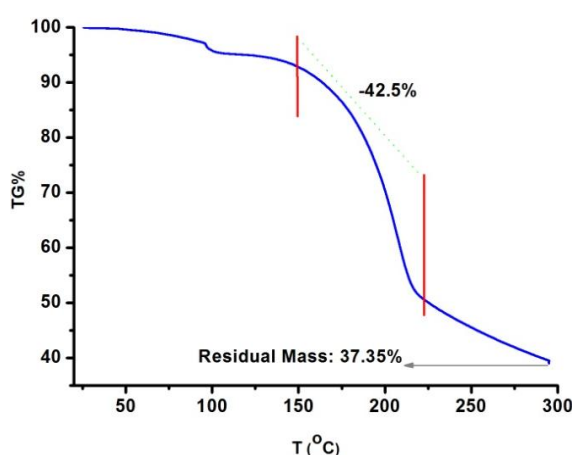
Fig.3.7: TG plot for A300 produced in Netzsch from carbonisation of the expanded alginic acid scCO$_2$ dried (A2).
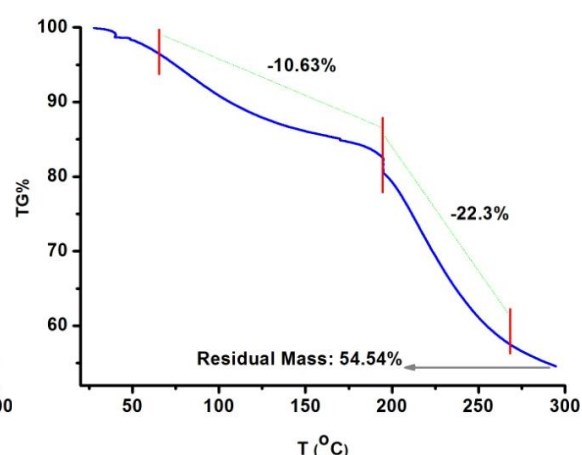
Fig.3.8: TG plot for A300 produced in Netzsch from carbonisation of the expanded alginic acid vacuum dried (A1).

Table.3.1: Temperature programme proposed to carbonise mesoporous alginic acid to certain temperatures to generate different textural properties of Algibons

Temperature $^{\circ}$C	Temperature rate $^{\circ}$C/min	Isotherm Time (min)	Emergency Temperature
Algibon300			
25			
100	1		
175	0.2	20	
250	0.2	40	
300	0.2	15	
320			Controlled
Algibon450			
25			
100	1		
175	0.2	20	
250	0.2	40	
300	0.2	15	
450	0.3		
470			Controlled
Algibon600			
25			
100	1		
175	0.2	20	
250	0.2	40	
300	0.2	15	
600	0.3		
620			Controlled
Algibon800			
25			
100	1		
175	0.2	20	
250	0.2	40	
300	0.2	15	
800	0.3		
820			Controlled
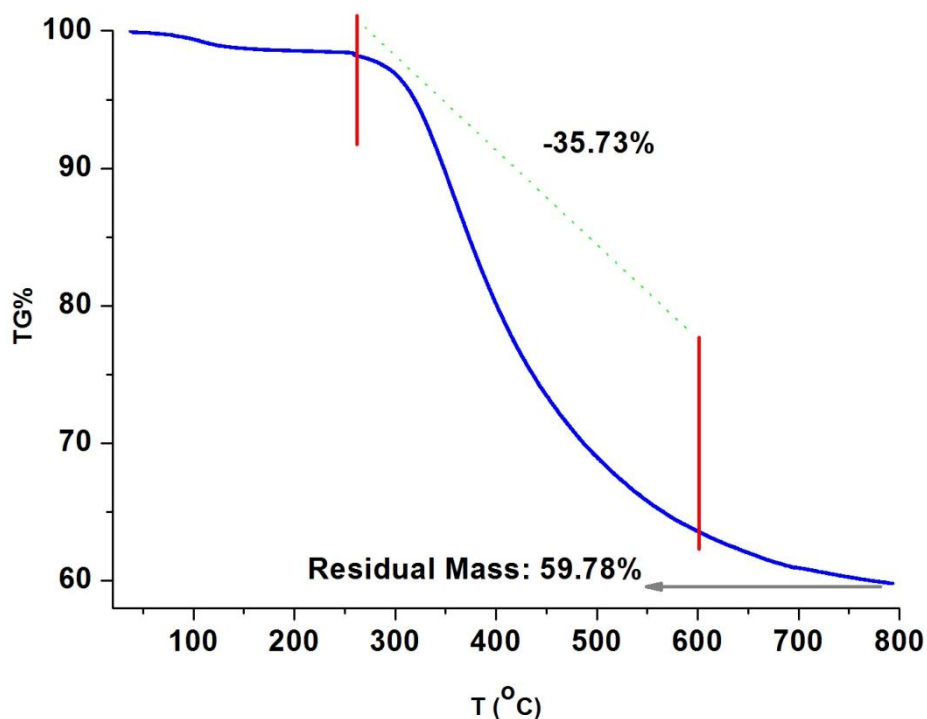
Fig.3.9: TG plot for Algibon800 produced from the Netzsch carbonised Algibon300 derived from expanded alginic acid scCO$_2$ dried (A2).

Figure 3.9 is the TG figure for the carbonisation of Algibon300 to Algibon800. It gives information that the mass lost between 300 and 600 ^{o}C is huge (36%). This means a gram of Algibon300 could yield 590 mg of Algibon800 or that a gram of expanded alginic acid could yield 200 mg Algibon800. Most of the mass lost occurs between 270 and 600 ^{o}C (about 36% of the total mass). Referring to Figure 3.8, in which expanded alginic acid vacuum oven dried (A1) employed, it is noticed that the percentage of mass lost is smaller and the amount of residual mass is about 55%, which is almost 15% more than in case of A300 produced from expanded alginic acid scCO$_2$ dried (A2) (see Figure 3.7). We can assume that the mesoporous alginic acid (A2) could be saturated with CO$_2$ gas from scCO$_2$ drying. As a result of the Netzsch carbonisation of A2 under N$_2$ gas, the immobilised CO$_2$ trapped in the pores of A2 would be removed from the pores and flowing N$_2$ gas throughout the thermal hydrolysis process preserved the pores from collapsing.[222]

3.3.4 Characterisation of the Algibon produced

A numbers of techniques were applied to characterise the textural properties of the Algibons generated including nitrogen sorption analysis, SEM (scanning

electron microscopy), Diffuse Reflectance Infrared Fourier Transform (DRIFT IR), Solid state NMR CHN test and Ash content.

3.3.4.1 Nitrogen sorption analysis

N_2-sorption analysis was conducted to determine the pores structure of the products. The pore volume of the Algibon yielded was drawn in Figure 3.10. From that figure and Table 3.2 conclude that the pore size distribution results are promising and the products are predominantly mesoporous. It is clear that the textural properties of the Algibons including A300, A450, A600 and A800 was better than of the previous ones obtained in Green Chemistry Centre of Excellence.[220] The pore volume of the Algibons was twice greater that of the Algibons produced in recent work. This may be due to the parameters applied in during carbonisation process helping to preserve its pores and avoid the collapsing.

Another interesting point is the previous work on generating Algibons was conducted in 2010 in the Green Chemistry Centre of Excellence, according to the data shown in table 3.3.[220] It is noticed that the current mesoporous alginic acid generated in chapter two can produce different textural properties of Algibons (see Table.3.2) in which their pore diameters are greater and pore volumes are twice larger than of the Algibons generated few years ago.
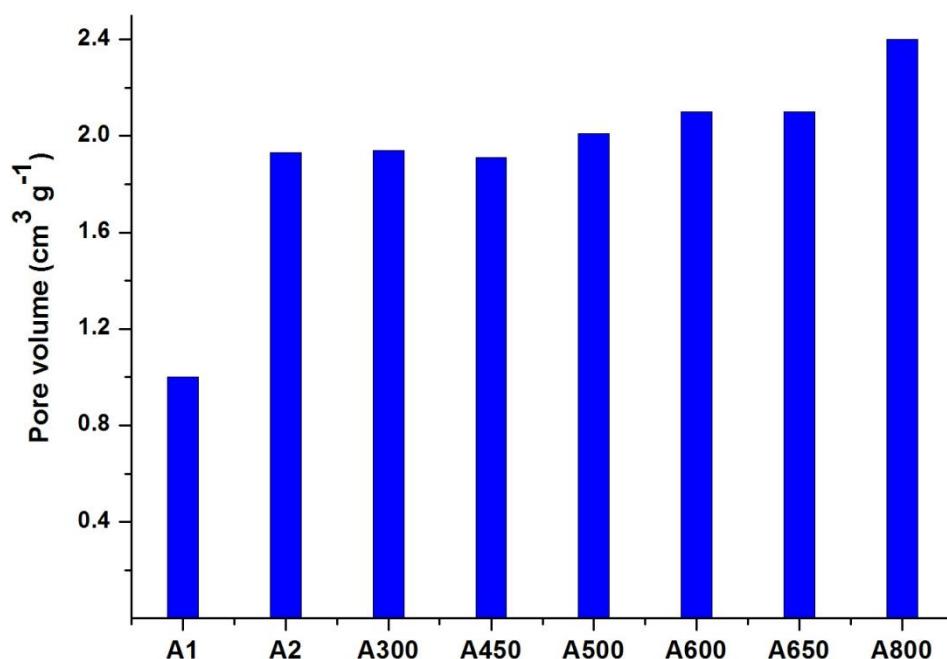
Fig.3.10: Pore volume of expanded alginic acid vacuum oven dried (A1) , expanded alginic acid super critical CO_2 dried (A2) and A300, A450, A500, A600, A650 and A800 derived from (A2) prepared in Netzsch.

Table.3.2: Pore size distribution of the expanded alginic acid and different temperature Algibons produced from the current method

New expanded alginic acid generated	S_{BET} (m^2/g)	Pore volume $(cm^3/g)_{BJH}$	Pore diameter $(nm)_{Ads}$	Pore diameter $(nm)_{des}$	Micro-porosity %	Meso-porosity %
Expanded alginic acid vacuum oven dried (A1)	235	1.02	16.4	14.5	6	83
Expanded alginic acid scCO$_2$ dried (A2)	274	2	33	29	2.5	96
A300	318	1.95	32	25	2.5	95
A450	456	1.83	31	24	6.0	93
A500	513	2.01	24	23	7.0	91
A600	593	2.1	24	23	7.1	91
A650	605	2.0	24	23	7.4	90.4
A800	585	2.4	28	22	7.1	91

Apv: BJH adsorption pore volume, Dpv: BJH desorption pore volume, Apd: BJH adsorption pore diameter, Dpd: desorption pore diameter.

Table.3.3: Pore size distribution of the expanded alginic acid and different temperature Algibons produced from recent work carried out in 2010.[220]

Recent expanded alginic acid generated	S_{BET} (m^2/g)	Pore volume $(cm^3/g)_{BJH}$	Pore diameter $(nm)_{Ads}$	Pore diameter $(nm)_{des}$	Micro-porosity %	Meso-porosity %
Expanded alginic acid vacuum oven dried (A1)	203	1.12	16	14	0.9	90
Expanded alginic acid scCO$_2$ dried (A2)	320	2.65	28	25	0.4	97
A300	216	0.9	18	16.5	1.1	95
A500	388	1	16	14.5	6	91
A600	360	1	18	16	5	92
A800	349	1	15.8	13.0	5	92

The reasons for generating a better quality of Algibons in this current study could be two fold. The first one it may be a heat structural stability of the expanded alginic acid which had been scCO$_2$ dried (A2). The second reason might be the carbonisation temperature programming and controlling of the

mesoporous alginic acid precursor. Thus during the carbonisation process the pore structure of the expanded alginic acid (A2) could survive throughout the thermal pyrolysis.

Here, linear isotherm plots for the A300, A450, A600 and A800 materials which were derived from the expanded alginic acid supercritical CO_2 dried precursor (A2), are plotted in Figure 3.11. The red colour line presents the adsorption linear isotherm and blue colour line presents the desorption linear isotherm. It is noticed that the isotherm plots for these mesoporous alginic acid precursor derived carbonaceous material products generated are isotherm type four[258]. Fortunately, this technology of Algibons production has been reproducible. Repeatability of these mesoporous materials is excellent as many time as is repeated. Change in their surface area, pore volume and average pore diameter as well as mesoporosity% is approximately about 2%.
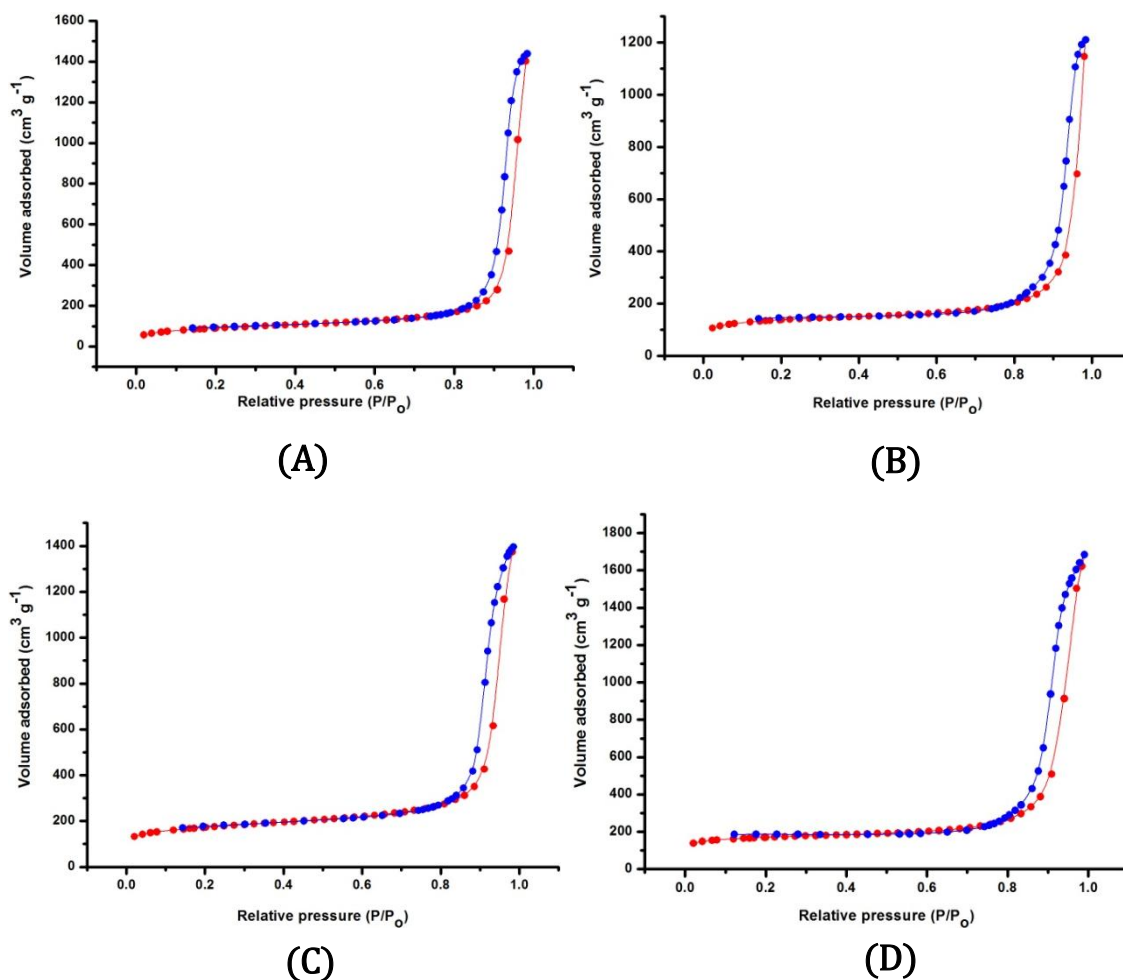
Fig.3.11: Linear isotherm plot of the generated products including (A) A300, (B) A450, (C) A600, (D) A800. Red colour present adsorption linear isotherm plot, blue colour present desorption linear isotherm plot.

It is also interesting to demonstrate the dV/dD pore size distribution of A300, A450, A600 and A800, they are in Figure 3.12. The red line is the adsorption pore size distribution and the blue line is the desorption pore size distribution. The results of nitrogen sorption analysis indicate that the pores shape of the Algibons generated in this chapter are a bottle flask like and large in size.[243-245]
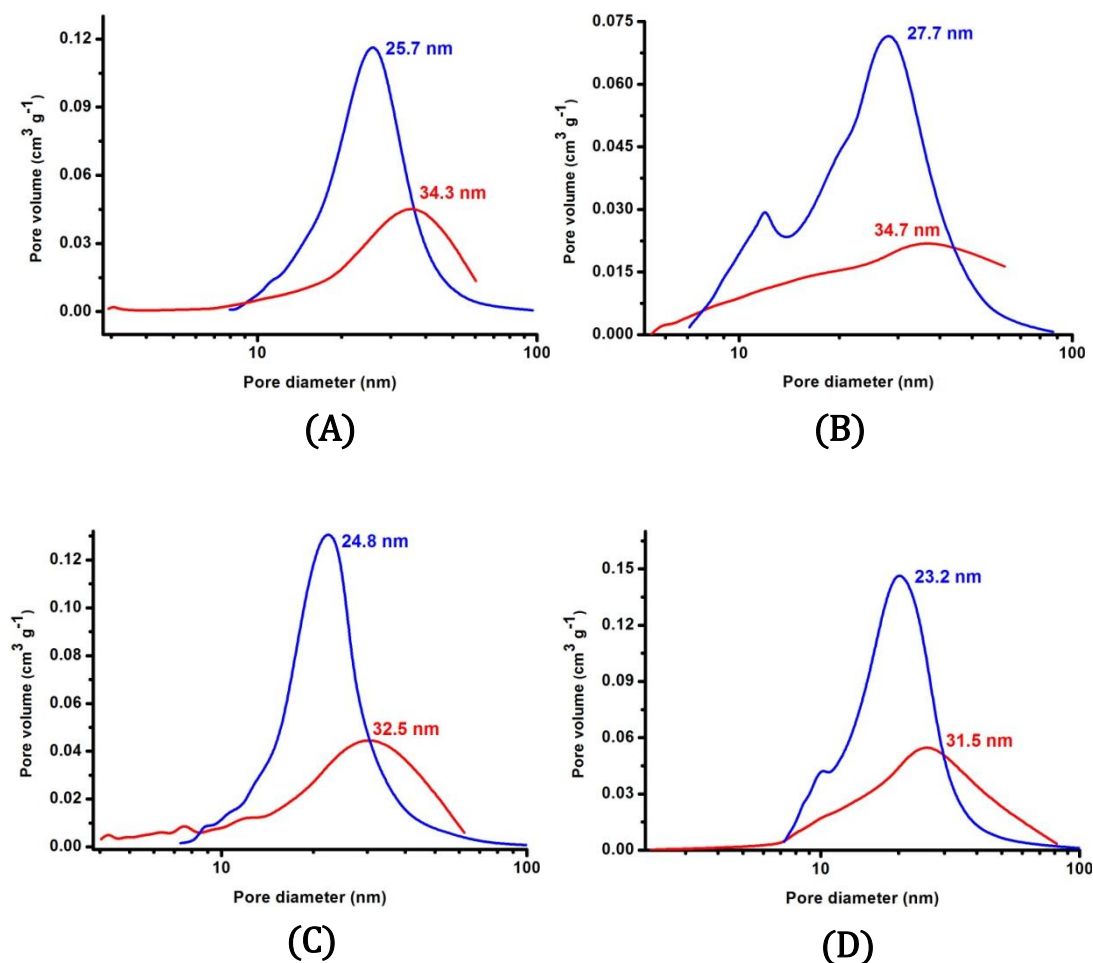
Fig.3.12: dV/dD pore size distribution of the generated products including (A) A300, (B) A450, (C) A600, (D) A800. Red line presents adsorption pore size distribution, blue line is desorption pore size distribution.

3.3.4.2 Scanning electron microscopy (SEM) test

The scanning electron micrograph (SEM) images, of expanded alginic acid scCO$_2$ dried products (A2) and its derivates including A300, A450 and A800, that were produced by thermal pyrolysis of A2, show the formation of an increasingly porous material (see Figure 3.10).

(A)   **(B)**

(C)   **(D)**
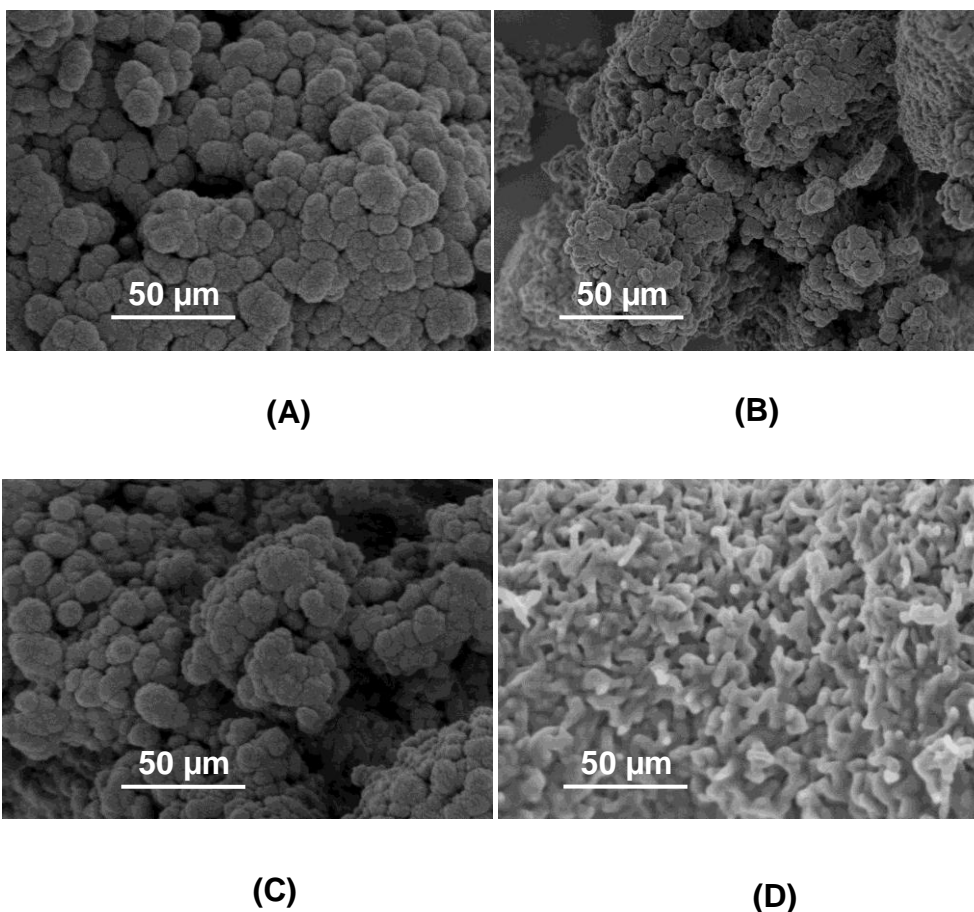
Fig.3.13: SEM of (A) expanded alginic acid scCO$_2$ dried (A2), (B) A300, (C) A450 and (D) A800.

The textural properties of mesoporous precursor (A2) and Algibons appears as a fluffy porous or web-like structure. Depending on the SEM images revealed in Figure 3.13, it appears they are highly uniform and in the range of meso-macro porosity. In particular SEM image of A800 demonstrates uniform particle size and shape.

3.3.4.3 DRIFT IR

Diffuse Reflectance Infrared Fourier Transform Infrared spectroscopy (DRIFT IR) was applied to check the different functionalities of the Algibons produced (see Figure 3.14). Analysis of alginic acid derived carbonaceous materials reveals a slow loss in polysaccharide character upon heating to 300 ^{o}C, as demonstrated by the changing of polysaccharide band spectrum between 1150 and 980 cm^{-1} area[267] relative to carboxylic bands means band between 1730 and 1619 cm^{-1} [268,269] proceeds. At 300 ^{o}C, the absorption bands from 1740 to 1562 cm^{-1} correspond to carbonyl and olefinic type groups. This confirms the

appearance of a band centered at 1605cm^{-1} due to conjugated (C=C) groups.[270]
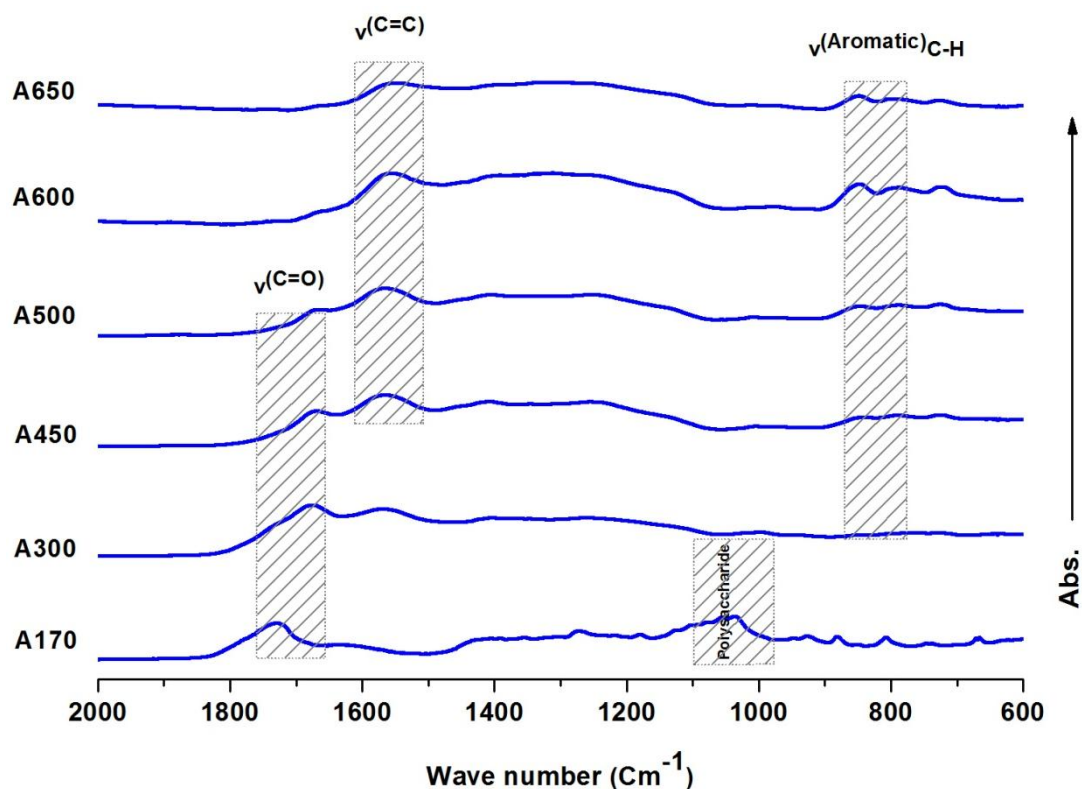
Fig.3.14: DRIFT IR for the Algibon generated at certain different temperatures of carbonisation

As the temperature reached 300 °C, C=O bands move to lower wave numbers from 1730 cm^{-1} to 1712 cm^{-1} and 1689 cm^{-1}. As the temperature reached 600 °C such this spectrum disappears. Because the decomposition/carbonisation of C-O containing groups such as olefinic, vinyl ethers, or lactones; which occur as the main polysaccharide backbone, proceeds.

Band belongs to the glycosidic bond, which is anomeric region occurs from 1000-600 cm^{-1} in A175, are also removed as the temperature reached 300 °C. A distinct aromatic feature occurs at temperature around 300 °C and over maintained at 600 °C by resolved spectral bands at 878, 820 and 765 cm^{-1}.[271]

3.3.4.4 Solid state NMR

This solid NMR spectroscopy was performed as an important technique to check the surface functional properties of the Algibons generated.

[13]C cross-polarization magic-angle spinning (CP MAS) NMR analysis in Fig.3.15 revealed similar functional groups for the solid materials as shown by

DRIFT IR in Figure 3.14. As the carbonisation temperature approached about 300 ^{o}C, the sharp extreme resonances of expanded alginic acid (A2) broaden and reduce in intensity. The Pyranose ring hydroxyl resonances between 72-63 ppm[272] transformed into a broad resonance centered at δ 75 ppm due to the dehydration of polysaccharide which caused drop in polysaccharide property.
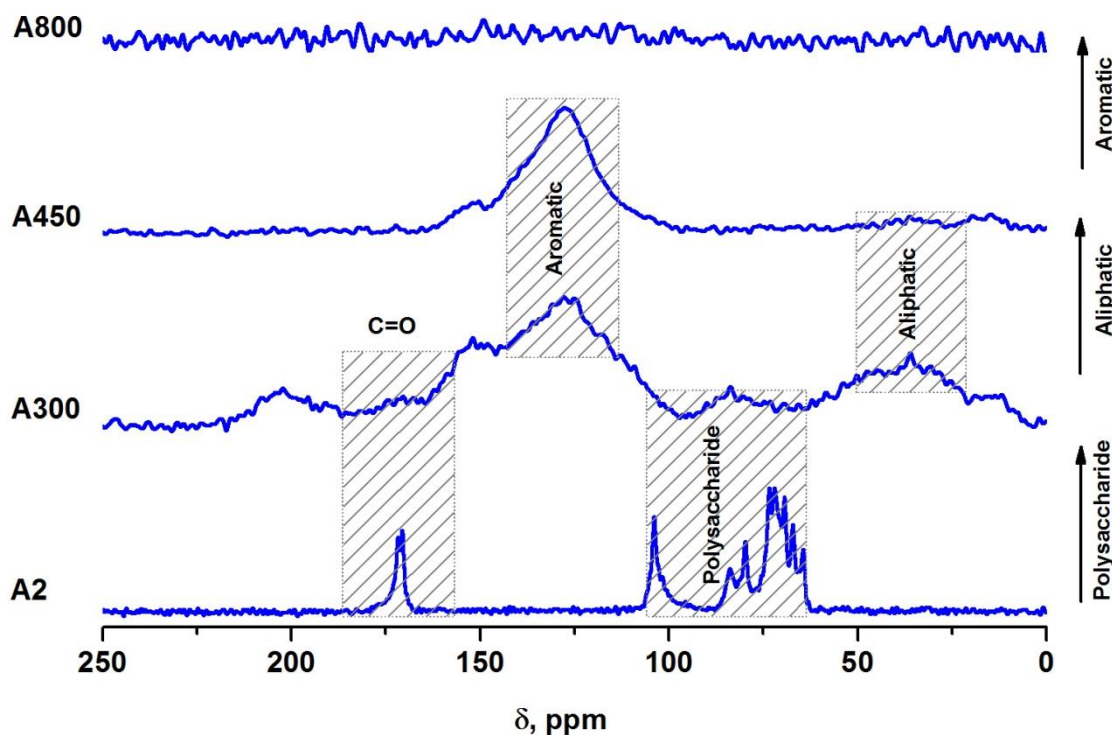
Fig.3.15: ^{13}C cross-polarization magic-angle spinning (CP MAS) NMR for expanded alginic acid (A2), A300, A450 and A800.

Resonances associated with cyclic ketones or lactones (δ 204.0 ppm) and furan or furfuryl type resonances (δ 150.9 ppm) are still also detected in slight intensity at temperature 300 ^{o}C[273].

It is observed that the structural decarboxylation/dehydration finished at 300 ^{o}C, but some residual bulk polysaccharide character slightly maintained yet. This resulted in broadening of the carbonyl resonance to a new peak centered at δ 174.0 ppm (associated with olefinic C-OH). The δ 170.1 ppm (δ COOH) resonance[274,275], which is very sharp in (A2), is removed at 300 ^{o}C. In addition, resonances associated with aliphatic character (δ 15-50 ppm)[276,277] is noticed as this decomposition reached 300 ^{o}C. Further changes can be noticed as the carbonisation temperature reached 300 ^{o}C the

glycosidic bond associated resonances cluster (δ 85 and 105 ppm)[278], which appears distinctly in (A2), also fall in intensity and disappear.

Increasing the carbonisation temperature further results in olefinic/furan type condensation to generate increased aliphatic character (δ 36.1 ppm), and a new broad resonance centered at δ 128 ppm as appears in A300 and is sharper in case of A450 which corresponds to the characteristic of aromatic systems.[279]

This NMR analysis can support the DRIFT IR bands, and informs compactly the conversion of the hydroxyl-rich polysaccharide material into aliphatic/alkene groups in which at the temperature approached 800 ^{o}C the materials generated (A800) becomes a strongly aromatic character. Researchers of Green Chemistry Centre of Excellence at The University of York have believed that some carboxyl groups may participate in cross-linking reactions between the associated polysaccharide chains to form a strong carbonaceous framework. This makes the A800 as the most cross-linked material produced with excellent stability.

3.3.4.5 CHN elemental analysis

Elemental analysis is a process of determination of element composition in a sample. For organic compound almost always refers to CHNX. C is carbon, H is hydrogen, N is nitrogen and X is either halogens or sulphur. The most common type of CHN test is carried out by combustion analysis.

Table.3.4: Elemental analysis for (A2), its derived mesoporous carbonaceous materials and AC

Porous material	CHN test		
	C%	H%	N%
Expanded alginic acid (A2)	36.6	4.7	--
A300	63.8	3.84	--
A450 (3)	73	3.22	--
A600 (4)	80.2	2.3	--
A800	82	1.3	--
AC	81	1.17	--

The combustion products like carbon dioxide, water and nitric acid correspond to carbon, hydrogen and nitrogen respectively in the sample. In this chapter the expanded alginic acid $scCO_2$ dried (A2), A300, A450, A600, A800 and Ac were elemental examined.

It is noticed in Table 3.4 that increase in the preparation temperature of the Algibons materials brings a significant increase in the percentage ratio of carbon/hydrogen. Such higher and longer thermal pyrolysis dramatically removed oxygen-containing functional groups including OH and COOH groups in the Algibons material. This could bridge this section to an article which reported that the lowest temperature prepared carbon material is the highest oxygen content material which presents a low ranked hydrophobic material, while, high temperature carbon material prepared, which has the lowest heteroatom content, is a high ranked hydrophobic material.[280] So that the A300 which is the highest oxygen content Algibon, is the lowest ranked hydrophobic one, however, A800, which is the most thermally dehydrated/decarboxylated material, is the top ranked hydrophobic material compared to the rest of Algibons generated. A small percent of nitrogen is noticed in A800, it may be as a result of nitrogen gas being adsorbed by A800 as carbonisation temperature approached 800 $^{\circ}$C.

3.3.4.6 Ash content test

Ash remains after the water and organic matter are removed by heating in the presence of 100% O_2 and 50% N_2.

Ash content test was carried out for the Algibons generated and activated carbon. The TG plot in Figure 3.16 introduces information that the high Algibon temperature contains a greater amount of the ash. In this experiment as a result of dehydration and a functional groups removal, at the end only residual carbon highly remained. From the TG plot it can be seen that the lowest amount of ash is in the expanded alginic acid (A2).

In A300 the ash left at the end is greater than in case of expanded alginic acid (A2). In addition, the amount of ash content in A800 was the highest which is approximately triple, twice and one-third times greater than in case of A300, A450 and A600 respectively. Because these carbonaceous materials had been already carbonised up to certain top temperatures which caused their surface

112

functional groups (OH and COOH) being gradually removed in response to temperature increased.
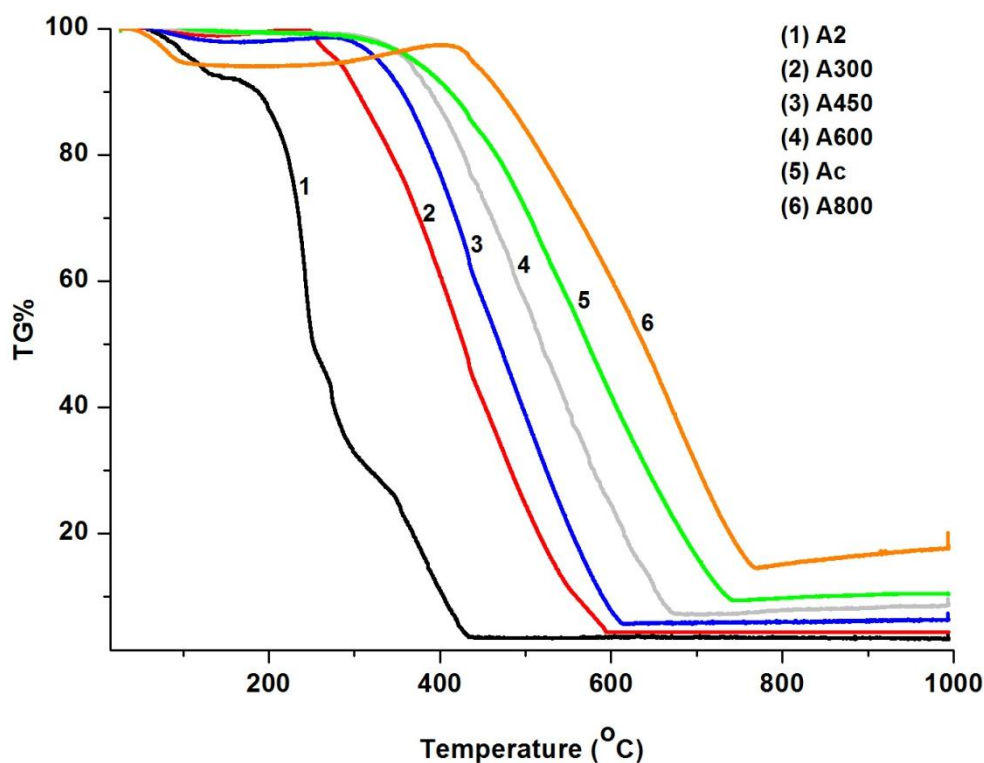
Fig.3.16: Ash content figure for the expanded alginic acid $scCO_2$ dried (A2), Algibons and Ac under (100 mL/min.) O_2 and (50 mL/min.) N_2.

Table.3.5: Ash content % for the Algibon and AC

Porous adsorbent material	Ash content %
A2 (1)	2.5
A300 (2)	4.2
A450 (3)	6.3
A600 (4)	8.5
AC (5)	11.2
A800 (6)	13.8

Activated carbon contains smaller amount of ash compared to A800 and greater amount than of A600. This could be related to the nature of the precursors which had been employed to generate Ac and Algibon as well as the thermal production process of both mesoporous carbonaceous materials and the AC.

It was reported that the high ash content indicates less oxygen content, this means, the high ash content products are like to be more hydrophobic and could be mechanically more stable.[273,279] The ash content results

113

demonstrate that the low temperature Algibon generated is more hydrophilic, but gradually changes to more hydrophobic when they are prepared at temperature 450 ^{o}C and over.

3.4 Conclusion

Applying the programmed and controlled thermal decomposition temperature for the mesoporous alginic acid precursor obtained (in chapter two) brought different textural properties of Algibons which resulted in a very promising mesoporous materials with super pore volume (up to 2.5 cm^3/g), pore diameter in between micro and macro and their surface area (S_{BET} under 650 m^2/g). They are predominantly mesoporous materials. The results demonstrated that the percentage of mesoporosity is over 90% like in high temperature Algibon, while, in some cases it is over 95%, such as in case of low temperature Algibon. Production of types of Algibon materials derived from the mesoporous alginic acid precursor generated (A2) depends on the carbonisation temperature approached.

The Algibon materials were characterised to find out more about their properties, some techniques were performed to analyse their porous structure such as BET, pore volume and pore diametre as well as surface functionalities of these products generated. The results of porosimetry obtained indicating that all types of Algibons produced (A300, A450, A600, and A800) were extremely mesoporous materials, their pores shape are bottle flask like. Nitrogen sorption analysis suggests that these carbonaceous materials follow adsorption isotherm four which also suggested the mesoporosity charactor. The results of porosimetry imply that the carbonisation temperature programme of the mesoporous precursor protects the pores from the collapsing.

SEM images revealed that Algibons particles are uniform, DRIFT IR and Solid NMR demonstrated that the low temperature Algibon is highly hydrophilic, however, high temperature Algibon is predominantly hyrdophobic.

The most important point of this part of this research is to declare the current method of Algibon generation is a successful method since it has been aimed to be reproducible on both small and large scale use.

This new adsorber can be a candidate for use in many technologically important applications in research and industry. Our desire will to use it in adsorption

technology to remove bulky organic dyes in water stream in particular and could be useful in metal uptake since being these types of pollutants in water stream are considerable threats to our environment and have significant risks to human health.

```
┌─────────────────────┐      ┌─────────────────────┐      ┌─────────────────────────┐
│ 200 g alginic acid   │      │                     │      │ Add 4 L ethanol and     │
│ in 4 L D.W  stir at  │ ───▶ │ Retrograde at 5 °C  │ ───▶ │ stir: 1st wash (1 h)    │
│ 100 °C for 160 min.  │      │ for 24 h in fridge  │      │ 2nd wash (30 min.)      │
│                      │      │                     │      │ 3rd wash (30 min.)      │
└─────────────────────┘      └─────────────────────┘      └─────────────────────────┘
                                                                       │
                                            [3 times]                  ▼
┌─────────────────────┐      ┌─────────────────────┐      ┌─────────────────────────┐
│ Different textural   │      │ Characterisation    │      │ Filtration using sinter │
│ properties of        │ ───▶ │ of Algibons         │      │ filter                  │
│ Algibons generated   │      │ produced            │      │                         │
└─────────────────────┘      └─────────────────────┘      └─────────────────────────┘
         ▲                                                             │
┌─────────────────────┐                                               ▼
│ Carbonisation of     │                                  ┌─────────────────────────┐
│ mesoporous           │                                  │ Add 4 L acetone and     │
│ precursor in Netschz │                                  │ stir for 30 min.        │
│ under N2             │                                  │                         │
└─────────────────────┘                                  └─────────────────────────┘
         ▲                                                             │
┌─────────────────────┐                         [3 times]             ▼
│ Quality control      │                                  ┌─────────────────────────┐
│ to determine textural│                                  │ Filtration using sinter │
│ property of the      │                                  │ filter                  │
│ mesoporous alginic   │                                  └─────────────────────────┘
│ acid generated       │                                               │
└─────────────────────┘                                               ◀─┘
         ▲                    ┌─────────────────────┐
┌─────────────────────┐      │ Dry the precipitate │
│ Mesoporous alginic   │ ◀─── │ in scCO2 at 50 °C/  │ ◀───
│ acid generated       │      │ 100 bar/3h,         │
│                      │      │ depressurise slowly │
│                      │      │ overnight           │
└─────────────────────┘      └─────────────────────┘
```

Fig.3.17: Algibon synthesis technology in Green Chemistry Centre of Excellence at The University of York, UK.

CHAPTER FOUR

Algibons Generated Application in Bulky Azo Dye Adsorption

4.1 Introduction

This part of the project involved the use of the developed Starbon technology to adsorb bulky organic dye molecules which are mostly used in the textile industry. This technology is based on the extremely large pore diameter and tuneable surface functionality of mesoporous carbonaceous materials which are derived from polysaccharide.[281] This study has proposed a few dyes called Procion Yellow H-EXL (PY), Remazol Black (RB), Procion Crimson H-EXL (PC) and Procion Navy H-EXL (PN) which are reactive azo dyes.[282] They represent approximately a third of the total dye market and more of half of the cotton market.[283] Their structure contains a reactive azo group which interact with the fibres and a chromophore group which gives rise to the colour.[284] Starbon has been already successfully used for the removal of smaller model dye at the Green Chemistry Centre of Excellence in 2012.[233] The objective of this chapter is to screen a variety of adsorbents including different types of Starbons, activated carbons and silica gel in industrial textile water treatment and choose the most efficient materials for the adsorption of dyes.

4.2 Experimental section

Firstly, standard stock solutions (140 mg/L) of the dyes (PY, RB, PC and PN) were prepared. From each standard stock solution a series of solutions containing each dye with concentrations 40, 60, 80, 100, 120 and 140 mg/L was prepared. At the first step of the investigation using these standard dyes solutions calibration curves for each dye was developed. After that, the minimum time for the adsorption equilibrium achievement of the dyes was estimated during kinetic experiments using 100 mg of each adsorbents materials to 100 mL of solution with optical density 1 A.U. of UV-Vis absorbance spectroscopy using a JASCO V-550 UV/VIS spectrometer, except for the RB dye in which 20 mg of each adsorbent was used in a 100 mL dye solution with optical density 1 A.U. of UV-Vis absorbance spectroscopy. Applied calibrations involving thermodynamic parameters of adsorption which were obtained were then analysed using Langmuir, Freundlich, Tempkin and Dubinin-Radushkevich models. The time of these experiments was always longer than the achievement time of adsorption equilibrium estimated during the kinetic experiments. The thermodynamic investigations were carried out using a mixture of 10 mg of adsorber and 10 mL of aqueous days solutions, (in the case

of RB, 5 mg adsorber was employed for 25 mL of RB solutions). The adsorption energy was calculated using adsorption experiments at different temperatures (25, 35, 45 and 55°C). A desorption experiment was conducted using i) Direct thermal regeneration of A800 loaded with dyes, ii) Dye unload and adsorber regeneration using distilled water or ethanol at 30 and 50°C and iii) Indirect thermal treatment of A800 loaded with the dyes which comprised of combination of warm ethanol wash and thermally treatment of the adsorber to 800°C. Furthermore, the A800 adsorbent was regenerated by means of the third procedure of desorption experiment which was successfully reused in the dye removal application.

4.3 Results and discussion

4.3.1 Calibration curve

UV-VIS spectra of each dyes solution in wavelength range between 200 and 900 nm have been recorded using UV-VIS Spectrometer "JASCO V-550 UV/VIS". Based on these investigations, the maximum wavelength (λ_{max}) was found for each of the dyes. The results are shown in the following Table 4.1. The linear relationship between absorption and concentration of a UV-VIS active compound is given by Lambert-Beer's law.[285] This law was used for the development of calibration curve between each dye absorption at the λ_{max} wavelength and its solution concentrations. It has been found that correlation coefficients (R^2) for the calibration are acceptable with a range between 0.994 and 0.999 (see Figure 4.1).

Table.4.1: Maximum wavelength for the dyes[282]

Dye	Abbreviation	Maximum wavelength λ_{max} (nm)
Procion Yellow H-EXL	PY	417
Remazol Black	RB	595
Procion Crimson H-EXL	PC	545
Procion Navy H-EXL	PN	607
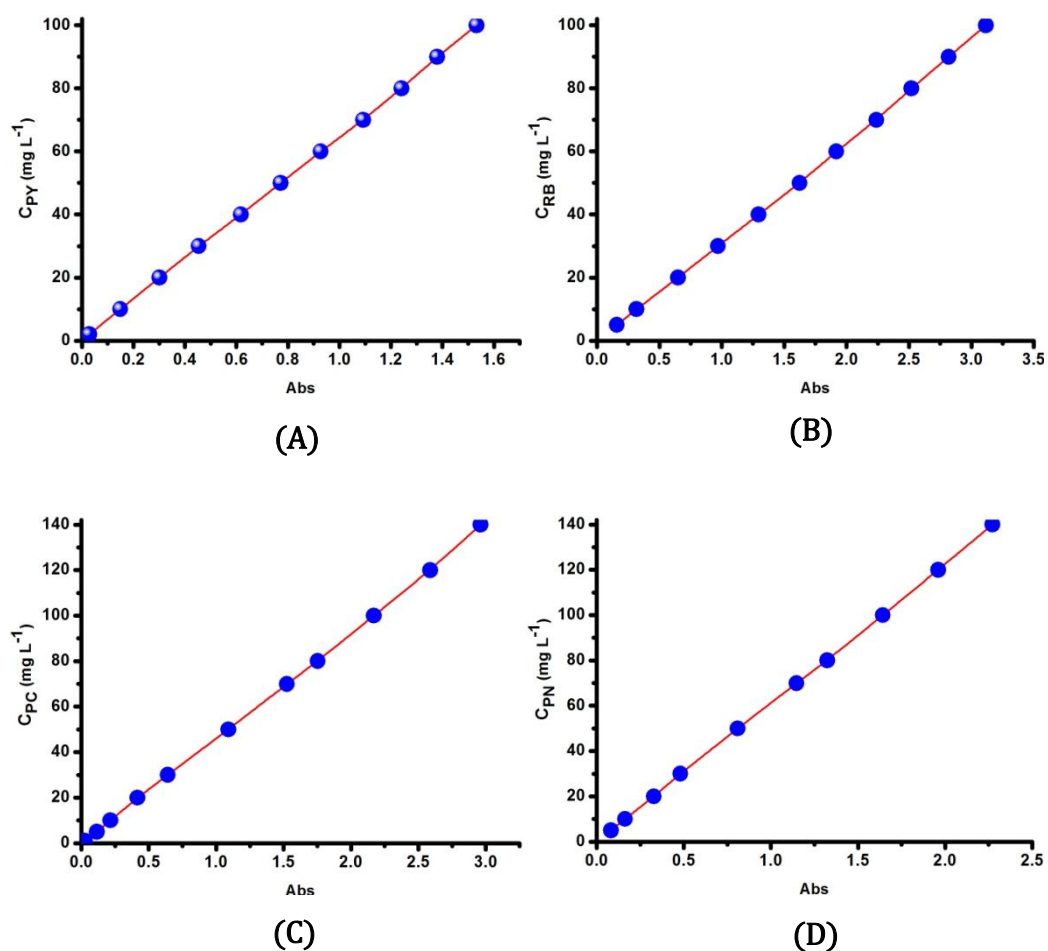
Fig.4.1: Calibration curves for (A) Procion Yellow (PY), （B）Remazol Black (RB), (C) Procion Crimson (PC), （D）Procion Navy (PN).

4.3.2 Adsorption kinetic

In this part of this chapter, the minimum time required to reach the dyes (i.e. PY, RB, PC and PN) adsorption equilibrium onto the surface of eight absorbents such as three different types of Algibons (A800, A450, A300) and Starbons (S800, S450, S300) as well as activated carbon and silica gel were determined. To give more details we refer the reader to Table 4.4 indicating the porosimetry of the adsorbents used. Another benefit of this investigation was to rank the applied adsorbents according to the rate of uptake of the dyes from the aqueous solution. Then each dye solution was prepared at a concentration that corresponds to one arbitrary unit of UV spectroscopy at the λ_{max} wavelength. (100 mg) of each adsorbent was employed for 100 mL of each individual dye solution prepared in the previous stage. An exception was made for RB in which case only 20 mg of adsorbent was employed for 100 mL of the Remazol black solution.
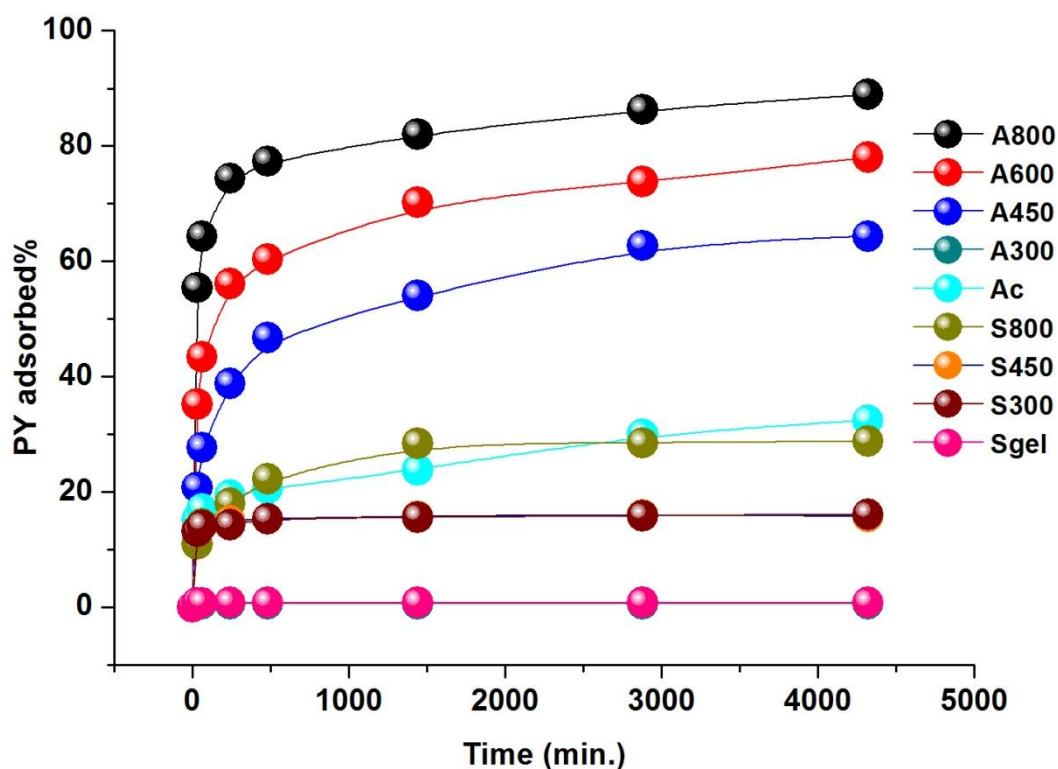
Fig.4.2: Percentage of PY adsorption using eight porous materials including A800, A450, A300, S800, S450, S300, AC and Silica gel (Sgel) as a function of time. Initial concentration of dye corresponds to one arbitrary unit of UV-VIS absorbance of PY solution.
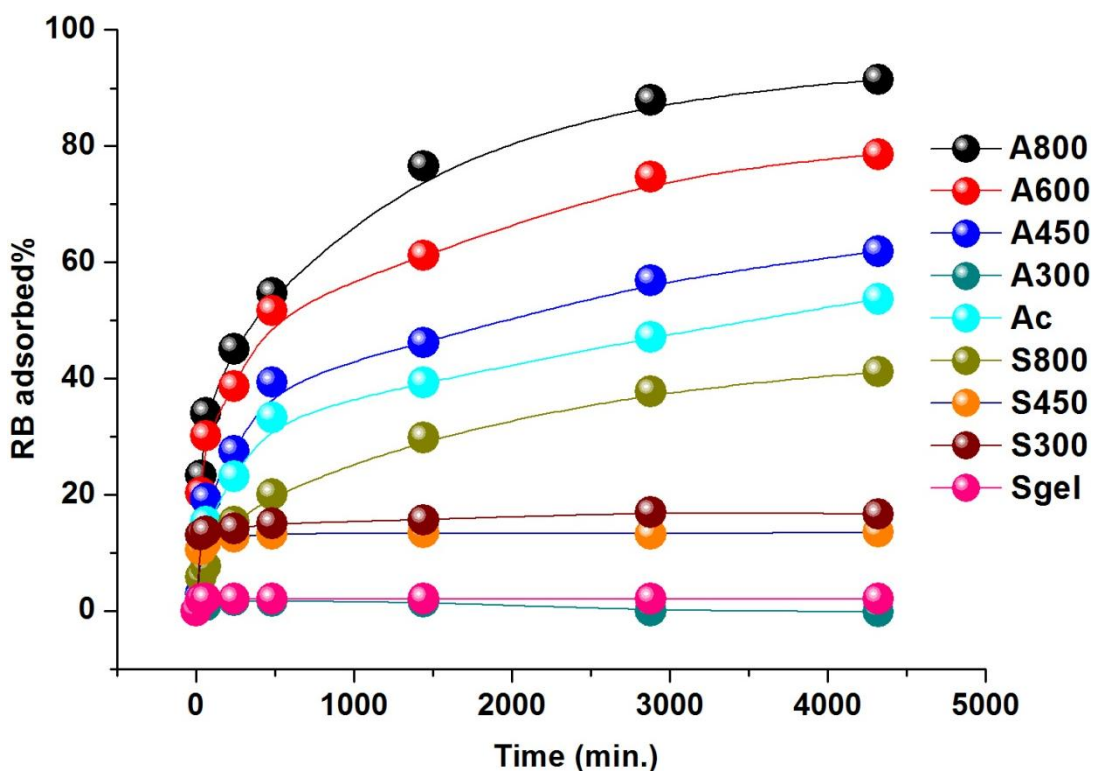
Fig.4.3: Percentage of RB adsorption using eight porous materials including A800, A450, A300, S800, S450, S300, AC and Silica gel (Sgel) as a function of time. Initial concentration of dye corresponds to one arbitrary unit of UV-VIS absorbance of RB solution.

120
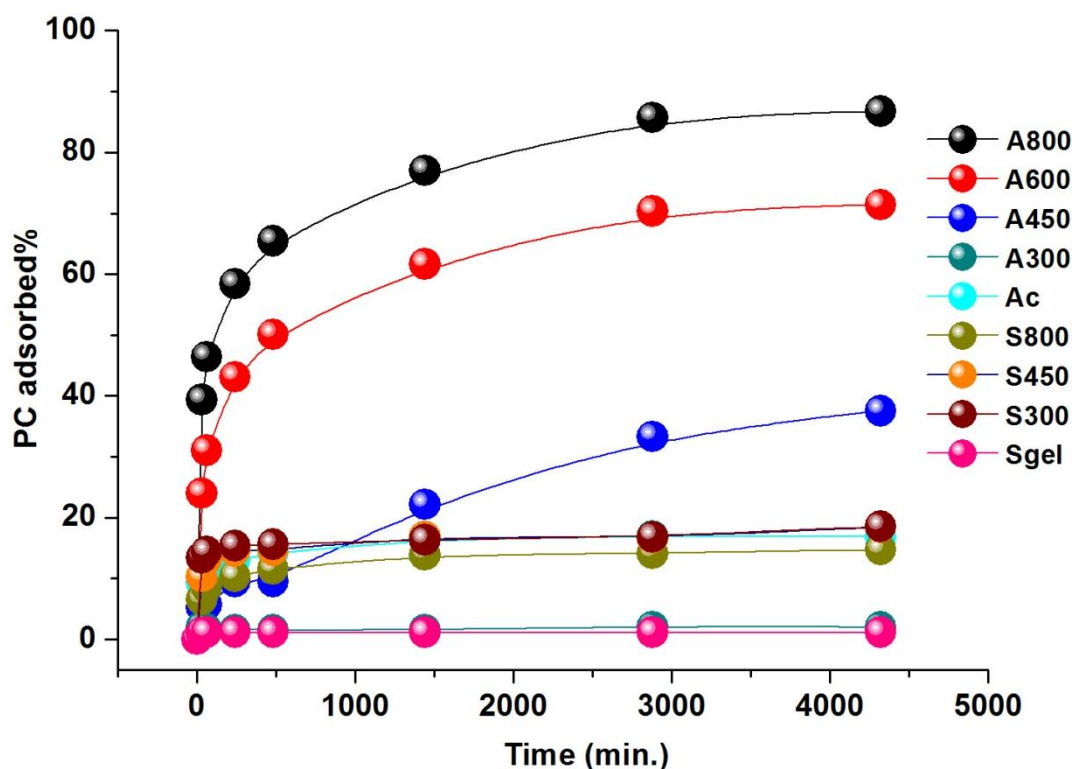
Fig.4.4: Percentage of PC adsorption using eight porous materials including A800, A450, A300, S800, S450, S300, AC and Silica gel (Sgel) as a function of time. Initial concentration of dye corresponds to one arbitrary unit of UV-VIS absorbance of PC solution.
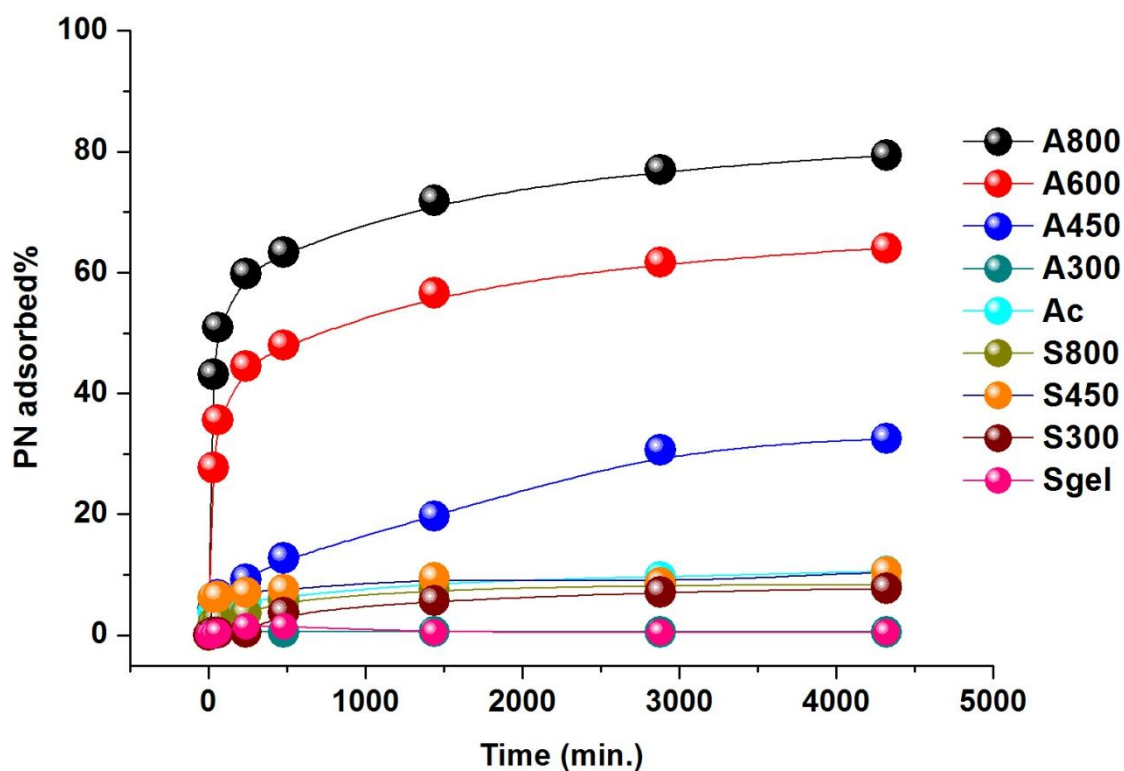
Fig.4.5: Percentage of PN adsorption using eight porous materials including A800, A450, A300, S800, S450, S300, AC and Silica gel (Sgel) as a function of time. Initial concentration of dye corresponds to one arbitrary unit of UV-VIS absorbance of PN solution.

It was observed that the colour of the dye solutions was reduced with time. To follow this kinetic process, a number of samples for UV-VIS measurement were taken at 30, 60, 240, 640, 1440, 2880, 4320 minutes. The kinetic curves which were obtained are shown in Figures 4.2 to 4.5.

The primary results of the kinetic investigation indicate that Algibons adsorbent at high temperatures could take up the dyes more efficiently than the other classes of adsorbents. This is probably due to the different textural properties of the adsorbent materials such as surface functionality as well as pore size, pore diameter and surface area.
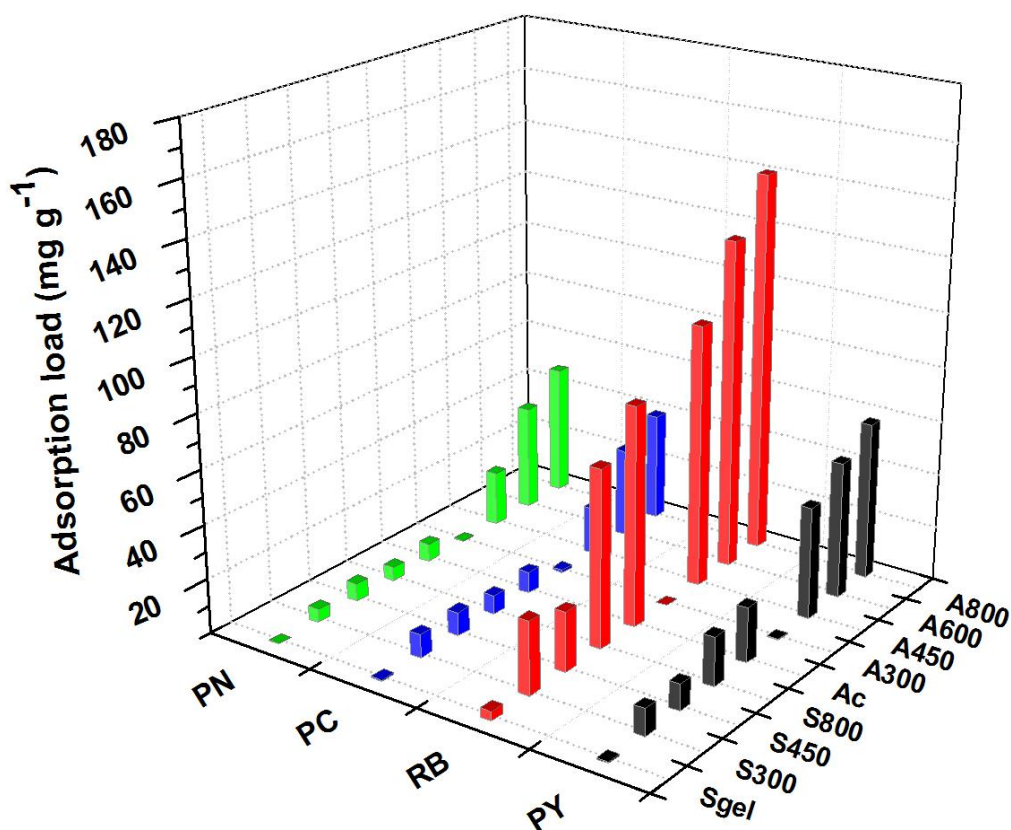
Fig.4.6: The amount of dyes adsorbed by one gram of each adsorbent obtained after 72 hours of contact time, with the initial concentration of each dye corresponding to one arbitrary unit of UV-VIS absorbance.
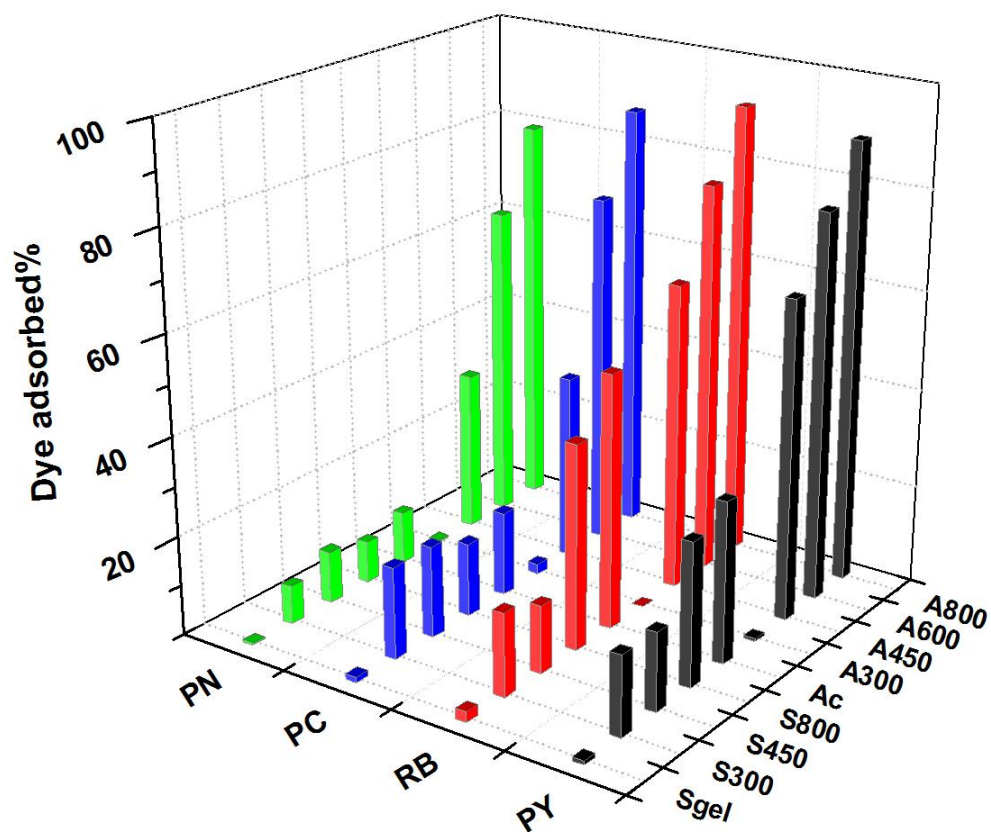
Fig.4.7: Degree of dyes adsorption by different adsorbents from the solutions after 72 hours of contact time, with the initial concentration of each dye corresponding to one arbitrary unit of UV-VIS absorbance.

Table.4.2: Dye adsorption load (mg g^{-1}) by each adsorbent employed as the contact time reached (72 hours) for each dye solution concentration which corresponds to one arbitrary unit of UV-VIS absorbance

Adsorption load (mg g^{-1})				
Dyes / Adsorbents	Procion Yellow (PY)	Remazol Black (RB)	Procion Crimson (PC)	Procion Navy (PN)
A800	58	141	40	48
A600	50.	122	33	39
A450	41	97	17	20
A300	0.4	0.1	1	0.3
AC	20	81	8	7
S800	18	65	7	5
A450	10	22	9	7
S300	9.6	27	8	5
Sgel	0.5	3	0.6	0.3

It is believed that the fact that the greatest RB uptake took place by the carbonaceous materials (see Fig.4.6 and 4.7) could be due to the smaller size and planar structure of this dye. In contrast to RB, the other dyes are larger and have a huge 3-D structure (see Fig.4.8 and 4.9, and Table 4.3) as was proved by modelling using Hyperchem software[286,287].
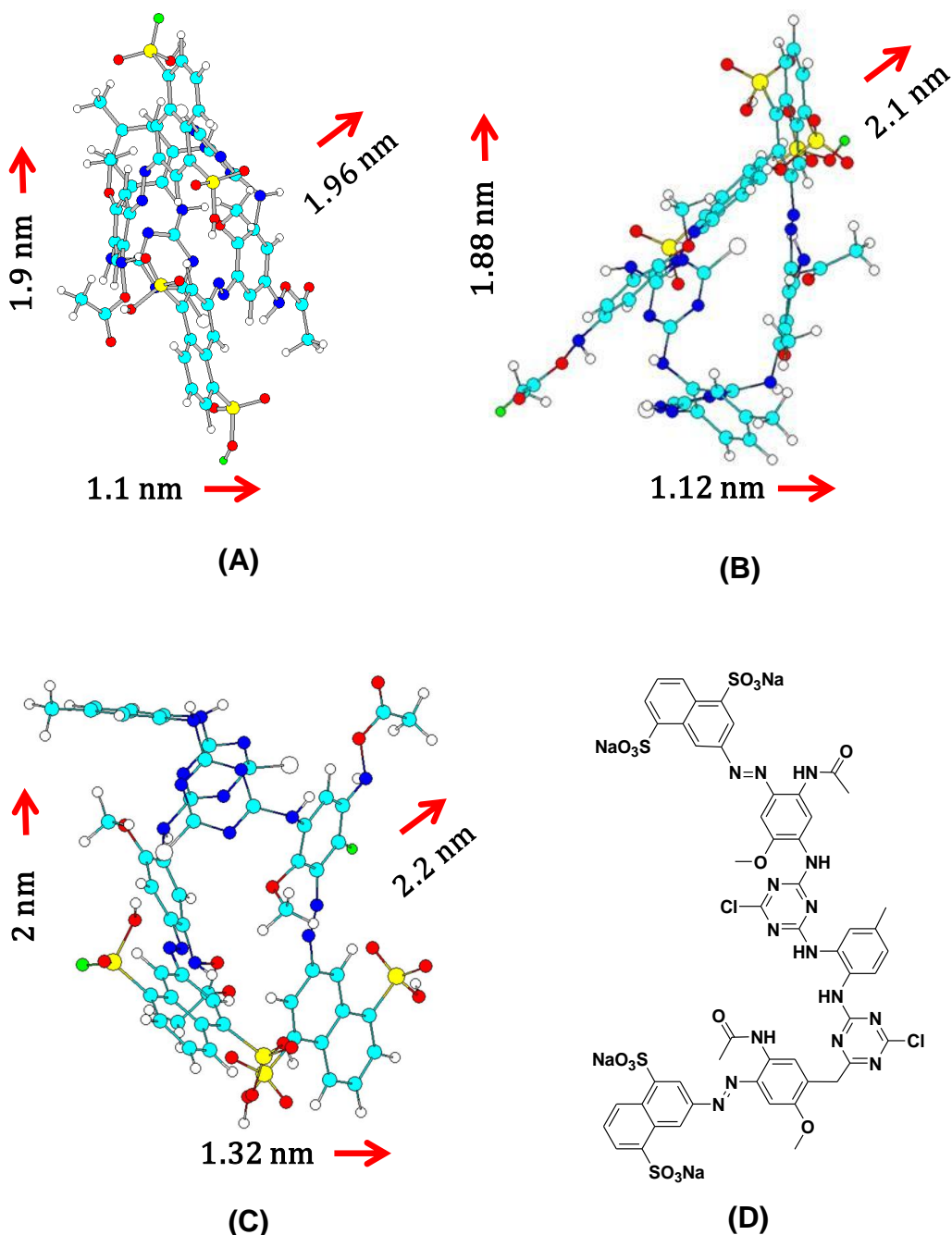
Fig.4.8: (A), (B) and (C) are three dimensional structures of Procion Yellow (PY) dye as drawn by Hyperchem software in space. (D) is the normal structure of Procion Yellow (PY) dye.
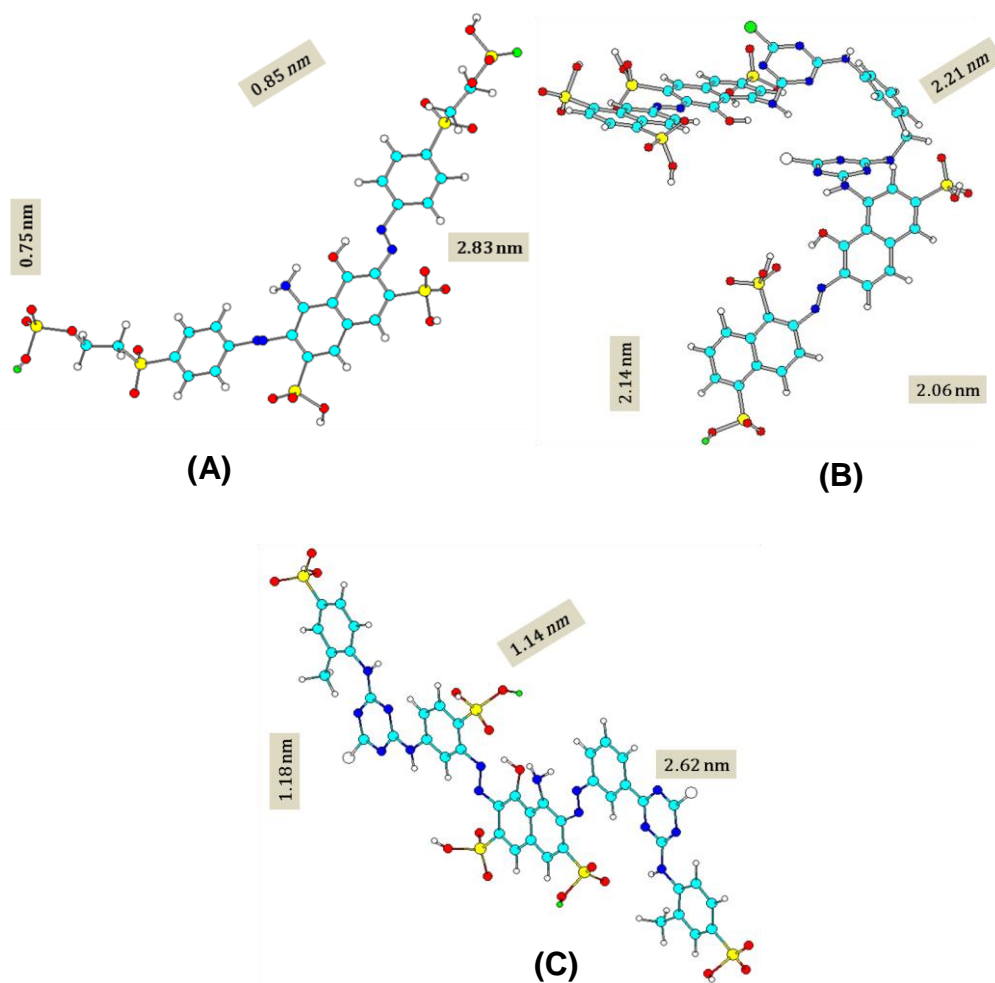
Fig.4.9: Three dimensional structures of (A) Remazol Black (RB), (B) Procion Crimson (PC) and (C) Procion Navy (PN) dyes as drawn by Hyperchem software.

Table.4.3: Calculation of the axis of each individual dye in space using Hyperchem software

Dye	X axis length	Y axis length	Z axis length
PY	1.32	2	2.2
RB	2.83	0.75	0.85
PC	2.06	2.14	2.21
PN	2.62	1.18	1.14

It is noted that the efficiency of the adsorption of the dyes by the carbonaceous adsorbents was much better than adsorption by the Sgel (Fig.4.6). This observation cannot be explained by surface very good textural properties of Sgel, which has a surface area of around 300 m^2/g as well as a pore volume which is twice as large and its pore diameter is ten times greater than that of the

activated carbon. Therefore poor Sgel performance could be due to the contrast between its surface hydrophilicity and the hydrophobicity of dye molecules.

It can be seen that, at high temperatures, the prepared Algibons, in particular, A800, has the highest dye adsorption rate compared to the other Algibons (A300, A450 and A600). This could be due to the highest pore volume, pore diameter of A800 and highest degree of carbon element percent of its surface/active sites (see Table 4.4). It has to be mentioned that, according to solid state NMR results, the most carbonised Algibons with graphite-like structure are also the most hydrophobic ones (see Fig.3.11). This hydrophobicity character significantly reduces the water molecules adsorption which is formed by means of hydrogen bonding to the oxygen containing surface/active sites of A800 adsorbent. Increase in hydrophilicity of the adsorbent can enhance the water molecules adsorption onto the adsorbent followed by clustering of further water molecules at the surface and sites of adsorbents.[288-293] That water clustering can prevent the accessibility of the dye species into the minor hydrophobic region of the hydrophilic adsorbent, it also lowers the interaction force between the dye molecules and the hydrophilic adsorbent.[294-300] This can obstruct the dye species access into the mesopores of hydrophilic Algibon. Therefore, the most hydrophobic Algibon (A800) allows better π-π interaction between aromatic rings of the bulky dye species and electron rich layer of adsorbent.[301]

This set of phenomena could significantly improve A800 performance in terms of adsorption of large aromatic dye molecule. In contrast, the very hydrophilic A300 adsorbent has no efficiency in terms of dye uptake, despite the fact that it has a high mesopore volume showing that the polar surface functionality of the A300 repulses the dye.

It was found that dye adsorption by the AC was lower than of the A800. The functionality of A800 and AC are very similar (see the results of CHN analysis in Table.4.4), so the difference between these materials could be explained by the high degree of AC microporosity with an average pore diameter twenty times smaller than the average diameter of A800. Morover, the exceptional mesoporous characteristics of A800 caused the faster rate of large dye uptake from the aqueous phase compared to AC.

The three dimensional structures of these four dyes are drawn using Hyperchem software (Figures 4.8 and 4.9) to logically emphasis the influence of the size and shape of the dyes on the adsorbent effectiveness for dye removal. According to the molecular structures, it appears that the diameter of the pores of the high temperature A800 prepared are very large which allow the bulky dyes to enter and diffuse through the mesoporous networking system.

Table.4.4: Porosimetry and CHN results for the porous adsorbents used in bulky dye adsorption

Adsorbent	S_{BET} (m^2/g)	Pore volume (cm^3/g)$_{BJH}$	Maximum pore diameter (nm)$_{Ads}$	Maximum pore diameter (nm)$_{des}$	Micro-porosity %	Meso-porosity %	CHN test	
							C%	H%
A800	555	2.4	27	20	7%	90	82	1.3
A600	593	2.1	24	23	7.1	91	80	2.3
A450	457	1.7	22	17	6%	92	73	3.22
A300	319	1.9	23	17	2%	93	63.8	3.84
AC	744	0.3	1.3	1.0	78%	10	81	1.17
Sgel	299	0.7	10.0	8.0	8%	85	--	--

Note: Starbons (S300, S450 and S8000) derived from starch were commercially approached. They were in storage for long time without well protection from moisture. Therefore, they collapsed gradually within 2 years. Porosimetry of S300, S450 and S800 indicated that their pore volume were ca (0.1 cm^3/g) and in macroporous region pore diameter ca (10 nm). Mesoporosity % in them were about few percentage. S300, S450 and S800 became extremely nonporous. Their surface area were (17 m^2/g) for S300, (25 m^2/g) for S450 and (297 m^2/g) for S800. Furthermore, to give more details we refer the reader to look at the figures of adsorption isotherm and pore size distribution plots for S300, S450 and S800 as well AC and Sgel in appendix four.

The differences between the ability of Algibons and AC in dyes adsorption is illustrated in Figure 4.10. The figure is based on nitrogen sorption analysis discussed in chapter three and textural properies of A800 and AC presented in Table 4.4. It explains how the pore volume and diameter of adsorbent can affect the dye uptake efficiency in terms of capturing the large dyes. As can be seen from Figure 4.10, the pores of the activated carbon adsorbent are dramatically smaller which limited its ability to take up the larger dyes. Therefore dye molecules could not be loaded into the pores of the activated carbon.
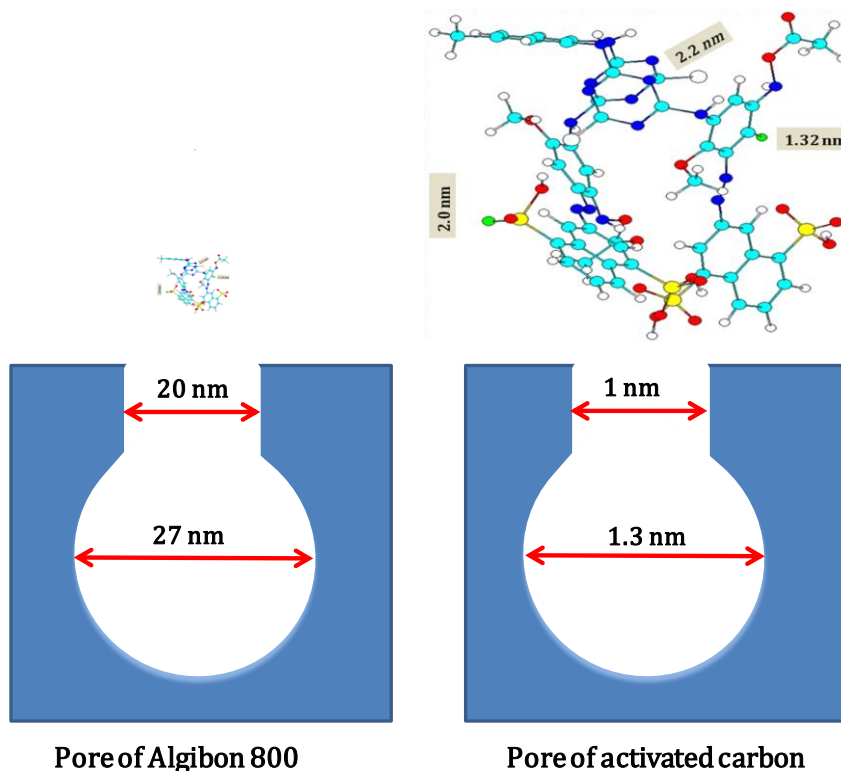
Fig.4.10: Comparison of the size and shape of dye molecule to the pores of A800 and AC.

4.3.3 Kinetic order model studies

In order to further understand the dye adsorption, the study of adsorption kinetics should be included so as to find an appropriate kinetic model. A lot of useful information can be obtained by using different kinetic models for analysis, such as chemical reaction, diffusion control and potential rate controlling steps. There are a wide variety of models available that can be examined in relation to adsorption kinetics. The most widely applied kinetic models are the pseudo-first and pseudo second-order models. The conformity between the models predicted values and experimental data is expressed by the correlation coefficients (R^2) value.

4.3.3.1 Pseudo-first-order model

For this model the linearised form of the Lagergren pseudo-first-order equation is used[302-304]:

$$\ln(Q_e - Q_t) = \ln Q_e - K_1\, t$$

Where Q_e is the amount of dye adsorbed (mg/g) at equilibrium, Q_t is the amount of dye adsorbed at time t (min), k_1 (min^{-1}) is the pseudo-first-order rate constant of adsorption. A straight line of $\ln(Q_e-Q_t)$ versus t suggests the applicability of this kinetic model.

4.3.3.2 Pseudo-second-order model

The following equation is used to determine the appropriateness of the pseudo-second-order model[305,306] for the adsorption process:

$$\frac{t}{Q_t} = \frac{1}{K_2 Q_e^2} + \frac{1}{Q_e} t$$

Where K_2 (g mg^{-1} min^{-1}) represents the pseudo-second-order rate constant. A straight line of t/Q_t versus t suggests the applicability of this kinetic model.

Table.4.5: Pseudo-first-order of kinetic parameters using different porous material adsorbents

Kinetic parameters of Pseudo first order reaction				
Adsorbent	**Dyes**	**Qe (mg/g)**	**K$_1$*10^{-3} (min^{-1})**	**R^2**
A800	PY	82	2.7	0.9538
	RB	331	1.0	0.9574
	PC	72	1.3	0.9730
	PN	57	1.0	0.9117
A450	PY	63	2.3	0.7925
	RB	112	1.9	0.9021
	PC	17	0.3	0.9403
	PN	33	0.5	0.9749
AC	PY	18	0.7	0.8865
	RB	87	1.6	0.9927
	PC	38	2.1	0.9105
	PN	11	0.7	0.9179

Table.4.6: Pseudo-second-order of kinetic parameters using different porous material adsorbents

Kinetic parameters of Pseudo second order reaction				
Adsorbent	Dyes	Qe (mg/g)	$K_2 \ast 10^{-3}$ (g mg^{-1} min^{-1})	R^2
A800	PY	55	9.1	0.999
	RB	130	3.2	0.993
	PC	34	2.5	0.997
	PN	20	3.1	0.9981
A450	PY	20	1.3	0.9954
	RB	80	14.3	0.999
	PC	21	15.6	0.991
	PN	13	4.1	0.9926
AC	PY	12	3.7	0.9927
	RB	59	4.3	0.9992
	PC	9	7.6	0.999
	PN	5	10.6	0.9928

From Tables 4.5 and 4.6 for pseudo-first-order parameters and pseudo-second-order parameters, it can be clearly noticed that the R^2 values for pseudo-second-order model are better than R^2 values for pseudo-first-order model. Almost every R^2 value for each adsorbent is in the acceptable range between 0.991 and 0.999. However, the calculated Q_e values in pseudo-second-order fit better with the experimental data than with the data obtained from the first kinetic equation. It indicates that the adsorption process for dye removal by these materials belongs to the second order kinetic model. That means dye adsorption followed a chemisorption as rate controlling mechanism.[307] Because of a strong interaction between the aromatic species of dye molecules and the hydrophobic region of the adsorbents.[301]

4.3.4 Dye adsorption study

This part of this chapter deals with the effect of dye concentration on dye adsorption load. To illustrate this point in Figure 4.11 the dye adsorption load (Q_e) is plotted versus concentration at equilibrium (C_e). It is noticed that the adsorption load is directly proportional to the increased concentration. This could be due to the high mesoporosity of A800 used which allows the bulky molecules to load into the large pores of A800.
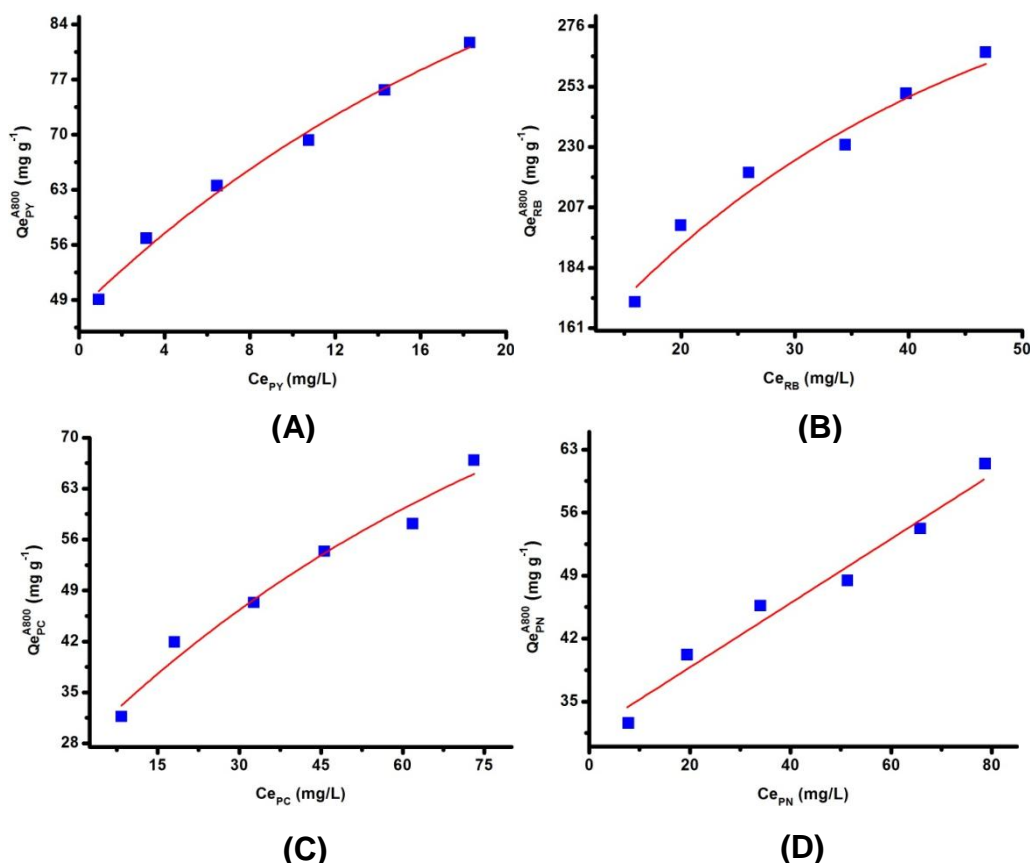
Fig.4.11: Dye adsorption load versus concentration using A800 for (A) PY, (B) RB, (C) PC and (D) PN.

4.3.4.1 Langmuir isotherm model

The Langmuir adsorption isotherm has been successfully applied to many adsorption processes. The linear form of this isotherm is represented by the following equations[184]:

$$\text{Linear equation:} \qquad \frac{C_e}{Q_e} = \frac{1}{Q_m\,K} + \frac{C_e}{Q_m} \qquad \textbf{[1]}$$

Inverse of slope is Q_m which is the maximum adsorption capacity of adsorbent to remove pollutant. Inverse of ([intercept]*[Qm]) is constant of equilibrium.

$$K = \frac{1}{Q_m \text{ Intercept}} \qquad \text{[2]}$$

Where C_e is the adsorbate concentration at equilibrium (mg/L), Q_e the adsorption load at equilibrium, K is constant of equilibrium. Q_m is the maximum monolayer adsorption capacity of the solid (mg/g).

This model assumes a monolayer coverage of adsorbate on the homogeneous surface of the adsorbent. This isotherm makes the simple assumption that adsorption is occurring at specific homogeneous sites within the adsorbent and that, once an adsorbate molecule is occupying this site, no further adsorption can take place on it.[308]

The essential characteristics of a Langmuir isotherm can also be expressed by a dimensionless constant called a separation factor or equilibrium parameter, R_L, defined by Weber and Chakkravorti as follows[309]:

$$R_L = \frac{1}{1 + K_L . C_o} \qquad \text{[3]}$$

Table.4.7: Equilibrium parameter (R_L) value pretending for Langmuir isotherm model

Value of R_L	Type of isotherm
$R_L > 1$	Unfavourable
$R_L = 1$	Linear
$0 < R_L < 1$	Favourable
$R_L = 0$	Irreversible

4.3.4.2 Freundlich adsorption isotherm model

K_F can be defined as the adsorption or distribution coefficient and represents the quantity of dye adsorbed onto A800 for a unit equilibrium concentration. Qe is the amount of dye (mg) adsorbed by a gram of a solid material. This model describes multilayer adsorption.[185] The slope 1/*n* ranging between 0 and 1 is a measure of adsorption intensity or surface heterogeneity, becoming more heterogeneous as its value gets closer to zero. A value for 1/*n* below one indicates a normal Langmuir isotherm while 1/*n* above one is indicative of cooperative adsorption.[310]

$$\mathbf{LnQ_e = lnK_F + \frac{1}{n}lnC_e} \qquad \textbf{[4]}$$

4.3.4.3 Temkin adsorption isotherm model

A Temkin isotherm contains a factor that explicitly takes into account the adsorbent-adsorbate interactions. The heat of adsorption of all the molecules in the layer would decrease linearly with coverage due to adsorbent-adsorbate interactions. The adsorption is characterized by a uniform distribution of binding energies, up to some maximum binding energy. The Temkin isotherm is expressed as follows[311, 312]:

$$\mathbf{Q_e = \frac{RT}{b}LnA + \frac{RT}{b}LnC_e} \qquad \textbf{[5]}$$

where RT/b= B (J/mol), which is the Temkin constant related to heat of sorption whereas *A* (L/g) is the equilibrium binding constant corresponding to the maximum binding energy. R (8.314 J/mol K) is the universal gas constant and T is the absolute solution temperature in Kelvin.

4.3.4.4 Dubinin-Radushkevich (D-R) adsorption isotherm model

The Dubinin and Radushkevich model can be used to describe adsorption onto porous solids. It assumes that there is not an homogeneous surface on the adsorbent. Assuming that the adsorption is limited to a monolayer, the D-R equation can be used to estimate the energy of adsorption. The equation is expressed as follows:

$$\mathbf{Q_e = Q_e e^{(-K\varepsilon^2)}} \qquad \textbf{[6]}$$

The linear form of the equation was used to model the adsorption as follows[313,314]:

$$\mathbf{lnQ_e = lnQ_m - K\varepsilon^2} \qquad \textbf{[7]}$$

$$\mathbf{\varepsilon = RT\,ln\left(1 + \frac{1}{C_e}\right)} \qquad \textbf{[8]}$$

Where Q_m signifies the monolayer saturation capacity (mg/g) and K the constant of adsorption energy which gives the mean free energy (E) of adsorption per molecule of adsorbate when it is transferred to the surface of the solid from the solution and can be calculated from the following equation:

$$\mathbf{E} = \frac{1}{\sqrt{2\mathbf{K}}} \qquad \textbf{[9]}$$

The mean adsorption energy (E) gives information about chemical and physical adsorption, where E in the range of 8-16 kJ mol^{-1} indicates physical adsorption of the adsorbate.

According to equations (1, 4, 5 and 6) of the adsorption isotherm model, all results are summarised in Tables 4.8-4.10 for A800's, A450's and Ac's isotherm parameters. Those R^2 values of the Langmuir isotherm for PY, RB, PC, PN which were obtained are in an acceptable range between 0.992 and 0.999. These four values of the correlation coefficient are higher than R^2 in the other three isotherms modes. In all cases, the Langmuir equation yielded the best fit of experimental data compared to the other isotherm models. This indicates that the dye molecules formed monolayer coverage on the adsorbent.[308] It indicates that the adsorbents have a uniform shape and size and dye molecules was adsorbed equivalently on the sites and interior pores of the adsorbent materials with may be no sidelong interaction and steric hindrance between the adsorbed dye molecules.[315]

In addition, the Q_m values calculated from Langmuir model fitted well with the experimental data. Further information from Freundlich model confirms the well fitted applicability of the Langmuir model for the dye removal. This is because all the 1/n values from the Freundlich model are between 0 and 1 which indicates a normal Langmuir.[310] Equilibrium parameter (R_L) values for the Langmuir isotherm model can be calculated based on the initial concentration of dye solution and the K (constant of equilibrium) found in Tables 4.8-4.10. (Plots of all of these experiments are listed in the Appendix four).

Table.4.8: Employing A800 and using different isotherm models to describe adsorption

A800	PY	RB	PC	PN
Langmuir: $\frac{C_e}{Q_e} = \frac{1}{Q_m K} + \frac{C_e}{Q_m}$				
K(L/mg)	0.6523	0.0615	0.1437	0.1214
Q_m (mg/g)	84.7	355	84	65.1
R^2	0.999	0.994	0.993	0.992

Freundlich: $LnQ_e = lnK_F + \frac{1}{n}lnC_e$				
K_F	48	62.8	16	19.58
1/n	0.16476	0.3733	0.32004	0.2441
R^2	0.95	0.91	0.96	0.916
Tempkin: $Q_e = \frac{RT}{b}LnA + \frac{RT}{b}LnC_e$				
B (J/mol)	10.3814	80.36384	14.824	10.828
A (L/g)	94	1.81	1.080	2.31
R^2	0.91	0.84	0.92	0.86
D-R: $lnQ_e = lnQ_e - K\varepsilon^2$				
Q_m (mg/g)	95	320	70	56.2
$Kx10^{-3}$ (mol^2/J^2)	1.6	4.1	2.6	1.9
E (J/mol)	2	0.35	0.4385	0.513
R^2	0.683	0.91	0.84	0.781

Table.4.9: Employing A450 and using different isotherm models to describe adsorption

A450	PY	RB	PC	PN
Langmuir				
K (L/mg)	0.0977	0.15208	0.0133	0.043
Q_m (mg/g)	72	146.8	23.6	40.3
R^2	0.997	0.994	0.994	0.992
Freundlich				
K_F	18.8	72.7	17.6	4.188
1/n	0.31281	0.1444	1.7563	0.8548
R^2	0.98	0.51	0.93	0.92
Tempkin				
B (J/mol)	15.303	0.1438	16.608	7.579
A (L/g)	1.2	0.2234	33.7	19.595
R^2	0.96	0.44	0.90	0.88
D-R				
Q_m (mg/g)	67	145	31	20.82
$Kx10^{-3}$ (mol^2/J^2)	2.5	2.25	4.28	2.15
E (J/mol)	0.63	0.47	3.3	0.153
R^2	0.88	0.38	0.90	0.871

Table.4.10: Employing AC and using different isotherm models to describe adsorption

AC	PY	RB	PC	PN
Langmuir				
K (L/mg)	0.1439	0.1554	0.1931	0.3635
Q_m (mg/g)	29	104.1	17.6	8
R^2	0.997	0.996	0.95	0.992

Freundlich				
K_F	17	18.1	1.42	9.188
1/n	0.101	0.15146	0.103	0.055
R^2	0.68	0.6	0.86	0.25
Tempkin				
B (J/mol)	2.5074	15.317	9.44937	0.4232
A (L/g)	393	0.3541	15.5	8.56
R^2	0.5	0.74	0.79	0.21
D-R				
Q_m (mg/g)	27	87	24.48	3.3
$K \times 10^{-3}$ (mol^2/J^2)	1.62	2.64	1.5	1.76
E (J/mol)	0.6	0.44	0.181	0.533
R^2	0.42	0.83	0.77	0.15

All the R_L values were between 0 and 1, indicating that the adsorption of dye on the prepared A800 was favourable at the conditions being studied. For example, for PC dye adsorption using A800, as the initial concentration increased from 40 to 140 mg/L, the R_L values decreased from 1.482×10^{-3} to 4.74×10^{-4}. This indicated that adsorption was more favourable at higher concentrations.[316]

4.3.5 Thermodynamics parameters for the adsorption

Thermodynamics is a tool in science used to describe processes that involve changes in temperature, transformation of energy, and the relationships between heat and work. Therefore, in order to understand dye adsorption in this chapter, the thermodynamic parameters such as enthalpy (ΔH) and entropy (ΔS) of adsorption are calculated. The parameters in this section can be used for the temperature effect on dye adsorption using the following equations[317]:

$$\Delta G = -RT \, LnK \quad [10]$$

$$LnK = -\frac{\Delta H}{RT} + \frac{\Delta S}{R} \quad [11]$$

Where K is the equilibrium constant obtained for each temperature from the Langmuir model, R is the molar gas constant (8.314 J/mol K) and T is the absolute temperature. ΔH and ΔS were obtained from the slopes and intercepts of the linear plots of lnK against 1/T. ΔH is the amount of energy gained or released as adsorption takes place between the adsorbate-adsorbent. ΔS

presents the degree of disorder or freedom at solid/liquid interface. These thermodynamic parameters are described as follows[318]:

ΔH= - value, which means that the adsorption between the adsorbate and adsorbent is exothermic. ΔH= + value, which means the adsorption between the adsorbate and the adsorbent is endothermic.

ΔS= + value, which means the adsorption is spontaneous. ΔS= - value, which means the adsorption is non-spontaneous. ΔG= - value means adsorption is spontaneous and vice verse.

4.3.6 Thermodynamic analysis of dyes adsorption

Further work was done to find thermodynamic parameters of adsorption such as energy (E_{ads}) and entropy (ΔS_{ads}) of adsorption using the two most promising adsorbers (A800 and AC). Langmuir equilibrium constants for each dye-carbonaceous system (i.e. RB-A800, RB-AC, PY-A800, PY-AC etc.) were obtained using the method described in section 4.3.4.1 for each dye at temperatures 25, 35, 45 and 55 ^{o}C respectively (Plots of all of these experiments are listed in the Appendix four). The constants of equilibrium together with the maximum dye adsorption values obtained for each experimental system can be found in Tables 4.11- 4.14. It can be noticed from these tables that the correlation coefficient (R^2) for all experiments is within an acceptable range (above 0.990).

Table.4.11: Results obtained for Procion Yellow (PY) dye when adsorption took place at different temperatures employing A800 and AC

Using **A800** adsorbent for **PY**: Adsorption was done at 25, 35, 45 and 55 ^{o}C				
T ^{o}C	Q_m (mg/g)	K (L/mg)	R^2	
25	84.7	0.6523	0.997	E_{ads} (Enthalpy)= -9 KJ/mol Entropy= 32.1 J/mol K
35	84.5	0.5428	0.99	
45	81.2	0.5189	0.991	
55	80	0.4689	0.96	
Using **AC** adsorbent for **PY**: Adsorption was done at 25, 35, 45 and 55 ^{o}C				
25	29.1	0.1439	0.993	E_{ads} (Enthalpy)= -51.2 K J/mol Entropy= 188.3 J/mol K
35	29	0.0593	0.991	
45	27.6	0.04118	0.96	
55	26	0.01998	0.94	

Table.4.12: Results obtained for Remazol Black (RB) dye when adsorption took place at different temperatures employing A800 and AC

Using **A800** adsorbent for **RB**: Adsorption was done at 25, 35, 45 and 55 ^{o}C				
T ^{o}C	Q_m	K (L/mg)	R^2	
25	355	0.0615	0.995	E_{ads} (Enthalpy)= -17.6 KJ/mol Entropy= 37 J/mol K
35	356	0.048	0.992	
45	348	0.038	0.993	
55	332	0.0323	0.91	
Using **AC** adsorbent for **RB**: Adsorption was done at 25, 35, 45 and 55 ^{o}C				
25	104.1	0.1554	0.996	E_{ads} (Enthalpy)= -46.7 K J/mol Entropy= 172.3 J/mol K
35	104.3	0.08593	0.99	
45	101	0.04152	0.991	
55	98	0.02928	0.95	

Table.4.13: Results obtained for Procion Crimson (PC) dye when adsorption took place at different temperatures employing A800 and AC

Using **A800** adsorbent for **PC**: Adsorption was done at 25, 35, 45 and 55 ^{o}C				
T ^{o}C	Q_m	K (L/mg)	R^2	
25	84	0.20158	0.998	E_{ads} (Enthalpy)= -26 KJ/mol Entropy= 113.2 J/mol K
35	84	0.05651	0.995	
45	82	0.03778	0.991	
55	80	0.02179	0.96	
Using **AC** adsorbent for **PC**: Adsorption was done at 25, 35, 45 and 55 ^{o}C				
25	17.6	0.1931	0.99	E_{ads} (Enthalpy)= -37.2 K J/mol Entropy= 138.7 J/mol K
35	18.1	0.1191	0.991	
45	18.2	0.06128	0.993	
55	15.5	0.05278	0.98	

Table.4.14: Results obtained for Procion Navy (PN) dye when adsorption took place at different temperatures employing A800 and Ac

Using **A800** adsorbent for **PN**: Adsorption was done at 25, 35, 45 and 55 ^{o}C				
T ^{o}C	Q_m	K (L/mg)	R^2	
25	65.2	0.1214	0.994	E_{ads} (Enthalpy)= -8.2 KJ/mol Entropy= 46.8 J/mol K
35	65.3	0.1129	0.996	
45	62	0.09721	0.993	
55	60	0.08911	0.97	
Using **AC** adsorbent for **PN**: Adsorption was done at 25, 35, 45 and 55 ^{o}C				
25	9	0.3635	0.995	E_{ads} (Enthalpy)= -13.7 K J/mol Entropy= 54.2 J/mol K
35	8.8	0.3199	0.997	
45	8	0.2743	0.99	
55	6.5	0.2179	0.95	

The linear dependencies of equilibrium constants obtained according to the temperature of the experiment in Arrhenius coordinates (lnK versus the inverse of the temperature (T in Kelvin degree) for A800 are shown in Figure 4.12. The energies of adsorption (from gradients) and entropy of adsorption (from intercepts) were found from these linear plots. The same procedure was repeated for AC.

Energy of adsorption (E_{ads}) found was distinctly smaller for A800 than of AC. This could be explained by the high degree of activated carbon (AC) microporosity. This means that, when the dye molecules are trapped in the mesoporous system of the material with a low degree of microporosity (e.g A800), the number of interactions made between the dye molecule and the adsorbent surface would be less than the numbers of interaction made between the dye species and surface of materials with high degree of microporosity (e.g. AC). A negative value of the enthalpy for all the systems implies that the dye adsorption process is exothermic (favourable) in nature.
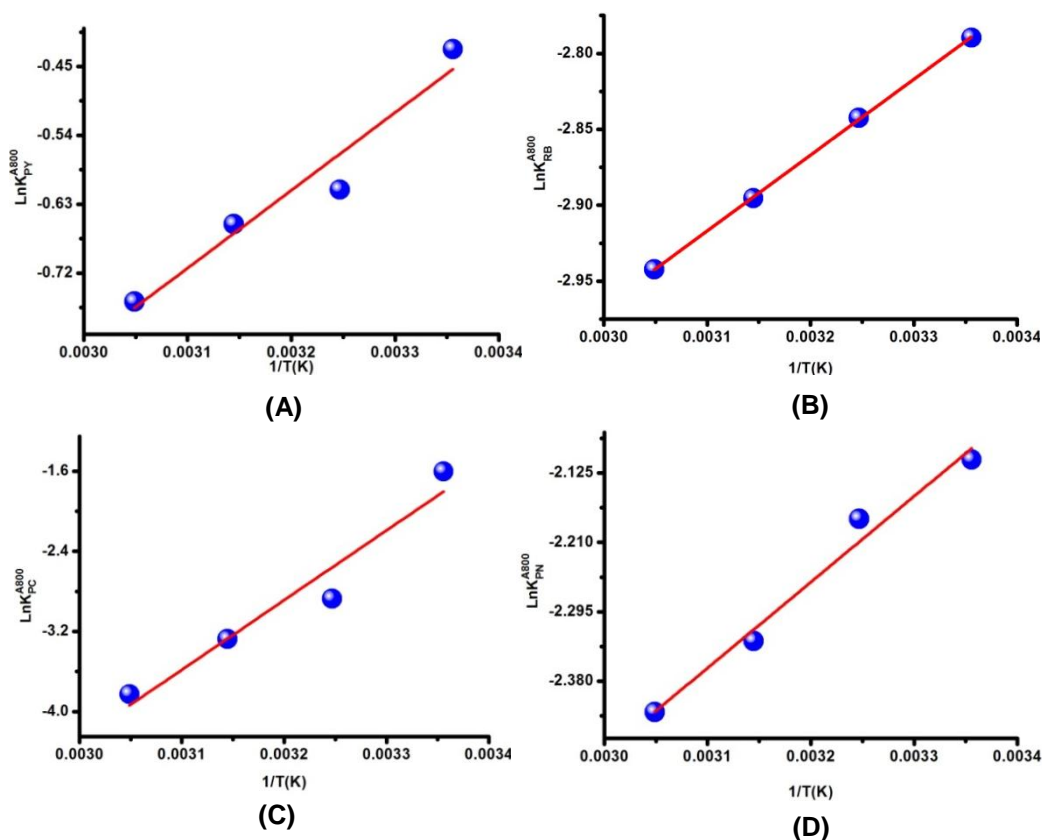
Fig.4.12: LnK versus 1/T(K) for (A) PY, (B) RB, (C) PC and (D) PN adsorption using A800.

As was mentioned above in 4.3.5, the ΔS is corresponding the degree of disorder at solid/liquid interface. All obtained ΔS values are positive which demonstrate that the dye adsorption process was accompanied by a disorder degree which increased within the solid/liquid interface.[319] A number of degrees of freedom had to be reduced for the dyes during the adsorption. Therefore the interface disordering could be relevant to the process of water molecule release. This process of water molecules replacement on the adsorbent surface will massively increase the entropy of the system due to a large number of molecules of water which were displaced as molecules of the dyes were adsorbed. In this case, the actual value of the entropy of adsorption would depend on the shape, size, nature of the dyes and the adsorbent materials.

Altogether experimental results demonstrate that ΔG values obtained are negative at all the temperatures (see Table 4.15). This indicates the thermodynamic feasibility and spontaneity of the dye adsorption.[320] The fact that the changes in free energy increases with an increase in temperature was also noted. This could be explained in terms of how the dye molecules diffused more rapidly from the liquid phase across the solid/liquid interface or external boundary layer and the internal pores of the adsorbent particles.[321] Another possible explanation may be because of the activation of more sites on the surface and interior pore wall of the adsorbents with increase in temperature, which might also cause a quicker rate of dye adsorption.

This explanation would mean that rate of dye adsorption could be faster with an increase in temperature which could cause a faster reaction between the dyes and adsorbents. But an increase in the temperature of the system decreased the maximum dye adsorption. Because elevating temperature might lower the force of adsorption between the dye molecules and the adsorbent.[322]

This means that the faster rate of dye uptake is more favourable with an increase in temperature, while the maximum dye adsorption is less favourable as temperature is increased.

It is concluded that enthalpy is negative and entropy is positive caused a negative Gibbs free energy for all dyes adsorption process system. Process like

that is favoured by both enthalpy and entropy terms which should be favourable or spontaneous.

Table.4.15: Free energy obtained for the dyes at different temperatures using A800 and AC adsorbents

Dyes and adsorbents used	ΔG (KJ/mol)			
	25 °C	35 °C	45 °C	55 °C
PY using A800	-18.536	-18.856	-19.176	-19.496
PY using AC	-107.224	-109.104	-110.984	-112.864
RB using A800	-28.626	-28.996	-29.366	-29.736
RB using AC	-97.956	-99.676	-101.396	-103.116
PC using A800	-59.674	-60.804	-61.934	-63.064
PC using Ac	-78.324	-79.704	-81.084	-82.463
PN using A800	-21.908	-22.368	-22.828	-23.288
PN using AC	-29.792	-30.332	-30.872	-31.412

In addition, the comparison and contrast between the adsorbent dye coverage, surface availability% and energy of adsorption (E_{ads}) for A800 and AC are given in Table 4.16. The surface coverage is lower than 100% for each dye. Therefore, the table demonstrates that, in all cases, monolayer adsorption took place. It is also very important to note that dye surface coverage for AC is always significantly lower than for A800 which is in agreement with high adsorption by the Algibon.

Table.4.16: Comparison between surface area of adsorbent dye coverage and energy of adsorption for A800 and AC adsorbers employed in dye removal

Dye	A800 Dye coverage (m^2/g)	A800 Surface availability %	E_{ads} for A800 (KJ/mol)	Ac Dye coverage (m^2/g)	AC Surface availability %	E_{ads} for Ac (KJ/mol)
RB	499	90%	17	47	20%	46.7
PY	136	25%	9	43	6%	51.2
PC	149	27%	26	32	4%	37.2
PN	169	30%	8.2	21	3%	13.7

4.3.7 Dye desorption experiment

The target of this experiment was to investigate an opportunity to recover dyes adsorbed by the A800 material. A800 was chosen for the dye desorption experiment since it has demonstrated the maximum dye adsorption capacity.

Firstly, adsorption of dye was carried out according to the methodology explained below: 1000 mg of each dye was individually dissolved in a sufficient amount of distilled water in a 500 mL volumetric flask and filled to the mark with distilled water. Before the adsorption experiment, 2.5 mL of each concentrated dye was diluted in 100 mL volumetric flask and measured using UV-VIS spectrometer. These measurements were recorded as initial absorbance (Ao) of the dyes.

To undertake the adsorption experiment, 250 mL of each individual concentrated dye was added into a 500 mL sized bottle flask reactor containing 1 gram of A800. Then adsorption was run for 72 hours with constant stirring. 2.5 mL of the filtrate of each dye solution, after adsorption had been carried out, was taken and then diluted into 100 mL. It was measured by UV-VIS spectrometer. These measurements was recorded as absorbance (Ai) of the dyes after adsorption for 72 hours. Then the amount of dye adsorbed by A800 was found.

The A800 loaded with the individual dye was filtrated and freeze dried. The regeneration of A800 used was carried out using three different techniques: i) Direct thermal treatment, ii) Dye recovery and adsorbent regeneration using solvent and iii) Indirect thermal treatment of A800 loaded with dye: it comprised a combination of warm ethanol (50 ^{o}C) followed by Starbon thermal treatment at 800°C. The third procedure was the most successful. This regeneration procedure of A800 yielded a very good result in which the pores of the A800 were preserved. The regenerated A800 was successfully reused in dye removal application. The following steps were conducted to unload the dyes in the case of A800.

4.3.7.1 Direct thermal regeneration of A800 loaded with dyes

After dye adsorption experiment took place the A800 was filtered out and freeze dried. The success of the approach was estimated by nitrogen adsorption

analysis of the A800 sample contaminated with the dyes. The results measured are shown in Table 4.17 and Figure 4.13

Table.4.17: Porosity analysis results for the initial A800 and the A800 loaded with the dyes

Materials	S_{BET} (m^2/g)	Pore volume (cm^3/g)$_{BJH}$	Pore diameter (nm)$_{Ads}$	Pore diameter (nm)$_{des}$	Meso-porosity%
Initial A800	426	0.84	15.1	14.4	73
A800 loaded with PY dye	284	0.21	92	49	5.6
A800 loaded with RB dye	303	0.17	82	45	4.1
A800 loaded with PC dye	324	0.199	86.5	46	5.2
A800 loaded with PN dye	281	0.188	87.3	46.0	4.5

Fig.4.13: Pore volume of the initial Algibon A800(i) before use in adsorption application, A800 loaded with PY dye (A800+PY), A800 loaded with RB dye (A800+RB), A800 loaded with PC dye (A800+PC), A800 loaded with PN (A800+PN).
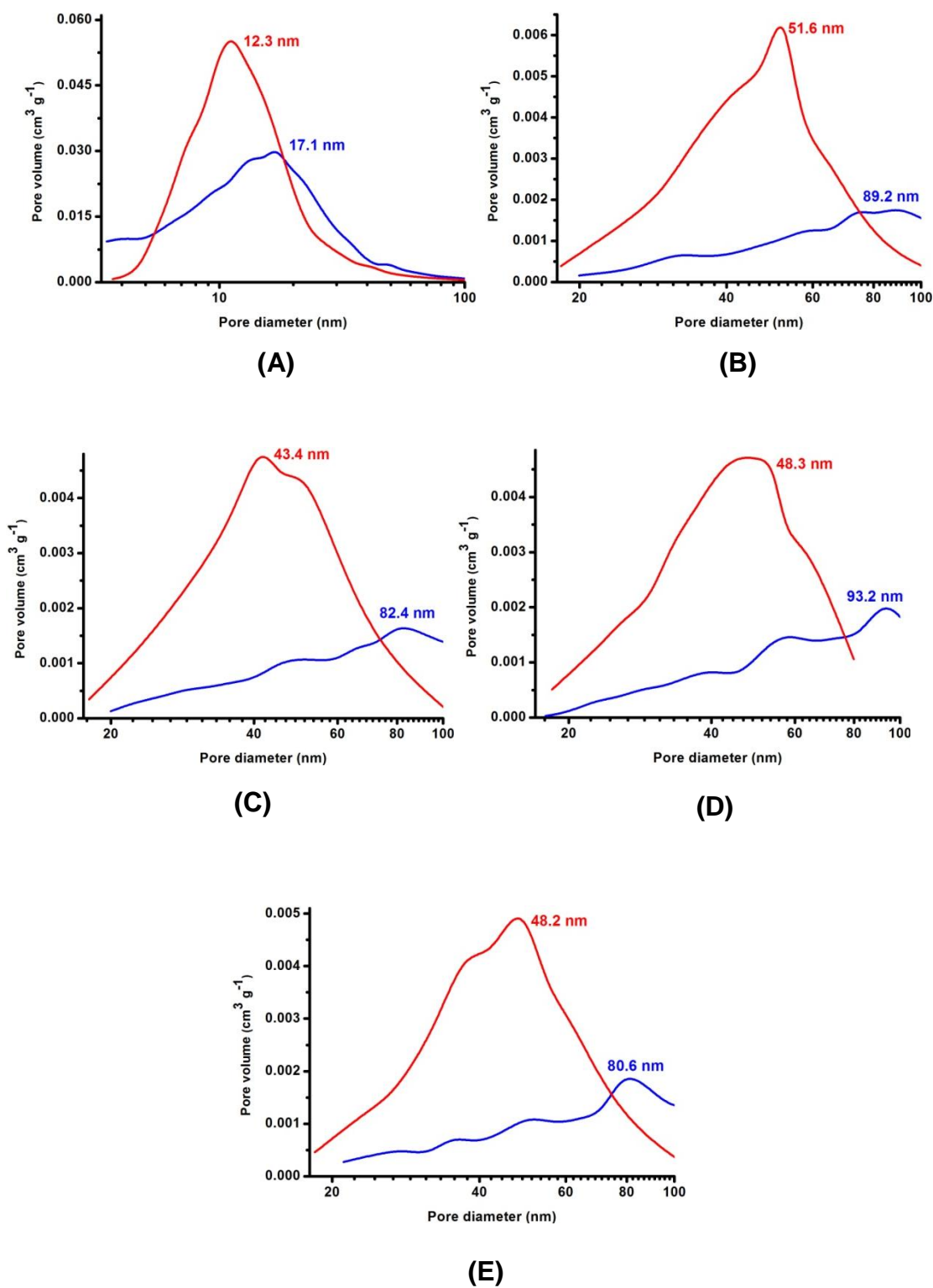
Fig.4.14: dV/dD pore volume (cm³/g) versus diameter (nm) for (A) initial A800, (B) A800 loaded with PY, (C) A800 loaded with RB, (D) A800 loaded with PC and (E) A800 loaded with PN. The blue line colour presents adsorption pore size distribution (dV/dD), the red line colour presents desorption pore size distribution (dV/dD).

It is observed that the pore volume of A800 loaded with the dyes decreased significantly compared to the initial A800 adsorbent before use (see Table.4.17).
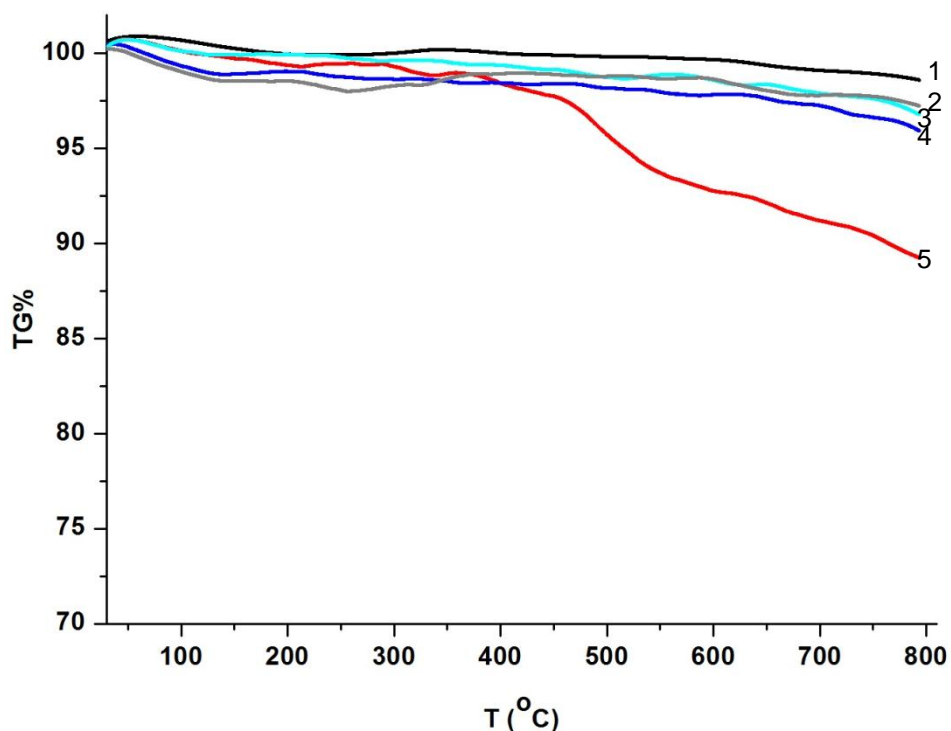
Fig.4.15: TG plot of initial A800 (black colour line 1), A800 loaded with: PN dye (grey colour line 2), PC dye (cyan colour line 3), RB dye (blue colour line 4) and PY dye (red colour line 5).

This is generally due to the dye molecules accumulating in the pores resulting in a massive reduction in the size of the pores in the mesoporous region of A800.

Therefore, in order to regenerate the adsorbent directly, thermal treatment of A800 loaded with the dyes was conducted at 10 ^{o}C/min. from room temperature to 800 ^{o}C (see TG plot in Fig.4.15). It is seen that mass loss for samples containing dyes almost levelled off while the original A800 did not change up to 800 ^{o}C.

The most important point to make is that the observed changes are quite small and corresponds to a few percentage of the adsorbed dye. This shows that the dyes are not desorbed as complex organics, but rather the dyes are not decomposed, possibly involving reaction with the support material.

Furthermore, the porosimetry results of the direct thermally treated A800 can be found in Table 4.18. This shows that direct treatment of the adsorber loaded with dyes does not help to regenerate the A800 nor recover the captured dyes.

Table.4.18: Porosity analysis results for the initial A800 and the direct thermally treated A800 loaded with the dyes

Materials	S_{BET} (m^2/g)	Pore volume (cm^3/g)$_{BJH}$	Pore diameter (nm)$_{Ads}$	Pore diameter (nm)$_{des}$
Initial A800	426	0.84	15.1	14.4
Direct thermally treated A800 loaded with PY dye	Not performed	Not performed	Not performed	Not performed
Direct thermally treated A800 loaded with RB dye	Not performed	Not performed	Not performed	Not performed
Direct thermally treated A800 loaded with PC dye	Not performed	Not performed	Not performed	Not performed
Direct thermally treated A800 loaded with PN dye	Not performed	Not performed	Not performed	Not performed

4.3.7.2 Dye unload and adsorber regeneration using solvent

It was noticed in 4.3.7.1 that direct thermal treatment of the A800 loaded with the dyes had not been successful. Therefore, It was proposed to apply a desorbent, including water, as the cheapest inorganic solvent and then ethanol as a green renewable and environmental friendly organic solvent to carry out the regeneration of the adsorbent material.
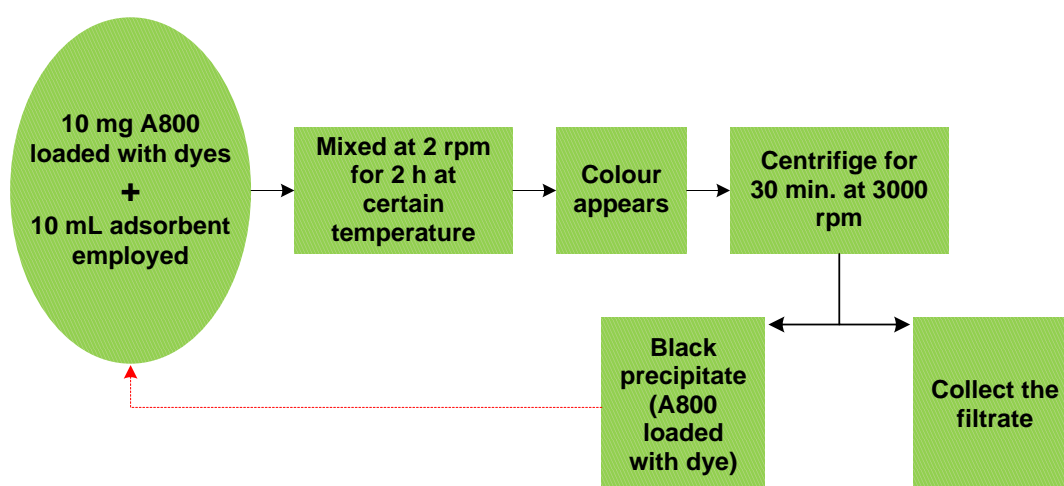
Fig.4.16: Desorption process.

Firstly desorption of the A800 loaded with the dyes was conducted using distilled water (D.W) at 30 and 50 ^{o}C at low stirring rate (2 rmp) to test the temperature influence on desorption process. In addition, desorption of the dyes was conducted at both temperatures employing ethanol to test the desorption efficiency of both desorbing agents to unload the dyes from the A800 and regenerate the adsorbent material used.

It was found that a temperature of 30 ^{o}C resulted in the desorption of small amounts of the dyes loaded with the A800 into the water aqueous phase. At 50 ^{o}C the desorption percentage increased by a few percent. The desorption percentage when ethanol was used was greater than that using water. Ethanol desorption efficiency at 50 ^{o}C was approximately 5% greater than of employing ethanol at 30 ^{o}C. Plots 4.17-4.21 demonstrate the competition between water and ethanol desorbents at both temperatures 30 and 50 ^{o}C.
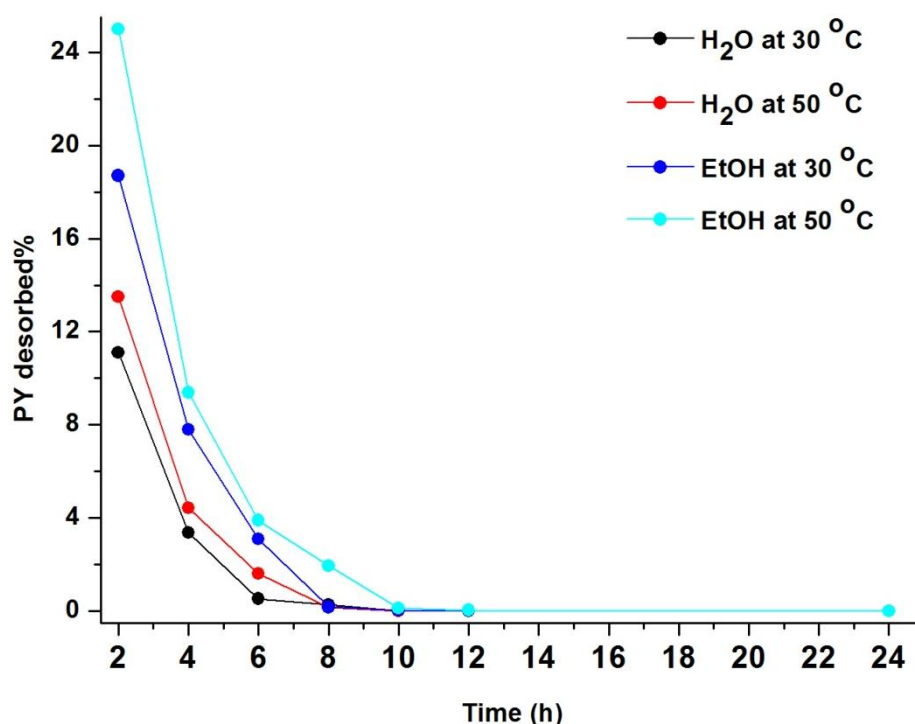
Fig.4.17: Procion Yellow (PY) desorption% using water and ethanol at 30 and 50 ^{o}C.
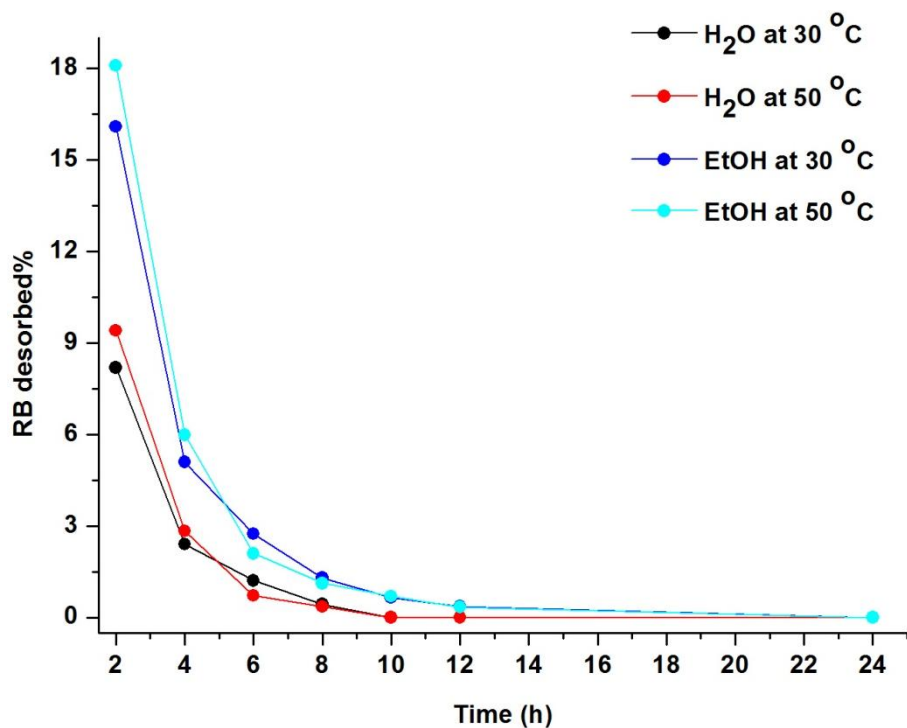
Fig.4.18: Remazol Black (RB) desorption% using water and ethanol at 30 and 50 ^{o}C.
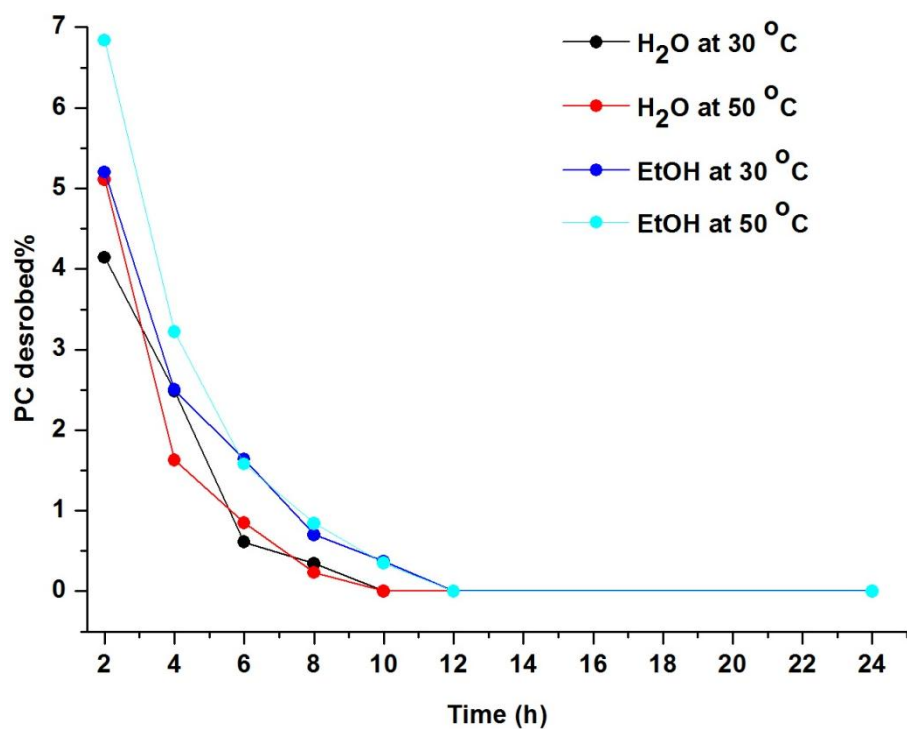
Fig.4.19: Procion Crimson (PC) desorption% using water and ethanol at 30 and 50 ^{o}C.

148
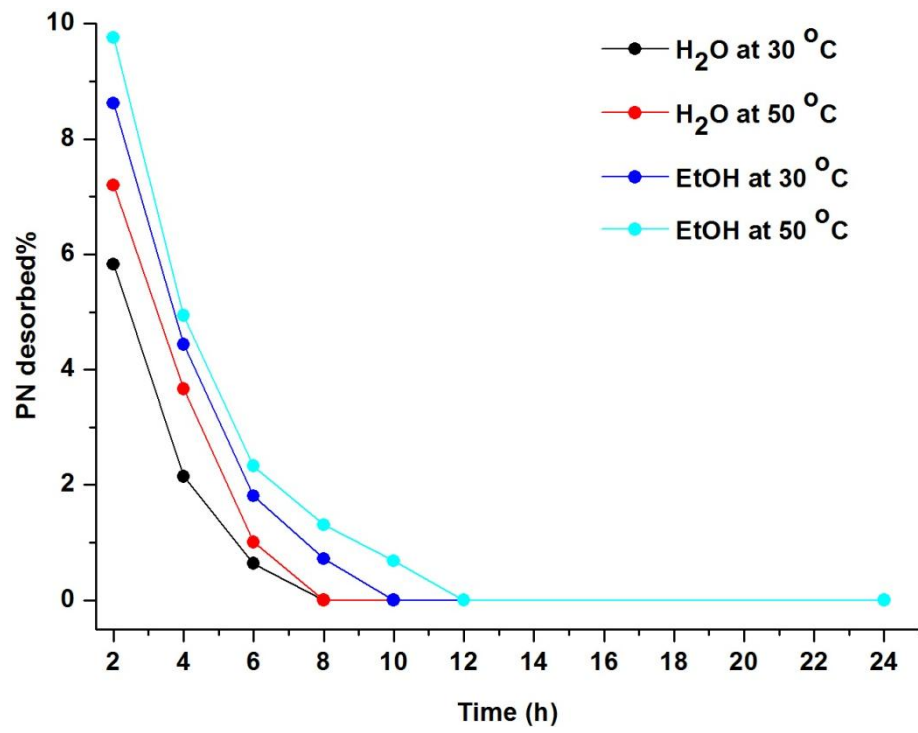
Fig.4.20: Procion Navy (PN) desorption% using water and ethanol at 30 and 50 ^{o}C.
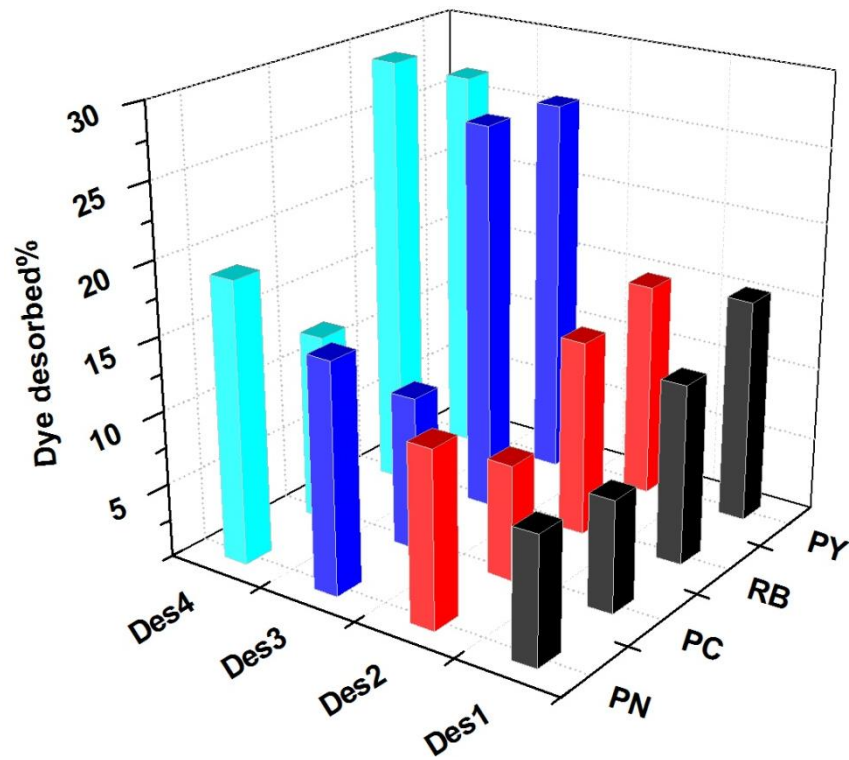
Fig.4.21: Total dyes desorped% using water and ethanol at 30 and 50 ^{o}C. Des1: H_2O at 30 ^{o}C, Des2: H_2O at 50 ^{o}C, Des3: EtOH at 30 ^{o}C and Des4: EtOH at 50 ^{o}C.

Figures 4.17 to 4.21 demonstrate that a H_2O desorbent at 30 ^oC can desorb the dyes up to certain levels between (6% for PC), (10% for PY), (11% RB) and (9% for PN), and its efficiency to desorb the dyes at 50 ^oC is increased by a few percent. This may be due to the better diffusion of warm water molecules through the hydrophobic A800 loaded with the dyes which caused the loaded dyes to become soluble.

Ethanol desorbes dyes better probably due to its good miscibility with hydrophobic and hydrophilic media. This diffusion was enhanced as the temperature of the system was increased to 50 ^oC which would cause the warm ethanol molecules to accelerate and penetrate better through the A800 loaded with the dyes.

Unfortunately, depending on the desorption study it was observed that these bulky dyes could only be unloaded up to a certain level which was just around 20% even with the use of warm ethanol. Therefore, the next step used for regenerating the Agibon used will be carried out by applying a combination of warm ethanol wash and thermal treatment.

4.3.7.3 Indirect thermal treatment of A800 loaded with dye

In this section, the loaded A800 with the dyes (0.5 gm) was firstly washed with warm ethanol at (50 ^oC) a few times to remove as much loaded dye as possible. It was then thermally treated in Netzsch by running and controlling a temperature programme (10 ^oC per minute up to 800 degree) under nitrogen gas. A combination of warm ethanol wash and then thermal treatment aimed to regenerate the A800 by thermal decomposition of the dyes. In this case, thermal decomposition of two dyes was carried out. One of these was a large bulky dye called Procion Crimson (PC); the other one was RB which is the smallest bulky dye among the dyes used.

There is a TG figure of regenerated A800 loaded with the PC and RB dyes which were thermally treated to 800 ^oC (see Figure 4.22), after warm ethanol wash had been done. There is a significant mass loss in lines 2 and 3 compared to the initial A800 (line 1). This seems to have occurred due to the thermal decomposition of the organic dyes in A800. Reason for excellent thermal decomposition of dyes in A800, after warm washing with ethanol, would relate to the miscible character of ethanol. Throughout desorption process,

ethanol at 50 ^{o}C could better undergo diffusion through the major part of the adsorbent. This could partially solublise some quantities or volumes of the dyes already loaded into the mesoporous hydrophobic region of Algibon. Therefore, this desorption using ethanol could assist in partly deblocking and reconnecting the inner nanostructured channel networking system of Algibon. Thereafter, throughout under nitrogen thermal treatment of the polluted A800 ethanol washed, the flow N_2 gas goes through the partially deblocked or reconnected nanostructured Algibon loaded with dyes. This caused the stream of nitrogen gas gradually evacuated the volatiles and gases emitted from the polluted A800 during the thermal dye decomposition up to 800 ^{o}C. This avoids the volatiles, for examples water, being collected and condensed in the pores of the thermally treated Algibon.
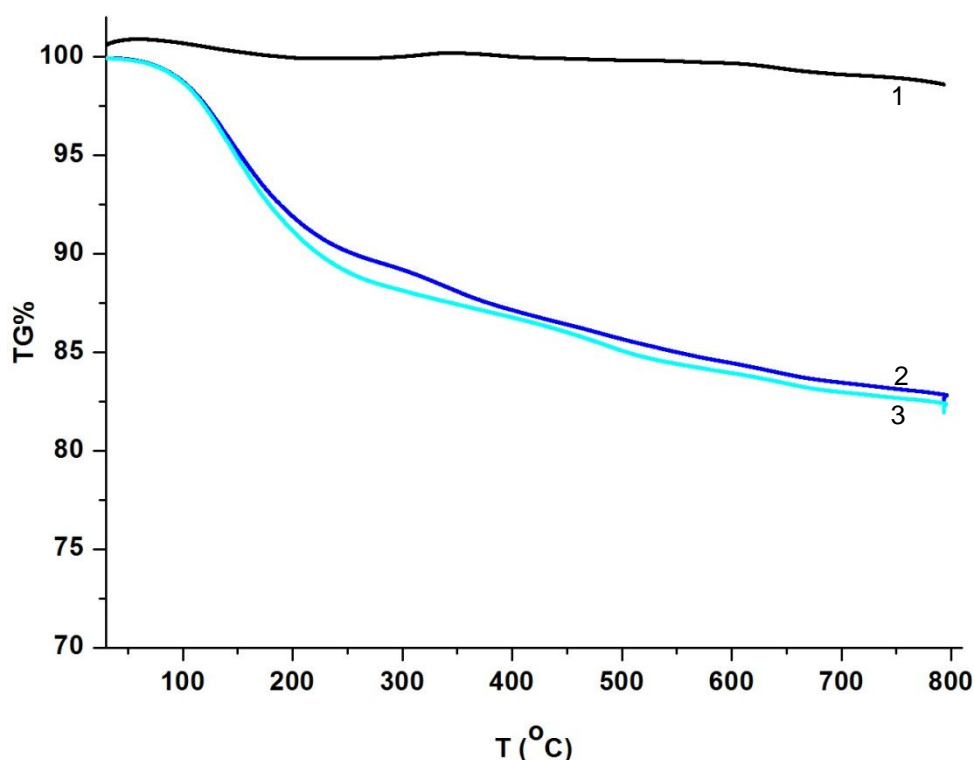
Fig.4.22: The TG figure of initial A800 is the black colour line 1, indirect thermal treatment of A800 loaded: with RB is the blue colour line 2, with PC dye is the cyan colour line 3.

Nitrogen adsorption analysis (porosimetery) was measured (see Table 4.19) for regenerating A800 by indirect thermal treatment. In Figure 4.23 the pore volume of A800 loaded with each single dye was plotted as well as compared to the pore volume of the initial Algibon A800(i) and the regenerated Algibon A800 (r). Fortunately, one of the important aims of the research was achieved since this

method of regeneration yielded a promising outcome since it was able to thermally decompose the organic dye in the pores of A800. According to the results obtained, the porous structure of the thermally regenerated A800 was maintained and was similar to the initial A800 before use.

Table.4.19: Porosity analysis results for the initial Algibon A800(i), Algibon loaded with dyes and the indirect thermaly regenerated Algibon A800(r)

Materials	S_{BET} (m^2/g)	Pore volume $(cm^3/g)_{BJH}$	Pore diametre $(nm)_{Ads}$	Pore diameter $(nm)_{des}$	Meso-porosity%
Initial Algibon A800(i)	426	0.84	15.1	14.4	73
A800 loaded with PY dye	284	0.21	92	49	5.6
A800 loaded with RB dye	303	0.17	82	45	4.1
A800 loaded with PC dye	324	0.199	86.5	46	5.2
A800 loaded with PN dye	281	0.188	87.3	46.0	4.5
Indirect thermally regenerated Algibon A800(r)	420.7	0.85	15	14.88	72.5
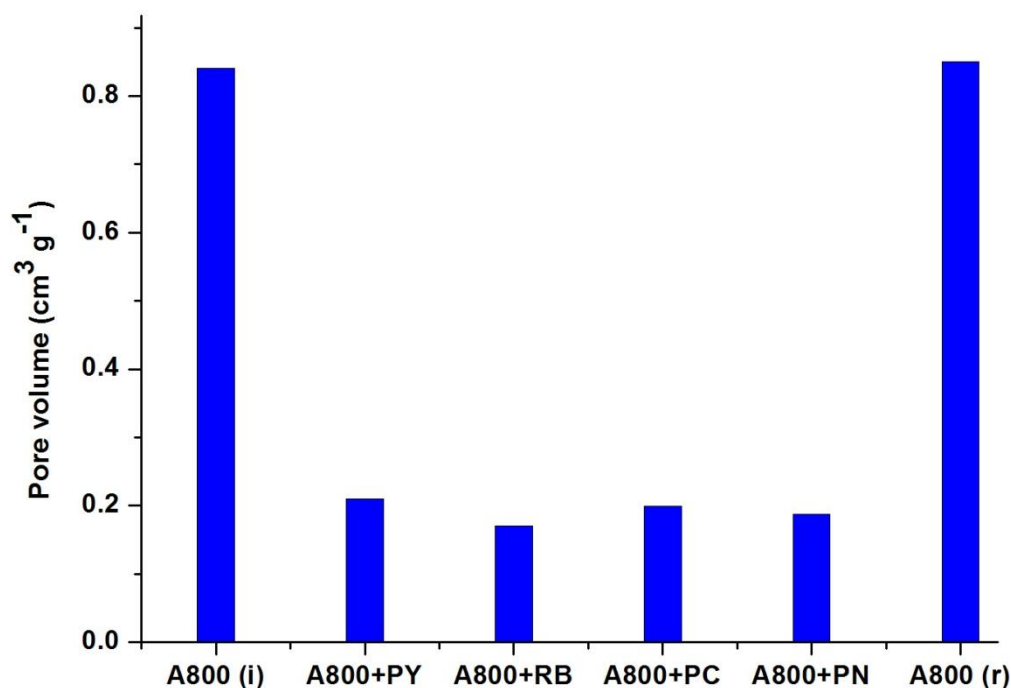
Fig.4.23: Pore volume of the initial Algibon A800(i) before use in dye adsorption application, A800 loaded: with PY dye (A800+PY), with RB dye (A800+RB), with PC dye (A800+PC), with PN (A800+PN) and indirect thermally regenerated Algibon A800 (r).

(A)   **(B)**
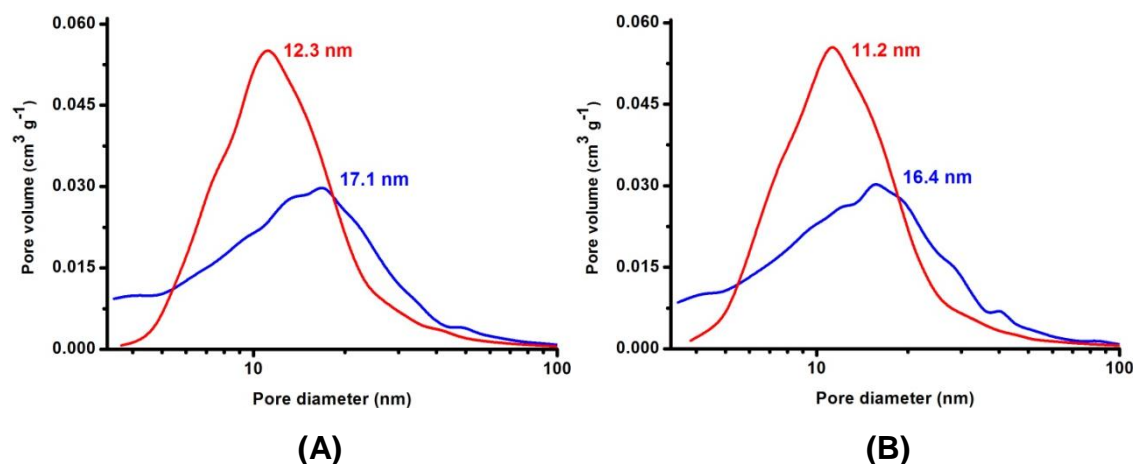
Fig.4.24: dV/dD pore volume (cm³/g) against pore diameter for (A) initial Algibon A800(i) and (B) indirect thermally regenerated Algibon A800(r). The blue line colour presents the adsorption pore size distribution (dV/dD), while the red line colour presents the desorption pore size distribution (dV/dD).

4.3.8 Re-employing regenerated A800 for dye adsorption application

This section gives information on the dye adsorption capacity for the regenerated Algibon adsorbent A800(r) which was restored by indirect thermal treatment.

The regenerated Algibon A800(r) was employed to remove dyes in water stream and compared to the initial Algibon A800(i). To do this, 10 mg of A800(r) was employed into 10 mL of each individual PN dye solution concentration (40, 60, 80, 100, 120 and 140 mg/L) and the adsorption took place for 72 hours with constant stirring. But in case of RB dye, only 5 mg of A800(r) was employed into 25 mL of different RB dye solution concentration (40, 60, 80, 100, 120 and 140 mg/L) and held for 72 hour with constant agitation. Then a Langmuir model was applied to find the dye maximum adsorption capacity by A800(r). The same steps were repeated for both dyes using initial Algibon A800 (i).

The results are presented in Table 4.20, (Plots of all of these experiments are listed in the Appendix four), show that the regenerated Algibon A800(r) has a similar dye adsorption capacity to the initial Algibon A800(i). This means that the A800(r) can be reused for dye removal in water streams successfully. Re-employing the regenerated adsorbent for water treatment could have some advantages including a reduction in the cost of A800 production, saving the

wasting of solvents and time as well as effort to generate A800 from the expanded alginic acid precursor.

Table.4.20: Comparing dye adsorption capacity by using the A800(r) and the A800(i)

A800 (i)	RB	PN
Langmuir		
K(L/mg)	0.1142	0.7107
Q_m (mg/g)	207	56
R^2	0.995	0.998
A800 (r)	**RB**	**PN**
Langmuir		
K(L/mg)	0.1243	0.6843
Q_m (mg/g)	198	54
R^2	0.993	0.996

4.4 Conclusion

Mesoporous carbonaceous materials, which had been derived from the expanded alginic acid precursor mentioned in chapter three, were employed in the adsorption of bulky organic dyes from water. The maximum dye adsorption capacity using A800 was compared to the activated carbon (AC). Its effectiveness for large dye uptake was compared magnificently better to the activated carbon. This is due to a high degree of mesoporosity and the unique surface functionality of the A800 used.

It was noticed that the adsorption between the adsorber and the substrates depends on the nature of the adsorbent, shape and size of the dye molecules. For instance, the adsorption capacity of RB dye by the adsorbents used was greater than the PY dye. This is due to the planar dimensional molecular structure of the RB compared to the molecular structure of PY which is bulkier and not planar in structure. This would mean that this dye cannot be captured as much or as well as was captured in the case of RB. It was found that the best type of adsorption isotherm model was the Langmuir model which

demonstrated that the adsorbent particles were uniform and that the type of adsorption was a monolayer adsorption. This means that the dyes were adsorbed as a single layer would be without lateral interaction between the adsorbed dye molecules.
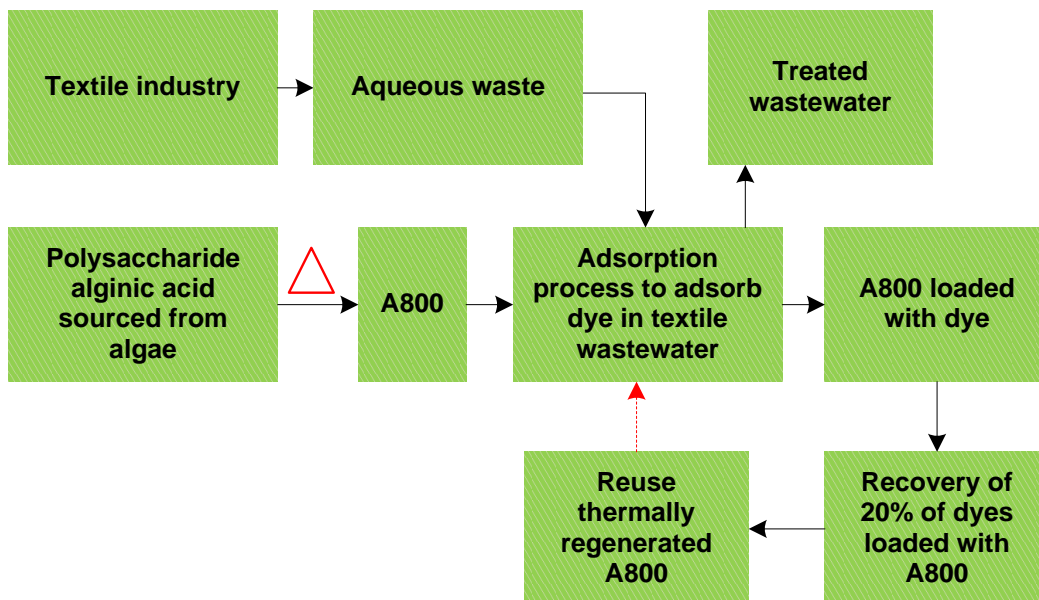
Fig.4.25: Dye adsorption in water stream using A800 and then regenerated A800 reuse in bulky dye removal application.

It is proposed that the mechanism of adsorption is π-π interaction between the aromatic like layer of the A800 adsorbent and the dyes.

It was demonstrated that the dye adsorption process at room temperature yielded a very good set of dye removal results. This is feasible for research and industry because it reduces energy consumption and the cost of dye adsorption treatment. Another interesting point is that A800 required less energy of adsorption compared to the Ac due to the less microporous properties of A800.

Desorption experiment revealed that dye desorption could be carried out using ethanol. Warm ethanol at 50 ^{o}C had better efficiency than ethanol at 30 ^{o}C. Desorption using ethanol showed better efficiency than water in both temperatures (30 and 50 ^{o}C). Indirect thermal treatment of A800 loaded with dye, which consists of warm ethanol wash and thermal pyrolysis, regenerated A800. The regenerated Algibon is called A800(r) and has a very good textural property in which the pore volume and diameter are similar to the initial Algibon

A800(i). This means A800 is very stable and its pores structure is preserved from collapsing throughout the entire processes.

The regenerated Algibon A800(r) obtained was re-employed to capture the dyes from water. The maximum dye adsorption capacity by the regenerated Algibon A800(r) is similar to the initial Algibon A800(i).

These critical and important results can have value in repair of the world where water pollution is due to large organic contaminants is a major problem. The ability to use material that can be derived from natural resources and their relative ease of regenerability and reuses are constituent with the modern trade toward a Circular Economy.

CHAPTER FIVE

Starbon Technology Used in Recovery of Metals From Waste Water

5.1 Introduction

This part of the project involved the use of the developed Starbon materials[323] to capture the metals mentioned on the EU's critical list of elements[324,325]. These metals are increasingly used in novel industrial areas such as the production of electric cars, energy saving light bulbs, fuel cells, catalytic converters, photovoltaic cell, generators (i.e. for wind, tidal and wave turbines), alloy in aircraft turbines industry, medical applications, catalysts as widely used in the chemical and related industries and many other types of industry which have grown rapidly during last few decades due to the demand for low carbon technologies and their importance for the development of a modern economy.[325-327] These elements are in shortage because of their vast usage and limited existence in a few geographical locations on the earth (see figure 5.1).[328] These elements are at great risk since it has been reported that some of them will run out within the next 50 years.[329-331] Therefore, the discovery of a proper methodology to capture such elements from the solid waste materials is vital for the protection of valuable resources, since metals can be recycled in the environment without losing their important properties.

However, although there are many conventional processes used for heavy metals recovery from wastewater, they are not specific (all metals removed altogether as a sludge), especially for dilute solutions and, in many cases, removing them requires high energy consumption [332,333].

The objective of this chapter was to screen the variety of carbonaceous materials derived from native polysaccharides (e.g. starch and alginic acid) in the metals adsorption from the water stream which resulted from digesting solid wastes. These ores were Pulverised fly ash (PFA), Red Mud (RM), Bottom ash (BA), Titano gypsum (TiG), Red Titano gypsum (RTiG) and Phospho Gypsum (PG).

A consultancy firm in North Yorkshire (Link2energy) has proposed to find a way of using a massive amount of such solid wastes which are rich in high value important metals. These ore materials contained toxic, valuable and critical metal ions including Ag, Cd, Li, Ti, Au, Sc, Be, Co, W, V and Ni.

The Starbon materials could improve the technological process of metals recovery due to specific adsorption by their controllable functional groups as

well as increasing the rate of sorption processes as a result of their mesoporosity. It has been found that Starbons worked well in the separation of the metals listed on the EU's critical list.[324,325] It was demonstrated that the A800 adsorbent material is the one of the best. Therefore the adsorption of a number of metals (i.e. Co, Cu, Ag and Cd) in a sample solution by the A800 material was further investigated including determination of types of adsorption, kinetic adsorption and evaluation of kinetic parameters of the process.
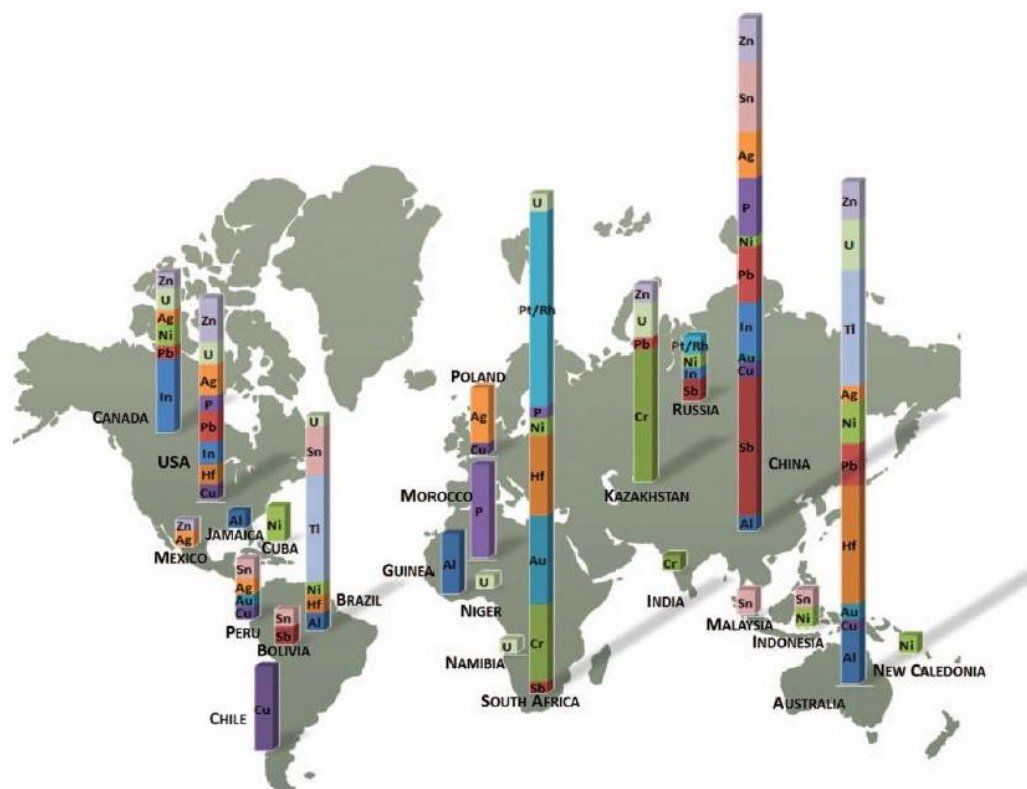
Fig. 5.1: Distribution of rare and precious metal reserves around the world.[328]

Table.5.1: List of EU critical elements[324,325]

Rare earths	Cobalt	Tungsten	Nickel	Tin	Beryllium
Gallium	Niobium	Molybdenum	Cadmium	Niobium	fluorspar
Platinum group metals	Tellurium	Selenium	Magnesium	Chromium	graphite
Tantalum	Germanium	Hafnium	Silver	Antimony	Indium

It has been decided to focus our research specifically on the recovery of the metals from the above table which presents the EU critical elements.

5.2 Experimental section

one gram of each ash (pulverised fly ash, red mud, bottom ash, titano gypsum, red titano gypsum and phospho gypsum) was individually added into a microwave cylinder container, then 50 mL of nitric acid (0.2 M) was added. The microwave cylinder container containing the ash and nitric acid was kept into the microwave reactor chamber. Temperature was controlled and held at 200 °C for one hour. The digested ash was then filtrated. 5 mL of the filtrate was mixed with 20 mL deionised ultra pure water. The water phase was syringe filtered. 10 µL of the collected clear water phase was taken by micropipette and diluted with 10 mL deionised ultra pure water. It was sent for inductively coupled plasma (ICP) to measure the initial amount of metals which existed in each ore.

To conduct the adsorption experiment, 10 mg of the Starbon adsorbent materials including Starbon300, Starbon800, A300 and A800 were individually added into the glass vial containing a small magnetic stirrer bar. Then 25 mL (5 mL filtrate+ 25 mL deionised ultra pure water) of the dilute form of the collected filtrate was employed into the glass vial containing 10 mg of the adsorbent materials and a small stirrer. Adsorption took place for 24 hours with constant agitation. The water phase was centrifuged for 30 min and syringe filtered. 10 µL of the collected clear water phase was taken by micropipette and diluted with 10 mL deionised ultra pure water. The final solutions were then sent for inductively coupled plasma (ICP) to measure the amount of metals removed. Further details are given in Table 5.2.

Table.5.2: Investigated materials for metals adsorption

Solid waste	Starbons			
	S300	S800	A800	A300
Fly ash (PFA)		▓		
Red mud (RM)		▓	▓	
Bottom ash (BA)	▓			
Titanogypsum (TG)	▓		▓	▓
Red (RTG)titanogypsum			▓	
Phosphogypsum (PG)		▓	▓	

The methodology used to estimate Starbon selectivity in metals adsorption is described as follows:

i) estimation of relevant amount of certain metal Me_n (Solution) in the solution as a ratio between concentration of this metal in the solution $[Me_n]^{solution}$ and sum of concentration of all elements in solution- $\Sigma_i [Me_i]^{solution}$.

ii) Estimation of relevant amount of certain metal Me_n (surface) on the surface as the ratio between surface concentration of this metal $[Me_n]^{surface}$ and the sum of concentration of all others elements on the surface-$\Sigma_i [Me_i]^{surface}$.

iii) Estimation of adsorption selectivity (Starbon selectivity effect) as a ratio:

Me_n (surface): Me_n (solution) = $[Me_n]$surface: $\Sigma_i [Me_i]$surface/$[Me_n]^{solution}$: $\Sigma i [Me_i]^{solution}$

Additionally, A800 was nominated for further experiment. It was individually applied (10mg of this adsorbent was added to 10 mL of series concentration solutions of a sample mixture containing Co, Cu, Ag and Cd and held for 24 hours). Isotherm metals adsorption using A800 was plotted, with different modes of adsorption applied which included Langmuir, Freundlich, Tempkin and Dubinning-Raduschkic. The maximum adsorption load from the Langmuir equation was found. At last, time contact was also conducted. The kinetic order including pseudo first and second order reaction was applied.

5.3 Results and discussion

5.3.1 Applications of Starbons for metal adsorption in water stream

It is known that global worry about the security of mineral supply has paid attention to many countries to re-evaluate their native resources, particularly the critical metals. They are called critical because of their dominance role in growing economies and the high risk of supply scarcity.[334]

In North Yorkshire there are several places with a significant amount of industrial solid waste that contains a large number of high value metals. For example, pulverised fly ash is a coal combustion waste product. In order to meet domestic energy requirements in the United Kingdom, annual production of pulverised fly ash is about five million tonnes. It is estimated that 35 per cent of this is sent to landfill.[335] This has attracted considerable attention from the British government.

Numerous metallic elements are known to occur in such solid wastes in concentrations ranging from a few parts per billion up to a several weight per cent, depending on the specific composition of the feedstock ore which has been used.[336]

The Yorkshire consultancy "Link2energy" approached the Green Chemistry Centre with a project which aimed to investigate the possibility of selective recovery of metals from solid wastes or ores. These wastes are pulverised fly ash (PFA), red mud (RM), bottom ash (BA), titano gypsum (TiG), red titano gypsum (RTiG) and phospho gypsum (PG) which are significantly enriched with certain critical and valuable metals. Therefore, significant attention in my PhD project was paid to recovery of these metals using Starbon technology. It was proposed that, in the first stage of the metal recovery process, solid waste needed to be digested, while in the second stage, a variety of Starbon materials including S800, S800, A300 and A800 were employed to screen their ability to capture the existed metals from the digested water stream. The digestibility of the solid ores under microwave conditions is shown in Figure 5.2.
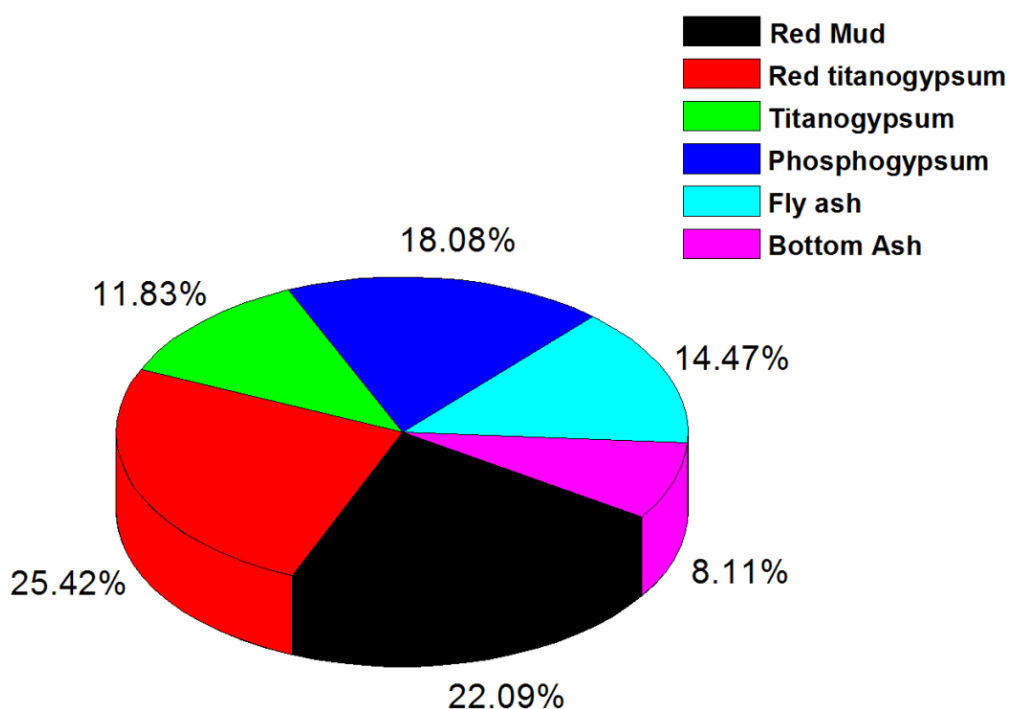
Fig.5.2: Degree of samples digestion microwave assisted, 0.2 M Nitric acid, T=200 $^{\circ}$C,1h.

It is noticed that digestion of Red Mud, Red Titanogypsum and Phosphogypsum occurs quite well. Titanogypsum and Bottom Ash did not solubilise well;

162

therefore, results of metals extraction from this materials could not be so well represented. However, bottom ash is likely to be silica-rich, and it is unlikely that silica will be solubilised under the operating conditions. However, as this is not one of the elements of interest in the context of the current project, it would be advantageous if the silica does not dissolve, as long as the key elements are solubilised.

Interestingly, the ICP analysis qualified the metals in the water stream after digestion process. The list of these critical EU elements are presented in Table 5.3.

Table.5.3: List of the critical EU elements found (ppm) in the digested solid wastes

Metals	PFA	Red Mud	Bottom ash	Titano-gypsum	Red Titano-gysum	Phospho-gypsum
Be	0.05	0.0	0.01	0.01	0.0	0.0
Co	0.1	0.01	0.03	0.03	0.07	0.0
La	0.38	0.32	0.18	0.29	0.16	0.16
Mg	48.62	3.56	26.39	40.74	19.21	1.27
Pd	0.0	0.0	0.0	0.0	0.0	0.0
Pt	0.0	0.0	0.0	0.0	0.0	0.0
Sb	0.0	0.0	0.0	0.0	0.0	0.0
Sc	0.11	0.1	0.04	1.77	0.17	0.0
W	0.03	0.03	0.02	0.0	0.01	0.02
Ga	0.14	n/a	0.04	0.0	n/a	0.0
Nb	0.0	n/a	0.0	0.0	n/a	0.0
Ge	0.36	n/a	0.0	0.0	n/a	0.0
Y	0.0	n/a	0.0	0.41	n/a	0.14
Nd	0.0	n/a	0.0	0.24	n/a	0.03

To test adsorption of metals in the digested ashes, 10 mg of S800 (Starbon derived from starch) was added to the collected filtrate of the fly ash (PFA) and held for 24 hours with constant stirring. After the adsorption process, Starbons were separated from the filtrates and filtrates samples were sent to ICP analysis. The same procedure was repeated for A800/Red Mud, S300/Titanogypsum, A300/Tytanogypsum and S800/Phosphogypsum, S800/Bottom ash and S300/Red Titanogypsum.
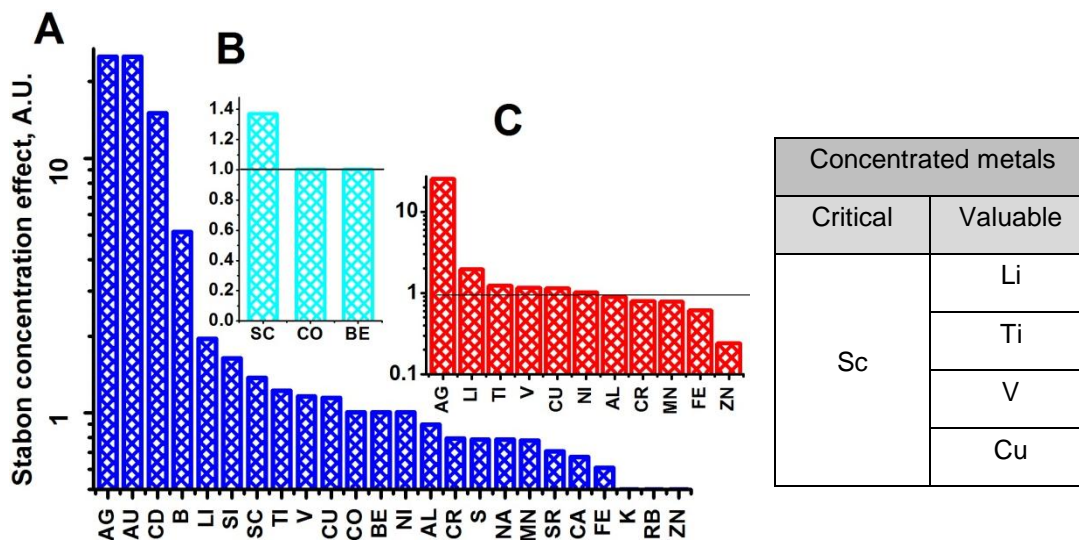
Fig.5.3: List of metals adsorbed by S800 in PFA. A: blue bars represent all elements. B: cyan bars represents elements from Critical EU list. C: red bars are valuable elements.

According to the ICP analysis it appears in Figure 5.3 that Starbon technology is efficient at recovering some high value elements such as Li, Ti, V and Cu which are in the list of valuable element as well as Sc which is in the list of critical elements. S800 has demonstrated the highest efficiency on relation to some metals in pulverised fly ash (PFA) ore.

It seems in Figures 5.3 and 5.4 that success in terms of the concentration of metals which is obtained depends on the types of the digested ash, the composition of the ash, the digestibility of the ore materials and, in addition, the nature of the adsorbents used.[337,338]
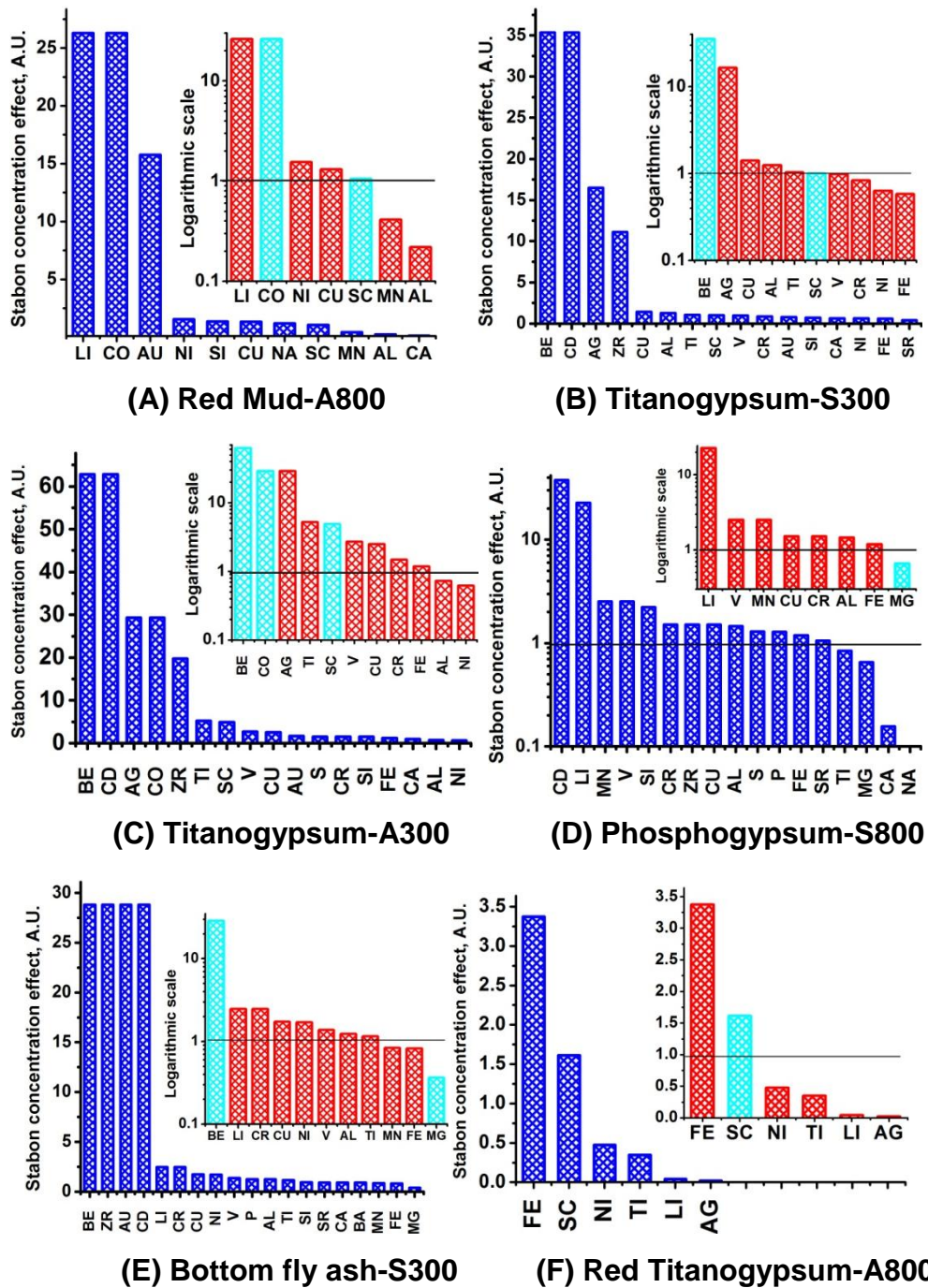
Fig.5.4: List of metals adsorbed in the contaminated water collected from the digested ash by different carbonaceous materials: (A) metals adsorbed by A800 in Red Mud; (B) metals adsorbed by S300 in Titanogypsum; (C) metals adsorbed by A300 in Titanogypsum; (D) metals adsorbed by S800 in Phosphogypsum; (E) metals adsorbed by S300 in Bottom fly ash; and (F) metals adsorbed by A800 in Red Titanogypsum. The blue bars presents all metals, the red bars are the valuable metals and the cyan bars are the critical metals.

Table 5.4 gives the high value metals which could be concentrated from ores using Starbon technology.

Table.5.4: The preferred metals adsorbed by Starbon materials used in the digested solid wastes

Solid waste	Adsorbent	Concentrated metals	
		Critical	Valuable
Fly ash	S800	Sc	Li Ti V Cu
Red mud	A800	Co	Li Ni Cu
Titanogypsum	S300	Be	Ag Cu Al
Titanogypsum	A300	Be Co Sc	Ag Ti Cu Cr Fe
Phosphogypsum	S800		Li V Mn Cu Cr Al Fe
Bottom fly ash	S300	Be	Li Cr Cu Ni V Ti
Red Titanogypsum	A800	Sc	Fe

In summary, some of the valuable elements like silver, lithium and titanium demonstrate an adsorption coefficient which is higher than 5 (see Table 5.5) indicating that there is a possibility of applying Starbon technology to their concentration. This implies that such metals ions are more desirably adsorbed

by the materials applied indicating the selectivity of Starbon technology for recovering them.

Table.5.5: Adsorption coefficient of valuable elements adsorbed using different Starbon adsorbents

Solid waste	Absorbent	Adsorption coefficient									
		Ag	Li	Ti	V	Cu	Al	Fe	Mn	Ni	Cr
PFA	S800	20	2	1.2	1.2	1.1	<1	<1	<1	<1	<1
Red M.	S800	<1	1.2	<1	<1	1.2	<1	<1	<1	<1	<1
	A800	<1	1.5	<1	<1	1.2	<1	<1	<1	1.5	<1
TitanoG	S300	29	<1	5.2	2.7	2.5	<1	1.2	<1	<1	1.5
	A300	16.5	<1	1	1	1.4	1.2	<1	<1	<1	<1
Red Ti.	A800	<1	<1	<1	<1	<1	<1	3.3	<1	<1	<1
PhosphG	S800	<1	22.3	<1	2.5	1.5	1.5	1.2	2.5	<1	<1
	A800	<1	7.1	<1	2.4	<1	<1	<1	2.4	<1	<1
BFA	S300	0	1	1	1	1	1	<1	<1	1	1

Adsorption coefficient: is the amount of metal ion concentrated onto the Starbon materials per the total amount of the metals ions in the system.

The experimental results (see Table 5. 6) demonstrate that some elements from the EU critical list[324,325] could be more concentrated on the Starbon surface such as scandium, cobalt, beryllium and tungsten. In particular, cobalt and beryllium demonstrate an adsorption coefficient which is higher than one. This means that three consecutive adsorption-desorption steps could potentially increase the concentration of these elements in the mixture signiicantly.

Table.5.6: Results showing the adsorption of critical elements using different Starbon adsorbents

Critical element	Ash material	Starbons	Adsorption coefficient
Sc	PFA	S800	1.4
	Titanogypsum	A300	3
	Red Titanogypsum	A800	1.5
Co	Red Mud	S800	20
	Red Mud	A800	26

	Titanogypsum	A300	20
Be	Titanogypsum	S300	32
	Titanogypsum	A300	40
W	Phosphogypsum	A800	7

Interestingly, Figure 5.5 gives information on how the composition of the raw materials, which had been digested by microwave technology, and the amount of metals which contained solid wastes may affect the process of metal adsorption. For example, different amounts of Gold (Au) adsorption were found in three different raw materials (i.e. Red Mud, Titanogypsum and Red Titanogypsum) using the A800 adsorbent. This is because the digestion of these raw materials brought complex species, such as soluble matrix species, into the aqueous phase. These complex soluble matrix species might have desposited or adsorbed on the adsorbent surface and interior layer including macro and mesoporous region. This would block the small pores in microporous region. As a consequence of that deposition the A800 adsorbent might have been partially or completely blocked. Therefore. this might have impaired the uptake of gold from the aqueous phase into the A800 regardless of the concentration of gold contained in the solid waste. Richer concentration of gold contained in waste stream should give a higher quantity of gold ions concentrated in the adsorbent employed.
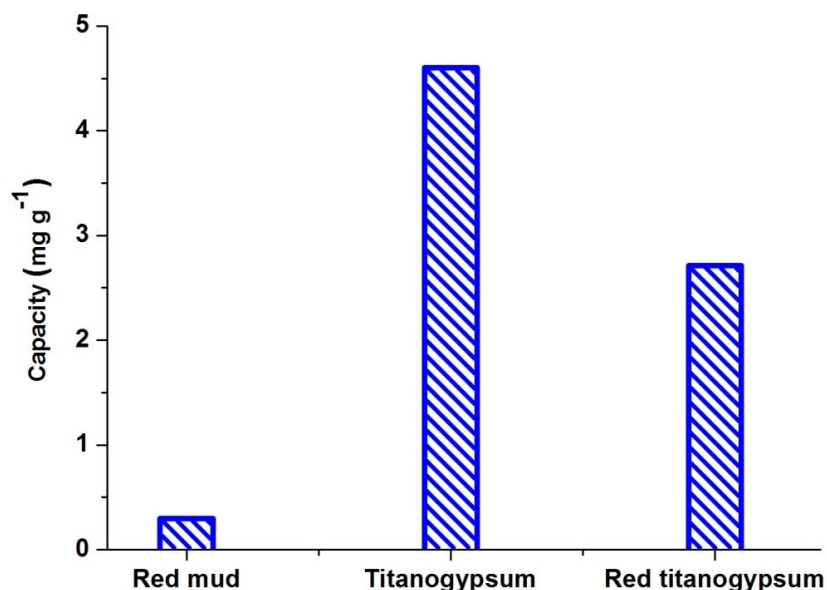
Fig.5.5: Raw material composition influence on gold adsorption by A800 adsorbent.

It appears in this section that Starbons have a good adsorptive capacity and specificity towards rare metals. It is also noticed that S800 is a better adsorber than S300. Algibon derived from alginic acid is better than Starbon which is derived from starch.

It is also important to understand that complex adsorption behaviour depends on the waste stream. For example, it was observed that gold is very good for S800/PFA, S800/red mud, A800/red mud and S300/bottom ash, but poor for S300 /titanogypsum. It is noticed that silver is good for S800/PFA, S300/Titanogypsum, A300/Titanogypsum, but poor for A800/Red mud, S800/Phosphogypsum, S300/Bottom ash and A800/Red Titanogypsum.

There are possible reasons for metals adsorption employing Starbon technology. One is microporosity[339] which could play a role in controlling the metal adsorption which occurs. The surface functionality of Starbons is another fundamental factor where the acidic functional groups in the active center of the Starbons materials cause metals adsorption to take place. This would be as a consequence of the replacement of the hydrogens on the Starbon surface with the metals ions in the aqueous phase.[340] Active sites where Starbons are present and which contain conjugated double bonds could also result in metals adsorption taking place as a result of the interaction between the π electron rich layers of the adsorbent and the vacant d-orbitals of the metal ion species.[340,341]

5.3.2 Systematic investigation on metal adsorption on Starbon based on A800

To investigate the influence of the nature of the metal ions on the kinetic parameters of adsorption, a detailed experimental analysis of the model system was carried out. A800, which demonstrates the most promising results and the most stable material with well-developed surface area, was chosen as the adsorber. A solution of four high value metals such as Co, Cu, Ag and Cd was proposed for adsorption. Concentrations of these metals were several thousand folds greater than those of the metals which had been adsorbed from the digested ashes. The experiments detailed below were conducted.

5.3.2.1 Concentration influence on adsorption

At the beginning of the experiment, each metal concentration in the initial mixture solution was 27.5 mg/L, 47.6 mg/L, 104.1 mg/L, 56.2 mg/L for Co, for Cu, for Ag and for Cd respectively. The solutions were prepared by dilution of corresponding salts with HNO_3 (pH 2). Final metals concentrations were obtained using ICP analysis. The series solutions with different initial concentration of metal ions were prepared as is described in Table 5.7.

Table.5.7: Series solutions of the metals prepared from the stock mixture solution sample

Series of solutions	Concentration of metal (mg/L)			
	Co	Cu	Ag	Cd
Solution1	1.372	2.382	5.206	2.812
Solution 2	2.745	4.765	10.411	5.624
Solution 3	6.864	11.912	26.029	14.061
Solution 4	13.729	23.824	52.057	28.121
Solution 5	27.458	47.648	104.115	56.243

The A800 adsorbent was added to different concentrations of the mixture solution containing Co, Cu, Ag and Cd. This work was carried out to further systematically test the efficiency of A800 in adsorbing the metals. Typical isotherms of metal adsorption onto the A800 surface are represented in Figure 5.6.

(A)   (B)
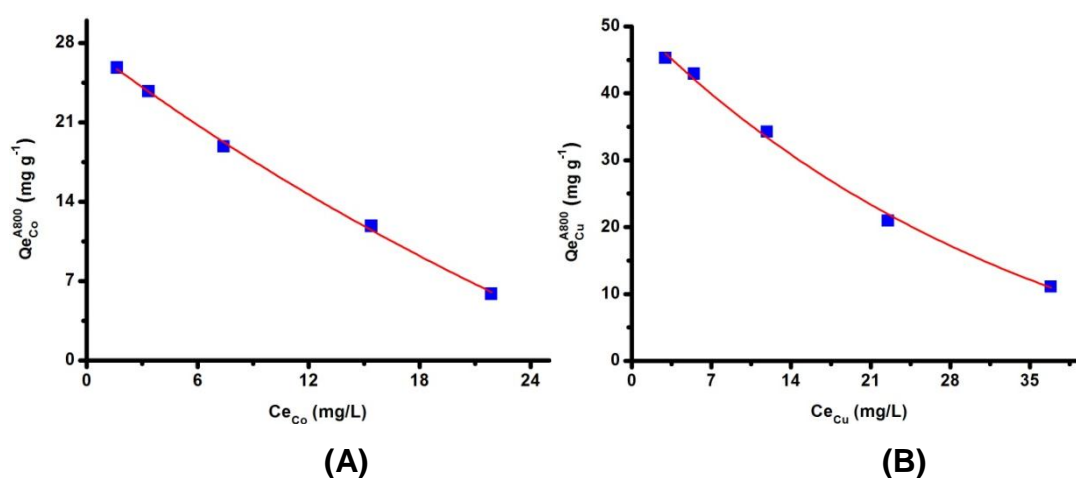
Fig.5.6: Isotherms of metals adsorption in the presence of A800 for (A) Cobalt, (B) Copper

5.3.2.2 Modelling metals adsorption types

In order to analyse the adsorption type of metals from effluents, it is necessary to find the most appropriate adsorption model. Starbon A800, which is the most stable material with a well-developed surface area, was proposed as the absorber for this investigation. In this section, four adsorption isotherm models such as Langmuir, Freundlich, Temkin and Dubinin-Radushkevich were applied.

The results of the calculation of the isotherm constant which is based on these four adsorption models are summarised in Table 5.8. Plots of all of these experiments are listed in the Appendix five.

Table.5.8: Employing A800 and using types of isotherm models to describe the adsorptive process

A800	Co	Cu	Ag	Cd
Langmuir				
K (L/mg)	0.572	0.381	0.224	0.556
Q_m (mg/g)	11.3	21.9	52.7	29.5
R^2	0.987	0.993	0.992	0.983
Freundlich				
K_F	41.2	94.1	218.13	100.71
1/n	0.513	0.4946	0.372	0.431
R^2	0.7576	0.7865	0.8133	0.7734
Tempkin				
B (J/mol)	7.33	12.544	23.684	13.389
A (L/g)	74.72	141.77	49.56	210.09
R^2	0.835	0.8266	0.8156	0.8349
D-R				
Q_m (mg/g)	9.10	16.93	45.95	22.32
$Kx10^{-3}$ (mol^2/J^2)	1.07	1.73	2.45	1.39
E (J/mol)	0.6835	0.542	0.204	0.599
R^2	0.443	0.457	0.545	0.391

The best R^2 values for all investigated systems (within the range 0.990 to 0.993) was found for the Langmuir isotherm adsorption model. In all cases, the Langmuir equation yielded the best fit of experimental data compared to other isotherm models. It indicates that the adsorption of metals has a monolayer character and that the surface of the adsorbent is uniform. Furthermore, the maximum adsorption capacity (Q_m) values calculated from Langmuir model fitted well with the experimental data.

Different values of metal maximum adsorption capacity (Q_m) may partly depend on the different state of their metallic ions, i.e. Ag has one positive ionic charge, while Cu, Co and Cd have two positive ionic charges. Their valence electron orbital configuration is also important which can give different metals ion radii. The stable oxidation state, valence electron configuration, ionic radius for each metal ion are shown in Table 5.9.[342-347]

Table.5.9: Valence orbital electronic configuration of the metal ions and their ionic radius

Metal ion	Atomic number	Valence electron	Ionic radius (A)
Silver metal ion (Ag^+)	47	$4d^{10}\ 5s^0$	1.26
Cadmium metal ion (Cd^{+2})	48	$4d^{10}\ 5s^0$	0.97
Cobalt metal ion (Co^{+2})	27	$3d^7\ 4s^0$	0.75
Copper metal ion (Cu^{+2})	29	$3d^9\ 4s^0$	0.73

Ag^+
I.R.=1.26 A

Cd^{+2}
I.R.=0.97 A

Co^{+2}
I.R.=0.75 A

Cu^{+2}
I.R.=0.73 A

Ionic radius (I.R.) increase
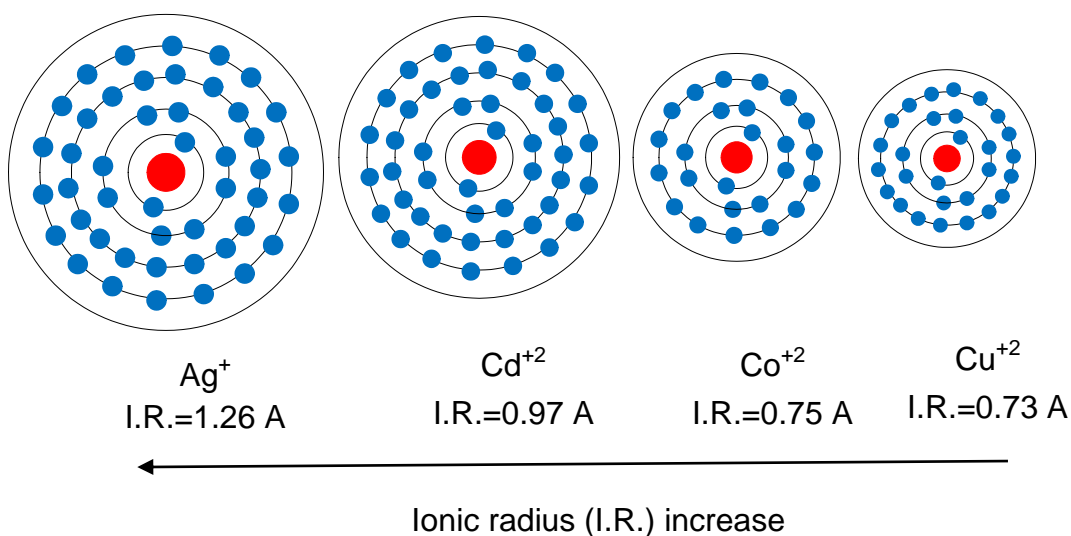
Fig.5.7: Size of the metals' ions

It is observed in Table 5.8 that the silver ion is the largest metal ion compared to cadmium, cobalt and copper ions respectively. Therefore, the silver ion is believed to have been filtrated and trapped better by the microporous region of the adsorbent. This resulted in the greatest silver maximum adsorption capacity (Q_m= 52 mg/g) by A800. The cadmium metal ion is smaller in size compared to silver, but larger than both cobalt and copper ions respectively. This is possibly the reason why Algibon's maximum adsorption capacity toward cadmium is smaller than in case of silver but bigger than in case of cobalt and copper.

However, the ionic radius of cobalt is nearly similar to copper, while the maximum adsorption capacity of cobalt by A800 is almost twice as less as in the case of copper. It seems that, in this case, the ionic radius may not have played a key role compared to the valence orbital electronic configuration of both cobalt and cobber which possibly would be a key factor. In the case of cobalt, the ion valence electron configuration is **$3d^7\ 4s^0$**, but for copper ion is **$3d^9\ 4s^0$**.[343] This difference in their electronic valence orbital arrangement possibly caused better copper adsorption to occur onto the A800 which was used.

The metal ion concentrations in the aqueous phase may also affect the amount of ion recovery by the adsorbent. For example, the greatest concentration of the metal ions in the mixture solution was silver (100 mg/L), which would cause the silver ion to be greatly concentrated into the A800. The same fact is perhaps right for cadmium whose ion concentration is the second largest in the solution mixture. This explanation seems to fit with copper and cobalt. It is observed that copper ion concentration (48 mg/L) is nearly twice as much as that of cobalt (27 mg/L). Therefore, difference in concentration could also be a cause for almost twice greater maximum adsorption capacity of Algibon to recover copper than in case of cobalt (see table 5.8). Despite the fact that both metal ions (Co and Cu) have different valence electronic configuration (see Table 5.9). This proposes a suggestion that the nature of the adsorbent and each metal ion may also have their own importance and play a key role. For instance, Algibon surface functional groups and the conjugated double bond contained active sites in Algibon might have caused this adsorbent to become a better adsorber for silver, cadmium and cupper, but may not be very excellent for the purpose of recovering cobalt.

Equilibrium parameter (R_L) value[348], pretending for Langmuir isotherm model, can be calculated from Table 5. 8 based on the constant of equilibrium (K) and initial concentration of metal solution which are found. All the R_L values were between 0 and 1, indicating that the adsorption of the metals on the A800 was favourable at the conditions being studied. For instance, for cobalt adsorption, the found constant of equilibrium (K) is 0.572. As the initial concentration increased from 1.5 to 27 mg/L, the R_L values decreased from 0.564 to 0.066. This implies that adsorption was more favourable at a higher concentration of metal in solution.

5.3.2.3 Kinetic adsorption

The adsorption kinetic study was carried out based on adsorption of four different metals (Co, Cu, Cd, Ag) onto the surface of A800. Samples were taken one by one at each contact time (e.g. 0, 10 min, 30 min, 60 min, 120 min, 240 min, 320 min, 1440 min). It was observed that the concentration of metals in the solution was decreasing as time increased. This means the metal ions need time to diffuse through the adsorbent in order to be bound. The results of metal uptake using A800 which depends on the adsorption time can be seen in Figure 5. 8.
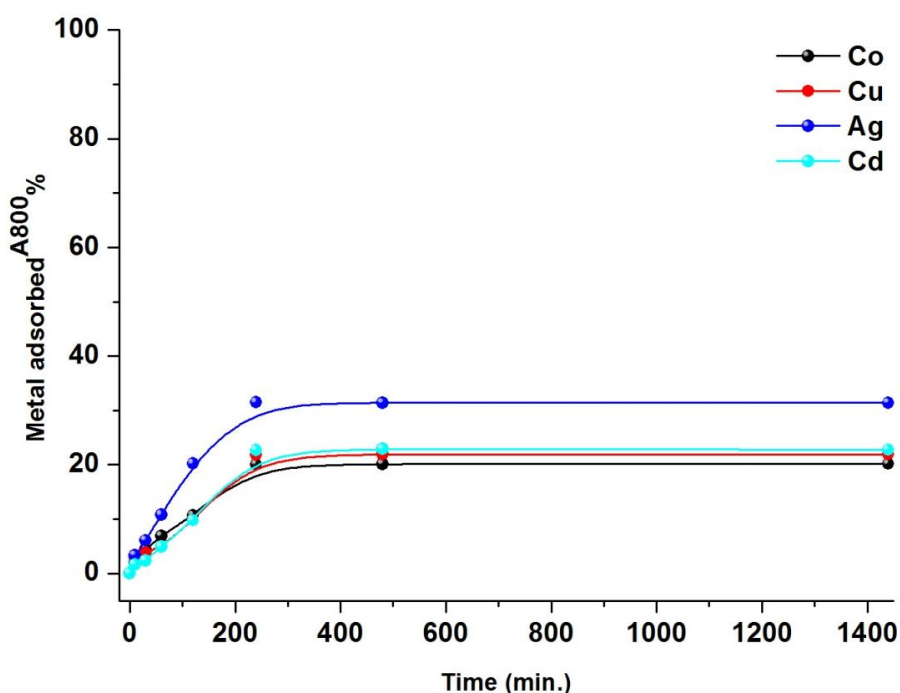
Fig.5.8: Contact time for metal adsorption employing A800 in aqueous media HNO_3 pH 2.

5.3.2.4 Kinetic order model studies

In order to further understand the metals adsorption, the study of adsorption kinetics should be included so as to determine an appropriate kinetic model. A lot of useful information could be obtained by using different kinetic models to analyse aspects such as chemical reaction and potential rate controlling steps. There are a wide variety of models available which can examine adsorption kinetics. The most widely applied kinetic models are the pseudo-first and pseudo second-order models. The conformity between the models predicted values and experimental data was expressed by the correlation coefficients (R^2) value (see Table 5. 10). Plots of all these experiments can be found in the Appendix five.

Table.5.10: Pseudo-first-order of kinetic parameters for metals adsorption using A800 adsorbent

Kinetic parameters of Pseudo first order reaction				
Adsorbent	Metals	Qe (mg/g)	K_1 (min^{-1})	R^2
A800	Co	1.1	$1.44*10^{-3}$	0.112
	Cu	1.6	$1.8*10^{-3}$	0.061
	Ag	6.7	$2.6*10^{-3}$	0.10
	Cd	21.6	$2.6*10^{-2}$	0.884

Table.5.11: Pseudo-second-order of kinetic parameters for metals adsorption using A800 adsorbent

Kinetic parameters of Pseudo second order reaction				
Adsorbent	Metals	Qe (mg/g)	K_2 (g mg^{-1} min^{-1})	R^2
A800	Co	6.3	$2.1*10^{-3}$	0.991
	Cu	7.4	$1.3*10^{-3}$	0.968
	Ag	24.3	$4.8*10^{-4}$	0.991
	Cd	11.4	$4.8*10^{-4}$	0.970

Values of R^2 demonstrated in tables 5.10 and 5.11 give clear information that the metal adsorption belongs to the second order kinetic. This is implying the applicability of this kinetic equation and the second-order nature of the adsorption process of the metals into the Algibon. This might be due to sharing or exchanging of electrons between the sorbent and sorbate.[349]

5.4 Conclusion

A variety of Starbon materials was tested for the adsorption of metals from the water stream produced during the digesting of solid waste materials. It appears that Starbons have a good adsorptive capacity and specificity towards certain metals. It was also noted that S800 is a better adsorber than S300. Algibon derived alginic acid is better than Starbon which is derived from starch. It was noted that complex behaviour affected metal removal in the waste stream. It is also important to know that complex behaviour depends on composition of the waste stream. For example, it was observed that Au was adsorbed very well using S800/PFA, S800/red mud, A800/red mud and S300/bottom ash systems, but poorly from S300 /titanogypsum. At the same time, Ag is adsorbed well from S800/PFA, S300/Titanogypsum, A300/Titanogypsum systems, but poorly from a system such as A800/Red mud, S800/Phosphogypsum, S300/Bottom ash and A800/Red Titanogypsum.

Microporosity could play a key role in controlling metals adsorption. Another key factor is the surface functionality of Starbons. The most promising active centre for metals adsorption could be acidic functional groups (the metals ions in the aqueous phase would replace the surface hydrogen) and active sites containing a conjugated double bond system which could adsorb metals due to the interaction between the π electron rich layers of the adsorbent and the empty d-orbitals of the metal ion species.

Further systematic work on four highly concentrated metals in the collected sample mixture containing (Co, Cu, Ag and Cd) demonstrated that A800 has a limited capacity to bind the metals. The adsorption of metals is very good as described by the Langmuir model which means that the metals were adsorbed as a monolayer. Adsorption is followed by a pseudo second order mechanism.

It is important to note that employing a benign adsorbent such as A800 for capturing metal ions in water streams, sourced from the digested ash or ore, could be carried out successfully. This may help ideas to be formulated which will enable a project to be designed successfully which will use various solid wastes as a resource to recover enriched metals. This could be feasible for a growing economy, minimising the amount of space occupied by waste as well as protecting human health from the threat of toxic metals and the environment more generally from pollution.

CHAPTER SIX

Experimental Section

6.1 Introduction

Renewable alginic acid polysaccharide material was expanded by applying a developed method of generating mesoporous alginic acid resulting in promising materials. The mesoporous alginic acid material produced was carbonised at various temperatures to obtain different textural properties of porous materials called Algibons. The carbonised expanded alginic acid corresponding to 300, 450 and 800 ^{o}C carbonisation temperature are denoted as A300, 450 and 800.

Some techniques were applied to characterise the Algibons produced such as Nitrogen sorption analysis to check the porosity structure including surface area (S_{BET}, pore volume and pore diameter). DRIFT IR and Solid State NMR spectroscopy were carried out to find out changes in surface functionalities of the Algibons generated. Elemental analysis was conducted to analyse the amount of carbon, hydrogen and nitrogen in the expanded material and its derivatives produced. Ash content test was applied to check the amount of the residue left in expanded alginic acid and its derivatives in the presence of oxygen.

The Algibons generated were employed for bulky organic dye adsorption in water stream. These compounds are reactive dyes called Procion Yellow H-EXL (PY), Remazol Black (RB), Procion Crimson H-EXL (PC) and Procion Navy H-EXL (PN).

The dyes adsorption loading for the Algibon generated was compared to the other commercially available porous materials including Starbon (starch derived Starbon300, 450 and 800 named as S300, 450 and 800), activated carbon (AC) as well as silica gel (Sgel).

Starbon technology was also used in recovery of high value metals from the water stream obtained from digesting solid wastes. These ores were named Pulverised fly ash (PFA), Red Mud (RM), Bottom ash (BA), Titano gypsum (TiG), Red Titano gypsum (RTiG) and Phospho Gypsum (PG). Selective adsorption of versatile textural Starbons (i.e. starch derived Starbons and alginic acid derived Algibons) towards the metals were investigated.

Further systematic investigation for adsorption of a number of metals (i.e. Co, Cu, Ag and Cd) in a sample solution by Algibon 800 material was additionally

carried out to determine types of adsorption, kinetic adsorption and evaluation of kinetic parameters of the process.

6.2 Chemicals

All materials were used as received without further purification. Procion Yellow H-EXL (PY), Remazol Black (RB), Procion Crimson H-EXL (PC) and Procion Navy H-EXL (PN) were purchased from Society of Dyers and Colourists in Bradford, UK. Powder activated carbon (Norit) was purchased from Fluka and was washed with deionised water at 75 ^{o}C, filtered and dried in a vacuum oven before they were employed. Starbon (S300, 450 and 800) were commercially obtained. Algibon (300, 450, 600 and 800) were made from alginic acid at Green Chemistry Centre of Excellence, University of York-UK.

Table.6.1: Polysaccharides carbonaceous materials and their abbreviation

Raw material	Prepared carbonisation temperature	Porous material produced	Abbreviation
Alginic acid	300 ^{o}C	Algibon300	A300
	450 ^{o}C	Algibon450	A450
	600 ^{o}C	Algibon600	A600
	800 ^{o}C	Algibon800	A800
Starch	300 ^{o}C	Starbon300	S300
	450 ^{o}C	Starbon450	S450
	800 ^{o}C	Starbon800	S800
Wood	1000 ^{o}C	Activated carbon	AC
Silica gel	600 ^{o}C	Silica gel	Sgel

6.3 General analytical techniques

6.3.1 Thermal gravimetric analysis

Thermal gravimetric analysis was carried out using a Netschz 409 STA thermal analyser. Samples (200 mg of each individual sample) were mounted in a 3.5 mL ceramic crucible and heated under nitrogen at a flow rate of (100 mL/min). The samples were heated at slow rate (under 0.5 ^{o}C/min as shown in Tables 6.9 to 6.12) to produce various temperature texture properties of Algibons (i.e. A300, 450-800).

6.3.2 Thermal gravimetric analysis infrared spectroscopy

The thermal gravimetric (TG) was carried out using 409 STA thermal analyser. Samples (50 mg of the sample) were mounted for the TG IR, in this case the TG was coupled with a Bruker Equinox 55 infrared via transfer line, the nitrogen flow was (100 mL/min). Different rate of temperatures (i.e. 5, 10 and 20 $^{\circ}$C/min.) were applied.

6.3.3 NMR spectroscopy

Solid state ^{13}C-MAS NMR analysis was carried out by Dr David Apperley, EPSRC solid state NMR service at The University of Durham, Department of Chemistry, Durham, DH1 3LE.

^{13}C-MAS NMR spectra were obtained using Varian VNMRS spectrometer at 100.56 MHz for ^{13}C. The spin rate of the MAS was set to 12 KHz spinning, with a wide spectra width and a rotor-synchronised echo. Spectral referencing was with respect to tetramethylsilane.

6.3.4 Simultaneous thermal analysis (STA)

Simultaneous thermal analysis (STA) measurement of dried expanded alginic acid was conducted on a Seiko STA. Super critical dried expanded alginic acid (15 mg) was weighed into an aluminium STA pan and analysed under nitrogen gas using a three stage profile in order to remove any prior thermal character. The sample was heated from room temperature to 625 $^{\circ}$C at 10 $^{\circ}$C/min. The results was processed in origin software to individually draw the TG and dTG versus T($^{\circ}$C) increased.

6.3.5 Electron microscopy

All electron microscopy images of the solid materials were carried out at the Instituto de Ciencia y Tecnología de Polímeros, CSIC, Madrid, Spain with the assistance of Dr Peter Shutterworth. Scanning electron microscopy (SEM) micrograph were recorded using a SU8000 Hitachi SEM applying an acceleration voltage of 1.0 or 3.0 kV-D 5.0 mm. Samples were coated with a ~5 nm Cr over layer to avoid charge accumulation during electron irradiation prior to analyses. Typical magnifications used for the solid materials were x5k, x10k, x20k, x25k, x60k and x100k.

6.3.6 DRIFT IR spectroscopy

Diffuse reflectance infrared spectroscopy (DRIFTS) was used to analyse the samples in Green Chemistry Centre of Excellence, University of York. A 10 mg of the Algibon was taken and diluted with 500 mg of pure KBr.

All experiments are performed with 16 scans and a resolution of 4 cm^{-1} in the spectral range 500-4000 cm^{-1} with a data interval of 1 cm^{-1}. The background spectrum is subtracted from the sample spectra. Diffuse reflectance measurements were performed in a conditioned atmosphere of room temperature. The IR spectra were obtained on a Bruker IFS55 FT IR spectrophotometer equipped with a mercury-cadmium-telluride detector (broad band 12000-420 cm^{-1}, liquid nitrogen cooled) with an aperture of 3.5 mm. The internal reflection element was a Golden Gate single pass diamond ATR. The spectra were recorded with a nominal resolution of 2 cm^{-1} by co-adding 500 scans. For all measurement, spectra of different Algibon samples were recorded.

6.3.7 CHN analysis

CHN test was carried out to determine the percentage of carbon, hydrogen and nitrogen in the solid samples (i.e. expanded alginic acid (EAA), A300, A450, A600, A800 and AC). The balance used is a Sartorius SE2 analytical balance, capable of weighing accurately to four decimal places on a milligram. 1.8 mg of the solid material to be analysed was weighed into disposable tin capsule. All the blanks and standards are weighed to allow for representative comparisons of the analyser's detector responses.

The sample capsule is then placed in a nickel sleeve and injected into a high temperature furnace (975°C) and burnt in high purity oxygen under static conditions. The tin capsules used for the sample container allow an initial exothermic reaction to occur, raising the temperature of combustion to over 1800°C. A further dynamic burst of oxygen is added at the end of the combustion process, to ensure total combustion of all inorganic and organic substances. The resulting combustion products pass through specialised reagents.

The concentration of water produced is proportional to the amount of hydrogen, the trapped CO_2 proportional to carbon and the amount of helium consumed corresponds to nitrogen in the original sample. At the end of each sample run

the spent nickel sleeves were ejected into a trap and the tin sleeves are disposed of as tin oxide waste.

6.3.8 Super critical CO$_2$ (scCO2)

Super critical CO$_2$ Thar SFE500 extractor operating at 50 ^{o}C/100 bar/min for 3 hours, was applied to dry the (100 g) of the filtrated wet expanded alginic acid generated. After pressurising was completed, the depressurising process was conducted slowly overnight. The resulting materials were dried to a fine light powder of expanded alginic acid.

6.3.9 porosimetry analysis

This analytical technique was used to determine the porosity properties of the solid materials, such as surface area, pore volume and pore diameter. The porosity of the sample was measured, after the prepared sample had been degassed (see scheme 3.1).

Sample preparation for porosimetry analysis

i) Mass of the porosimetry tube was recorded emptily on sensitive balance.

ii) 25 to 50 mg of each of the solid material was individually weighed in the porosimetry tube.

iii) Mass of the porosimetry tube and the solid sample were together recorded.

iv) Degassing the sample was carried out at 100 ^{o}C to 140 ^{o}C under nitrogen flow (100 mL/min.).
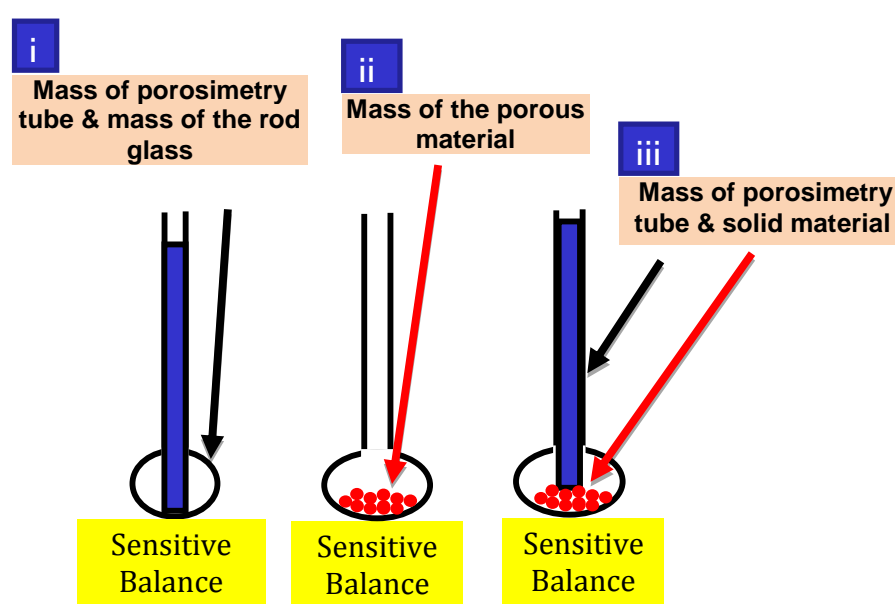
Fig.6.1: Preparing the porous materials (expanded alginic acid and its derivatives "Algibons") for degassing before porosimetry measurement was taken place.

Nitrogen sorption analysis

Porosimetry analysis was carried out using Micrometritic Tristar. Each of the solid material sample prepared for the porosity analysis was degassed one by one at 100 ^{o}C (for expanded materials such as expanded alginic acid) to 140 ^{o}C (for carbonised materials such as Algibon) for at least 5 hours under flowing nitrogen gas. Data obtained was done by using Micrometritic Tristar software. N$_2$ sorption isotherm was measured at -196 ^{o}C. Specific surface areas were calculated through the BET method. BJH method was used to calculate the mesopore volumes and pore size distribution; t-Plot analysis used nitrogen adsorption data in the P/P$_0$ range of 0.005 to 0.98.

6.3.10 Freeze drying technique

0.5 to 1 g of the well filtered wet solid material was added into the round bottom flask. The round bottom flask containing the sample was cooled down in liquid nitrogen cylinder for at least 15 min. The flask was then attached to the freeze drier tap channel. The system is now ready to run as the average temperature of the system is under -150 ^{o}C under extreme vacuum pressure. The freeze drying is started as the tap channel is manually opened and gradually. It was left for 24 hours. Next day the tap channel was closed tightly and the dried material collected.

6.3.11 UV-Vis analysis

UV-visible spectral analysis was recorded using a JACO V550 UV-visible spectrometer between 200 and 900 nm against a water reference. Auto zero was done.

Calibrations were carried out for all dyes compounds used in this thesis. Standard aqueous solutions of known concentrations were prepared and analysed. Distilled water was used as background.

Table.6.2: UV-vis λ_{max} absorbance spectroscopy used for calibration of the dyes

Dye name	Abbreviation	λ_{max} (nm)
Procion Yellow H-EXL(PY)	PY	416
Remazol Black (RB)	RB	600
Procion Crimson H-EXL (PC)	PC	545
Procion Navy H-EXL (PN)	PN	606

6.3.12 Inductively coupled plasma atomic emission spectroscopy (ICP-OES)

Perkin Elmer® Optima™ 7300 DV ICP-OES instrument (Shelton, CT, USA) was used which is equipped with WinLab32™ for ICP Version 4.0 software for simultaneous measurement of all analytes wavelengths of interest. By connecting a Segmented-array Charge-coupled Device (SCD) detector and an echelle optical system. High radio frequency (RF) power was applied to generate a robust plasma. The ICP-OES instrument was started and taken to operation conditions and let stabilized. The sample introduction system was checked and the wavelengths were tuned. The instrument was standardised.

Then the received sample solutions containing metal ions were converted to aerosols via a nebulizer. The aerosols are transported to the inductively coupled plasma which is a high temperature zone (8000-10000 °C). The analytes are heated to different (atomic and/or ionic) states. They produce characteristic optical emissions. These emissions are separated based on their respective wavelengths and their intensities which were measured by spectrometry. The intensities are proportional to the concentrations of analytes in the aqueous sample. The quantification is an external multipoint linear standardization by comparing the emission intensity of an unknown sample with that of a standard sample. Eventually, the amount of metal ions were recorded in each sample.

6.4 Preparation of alginic acid derived Algibon

One gram native alginic acid was added to 20 mL glass vial with plastic lid containing deionised water. It was heated at 100 °C with constant agitation (5 rpm) for 160 minutes and cooled to room temperature before being stored for 24 hours at 5 °C in the fridge for retrogradation. The resulting biphasic mixture was separated by vacuum filtration using a sintered glass funnel (ID 2nm) to remove excess water. The gel (residue) was subjected to solvent exchange by three repeated wash each with ethanol (20 mL) followed by acetone (20 mL). For each wash, the mixture was constantly agitated (5 rpm) for 30 minutes except for the first wash with ethanol which took one hour, and allowed for several minutes to separate into a clear liquid and solid phase and filtered. For the final solvent exchange with acetone, filtration was left for 15 minutes to remove as much acetone as possible. Thereafter, the expanded alginic acid was dried in vacuum oven overnight at 50 °C to give a light fine powder of

expanded alginic acid. Porosity of the product was tested by nitrogen sorption analysis.

Large scale of expanded alginic acid was prepared by charging 200 g of native alginic acid into a modified pressure cooker attached with a mechanical stirrer. 4 L distilled water was added into the pressure cooker containing the native alginic acid. The pressure cooker lid was attached and closed. The solution was mixed at room temperature for at least 15 minutes after which it was heated at 100 ^{o}C for 160 minutes and cooled to room temperature before being stored for 24 hours at 5 ^{o}C in the fridge. The mixture was separated by large vacuum filtration using a sintered glass funnel (ID 2nm) to remove excess water. The retrograded gel was subjected to solvent exchange by three repeated wash each with ethanol (4 L) followed by acetone (4 L). For each wash, the mixture was constantly stirred (5 rpm) for 30 minutes with the exception of the first wash with ethanol which was for one hour. It was allowed for several minutes to separate into a clear liquid and solid phase and filtered. For the final solvent exchange with acetone, filtration was left for 15 minutes to remove as much acetone as possible. Thenceforth, the expanded alginic acid was dried in a Thar SFE500 super critical CO_2 extractor operating at 50 ^{o}C/100 bar for 200 g for approximately 3 hours. The depressurisation of the system was gradually carried out overnight. Finally, light fine powder of expanded alginic acid obtained. This material is called expanded alginic acid $scCO_2$ dried (A2) and the porous structure of this product was examined using nitrogen porosimeter. This mesoporous material was carbonised at rate 1 ^{o}C/min up to 175 ^{o}C and from 175 ^{o}C at below 0.5 ^{o}C/min to various preparation temperatures (i.e. 300, 450, 600 and 800 ^{o}C) in nitrogen atmosphere in Netzsch to generate Algibons (i.e. A300, A450, A600 and A800). The quality of the Algibons generated was tested by nitrogen sorption analysis.

6.4.1 Preparation of expanded alginic acid

The preparation was first done on a small scale to establish the conditions which gave the best results for the expanded alginic acid production. Thereafter it was scale-up using the same procedure. The influence of gelatinisation temperature, time and the effect of retrogradation time on the expanded material were investigated. The effect of using different types of low surface tension organic fluids employed in solvent exchange on the porosity of the

expanded material was investigated. The following experiments were carried out to obtain a suitable method for preparing the mesoporous alginic acid.

6.4.1.1 Experiment one: Gelation studies at 80 ^{o}C over varying time periods

The following stages of expansion process were performed to produce expanded alginic acid in this experiment. At first, gelation of native alginic acid at 80 ^{o}C was carried out at varying period of times.

Sample Preparation

4 samples of 5% (1 gm of alginic acid/20 mL distilled water) were put into glass vial tube (sized 35 mL) containing a small magnetic stirrer bar to mix the solution well, and the glass vials were covered with plastic lids. These samples are called Sa1, Sa2, Sa3 and Sa4 respectively.

Gelatinisation

The four individual samples prepared (5%) of alginic acid were put into an aluminium heating block tube for gelatinisation. The gelation temperature was set at 80 ^{o}C and on reaching the set temperature the set up was held with constant agitation (5 rpm) for 40, 80, 120 and 160 minutes for samples Sa1, Sa2, Sa3 and Sa4 respectively.

Table.6.3: Gives information on gelatinisation of native alginic acid at 80 ^{o}C and different certain times with constant stirring in aluminium heating block tube

Samples	Concentration (1 g of alginic acid/20 mL D.W)	Gelatinisation Temperature	Gelatinisation time
Sa1	5%	80 ^{o}C	40 min
Sa2	5%	80 ^{o}C	80 min
Sa3	5%	80 ^{o}C	120 min
Sa4	5%	80 ^{o}C	160 min

Retrogradation

Retrogradation was performed after gelatinisation had yielded a water-gel product. Samples Sa1, Sa2, Sa3 and Sa4 were removed from the heating source, allowed to cool down and then transferred into a fridge at 5 ^{o}C for 24 hours.

Solvent exchange

The resulting biphasic mixture from the retrogradation stage was separated by vacuum filtration using a sintered glass funnel (ID 2nm) to remove excess water. The gel was solvent exchanged by three repeated wash each with ethanol (20 mL) followed by acetone (20 mL). For each wash, the mixture was constantly agitated (5 rpm) for 30 minutes except for the first wash with ethanol which took one hour, and allowed for several minutes to separate into a clear liquid and solid phase and filtered. For the final solvent exchange with acetone, filtration was left for 15 minutes to remove as much acetone as possible.

Drying process

The samples' precipitates were dried in the vacuum oven overnight at 50 ^{o}C after solvent exchange had completed. For the drying process, the samples were collected in beakers (400 mL) and covered with pierced aluminium foil. The quality of the resulting powdery product, that is, expanded alginic acid was tested by nitrogen sorption analysis.

6.4.1.2 Experiment two: Gelation studies at 90 ^{o}C over varying time periods

The same procedure stated in section 6.4.1.1 was used for all stages of preparation except for gelation process which was carried out at temperature of 90 ^{o}C. The summary of this experiment is illustrated below in Table 6.4.

Table.6.4: Provides information about preparation of expanded alginic acid gelatinised at 90 ^{o}C over different period of times with constant stirring in aluminium heating block tube

Sample name	CAa in Dw	Gn Cn		Rt Cn	Solvent exchange with ethanol (3times) Volume (mL) of ethanol used Stirring duration			Solvent exchange with acetone (3times) Volume (mL) of acetone used Stirring duration			Total volume of solvent used	Drying process in vacuum oven Temperature/ time
		T	Time		1st (1h)	2nd (30 min)	3rd (30 min)	1st (30 min)	2nd (30 min)	3rd (30 min)		
Sb1	(1 g/20 mL) (5%)	90 ^{o}C	40 min	+5 ^{o}C / 1 day	20 mL	20 mL	20 mL	20 mL	20 mL	20 mL	120 mL	50 ^{o}C/ 24 h
Sb2	(1 g/20 mL) (5%)	90 ^{o}C	80 min	+5 ^{o}C /1 day	20 mL	20 mL	20 mL	20 mL	20 mL	20 mL	120 mL	50 ^{o}C/ 24 h
Sb3	(1 g/20 mL) (5%)	90 ^{o}C	120 min	+5 ^{o}C/ 1 day	20 mL	20 mL	20 mL	20 mL	20 mL	20 mL	120 mL	50 ^{o}C/ 24 h
Sb4	1 g/20 mL) (5%)	90 ^{o}C	160 min	+5 ^{o}C /1 day	20 mL	20 mL	20 mL	20 mL	20 mL	20 mL	120 mL	50 ^{o}C/ 24 h

CAa in DW: Concentration of alginic acid in distilled water
Gn Cn: Gelatinisation conditions
Rt Cn: Retrogradation conditions
EtOH: Ethanol
Acet: Acetone

6.4.1.3 Experiment three: Gelation studies at 100 ^{o}C over varying time periods

Similar technological stages were performed as operated for expanding alginic acid in section (6.4.1.1 Experiment one), but with gelatinisation temperature being 100 ^{o}C throughout changing time periods. The conditions of this experiment are placed in Table 6.5.

Table.6.5: Summarizes the preparation of expanded alginic acid gelatinised at 100 ^{o}C over different period of times with constant stirring in aluminium heating block tube

Sample name	CAa in Dw	Gn Cn		Rt Cn	Solvent exchange with ethanol (3times) Volume (mL) of ethanol used Stirring duration			Solvent exchange with acetone (3times) Volume (mL) of acetone used Stirring duration			Total volume of solvent used	Drying process in vacuum oven Temperature/ time
		T	Time		1st (1h)	2nd (30 min)	3rd (30 min)	1st (30 min)	2nd (30 min)	3rd (30 min)		
Sc1	(1 g/20 mL) (5%)	100 ^{o}C	40 min	+5 ^{o}C / 1 day	20 mL	20 mL	20 mL	20 mL	20 mL	20 mL	120 mL	50 ^{o}C/ 24 h
Sc2	(1 g/20 mL) (5%)	100 ^{o}C	80 min	+5 ^{o}C /1 day	20 mL	20 mL	20 mL	20 mL	20 mL	20 mL	120 mL	50 ^{o}C/ 24 h
Sc3	(1 g/20 mL) (5%)	100 ^{o}C	120 min	+5 ^{o}C/ 1 day	20 mL	20 mL	20 mL	20 mL	20 mL	20 mL	120 mL	50 ^{o}C/ 40 h
Sc4	(1 g/20 mL) (5%)	100 ^{o}C	160 min	+5 ^{o}C /1 day	20 mL	20 mL	20 mL	20 mL	20 mL	20 mL	120 mL	50 ^{o}C/ 24 h

CAa in DW: Concentration of Alginic acid in distilled water
Gn Cn: Gelatinisation conditions
Rt Cn: Retrogradation conditions
EtOH: Ethanol
Acet: Acetone

6.4.1.4 Experiment four: Gelation studies at 110 ^{o}C over varying time periods

Same procedure of sample preparation and stages of expansion process (i.e. gelation, retrogradation, solvent exchange with ethanol and acetone followed by vacuum oven dried) were performed, however, the gelation temperature was fixed at 110 ^{o}C over 40, 80, 120 and 160 min. The states of this experiment are presented in Table 6.6.

Table.6.6: Shows the preparation of expanded alginic acid gelatinised at 110 ^{o}C over varying time period with constant stirring in aluminium heating block tube

Sample name	CAa in Dw	Gn Cn		Rt Cn	Solvent exchange with ethanol (3times) Volume (mL) of ethanol used Stirring duration			Solvent exchange with acetone (3times) Volume (mL) of acetone used Stirring duration			Total volume of solvent used	Drying process in vacuum oven Temperature/ time
		T	Time		1st (1h)	2nd (30 min)	3rd (30 min)	1st (30 min)	2nd (30 min)	3rd (30 min)		
Sd1	(1 g/20 mL) (5%)	110 ^{o}C	40 min	+5 ^{o}C / 1 day	20 mL	20 mL	20 mL	20 mL	20 mL	20 mL	120 mL	50 ^{o}C/ 24 h
Sd2	(1 g/20 mL) (5%)	110 ^{o}C	80 min	+5 ^{o}C /1 day	20 mL	20 mL	20 mL	20 mL	20 mL	20 mL	120 mL	50 ^{o}C/ 24 h
Sd3	(1 g/20 mL) (5%)	110 ^{o}C	120 min	+5 ^{o}C/ 1 day	20 mL	20 mL	20 mL	20 mL	20 mL	20 mL	120 mL	50 ^{o}C/ 40 h
Sd4	g/20 mL) (5%)	110 ^{o}C	160 min	+5 ^{o}C /1 day	20 mL	20 mL	20 mL	20 mL	20 mL	20 mL	120 mL	50 ^{o}C/ 24 h

CAa in DW: Concentration of Alginic acid in distilled water
Gn Cn: Gelatinisation conditions
Rt Cn: Retrogradation conditions
EtOH: Ethanol
Acet: Acetone

6.4.1.5 Experiment five: Effect of time on retrogradation process

The same procedure for sample preparation was performed as described in section (6.4.1.1 experiment one). The gelatinisation temperature and time (100 ^{o}C/160 min.) found were applied for gelatinisation process. Retrogradation was conducted at (5 ^{o}C) but for varying time periods. Information on this experiment is below in Table 6.7. The final products were tested by porosimetry analysis.

Table.6.7: Shows retrogradation process at 5 $^{\circ}$C over varying period of time for expanded alginic acid

Sample name	CAa in Dw	Gn Cn		Rt Cn	Solvent exchange with ethanol (3times) Volume (mL) of ethanol used Stirring duration			Solvent exchange with acetone (3times) Volume (mL) of acetone used Stirring duration			Total volume of solvent used	Drying process in vacuum oven Temperature/ time
		T	Time		1st (1h)	2nd (30 min)	3rd (30 min)	1st (30 min)	2nd (30 min)	3rd (30 min)		
Se1	(1 g/20 mL) (5%)	100 $^{\circ}$C	160 min	zero	20 mL	20 mL	20 mL	20 mL	20 mL	20 mL	120 mL	50 $^{\circ}$C/ 24 h
Se2	(1 g/20 mL) (5%)	100 $^{\circ}$C	160 min	5 $^{\circ}$C / 0.5 day	20 mL	20 mL	20 mL	20 mL	20 mL	20 mL	120 mL	50 $^{\circ}$C/ 24 h
Se3	(1 g/20 mL) (5%)	100 $^{\circ}$C	160 min	5 $^{\circ}$C / 1 day	20 mL	20 mL	20 mL	20 mL	20 mL	20 mL	120 mL	50 $^{\circ}$C/ 24 h
Se4	(1 g/20 mL) (5%)	100 $^{\circ}$C	160 min	5 $^{\circ}$C / 2 day	20 mL	20 mL	20 mL	20 mL	20 mL	20 mL	120 mL	50 $^{\circ}$C/ 24 h
Se5	(1 g/20 mL) (5%)	100 $^{\circ}$C	160 min	5 $^{\circ}$C /3 days	20 mL	20 mL	20 mL	20 mL	20 mL	20 mL	120 mL	50 $^{\circ}$C/ 24 h
Se6	(1 g/20 mL) (5%)	100 $^{\circ}$C	160 min	5 $^{\circ}$C/ 4 days	20 mL	20 mL	20 mL	20 mL	20 mL	20 mL	120 mL	50 $^{\circ}$C/ 40 h
Se7	(1 g/20 mL) (5%)	100 $^{\circ}$C	160 min	5 $^{\circ}$C/ 5 days	20 mL	20 mL	20 mL	20 mL	20 mL	20 mL	120 mL	50 $^{\circ}$C/ 24 h

CAa in DW: Concentration of alginic acid in distilled water, Gn Cn: Gelatinisation conditions, Rt Cn: Retrogradation conditions, EtOH: Ethanol, Acet: Acetone

6.4.1.6 Experiment six: Effect of solvent choice for drying retrograded gel

The procedure of sample preparation, gelatinisation (100 $^{\circ}$C/160 min.), retrogradation (5 $^{\circ}$C for 1 day) were followed as described in section (6.4.1.5 experiment five). Effect of using different organic fluids for gel solvent exchange was investigated. All retrograded gel samples, after complete wash, were

vacuum oven dried at 50 ^{o}C overnight. Another retrograded gel sample which was solvent exchanged with ethanol and then acetone was scCO$_2$ dried at 50 ^{o}C for three hours. Porosity of all final products from drying was measured by nitrogen sorption analysis. Summary of this experiment is in Table.6.8.

Table.6.8: Shows the use of different organic fluids for solvent exchanging the water in the alginic acid gel

Sample name	CAa in Dw	Gn Cn		Rt Cn	Solvent exchange with ethanol (3times)			Solvent exchange with different solvents (3times)			Total volume of solvent used	Drying process
					Volume (mL) of solvent used			Volume (mL) of solvent used				
					Stirring duration			Stirring duration				Temperature/ time
		T	Time		1st (1h)	2nd (30 min)	3rd (30 min)	1st (30 min)	2nd (30 min)	3rd (30 min)		
Sf1	(1 g/20 mL) (5%)	100 ^{o}C	160 min	+5 ^{o}C / 1 day	20 mL EtOH	20 mL EtOH	20 mL EtOH	No	No	No	60 mL	50 ^{o}C/ 24 h Vacuum oven
Sf2	(1 g/20 mL) (5%)	100 ^{o}C	160 min	+5 ^{o}C /1 day	20 mL EtOH	20 mL EtOH	20 mL EtOH	20 mL EtOH	20 mL EtOH	20 mL EtOH	120 mL	50 ^{o}C/ 24 h Vacuum oven
Sf3	(1 g/20 mL) (5%)	100 ^{o}C	160 min	+5 ^{o}C/ 1 day	20 mL EtOH	20 mL EtOH	20 mL EtOH	20 mL MeOH	20 mL MeOH	20 mL MeOH	120 mL	50 ^{o}C/ 24 h Vacuum oven
Sf4	(1 g/20 mL) (5%)	100 ^{o}C	160 min	+5 ^{o}C/ 1 day	20 mL EtOH	20 mL EtOH	20 mL EtOH	20 mL Hex	20 mL Hex	20 mL Hex	120 mL	50 ^{o}C/ 24 h Vacuum oven
Sf5	(1 g/20 mL) (5%)	100 ^{o}C	160 min	+5 ^{o}C / 1 day	20 mL EtOH	20 mL EtOH	20 mL EtOH	20 mL Acet	20 mL Acet	20 mL Acet	20 mL	50 ^{o}C/ 24 h Vacuum oven
Sf6	(1 g/20 mL) (5%)	100 ^{o}C	160 min	+5 oC / 1 day	20 mL EtOH	20 mL EtOH	20 mL EtOH	20 mL Acet	20 mL Acet	20 mL Acet	120 mL	50 ^{o}C/ scCO$_2$ 24 h

CAa I DW: Concentration of alginic acid in distilled water
Gn Cn: Gelatinisation conditions, Rt Cn: Retrogradation conditions; EtOH: Ethanol, MeOH: Metahnol, Hex: Hexane, Acet: Acetone, scCO$_2$: Super critical CO$_2$.

6.4.2 Production of Algibons from the mesoporous alginic acid precursor via temperature-controlled carbonisation

A temperature programme and control was proposed to carbonise the mesoporous alginic acid obtained to generate Algibons. This carbonisation process was taken place in Netzsch 409 STA thermal analyser under nitrogen

gas on small technical scale. 200 mg of mesoporous alginic acid scCO$_2$ dried was employed in a 3.5 mL ceramic crucible and heated under a flow rate of nitrogen 100 ml/min with slow heating temperature rate. This carbonisation temperature programme generated a promising quality of mesoporous Algibons. Products porosity were tested by nitrogen sorption analysis. The following temperature programmes were applied to obtain different textural properties of Algibons.

6.4.2.1 Carbonisation temperature profile for Algibon300 production

Carbonisation temperature programme was applied in the Netzsch to pyrolysis the mesoporous alginic acid to 300 ^{o}C to generate A300 (see Table 6.9).

Table.6.9: Temperature programming control run for generating A300 from the precursor

Temperature ^{o}C	Temperature rate ^{o}C/min	Time of isotherm temperature	Time of emergency rest temperature
25			
100	1		
175	0.2	20 min	
250	0.2	40 min	
300	0.2	20 min	
320			Controlled

Based on the temperature programme was used to prepare A300, the same temperature rate (revealed in Table 6.9) was applied from room temperature up to 300 ^{o}C for generating the other Algibons, but temperature rate 0.3 ^{o}C/min was applied from 300 ^{o}C to 350, 400, 600 and 800 ^{o}C to produce A350, A400, A450 and A800 respectively.

6.4.2.2 Carbonisation temperature profile for Algibon450 production

Temperature programme of A450 preparation is placed in Table 6.10. Carbonisation process was conducted in an inert nitrogen atmosphere in Netzsch.

Table.6.10: Temperature programming was run for generating A450 from the precursor achieved

Temperature °C	Temperature rate °C/min	Time of isotherm temperature	Time of emergency rest temperature
25			
100	1		
175	0.2	20 min	
250	0.2	40 min	
300	0.2	20 min	
450	0.3	15 min	
470			Controlled

6.4.2.3 Carbonisation temperature profile for Algibon600 production

Temperature of A600 preparation is in Table 6.11.

Table.6.11: Temperature programming was run for generating A600 from the precursor achieved

Temperature °C	Temperature rate °C/min	Time of isotherm temperature	Time of emergency rest temperature
25			
100	1		
175	0.2	20 min	
250	0.2	40 min	
300	0.2	20 min	
600	0.3	15 min	
620			Controlled

6.4.2.4 Carbonisation temperature profile for Algibon800 production

Temperature of A800 preparation is in Table 6.12.

Table.6.12: Temperature programming was run for generating A800 from the precursor achieved

Temperature °C	Temperature rate °C/min	Time of isotherm temperature	Time of emergency rest temperature
25			
100	1		
175	0.2	20 min	
250	0.2	40 min	
300	0.2	20 min	
800	0.3	15 min	
820			Controlled

6.5 Dye adsorption experiments using porous adsorbents (Porous adsorbents application in bulky dye adsorption)

Standard stock solution of the four dyes used were prepared in volumetric flasks using distilled water at the following concentration: Procion Yellow (PY) 140 mg/L, Remazol Black (RB) 140 mg/L, Procion Crimson (PC) 140 mg/L, Procion Navy (PN) 140 mg/L. All dyes were completely dissolved with sufficient amount of water and stirred well and completed to the mark in 1000 mL volumetric flask by distilled water. The samples were taken to be analysed by UV-vis spectroscopy for initial concentration before use in adsorption studies. From each standard stock solution a series of solutions containing each dye was prepared. At the first step of the investigation using these standard dyes solutions calibration curves for each dye was developed. After that, the minimum time for the adsorption equilibrium achievement of the dyes was estimated during kinetic experiments using eight adsorbents (i.e. S300, S450, S800, A300, A450, A800, Ac and Sgel) to each dye solution with optical density 1 A.U. of UV-Vis absorbance spectroscopy using a JASCO V-550 UV/VIS spectrometer. Then sample were taken for UV-Vis measurement at certain time contacts.

The dye adsorption loads by the materials (Q_e) were determined at equilibrium which represent the amount of dye in milligram adsorbed by one gram of each adsorbent used.

Hyperchem software was used to draw the three dimensional structure of the dyes. Nitrogen sorption analysis was measured for the adsorbents used for dye removal. Both drawn 3-D dyes structures and the porosimetry results were taken to further supporting the explanation of different rate of dye uptake by the carbonaceous materials used. The bulky organic dye size was compared to the pores of A800 and Ac which were proposed based on the pore size distribution.

Kinetic order model study was carried out for dye adsorption using A800, A450 and AC to find an appropriate kinetic model.

Dye adsorption study was further investigated by processing the results obtained in four known models which were Langmuir, Freundlich, Tempkin and Dubinin-Radushkevich adsorption. Langmuir equation, which was the successful model, was applied to draw a plot between C_e/Q_e versus C_e, it gave the maximum adsorption capacity (Q_m) and constant of equilibrium (K).

Thermodynamic adsorption study were conducted for the four dyes using A800 and AC adsorbents at four different temperatures: 25, 35, 45 and 55 ^{o}C. From the applied Langmuir equation, the constant of equilibriums (K) for dye adsorption at 25, 35, 45 and 55 ^{o}C were found. The slope and the intercept from the plot between the obtained constant of equilibrium (K) versus (1/T in Kelvin) gave enthalpy or energy of adsorption (E_{ads}) and entropy of the system respectively. Eventually, free energy values for each dye using A800 and Ac were calculated from the found enthalpy (E_{ads}) and entropy at temperatures 25, 35, 45 and 55 ^{o}C.

The regeneration of Algibon used was carried out using three different techniques: i) Direct thermal treatment, ii) Dye recovery and adsorbent regeneration using solvent and iii) Indirect thermal treatment of A800 loaded with dye. The regenerated A800 was successfully reused in dye removal application.

6.5.1 Calibration curve for the dyes used

Series of dyes concentrations (5, 10, 20, 30, 40, 50, 60, 70, 80 100, 120, 140 mg/L) were prepared. One mL of every series of dye concentrations was

individually taken for UV-spectroscopy measurement, aimed to determine the maximum wavelength (λ) which will be used for further UV-vis spectroscopy measurement.

Table.6.13: Maximum wavelength for the dyes described in this research work

Dye	Maximum wavelength λ_{max} (nm)
Procion Yellow (PY)	417
Remazol Black (RB)	595
Procion Crimson (PC)	545
Procion Navy (PN)	607

6.5.2 Adsorption kinetic procedure

For the kinetic adsorption studies each dye solution was prepared at a concentration that corresponded to one arbitrary unit of UV spectroscopy at the λ_{max} wavelength. 100 mg of each absorbent (i.e. three different types of Algibons (A800, A450, A300) and Starbons (S800, S450, S300) as well as activated carbon and silica gel were individually added into 100 mL of that dye solution had concentration corresponded to one arbitrary unit of UV spectroscopy. But in case of RB only 20 mg of each adsorbent was employed for 100 mL of the Remazol black solution. To follow the kinetic process, a number of samples were taken at 30, 60, 240, 640, 1440, 2880, 4320 minutes for UV-VIS measurement. The kinetic curves were plotted between the dye adsorbed% versus the contact times for each dye using eight adsorbents.

The dyes adsorption loads were plotted for every adsorbent as contact time reached equilibrium (4320 min.). The following law was applied to calculate the dye adsorption load by each adsorbent material employed:

$$Qe = \frac{(C_o - C_e) * V}{m}$$

Q_e is the amount of dye in milligram adsorbed by one gram of adsorbent used, it is measured by (mg/g). C_o is the initial concentration of the dye solution; Ce is the concentration of the dye solution (mg/L) as adsorption reached equilibrium, V volume of the solution used (L) and m is the mass of the adsorbent used (g).

198

6.5.3 Types of kinetic order model

The following kinetic order models were applied to check the pseudo first and second order model:

6.5.3.1 Pseudo first order model

For this model the linearised form of the Lagergren pseudo-first-order equation is used:

$$\ln(Q_e - Q_t) = \ln Q_e - K_1 \, t$$

Where Q_e is the amount of dye adsorbed (mg/g) at equilibrium, Q_t is the amount of dye adsorbed at time t (min), k_1 (min^{-1}) is the pseudo-first-order rate constant of adsorption. A straight line of $\ln(Q_e - Q_t)$ versus t suggests the applicability of this kinetic model.

Plot between $\ln(Q_e - Q_t)$ versus time t gives a slope which corresponds to constant of kinetic first order reaction (K_1). Exponential of the intercept of that plot corresponds to the dye adsorption load at equilibrium.

6.5.3.2 Pseudo second order model

The following equation used to determine the appropriateness of the pseudo-second-order model for the adsorption process:

$$\frac{t}{Q_t} = \frac{1}{K_2 Q_e^2} + \frac{1}{Q_e} t$$

Where K_2 (g mg^{-1} min^{-1}) represents the pseudo-second-order rate constant. A straight line of t/Q_t versus t suggests the applicability of this kinetic model.

Plot between t/Q_t against time t gives a slope. The inverse of that slope is dye adsorption load at equilibrium. The inverse of [$(Q_e)^2$ * intercept of that plot] is the constant of kinetic second order reaction (K_2).

6.5.4 Dye adsorption study

From each dye standard stock solution a series of solutions containing each dye with concentrations (40, 60, 80, 100, 120 and 140 mg/L) was prepared. 10 mL of each dye series of concentrations was employed to 10 mg of A800 adsorbent, except in case of RB dye, 25 mL of RB series of concentrations were employed to 5 mg A800. Adsorption process held for 72 hours. After

adsorption completed, each set of series samples were taken for UV-Vis spectrometry measurement. The same steps were repeated for the dyes using A450 and AC adsorbents.

The obtained results were processed in different kinds of adsorption isotherm models such as Langmuir, Freundlich, Temkin and Dubinin-Radushkevich adsorption.

6.5.4.1 Langmuir adsorption equation

The data obtained was processed in Langmuir equation:

$$\frac{C_e}{Q_e} = \frac{1}{Q_m\,K} + \frac{C_e}{Q_m}$$

K is constant of equilibrium, C_e concentration of the dye or sample at equilibrium and Q_m is maximum adsorption capacity.

Inverse of slope from the plot between C_e/Q_e versus C_e for each dye corresponded to the dye maximum adsorption capacity (Q_m) and constant of equilibrium (K) can be found as following:

$$K = \frac{1}{Q_m * \text{Intercept}}$$

The found K can be applied in the following equation:

$$R_L = \frac{1}{1 + K_L \cdot C_o}$$

R_L is Equilibrium parameter, K is the constant of equilibrium found and C_o is the initial concentration of the dyes. If R_L is greater than one means the adsorption is unfavourable, equal to one means adsorption is linear. R_L greater than zero and smaller than one means it is favourable. If it is zero means adsorption is irreversible.

6.5.4.2 Freundlich adsorption equation

The Freundlich equation was applied to the data:

$$LnQ_m = lnK_F + \frac{1}{n}lnC_e$$

Q_m is maximum adsorption capacity, K_F constant of Freundlich and n heterogeneity factor, and signifies the intensity of adsorption.

K_F and n can be obtained from the plot between $\ln Q_e$ against $\ln C_e$. The slope and intercept of that plot corresponded to K_F and n respectively.

6.5.4.3 Temkin adsorption equation

This model of adsorption was carried out to process the data:

$$Q_e = \frac{RT}{b} LnA + \frac{RT}{b} LnC_e$$

RT/b= B (J/mol) presents the Temkin constant related to heat of sorption, A is measured in (L/g), which is (intercept divided by slope), is the equilibrium binding constant gives the maximum binding energy (J/mol). R (8.314 J/mol K) is the universal gas constant and T is the absolute solution temperature in Kelvin degree.

Plot between the Q_e versus LnC_e gives slope and intercept. Slope corresponds to B (heat of adsorption). Exponential of A corresponds to maximum binding energy.

6.5.4.4 Dubinin-Radushkevich adsorption equation

The received results were processed in Dubinin-Radushkevich equation:

$$Q_e = Q_e e^{(-K\varepsilon^2)}$$

This equation can be written for the linear form of adsorption model as follow:

$$\ln Q_e = \ln Q_m - K\varepsilon^2$$

$$\varepsilon = RT \ln\left(1 + \frac{1}{C_e}\right)$$

Where Q_m signifies the monolayer saturation capacity (mg/g) and K the constant of adsorption energy which gives (E) the mean free energy (J/ mol) of adsorption per molecule of adsorbate when it is transferred to the surface of the solid from the solution and can be determined from the equation written below:

$$E = \frac{1}{\sqrt{2K}}$$

Plot between lnQ$_e$ versus $\mathcal{E}$ gives a slope which corresponds to the constant of adsorption energy (K) and the exponential of the intercept of that plot presents the maximum adsorption capacity Q$_m$ (mg/g).

6.5.5 Effect of temperature on adsorption isotherm

A stock solution of each individual dye was prepared. For example, (140 mg/L) stock solution of PC dye was made. A series of solutions from the stock solution was prepared including (40, 60, 80, 100, 120 and 140 mg/L).

10 mL of each of the single PC dye solution was poured into the glass vial plastic lead containing 10 mg of A800 and magnetic stirrer bar. The adsorption was carried out at 25 ^{o}C for 72 hours with constant stirring. The same steps were conducted, but at 35, 45 and 55 ^{o}C. At the end 24 samples were collected and took for UV-vis spectroscopy measurement.

The same procedure was repeated to the other dyes, but in case of RB dye, 5 mg of A800 was employed to 25 mL of each RB dye solution. In the end, the Langmuir equation was applied for the points obtained at the various temperatures applied. The maximum adsorption capacity (Q$_m$) and constant of equilibrium (K) was found for each system.

The constants of equilibrium (K) found were converted to Lnk. Plot between lnK versus 1/T in Kelvin degree gave slope and intercept which corresponded to the energies of adsorption (from gradients) and entropy of adsorption (from gradient).

The same steps were repeated in order to find the enthalpy (E$_{ads}$) and entropy (ΔS) for each individual dye using activated carbon.

Changes in free energies (ΔG) were found for each dye using A800 and Ac at 25, 35, 45 and 55 ^{o}C.

Surface area dye coverage for both Algibon800 and activated carbon adsorbents was determined using the following equation:

$$\theta = \frac{Q_m *(\textbf{Avogadro number})*(\textbf{dye surface area})}{\textbf{Dye molecular weight}}$$

θ is surface area of adsorbent dye coverage (m^2/g), Q_m is maximum adsorpation capacity of each dye (mg/g) at ambient temperature, Avogadro number is $6.023*10^{23}$ mol^{-1} and molecular wight of each dye is 1416 g/mol for Procion Yellow (PY) ($C_{49}H_{39}O_{18}S_4Cl_2N_{15}Na_4$), 893 g/mol for Remazol Black (RB) ($C_{24}H_{17}O_{19}S_6Na_4$), 1608 g/mol for Procion Crimson (PC) ($C_{53}H_{33}O_{26}S_8Cl_2N_{14}$) and 1336 g/mol for Procion Navy (PN) ($C_{42}H_{32}O_{19}S_6Cl_2N_{15}Na$).

6.5.6 Dye desorption experiment

It began with adsorption of dye. 1000 mg of each dye was individually dissolved in a sufficient amount of distilled water in a 500 volumetric flask and completed to the label with distilled water. Before the adsorption experiment, 2.5 mL of each concentrated dye was diluted in 100 mL volumetric flask and measured applying UV-VIS spectrometer. These measurements were taken as initial absorbance (Ao) of the dyes.

To undertake the adsorption experiment, 250 mL of each individual concentrated dye was added into a 500 mL sized glass bottle reactor containing 1 gram of A800. Then adsorption was run for 72 hours with constant agitation. After adsorption had been carried out, 2.5 mL of the filtrate of each dye solution was taken and then diluted into 100 mL. It was measured by UV-VIS spectrometer. These measurements were taken as absorbance (Ai) of the dyes after adsorption reached equilibrium. Then the amount of dye adsorbed by A800 was found as following:

Amount of dye adsorbed by A800 = amount of initial dye-amount of dye remained

The A800 loaded with the individual dye was filtrated and freeze dried. 50 mg of A800 contaminated with each dye was taken for porosimetry analysis. Their pore size distribution (**dV/dD**) were drawn versus **pore diameter** (nm) and compared to the initial A800.

The regeneration of A800 used was carried out using three different procedures:

6.5.6.1 Direct thermal treatment

Thermal gravimetric analysis was applied using a Netzsch 409 STA thermal analyser. Samples (100 mg of each individual sample) were mounted in a 3.5 mL ceramic crucible and heated from room to 800 ^{o}C (rate of heat was 10 ^{o}C

per minute) under a flow nitrogen rate (100 mL/min). 50 mg of the thermally treated dyes contained A800 were collected and analysed by nitrogen sorption analysis.

6.5.6.2 Dye recovery and adsorbent regeneration using solvent

10 mg of dyes containing A800 were individually added into a vial glass (35 mL size) plastic led containing a magnetic stirrer bar. 10 mL of distilled water was poured into the system. The samples were put into the aluminium heating tube block. The system was heated to 30 ^{o}C. The loaded A800 with the dyes was constantly mixed at stirring rate (2 rpm) and held for two hours. After two hours of stirring at 30 C, the samples were centrifuged for 30 minutes. The samples filtrates were collected using syringe filter. The collected filtrates were taken for UV-VIS spectrometry measurement.

Second portion of 10 mL distilled water was added into the remaining contaminated A800 with the dyes which were in the bottom of the vial glass. The system was mixed for another two hours at 30 ^{o}C at the same rate of stirring. Then it was centrifuged and the filtrate was syringe filtered and sent for measurement. The same steps were repeated to further wash the dye containing A800 until the colour disappeared. The last portion of distilled water (10 mL) was added and the system was left for 24 hours. To ensure disappearance of the colour was completed.

The same procedure was conducted for dyes desorption from the A800 using distilled water at 50 ^{o}C. Desorption using ethanol at both temperatures 30 and 50 ^{o}C was done by carrying out the same procedure described.

6.5.6.3 Indirect thermal treatment of A800 loaded with dye

This procedure consisted of the combination of warm ethanol followed by Starbon thermal treatment.

500 mg of each individual A800 were loaded with the dyes, after they had been freeze dried; the contents were added into beakers containing a magnetic stirrer bar. 100 mL of ethanol was then added into each system. The systems were heated to 50 ^{o}C and held for 1 hour. The solution were filtrated and the collected precipitates (dyes contained A800) were returned to the beaker the same steps were repeated two times more. The final precipitates were collected and dried in oven at 100 ^{o}C overnight.

150 mg of each dye that contained A800, had been ethanol washed, were respectively mounted in a 3.5 mL ceramic crucible in a Netzsch 409 STA thermal analyser. The system was heated to 800 ^{o}C (rate of thermal treatment was 10 ^{o}C per minute) under nitrogen flow rated 100 mL per minute. The thermally treated dyes containing A800 were collected. The regenerated Algibons were analysed using nitrogen sorption analysis.

6.5.7 Regenerated Algibon application in dye removal

10 mg of the regenerated Algibon A800(r) was added into each individual series of concentrations (i.e. 40, 60, 80, 100, 120 and 140 mg/L) of PN. Magnetic stirrer bars were added to the systems with stirring constantly continued for 72 hours at normal temperature. The samples filtrates were collected and sent for UV-VIS measurement.

The same procedure was repeated for RB dye, but in this case 5 mg of the regenerated A800 was employed for 25 mL of each individual concentration of the RB dye solution. Langmuir equation was applied for both dyes using regenerated Algibon A800(r). The dyes maximum adsorption capacities were found. The same steps were applied for both dyes using initial Algibon A800(i).

6.6 Metal adsorption procedure

6.6.1 Metals recovery in digested solid waste

One gram of each ash (Pulverised fly ash, Red Mud, bottom ash, Titano gypsum, Red Titanogypsum and Phosphogypsum) was individually added into a microwave cylinder container, and then 50 mL of nitric acid (0.2 M) was added. The microwave cylinder container containing the ash, nitric acid and magnetic stirrer bar was kept in the microwave reactor chamber. Temperature was controlled and held on 200 ^{o}C for one hour. The water phase from the digested ash was then filtrated. 5 mL of the filtrate was mixed with 20 mL deionised ultra pure water. 10 mg of the Starbon adsorbent materials including Starbon300, Starbon800, A300 and A800 were employed into the glass vial containing a small magnetic stirrer bar. The 25 mL of the prepared diluted form of the filtrate collected was employed into the glass vial containing the adsorbent materials and a small magnetic stirrer bar. After 24 hours contact time, the samples were centrifuged for 30 minutes and the water phase was syringe filtered. 10 µL of the water phase collected was taken by micropipette

and diluted with 10 mL deionised ultra pure water. The final solutions were then sent for inductively coupled plasma atomic emission spectroscopy (ICP-AES) to measure the amount of metals removed. The initial concentration of each metal ion in every solid waste was already determined.

Methodology of estimation of Starbon selectivity in metals adsorption is described below:

i) estimation of relevant amount of certain metal Me_n (Solution) in the solution as a ratio between concentration of this metal in the solution $[Me_n]^{solution}$ and sum of concentration of all elements in solution- $\Sigma_i [Me_i]^{solution}$.

ii) Estimation of relevant amount of certain metal Men (surface) on the surface as a ratio between surface concentration of this metal $[Me_n]^{surface}$ and sum of concentration of all others elements on the surface-$\Sigma_i [Me_i]^{surface}$.

iii) Estimation of adsorption selectivity (Starbon selectivity effect) as a ratio:

Me_n (surface): Me_n (solution) = $[Me_n]$ surface: $\Sigma_i [Mei]surface/[Men]^{solution}$: $\Sigma i [Mei]^{solution}$

Table.6.14: Investigated materials for metals adsorption

Solid waste	Starbons			
	S300	**S800**	**A800**	**A300**
Fly ash (PFA)		█████		
Red mud (RM)		█████	█████	
Bottom ash (BA)	█████			
Titanogypsum (TG)	█████		█████	█████
Red (RTG)titanogypsum			█████	
Phosphogypsum (PG)		█████	█████	

6.6.2 Further study on metal adsorption using Algibon

Further systematic investigation on metal adsorption on Starbon based on A800 was carried out in a mixture sample comprising of four metals including (Cu, Co, Ag and Cd) metals ions.

Table.6.15: Series solutions of metals ions prepared from the stock mixture solution

Series of solutions	Concentration of metal (mg/L)			
	Co	Cu	Ag	Cd
Solution1	1.372	2.382	5.206	2.812
Solution 2	2.745	4.765	10.411	5.624
Solution 3	6.864	11.912	26.029	14.061
Solution 4	13.729	23.824	52.057	28.121
Solution 5	27.458	47.648	104.115	56.243

To measure the initial concentration of this sample, 10 µL of the sample solution mixture was added into 10 mL of deionised ultra pure distilled water. The initial metal ions concentrations and the diluted metals ions solutions concentrations, which were prepared from the original mixture sample solution, were measured by ICP.

10 mg of A800 adsorbent was individually employed to 10 mL of the series concentrations solutions of the mixture containing Co, Cu, Ag and Cd metals ions and adsorption held for 24 hours with stirring. The samples were centrifuged for 30 minutes and the filtrates were separated by syringe filter. The collected filtrates were sent for ICP measurement.

The obtained results were processed by applying types of adsorption isotherm equations like Langmuir, Freundlich, Tempkin and Dubinning-Raduschkic. Maximum adsorption capacity from Langmuir equation was found for each metal.

6.6.2.1 Metal kinetic adsorption

For the kinetic adsorption studies 100 mg of A800 adsorbent was employed for the initial mixture sample solution. The samples were taken one by one at each contact time (i.e. 0, 10 min, 30 min, 60 min, 120 min, 240 min,, 320 min, 1440 min). The kinetic curve was plotted between the metal adsorbed% versus the contact times for each metal using Algibon.

6.6.2.2 Metal kinetic order adsorption model

The following kinetic order equations were used to study the pseudo first and second order model:

6.6.2.2.1 Metal kinetic pseudo first order equation

The following equation was applied for this model of pseudo-first-order:

$$\ln(Q_e - Q_t) = \ln Q_e - K_1\, t$$

Where Q_e is the amount of metal adsorbed (mg/g) at equilibrium, Q_t is the amount of metal adsorbed at time t (min), k_1 (min^{-1}) is the pseudo-first-order rate constant of adsorption. A straight line of $\ln(Q_e\text{-}Q_t)$ versus t suggests the applicability of this kinetic model.

Plot between $\ln(Q_e\text{-}Q_t)$ versus time t gives a slope which represents the constant of kinetic first order reaction (K_1). Exponential of the intercept of that plot corresponds to the metal adsorption load at equilibrium.

6.6.2.2.2 Metal kinetic pseudo second order equation

The following equation used to determine the appropriateness of the pseudo-second-order model for the adsorption process:

$$\frac{t}{Q_t} = \frac{1}{K_2 Q_e^2} + \frac{1}{Q_e}\, t$$

Where K_2 (g mg^{-1}min^{-1}), represents the pseudo-second-order rate constant. A straight line of t/Q_t versus t suggests the applicability of this kinetic model.

Plot between t/Q_t against time t gives a slope. The inverse of that slope represents the metal adsorption load at equilibrium (Q_e). The inverse of [$(Q_e)^2$ * intercept of that plot] presents the constant of kinetic second order reaction (K_2).

CHAPTER SEVEN

Thesis Conclusion and Future Work

7.1 Conclusion observed

7.1.1 Preparation of expanded alginic acid precursor

A novel robust procedure of alginic acid expansion has been developed. It includes optimisation of parameters of each stage of expansion such as gelation, retrogradation, solvent exchange and drying. It has been found that the optimum procedure of alginic acid expansion has to be included:

1) Gelation: 160 minutes at temperature 100 ^{o}C.
2) Retrogradation: 24 hours at temperature 5 ^{o}C.
3) Solvent exchange: three ethanol followed by three acetone.
4) Drying: using scCO$_2$ 3h at 50°C and pressurised to 100 bar. Slowly depressurised for time12h.

The textural properties (pore volume ca 2 cm^3/g and pore diameter around 25 nm) of the mesoporous materials produced using optimised method.

7.1.2 Generating Algibons from the mesoporous alginic acid produced

Using thermal gravimetric analysis (TGA) and thermal gravimetric analysis coupled with Fourier transform Infrared spectroscopy (TG-FTIR) techniques, the mechanism of decomposition of the expanded alginic acid has been determined. Temperature profile for preparation of the Algibons at specific temperature (e.g. 300, 450, 600 and 800 °C) has been applied. It has been found that it is very important to keep the heating rate for carbonisation of the alginic acid at (0.3 ^{o}C/min.) under point 250°C.

The textural properties (pore volume ca 2.5 cm^3/g and pore diameter around 25 nm) of the mesoporous materials generated using the current method are substantially better than previously reported (V$_{pore}$= 1 cm^3/g; D$_{pore}$ = 16 nm).

Based on optimum procedure developed during the first part of this project a range of Algibons were generated and characterised using nitrogen adsorption, DRIFT-IR, TGA, SEM , elemental composition analysis, ash content and solid NMR.

7.1.3 Investigation of Algibons as adsorbent for reactive dye adsorption

The Algibons were employed in chapter four to capture potentially harmful compounds from aqueous water stream. It has been shown that Algibons significantly (up to six folds) overcome the typical microporous activated carbon

(AC) in removing bulky dyes which are globally used in cotton market and textile industry.   For bulky dye removal, the work demonstrated that adsorbent with a higher mesoporous character, A800, was found to be the best adsorber. This material also demonstrated much higher rate of adsorption for large dye molecules than microporous material such as AC. The adsorption of the dyes using Ac was not performed well, due to the small pore size and diameter of the Ac which limited its effectiveness for dye uptake.

The obtained results highlight that preparation temperature of Algibons is crucial in dye capture, demonstrating importance of adsorber surface functionality for dye removal efficiency. It was noticed that Algibons prepared at high temperature and therefore containing high carbon content exhibit better dye uptake. The high efficiency of the A800 adsorbent could be explained by π-π interaction between conjugated surface functional group of the adsorber and the aromatic rings of the dyes.

Overall, the work with Algibon preparation and application in bulky dye capture was very successful.

Algibons loaded with the dyes were regenerated by water and ethanol. They could unload the dyes up to certain level which was around 20%. Thermal treatment was carried out for the contaminated A800 with the dyes after warm ethanol wash had been conducted. It was observed that the textural property of the regenerated A800 was maintained. This implies the success in regenerating A800 used. The regenerated Algibon A800(r) was reused in bulky dye adsorption demonstrating similar efficiency to the initial material A800(i).

7.1.4 Metal ions removal using Algibon generated

Recovering high value elements including the valuable and critical from the rich metal contained solid wastes has been carried out using Novel Starbon materials. It has been found that the adsorption of metals is very sensitive to the nature of the Starbon surface functionality which has made possible selective adsorption of these metals using Starbon technology.

It appeared that Starbons had a good performance specificity towards the rare metals. It was also noticed that S800 was a better adsorber than S300. Algibon derived alginic acid is better than Starbon derived from starch. For example, it was observed that Au was efficiently adsorbed from the systems such as

S800/PFA, S800/red mud, A800/red mud and S300/bottom ash, but poorly from S300 /titanogypsum one. Likewise, Ag was efficiently adsorbed from S800/PFA, S300/Titanogypsum, A300/Titanogypsum sytems, but poorly from sytems such as A800/Red mud, S800/Phosphogypsum, S300/Bottom ash and A800/Red Titanogypsum.

In metals adsorption microporosity could play a great role as well as surface functionality of Starbons materials. The acidic functional groups in the active sites of the adsorber would bind the metals into the adsorbents as a result of replacing the surface hydrogens with the metals ions in the discharge. Adsorption could happen as a consequence of interaction between the π electron rich layers of the adsorbent and the vacant d orbitals of the metal ion species.

Additional research was carried out systematically on four concentrated metals ions (Co, Cu, Ag and Cd) containing mixture of sample solution based on Algibon. It was found that A800 recovered the metals ions discriminately. Metals adsorption was described by Langmuir adsorption isotherm which means the metals were adsorbed as a monolayer. The adsorption kinetic was followed by pseudo second order mechanism.

Despite the fact that Starbon materials are very successful at selectively recovering low concentration of high value metals ions. But it appears that Starbons would remove them discriminately when metals ions are in concentrated level.

Starbons application in receiving the important elements from the metals rich contained solid waste is of a great success achievement although it is acknowledged that Starbons technology could be established, particularly in the third world countries where local resource can be employed, to design a project to successfully treat wastewater containing metals. Applications of Starbon technology in both cases can be feasible for growing economy, minimising occupied space by wastes as well as to protect all life form from risk and the environment from pollution.

7.2 Future work

7.2.1 Reactive dye adsorption from industrial aqueous waste

It is known that Starbon materials could be produced in different shape including monolith. It will be interesting to apply Starbon monolith to the wastewater containing dyes. Furthermore, at the current investigation Algibons have only been tested for single component solutions and model systems. Although, in reality it is necessary to test Algibon performance for complex dyes mixture for their selectivity and efficiency. This implies that Starbons can either specifically or randomly adsorb dyes which suggests they could be deployed for treatment of water stream contaminated with dyes.

7.2.2 Regeneration of Algibon adsorbent

It is necessary to reduce waste and increase the green certificate of the Starbon material regeneration. It is very worthy to try to find out a method which not only regenerate the adsorbent, but also recover the dyes. This means the dyes are not destroyed. If this could be set up, it would be ideal. This way could allow both the adsorbent and the dye loaded be reused. The proposed methods for desorption of dyes without destroying them may be using pH change employing HCl or NaOH despite the fact that using strong acid and base are not environmentally friendly causing problem to the ecosystem.

7.2.3 Further work on metal ion removal

Owing to time limit, it was not possible during this work to do further experiment on using low temperature prepared Algibon and Starbon (i.e S300 and S800) for high concentration of metals ions removal in discharge. It would be a good idea if efficiency of A300, S300 and S800 will be compared with the A800 used.

Possibility of applying this novel technology in the industrial zone of Sulaimani city in Kurdistan region of Iraq would be very much appreciated in the future work. It can be extended to the neighbouring regional countries for wastewater treatment containing pollutants in collaboration with Green Chemistry Centre of Excellence at The University of York, UK. Another crucial future work could be the application of this technology to recover selective extraction of valuable components from soil or rocks in some areas of Kurdistan region. These natural resources are rich in various minerals. With proper control of these minerals using this technology, we can recover mixtures which will be very useful in applications including binders for construction, using it as a filler or tar to occupy the space between the support materials which are employed in restoration and

construction of asphalt road as well as playground, basketball court, driveway and it might also be useful in housing.

Appendices

Appendix one

Table.8.1.1: Typical composition of untreated domestic watstewater[38]

Contaminants	Unit	Concentration		
		Weak	Medium	Strong
Total solids (TS)	mg/L	350	720	1 200
Total dissolved solids (TDS)	mg/L	250	500	850
Fixed	mg/L	145	300	525
Volatile	mg/L	105	200	325
Suspended solids	mg/L	100	220	350
Fixed	mg/L	20	55	75
Volatile	mg/L	80	165	275
Settleable solids	mL/L	5	10	20
BOD5, 20ºC	mg/L	110	220	400
TOC	mg/L	80	160	290
COD	mg/L	250	500	1 000
Nitrogen (total as N)	mg/L	20	40	85
Organic	mg/L	8	15	35
Free ammonia	mg/L	12	25	50
Nitrites	mg/L	0	0	0
Nitrates	mg/L	0	0	0
Phosphorus (total as P)	mg/L	4	8	15
Organic	mg/L	1	3	5
Inorganic	mg/L	3	5	10
Chlorides	mg/L	30	50	100
Sulfate	mg/L	20	30	50
Alkalinity (as CaCO3)	mg/L	50	100	200
Grease	mg/L	50	100	150
Total coliforms	No/100 ml	10^6-10^7	10^7-10^8	10^7-10^9
Volatile organic compounds	μg/L	<100	100-400	>400

Table.8.1.2: Important contaminants in wastewater[39]

Contaminants	Reason for importance
Suspended solids (SS)	can lead to development of sludge deposits and anaerobic conditions when untreated wastewater is discharged to the aquatic environment.
Biodegradable organics	are principally made up of proteins, carbohydrates and fats. They are commonly measured in terms of BOD and COD. If discharged into inland rivers, streams or lakes, their biological stabilization can deplete natural oxygen resources and cause septic conditions that are detrimental to aquatic species.
Pathogenic organisms	found in waste-water can cause infectious diseases.
Priority pollutants	including organic and inorganic compounds, may be highly toxic, carcinogenic, mutagenic or teratogenic.
Refractory organics	that tend to resist conventional waste-water treatment include surfactants, phenols and agricultural pesticides.
Heavy metals	usually added by commercial and industrial activities must be removed for reuse of the waste-water.
Dissolved inorganic constituents	such as calcium, sodium and sulphate are often initially added to domestic water supplies, and may have to be removed for waste-water reuse.

Table.8.1.3: Information on Procion Yellow (PY) dye[140]

	Procion Yellow (PY)	
1	Form	Granular
2	Colour	Yellowish orange
3	Odour	Odourless
4	Molecular weight	1416 g/mol ($C_{49}H_{39}O_{18}S_4Cl_2N_{15}Na_4$)
5	Chemical characterisation	Azo reactive dyestuff preparation
6	Melting point	> 100 ^{o}C
7	Solubility in water	70 g/L (20 ^{o}C)
8	pH value	8-10 (10 g/L, 20 ^{o}C)
9	Hazardous decomposition	Not determined yet
10	Acute oral toxicity	LD50 >2000 mg/Kg (rat)
11	Acute inhalation toxicity	Not determined yet
12	Acute dermat toxicity	LD50 >2000 mg/Kg (rat)
13	Sensitisation	High concentration may result irritation of mucous membrane
14	Mutagenity	Not tetermined yet
15	Biodegradability	< 20% (slightly eliminable from water
16	Fish toxicity	LC50> 100 mg/L
17	Algae toxicity	EC50 > 100 mg/L
18	Bacteria toxicity	EC20 > 100 mg/L
19	Chemical Oxygen demand (COD)	1.113 mg/g
20	Biological oxygen demand (BOD)	< 100 mg/g (5 days)
21	Hazardous	Irritant and serious risk to damage eye

Table.8.1.4: Information on Remazol Black (RB) dye[140]

	Remazol Black (RB)	
1	Form	Powder
2	Colour	Black
3	Odour	Odourless
4	Molecular weight	893 g/mol ($C_{24}H_{17}O_{19}S_6Na_4$)
5	Chemical characterisation	Azo reactive dyestuff preparation
6	Melting point	Not determined yet
7	Solubility in water	> 100 g/L (20 ^{o}C)
8	pH value	4.5-7 (10 g/L, 20 ^{o}C)
9	Hazardous decomposition	Not determined yet
10	Acute oral toxicity	LD50 >2000 mg/Kg (rat)
11	Acute inhalation toxicity	Not determined yet
12	Acute dermat toxicity	Not determined yet
13	Sensitisation	May cause sensitisation by inhalation and skin contact
14	Mutagenity	Not tetermined yet
15	Biodegradability	10-25%
16	Fish toxicity	LC50> 100 mg/L
17	Algae toxicity	Not determined yet
18	Bacteria toxicity	EC20 > 1000 mg/L
19	Chemical Oxygen demand (COD)	Not determined yet
20	Biological oxygen demand (BOD)	Not determined yet
21	Hazardous	Harmful and may cause problem to inhalation and skin

Table.8.1.5: Information on Procion Crimson (PC) dye[140]

	Procion Crimson (PC)	
1	Form	Granule
2	Colour	Red
3	Odour	Odourless
4	Molecular weight	1608 g/mol ($C_{53}H_{33}O_{26}S_8Cl_2N_{14}$)
5	Chemical characterisation	Azo reactive dyestuff preparation
6	Melting point	> 100 ^{o}C
7	Solubility in water	> 140 g/L
8	pH value	7-9 (10 g/L, 20 ^{o}C)
9	Hazardous decomposition	Not determined yet
10	Acute oral toxicity	LD50 > 2000 mg/Kg (rat)
11	Acute inhalation toxicity	Not determined yet
12	Acute dermat toxicity	LD50 > 2000 mg/Kg (rat)
13	Sensitisation	Not yet observed
14	Mutagenity	Not tetermined yet
15	Biodegradability	< 20%
16	Fish toxicity	LC50> 100 mg/L
17	Algae toxicity	EC50 > 100 mg/L
18	Bacteria toxicity	IC50 > 1000 mg/L
19	Chemical Oxygen demand (COD)	1.22 mg/g
20	Biological oxygen demand (BOD)	< 30 mg/g
21	Hazardous	Irritant to skin and serious risk to damage eye

Table.8.1.6: Information on Procion Navy (PN) dye[140]

	Procion Navy (PN)	
1	Form	Powder
2	Colour	Deep blue
3	Odour	Odourless
4	Molecular weight	1336 g/mol ($C_{42}H_{32}O_{19}S_6Cl_2N_{15}Na$)
5	Chemical characterisation	Azo reactive dyestuff preparation
6	Melting point	Not determined yet
7	Solubility in water	150 g/L (20 ^{o}C)
8	pH value	6-7.5 (10 g/L, 20 ^{o}C)
9	Hazardous decomposition	Not determined yet
10	Acute oral toxicity	LD50 > 2000 mg/Kg (rat)
11	Acute inhalation toxicity	Not determined
12	Acute dermat toxicity	LD50 > 2000 mg/Kg (rat)
13	Sensitisation	Not yet observed
14	Mutagenity	Not determined
15	Biodegradability	50%
16	Fish toxicity	LC50> 100 mg/L
17	Algae toxicity	Not determined yet
18	Bacteria toxicity	EC10 > 1000 mg/L
19	Chemical Oxygen demand (COD)	Not determined
20	Biological oxygen demand (BOD)	Not determined
21	Hazardous	Could be not harmful

Appendix two
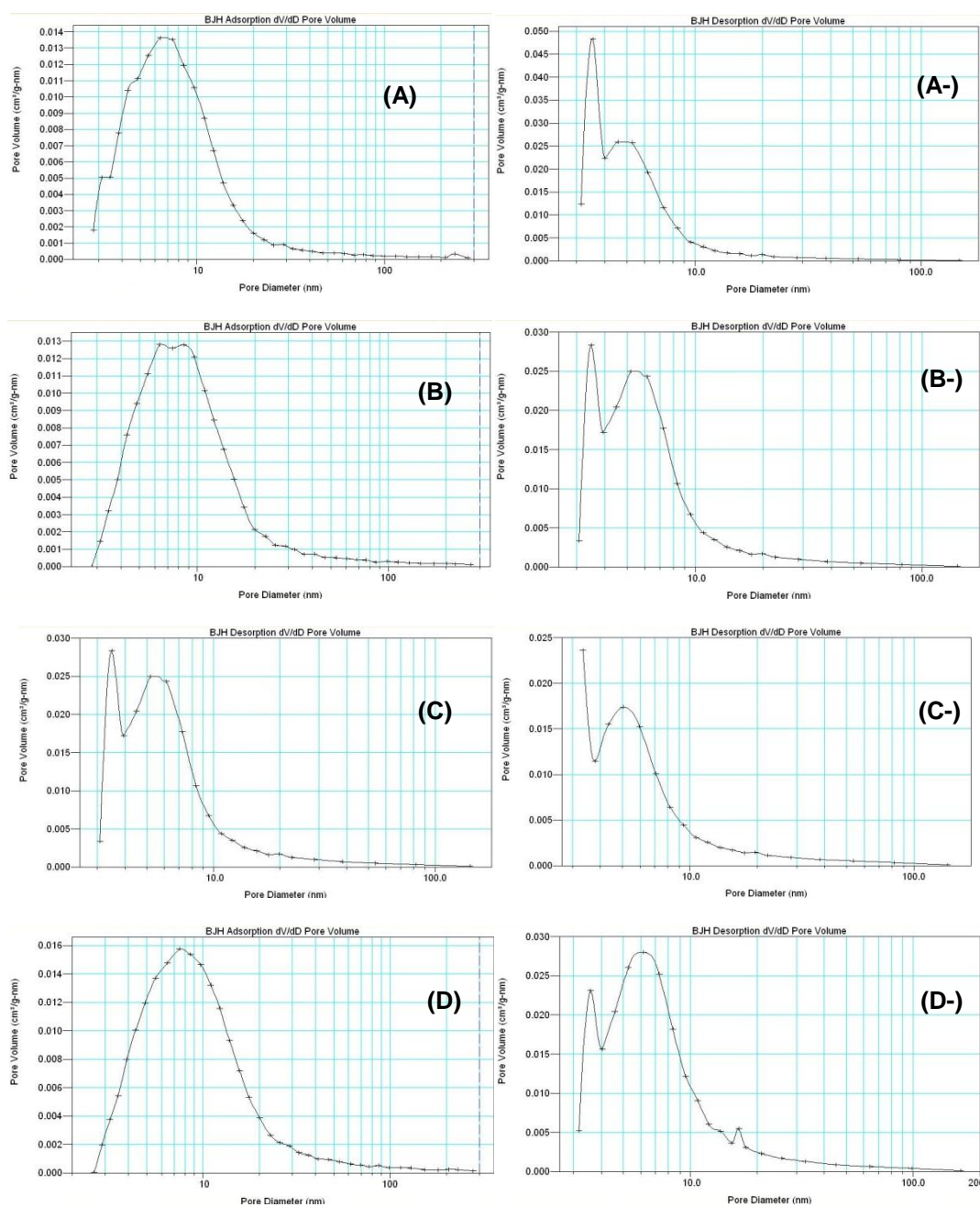
Fig.8.2.1: dV/dD pore size distribution of expanded alginic acid when gelation carried out at 80 ^{o}C for (A) 40 min.(adsorption pore size distribution), (A-) 40 min. (desorption pore size distribution); (B) 80 min (adsorption), (B-) 80 min (desorption); (C) 120 min (adsorption), (C-) 120 (desoption) and (D) 160 min (adsorption), (D-) 160 min (desorption).
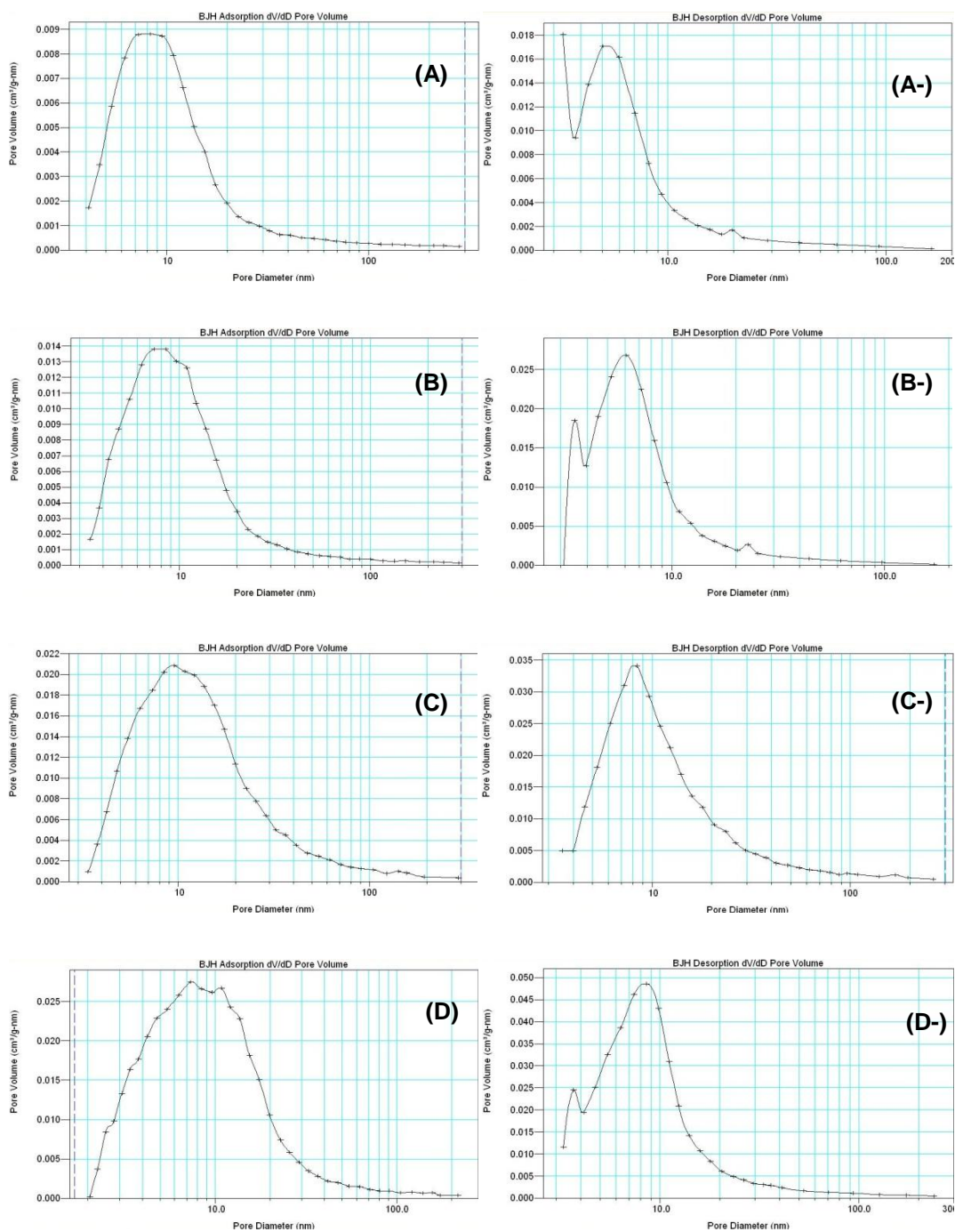
Fig.8.2.2: dV/dD pore size distribution of expanded alginic acid when gelation carried out at 90 °C for (A) 40 min.(adsorption pore size distribution), (A-) 40 min. (desorption pore size distribution); (B) 80 min (adsorption), (B-) 80 min (desorption); (C) 120 min (adsorption), (C-) 120 (desoption) and (D) 160 min (adsorption), (D-) 160 min (desorption).
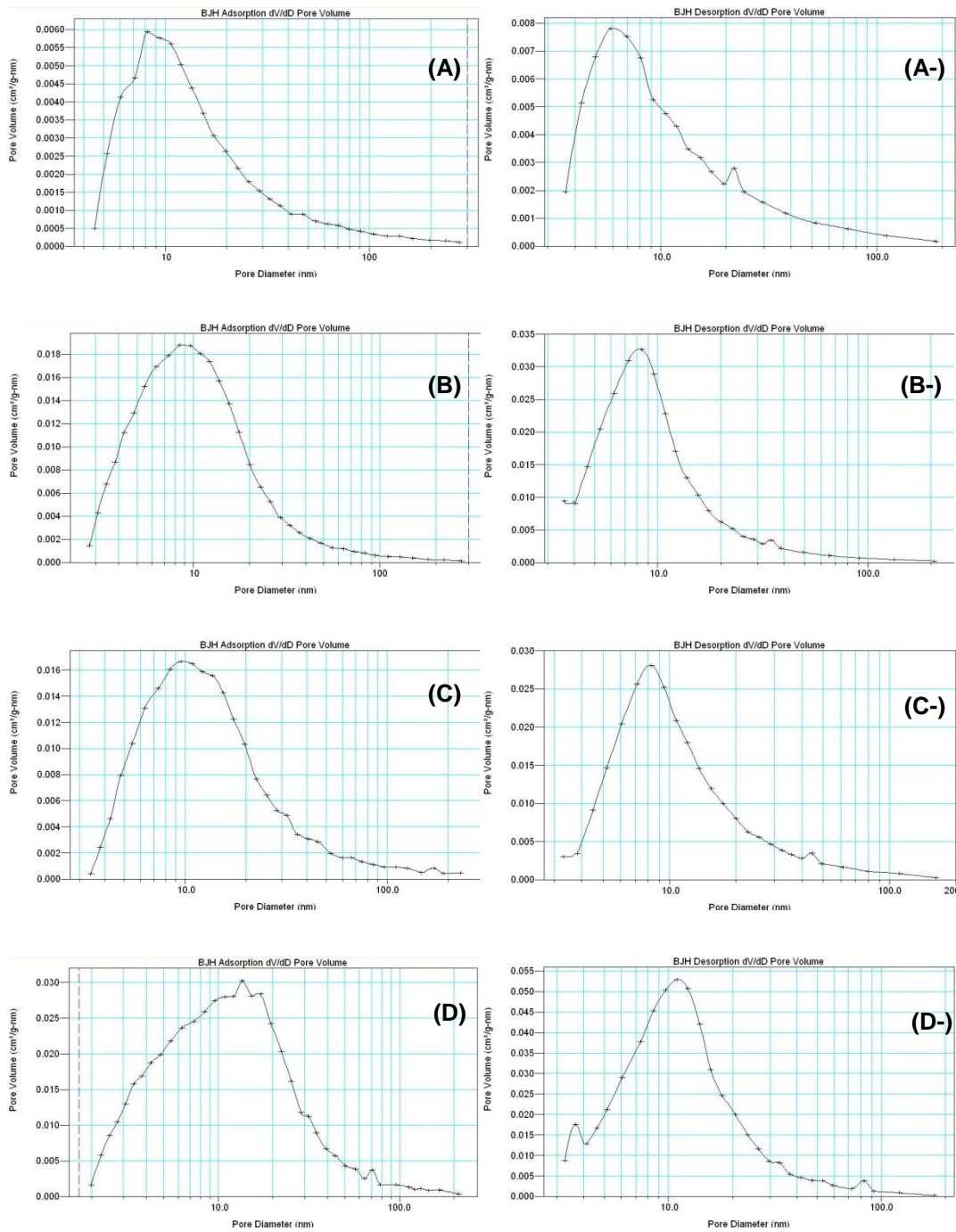
Fig.8.2.3: dV/dD pore size distribution of expanded alginic acid when gelation carried out at 100 °C for (A) 40 min.(adsorption pore size distribution), (A-) 40 min. (desorption pore size distribution); (B) 80 min (adsorption), (B-) 80 min (desorption); (C) 120 min (adsorption), (C-) 120 (desoption) and (D) 160 min (adsorption), (D-) 160 min (desorption).
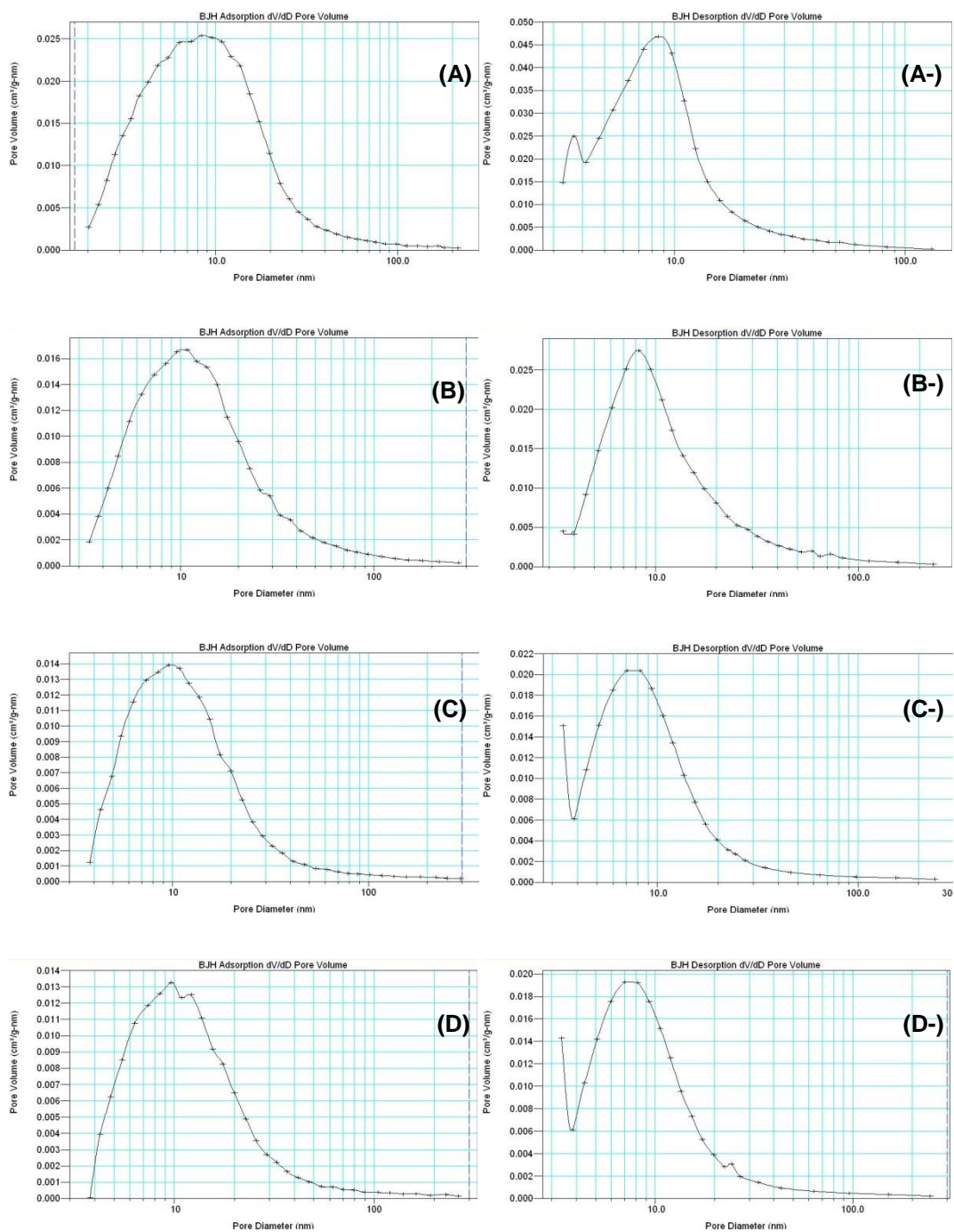
Fig.8.2.4: dV/dD pore size distribution of expanded alginic acid when gelation carried out at 110 °C for (A) 40 min.(adsorption pore size distribution), (A-) 40 min. (desorption pore size distribution); (B) 80 min (adsorption), (B-) 80 min (desorption); (C) 120 min (adsorption), (C-) 120 (desoption) and (D) 160 min (adsorption), (D-) 160 min (desorption).
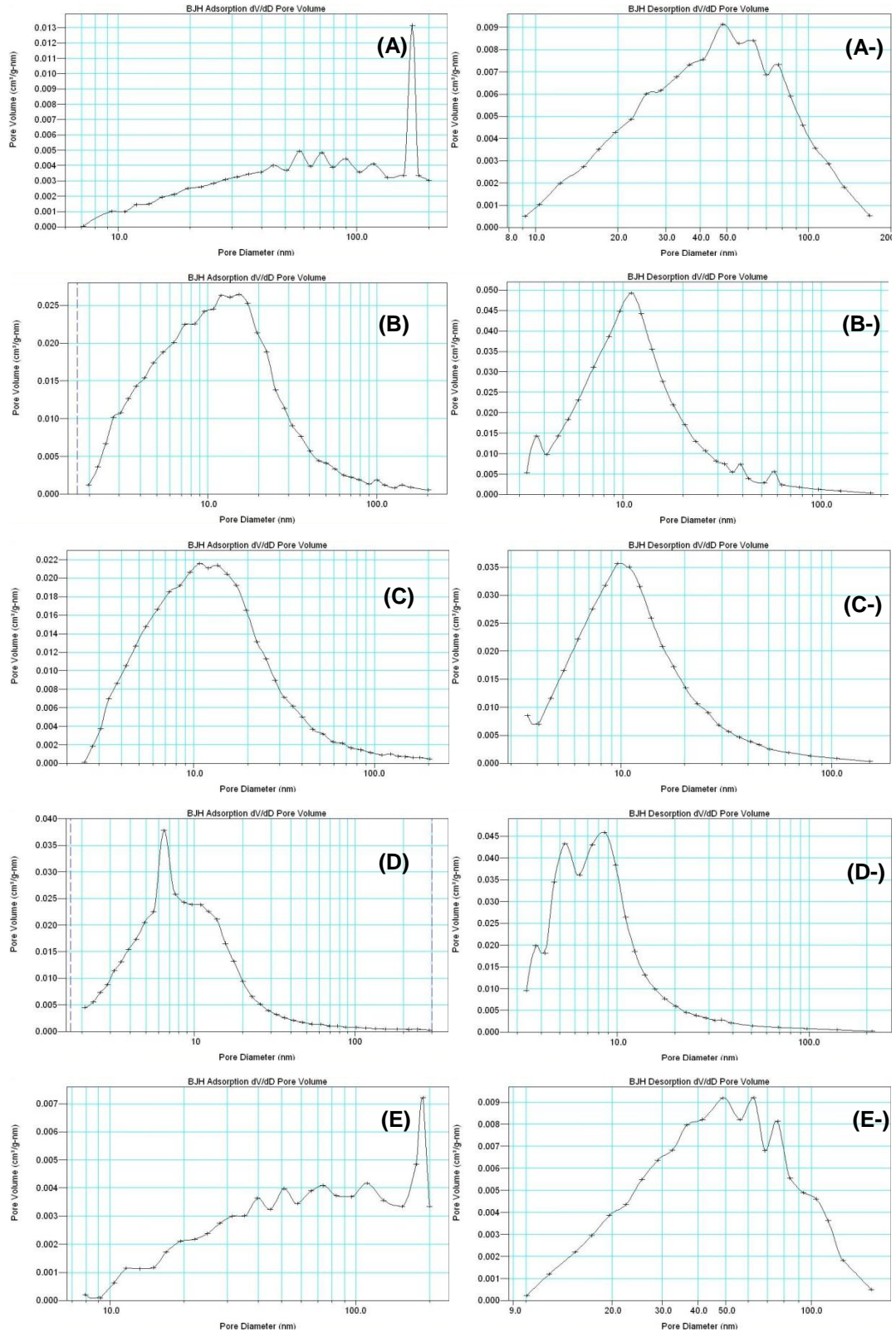
Fig.8.2.5: dV/dD pore size distribution of expanded alginic acid when retrogradation was carried out at 5 ^{o}C for (A) 12 h (adsorption pore size distribution (Apsd)), (A-) 12 h (desorption pore size distribution (Dpsd)); (B) 24 h (Apsd), (B-) 24 h (Dpsd); (C) 48 h (Apsd), (C-) 48 h (Dpsd); (D) 72 h (Apsd), (D-) 48 h (Dpsd); (E) 96 h (Apsd), (E-) 96 h (Dpsd).
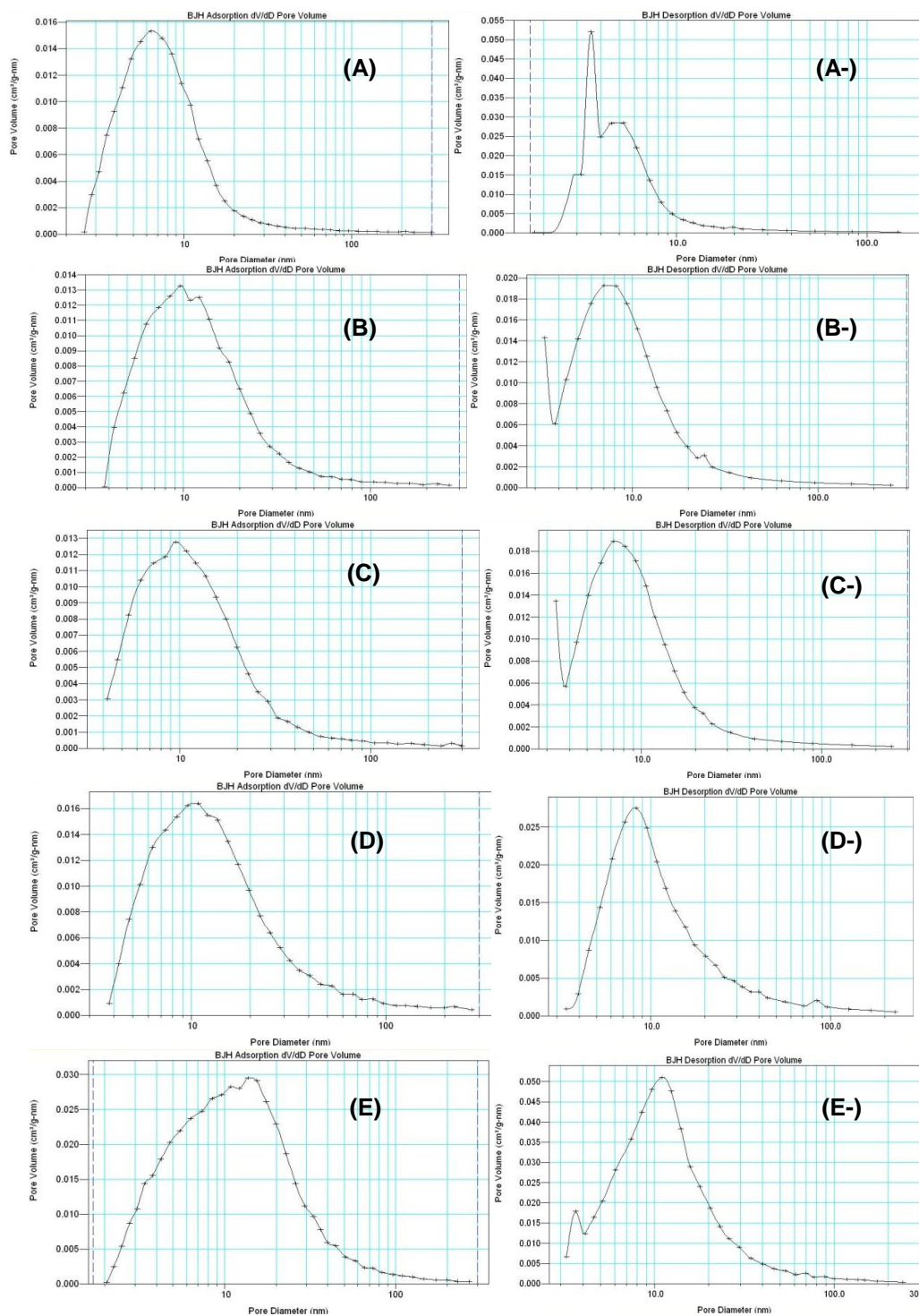
Fig.8.2.6: dV/dD pore size distribution for expanded alginic acid when the retograded gel was washed with (A) 3 times ethanol (adsorption pore size distribution (Apsd)), (A-) 3 times with ethanol (desorption pore size distribution (Dpsd)); (B) 3 times ethanol plus 3 times ethanol (Apsd), (B-) 3 times ethanol plus 3 times ethanol (Dpsd); (C) 3 times ethanol plus plus 3 times methanol (Apsd), (C-) 3 times ethanol plus 3 times methanol (Dpsd); (D) 3 times ethanol plus 3 times hexane (Apsd), (D-) 3 times ethanol plus 3 times hexane (Dpsd); (E) 3 times ethanol plus 3 times acetone (Apsd), (E-) 3 times ethanol plus 3 times acetone (Dpsd), all following by vacuum oven dried.
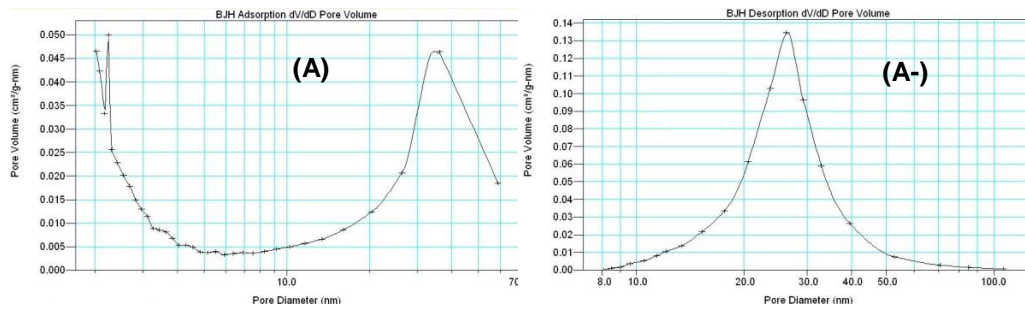
Fig.8.2.7: dV/dD pore size distribution for expanded alginic acid when the retograded gel was washed with (A) 3 times ethanol plus 3 times with acetone (adsorption pore size distribution (Apsd)), (A-) 3 times with ethanol plus 3 times with acetone desorption pore size distribution (Dpsd)) following by scCO$_2$ dried.
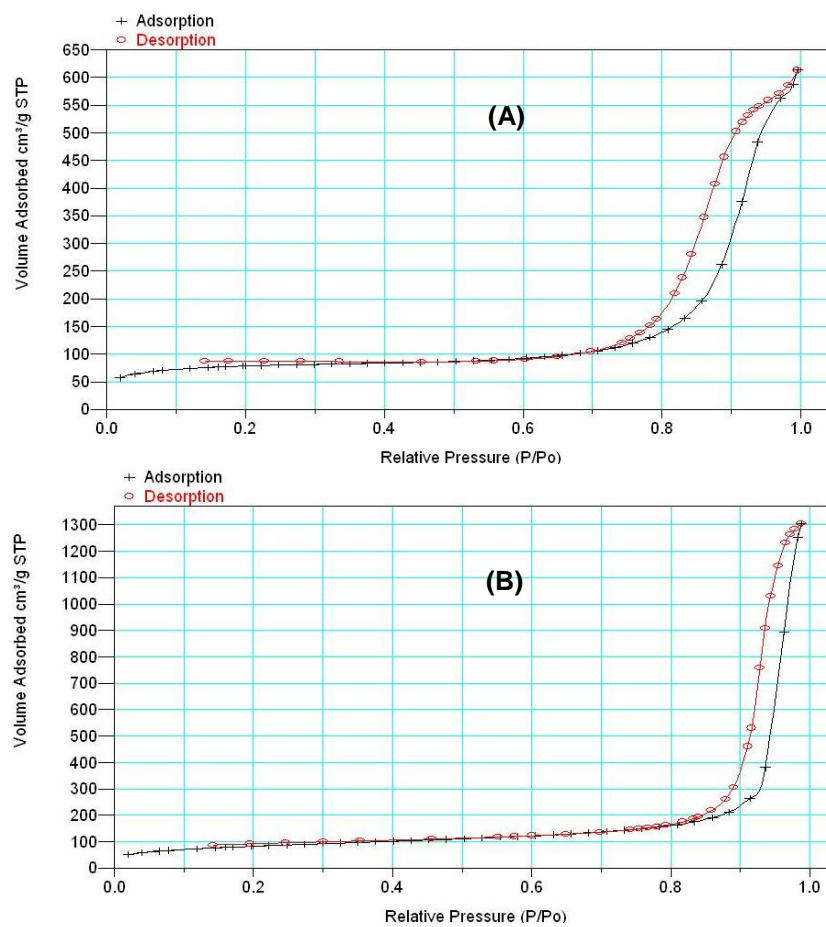
Fig.8.2.8: Linear isotherm plot for (A) expanded alginic acid, where the parametres of expansion are: gelation was done at 100 ^{o}C for 160 min, retrogradation was for 24 h at 5 ^{o}C, solvent exchange was 3 times with ethanol plus 3 times with acetone following acid vacuum oven dried (A1) and (B) expanded alginic acid, where the parametres of expansion are: gelation was done at 100 ^{o}C for 160 min, retrogradation was for 24 h at 5 ^{o}C, solvent exchange was 3 times with ethanol plus 3 times with acetone following scCO$_2$ dried.
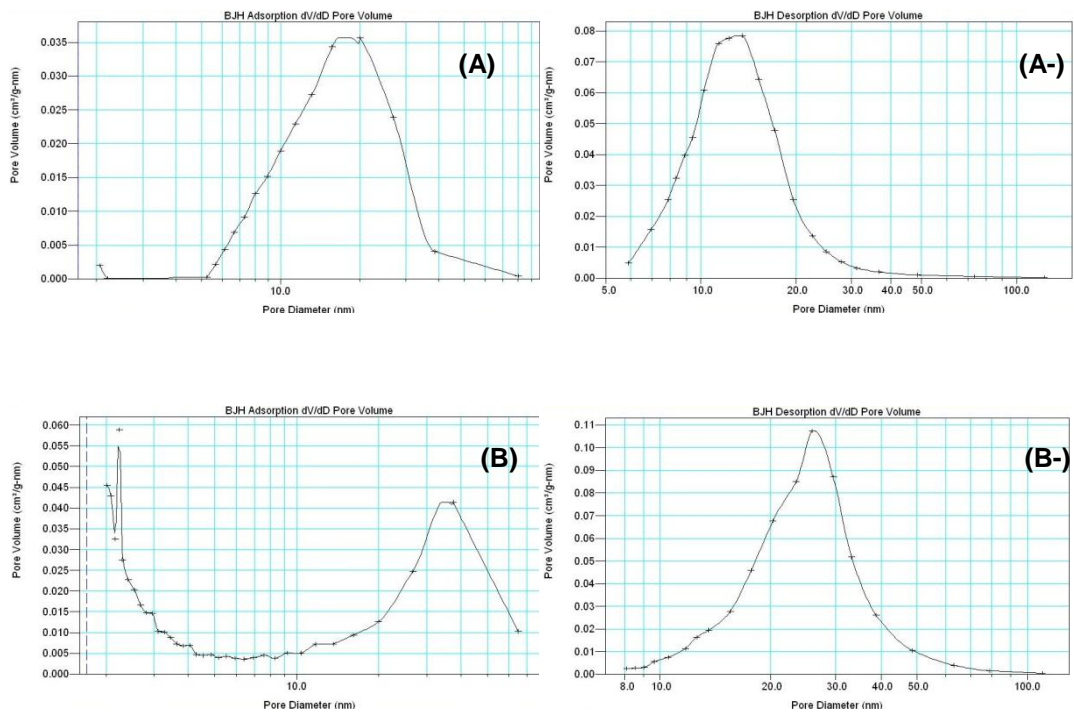
Fig.8.2.9: dV/dD pore size distribution for expanded alginic acid when the retograded gel was washed with (A) 3 times ethanol plus 3 times with acetone (adsorption pore size distribution (Apsd)), (A-) 3 times with ethanol plus 3 times with acetone desorption pore size distribution (Dpsd)) following by scCO$_2$ dried.

Appendix three
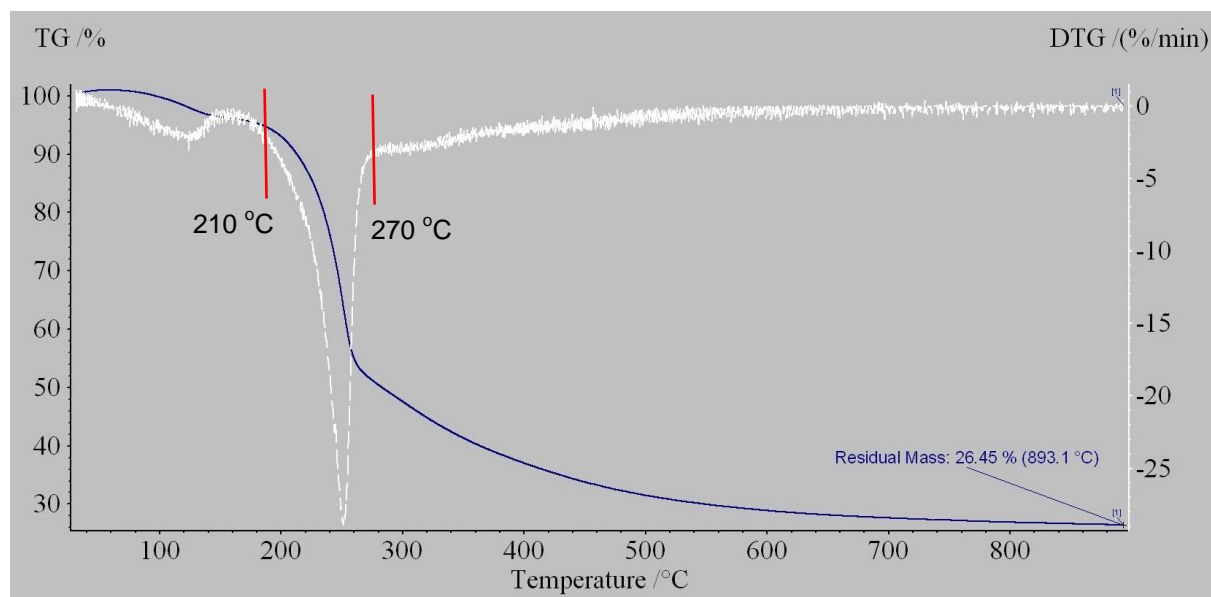
(A)
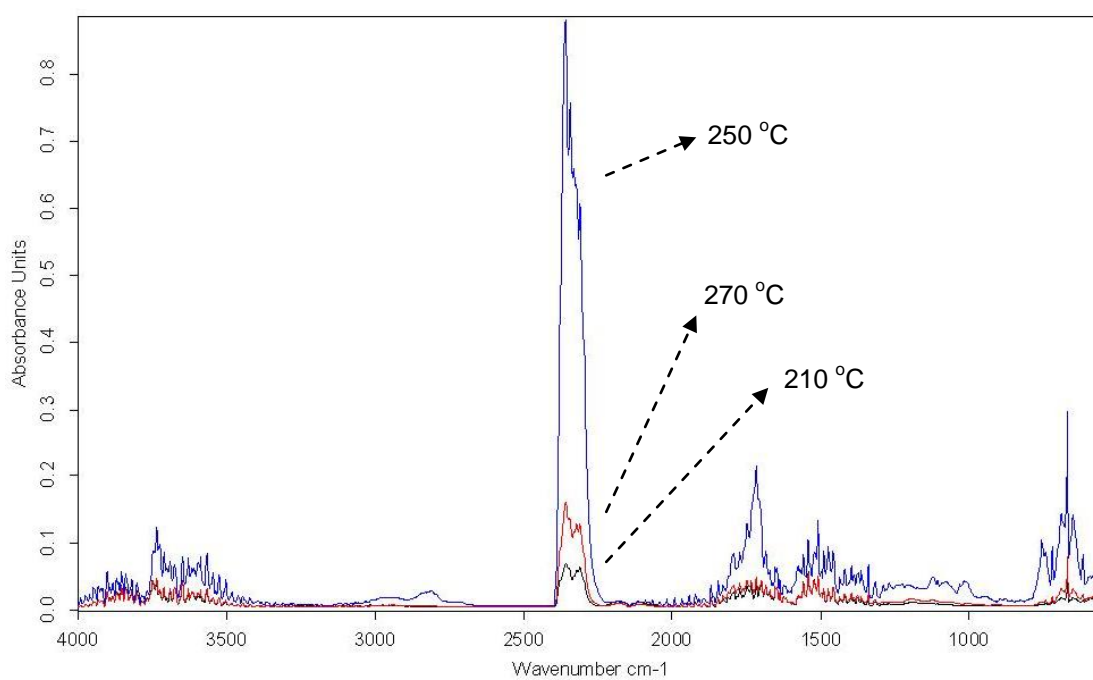
(B)

Fig.8.3.1: (A) TG figure of thermal pyrolysis of expanded alginic acid precursor from room temperature to 900 $^{\circ}$C using temperature rate (20 $^{\circ}$C/min.); (B) Spectrum of the components released at 210, 250 and 270 $^{\circ}$C respectively throughout the carbonisation of the expanded alginic acid.
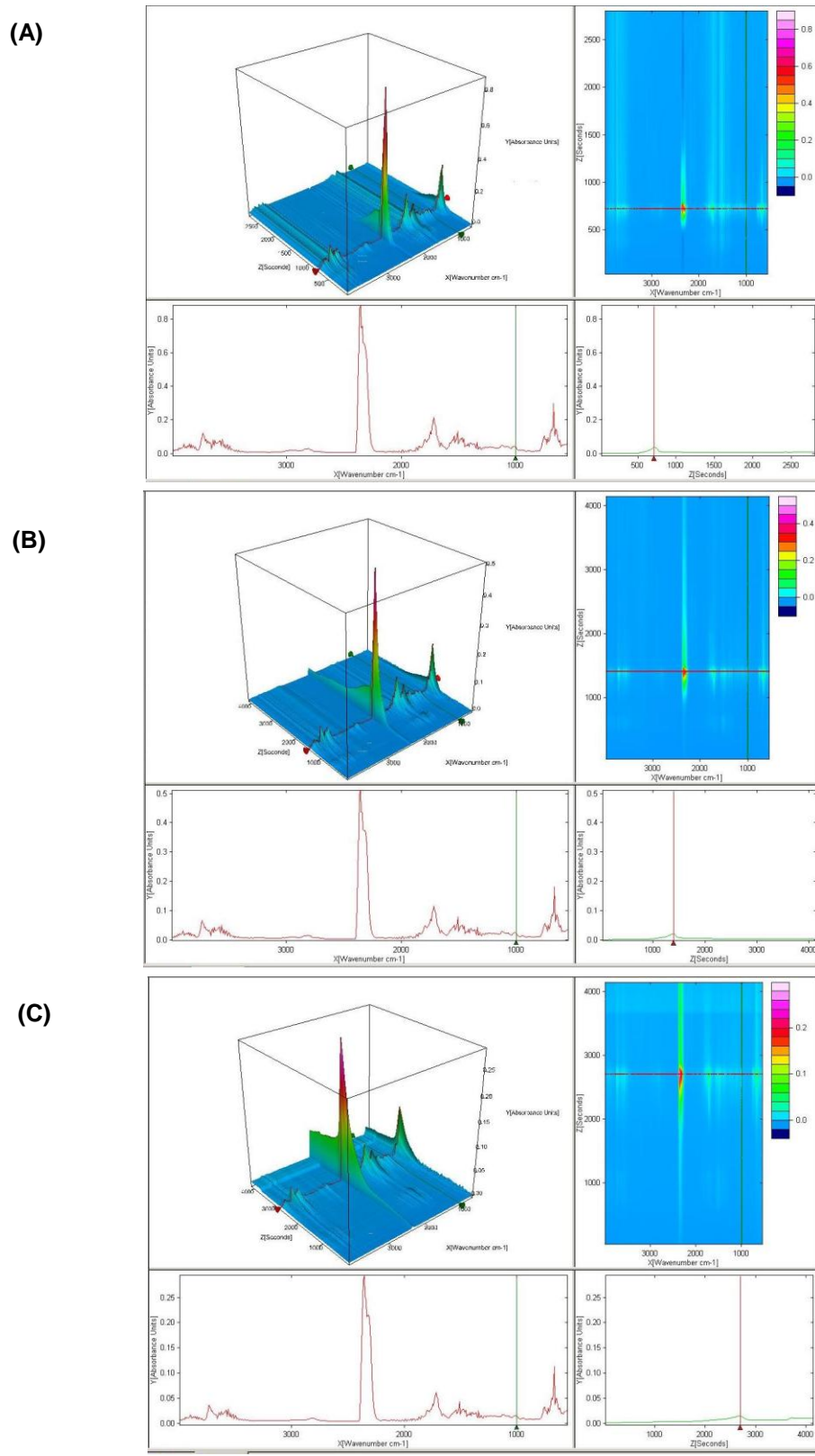
Fig.8.3.2: TG IR figures in three and two dimension for carbonisation of expanded alginic acid under nitrogen up to 800 $^{\circ}$C using temperature rates (A): 20 $^{\circ}$C/min, (B): 10 $^{\circ}$C/min and (C): 5 $^{\circ}$C/min.
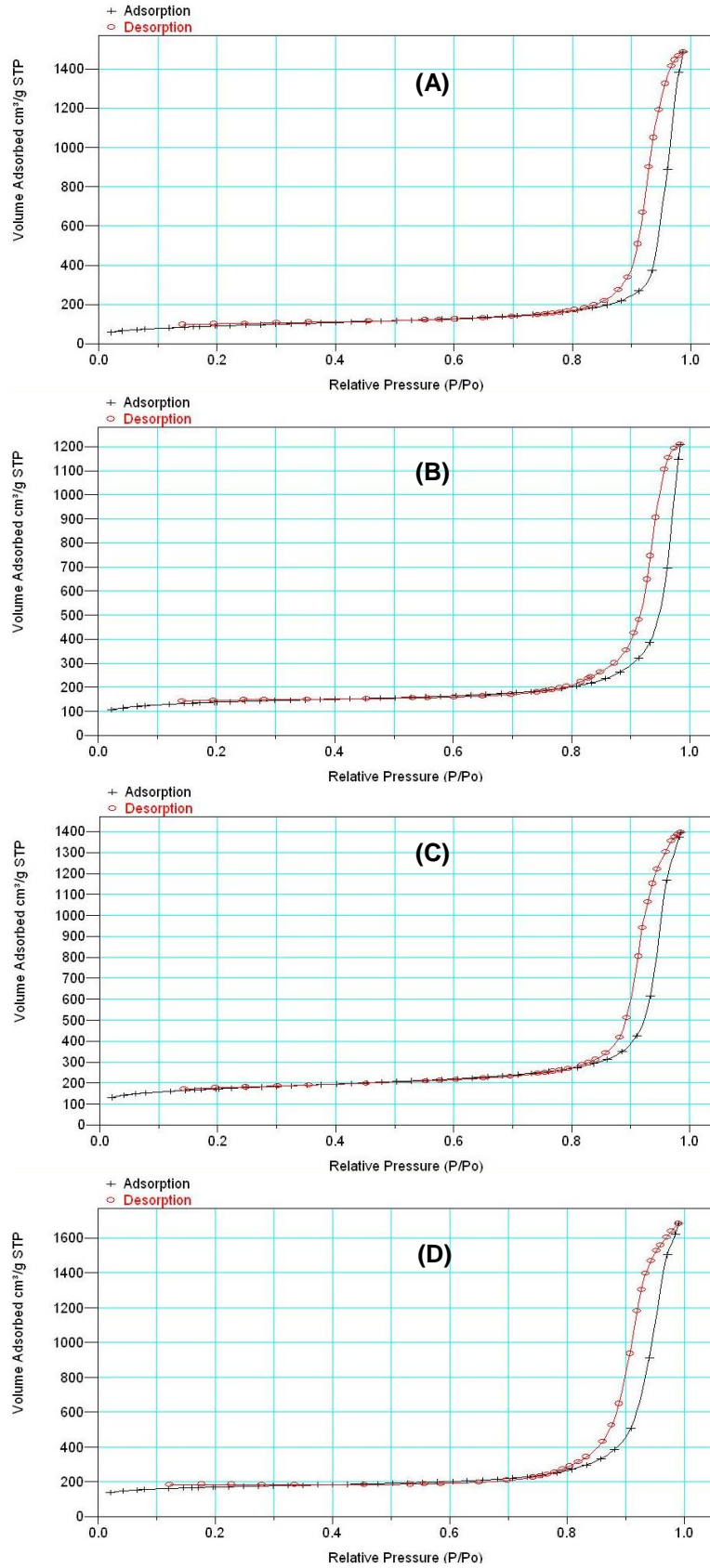
Fig.8.3.3: Linear isotherm plot for (A) A300, (B) A450, (C) A600 and (D) A800.
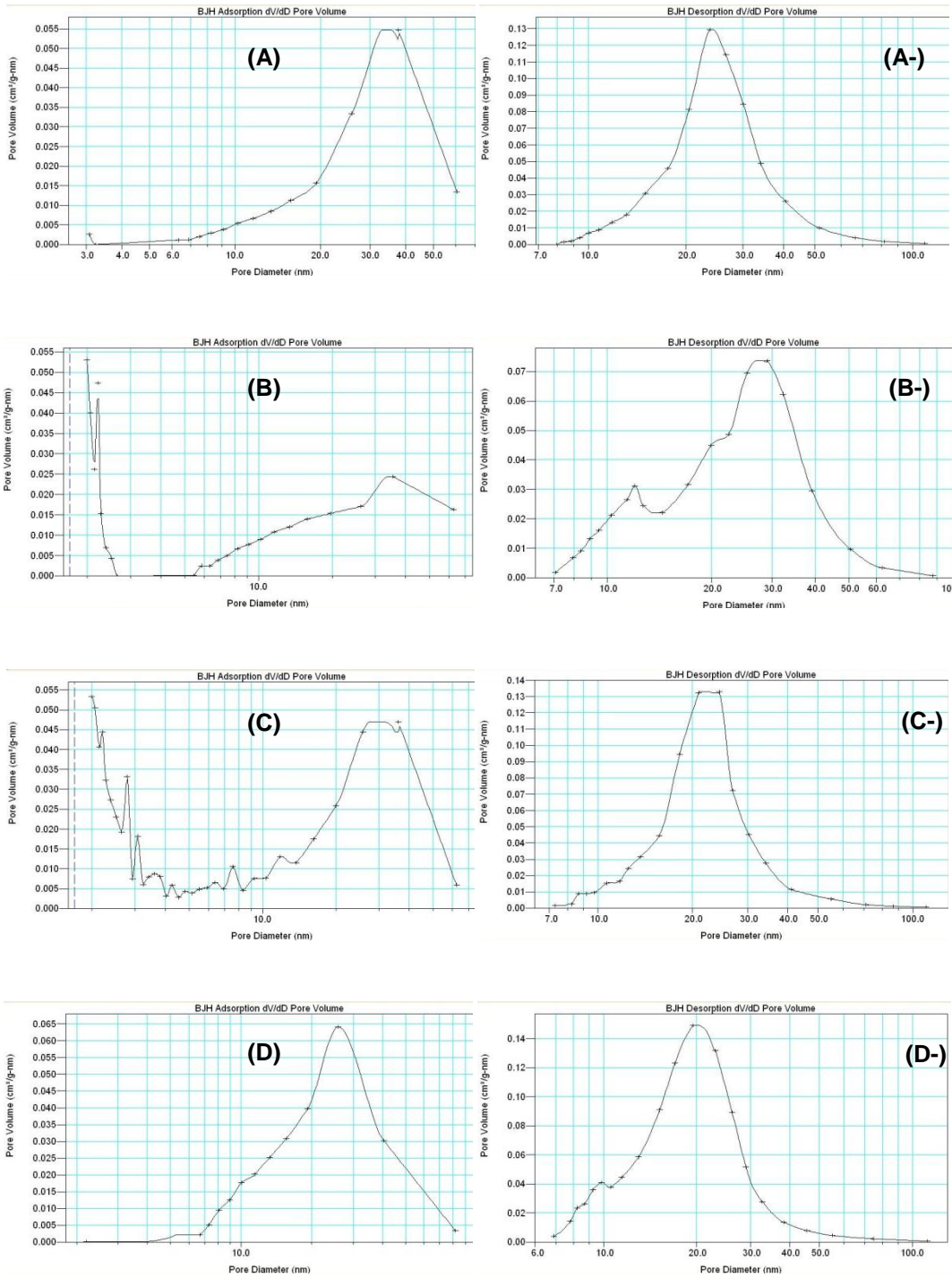
Fig.8.3.4: dV/dD pore size distribution for (A) A300 (adsorption pore size distribution (Apsd)), (A-) A300 (desorption pore size distribution (Dpsd)); (B) A450 (Apsd), (B-) A450 (Dpsd); (C) A600 (Apsd), (C-) A600 (Dpsd); (D) A800 (Apsd), (D-) A800 (Dpsd).

232
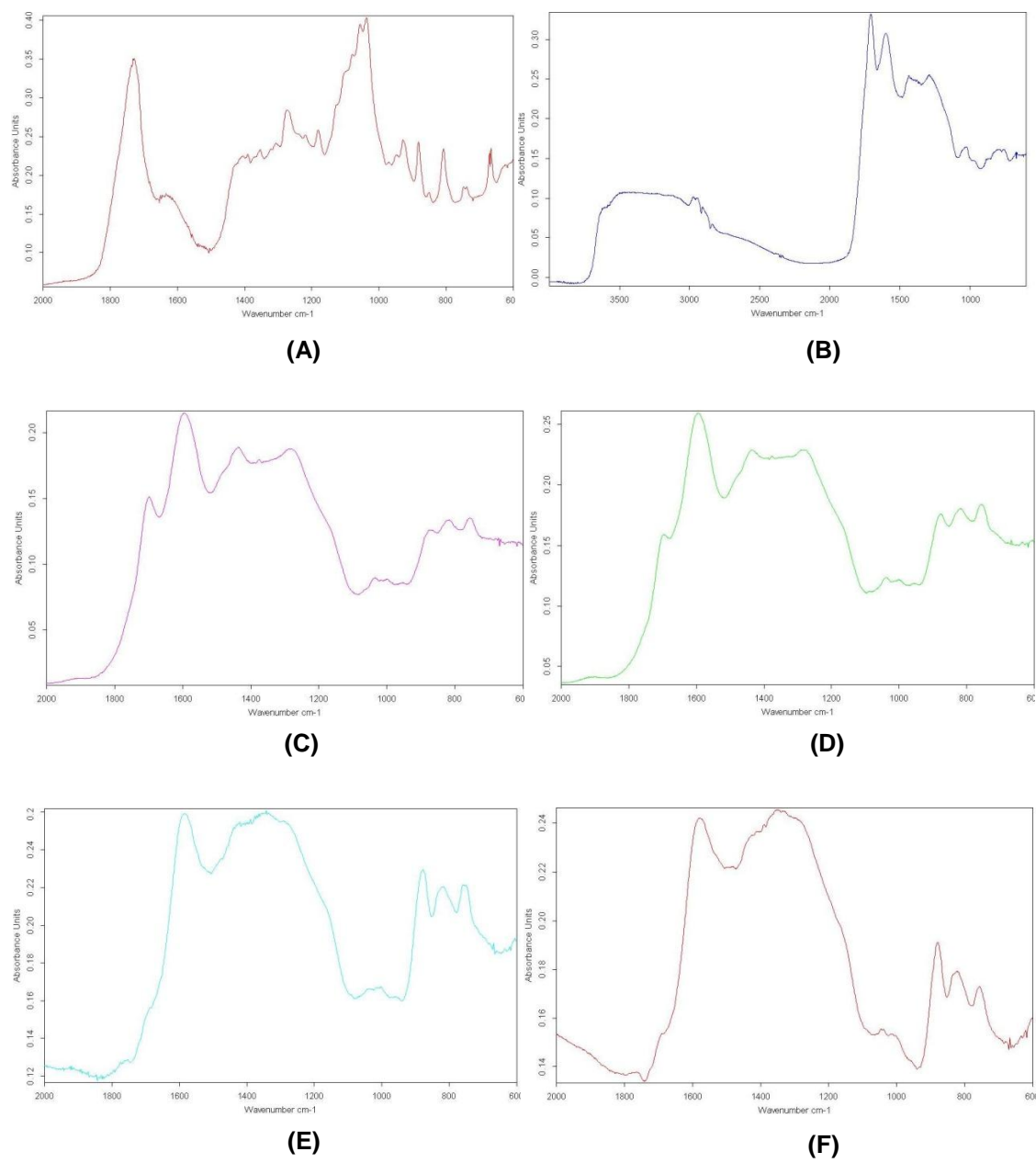
Fig.8.3.5: DRIFT IR for (A) A190, (B) A300, (C) A450, (D) A500, (E) A600 and (F) A650.

Fig.8.3.6: NMR solid state for (A) expanded alginic acid scCO$_2$ dried (A2), (B) A300, (C) A450, (D) A600 and (E) A800.
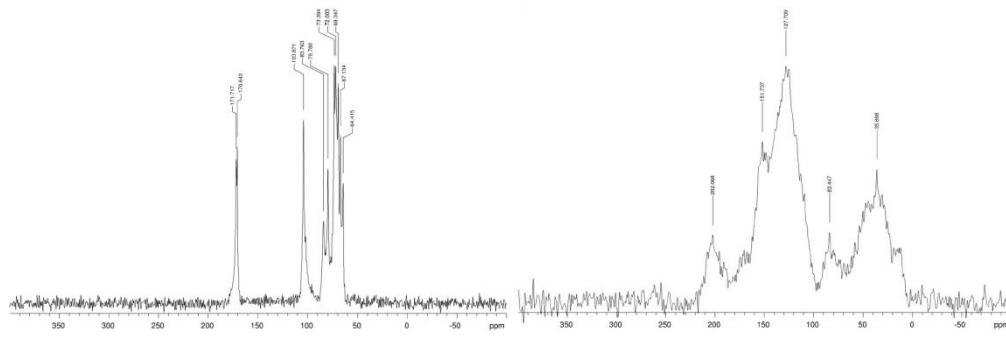
CHN Microanalytical Service Results

(A)

Name	H. Abdoul			Compound ID	① Expanded Alginic Acid (EAA)	
Element	**% C**	**% H**		**% N**	**% Rest**	
Observed 1	36.57	4.70		–	58.73	
Observed 2	36.82	4.65		–	58.53	
Mean	36.695	4.675		–	–	
Calc (theory)						

Comments: Check std within specified limits YES / NO. Counter/run no: 19104

CHN Microanalytical Service Results

(B)

Name	H. Abdoul		Compound ID	Algibon 300 (A300)	
Element	**% C**	**% H**	**% N**	**% Rest**	
Observed 1	63.80	3.84	0.22	32.14	
Observed 2	63.58	3.78	0.18	32.46	
Mean	63.691	3.810	0.199	–	
Calc (theory)					

Comments: Check std within specified limits YES / NO. Counter/run no: 19104

CHN Microanalytical Service Results

(C)

Name	H. Abdoul		Compound ID	③ Algibon 450 (A450)	
Element	**% C**	**% H**	**% N**	**% Rest**	
Observed 1	73.05	3.22	–	23.73	
Observed 2	72.97	3.26	–	23.77	
Mean	73.009	3.240	–	–	
Calc (theory)					

Comments: Check std within specified limits YES / NO. Counter/run no: 19104

CHN Microanalytical Service Results

(D)

Name	H. Abdoul		Compound ID	④ Algibon 600 (A600)	
Element	**% C**	**% H**	**% N**	**% Rest**	
Observed 1	80.61	2.27	–	17.12	
Observed 2	80.59	2.31	–	17.10	
Mean	80.602	2.289	–	–	
Calc (theory)					

Comments: Check std within specified limits YES / NO. Counter/run no: 19104

CHN Microanalytical Service Results

(E)

Name	H. Abdoul		Compound ID	⑤ Algibon 800 (A800)	
Element	**% C**	**% H**	**% N**	**% Rest**	
Observed 1	81.38	1.34	0.29	16.99	
Observed 2	81.62	1.44	0.25	16.69	
Mean	81.500	1.391	0.271	–	
Calc (theory)					

Comments: Check std within specified limits YES / NO. Counter/run no: 19104

CHN Microanalytical Service Results

(F)

Name	H. Abdoul		Compound ID	⑥ Activated carbon (AC)	
Element	**% C**	**% H**	**% N**	**% Rest**	
Observed 1	81.41	1.14	0.57	16.88	
Observed 2	81.35	1.20	0.49	16.96	
Mean	81.378	1.169	0.530	–	
Calc (theory)					

Comments: Check std within specified limits YES / NO. Counter/run no: 19104

Fig.8.3.7: CHN elemental analysis test for (A) expanded alginic acid, (B) A300, (C) A450, (D) A600, (E) A800 and (F) AC.
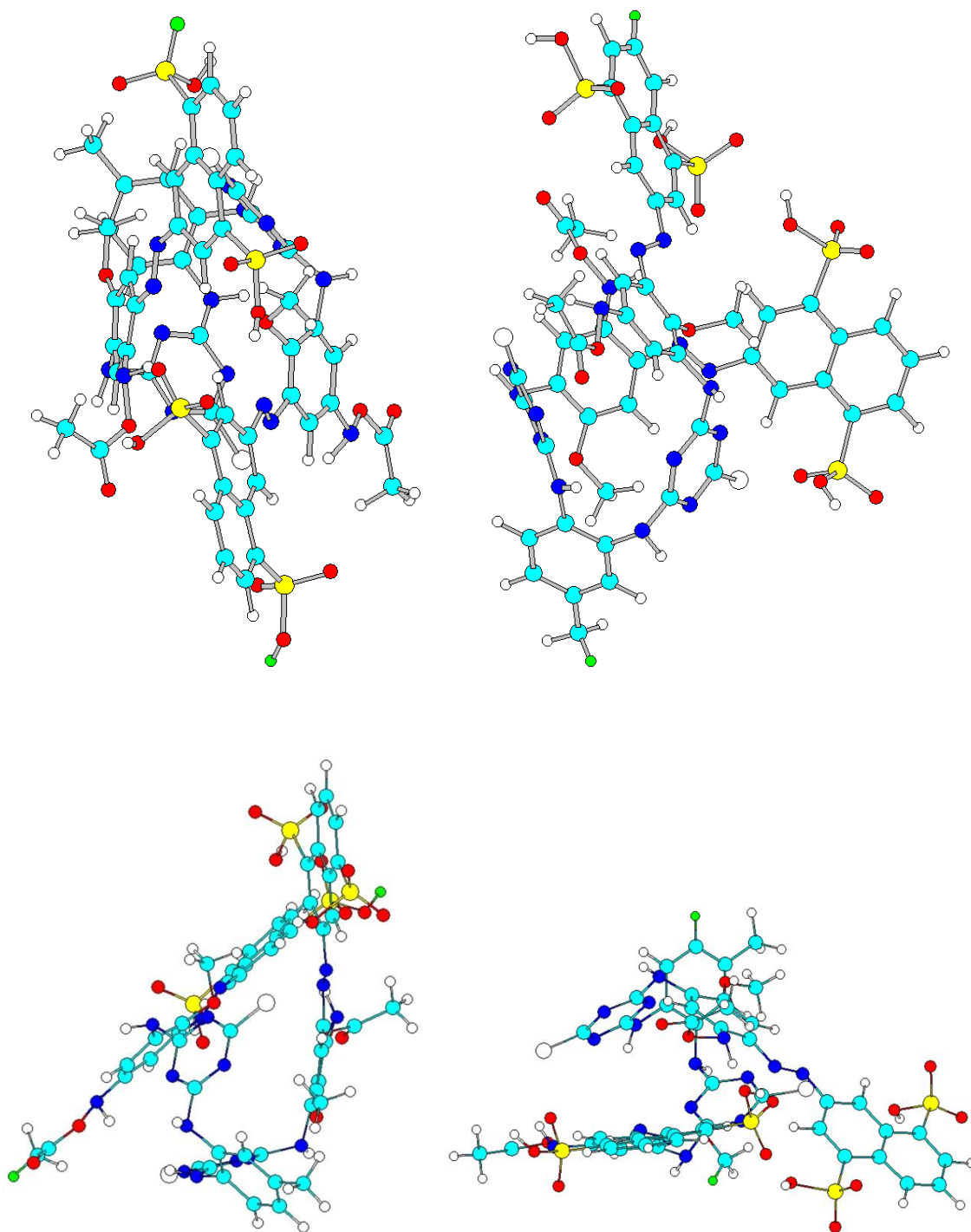
Fig.8.4.1: Different dimensional structures of Procion Yellow (PY) dye molecule in space.
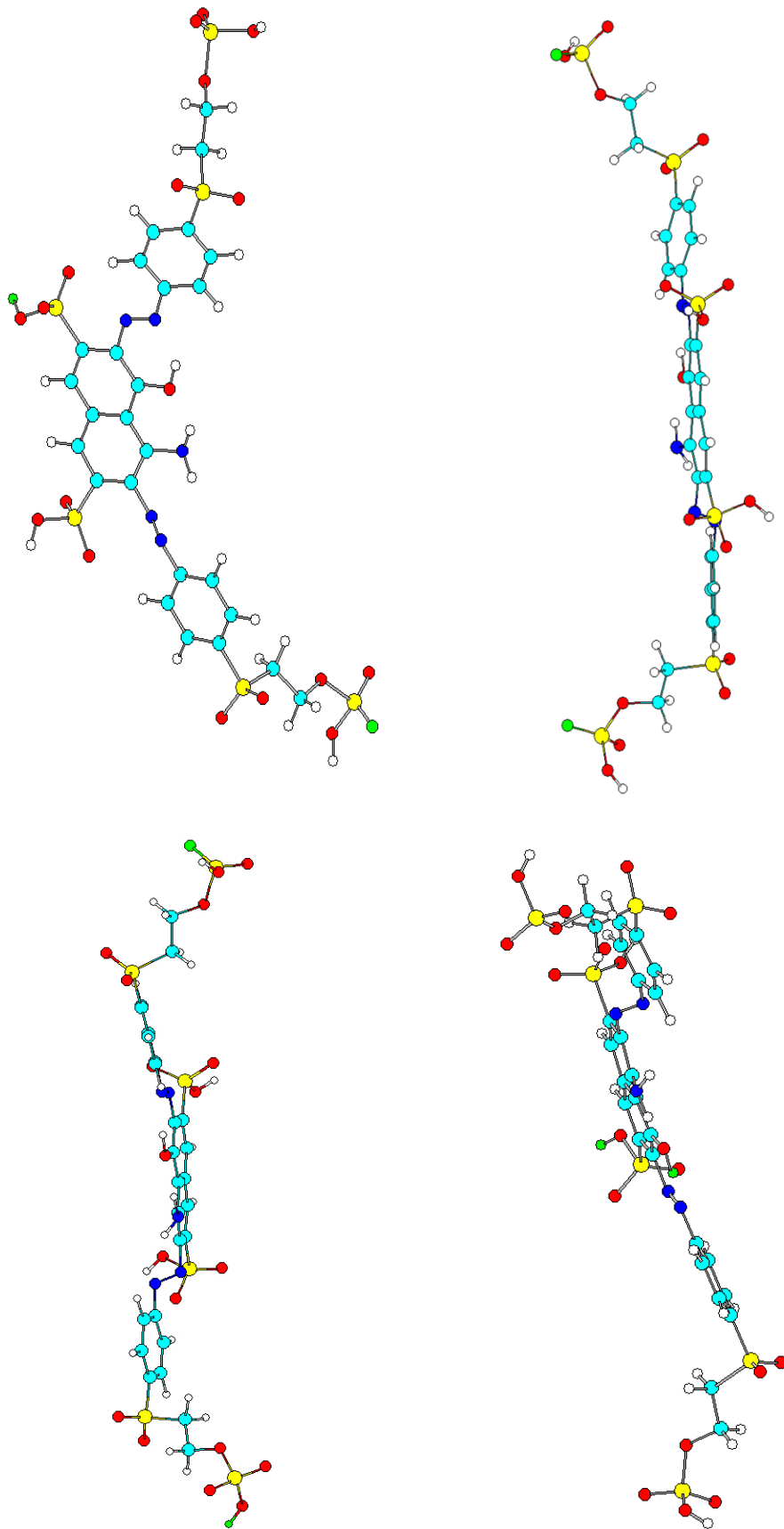
Fig.8.4.2: Different dimensional structures of Remazol Black (RB) dye molecule in space.
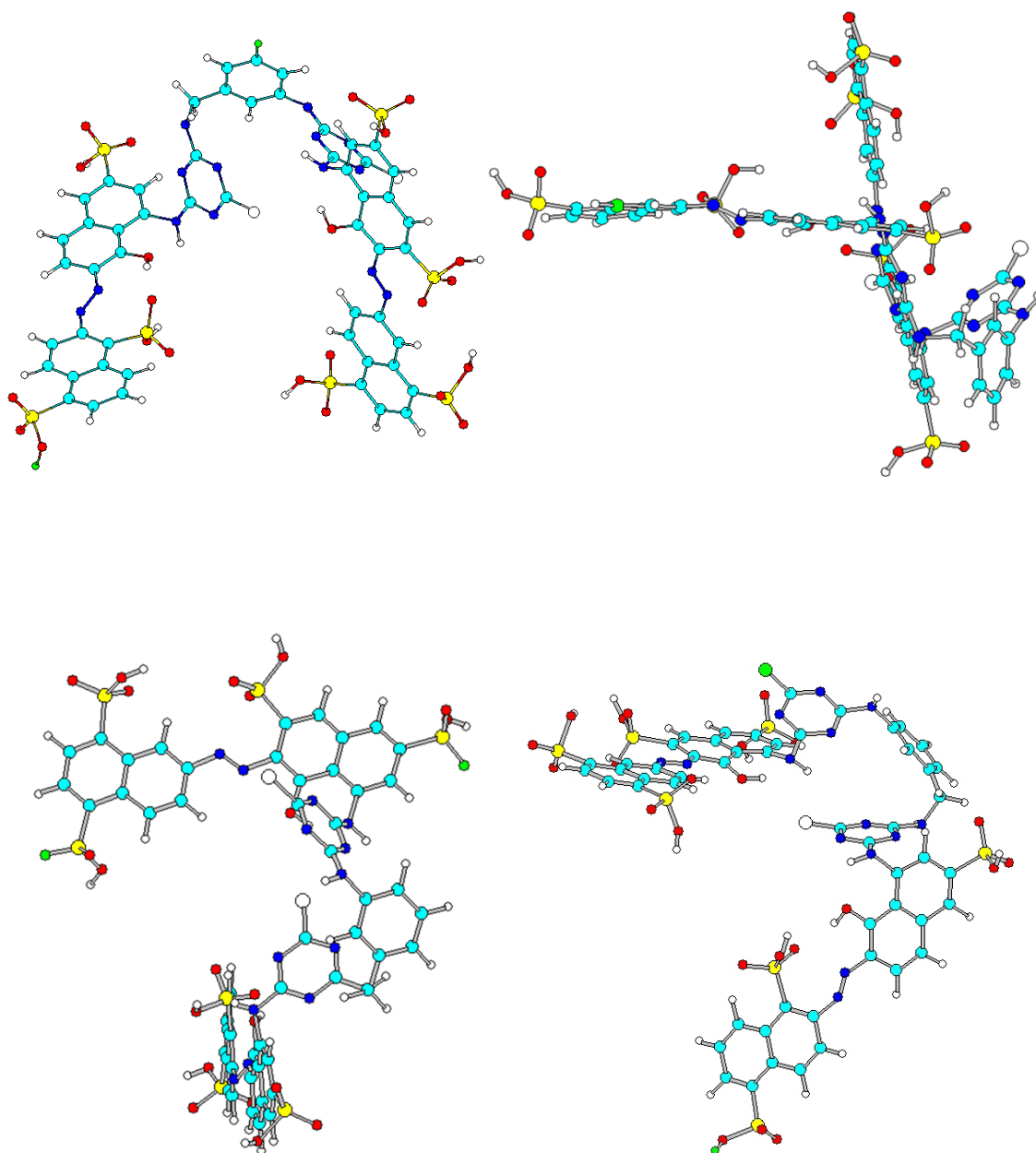
Fig.8.4.3: Different dimensional structures of Procion Crimson (PC) dye molecule in space.
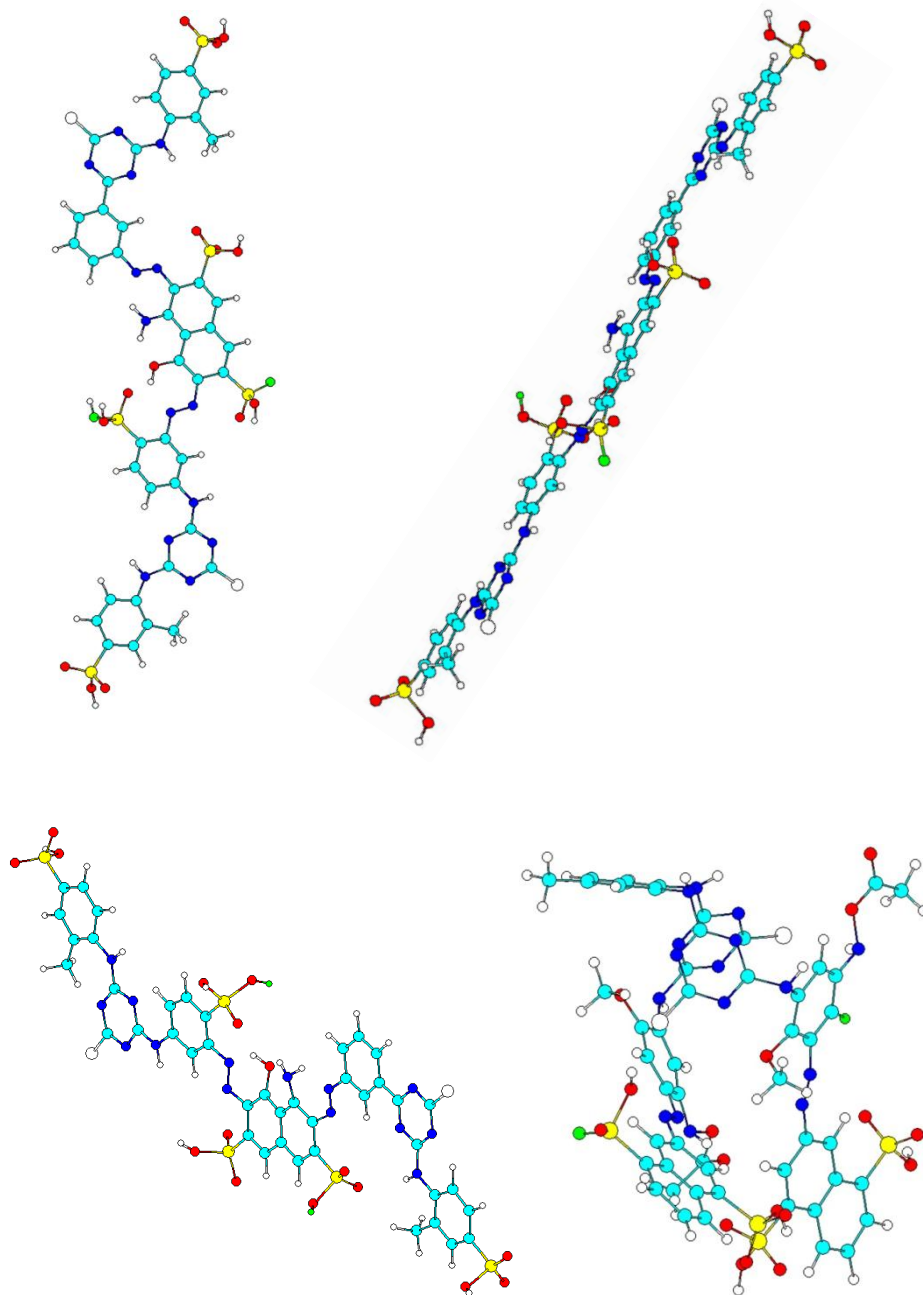
Fig.8.4.4: Different dimensional structures of Procion Navy (PN) dye molecule in space.

Table.8.4.1: Dye molecular characterisation using Hyperchem

Dye Characters	Procion Yellow (PY)	Remazol Black (RB)	Procion Crimson (PC)	Procion Navy (PN)
Molecular properties, Energy (Kcal/mol)				
Total energy	-367591.9	-252964	-983457.9	-323168.6
Binding energy	-14390.07	-8399.813	-1378766	-12149.61
Heat of formation	-282.7529	-559.1024	-1393174	-327.9358
Electronic energy	-5774954	-2389191	-4413163	-37711183
Nuclear energy	5407362	2136227	5396621	3448014
Dipole moment (D)				
Total dipole moment	3.38252	0.86467	9861.30469	9.08116
Dipole X	-1.48108D	0.60233	-7223.64502	5.23025
Dipole Y	-2.96028 D	0.47120	3705.64331	-.6.65169
Dipole Z	-069612 D	0.40350	5597.54297	3.29651
RMS gradient (Kcal/A.mol)				
RMS gradient	1.93814	0.14077	2314.82031	0.26737
Gradient X	1.64924	0.06360	1149.61609	0.4827
Gradient Y	0.57621	0.08824	1179.87256	0.20748
Gradient Z	0.83925	0.08935	1626.24622	0.16159
QSAR properties				
Surface area	1255.54 A^2	1144.71 A^2	1501.28 A^2	1321.02 A^2
Volume	2833.50 A^3	1965.74 A^3	3206.67 A^3	2675.44 A^3
Hydration Energy	-49.10 Kcal/mol	-61.65 Kcal/mol	-8011 Kcal/mol	-69.83 Kcal/mol
Polarisability	115.25 A^3	60.03 A^3	117.78 A^3	97.34 A^3
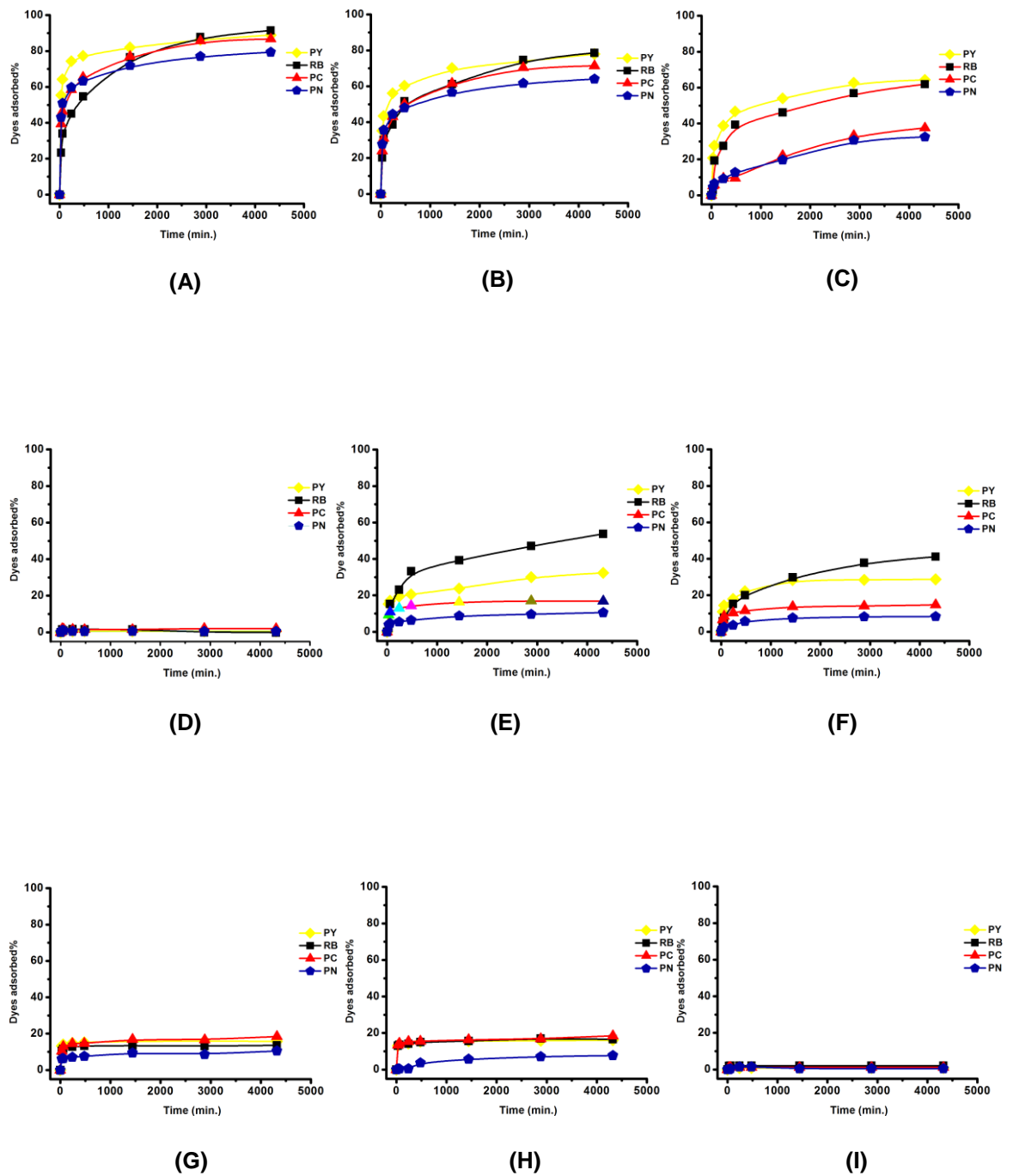
Fig.8.4.5: Adsorption kinetic of each individual porous material including (A) A800, (B) A600, (C) A450, (D) A300, (E) S800, (F) S450, (G) S300, (H) AC and (I) Silica gel (Sgel) for the dyes (PY, RB, PC and PN) adsorbed%. Initial concentration of each dye corresponds to one arbitrary unit of UV-VIS absorbance of dye solution.
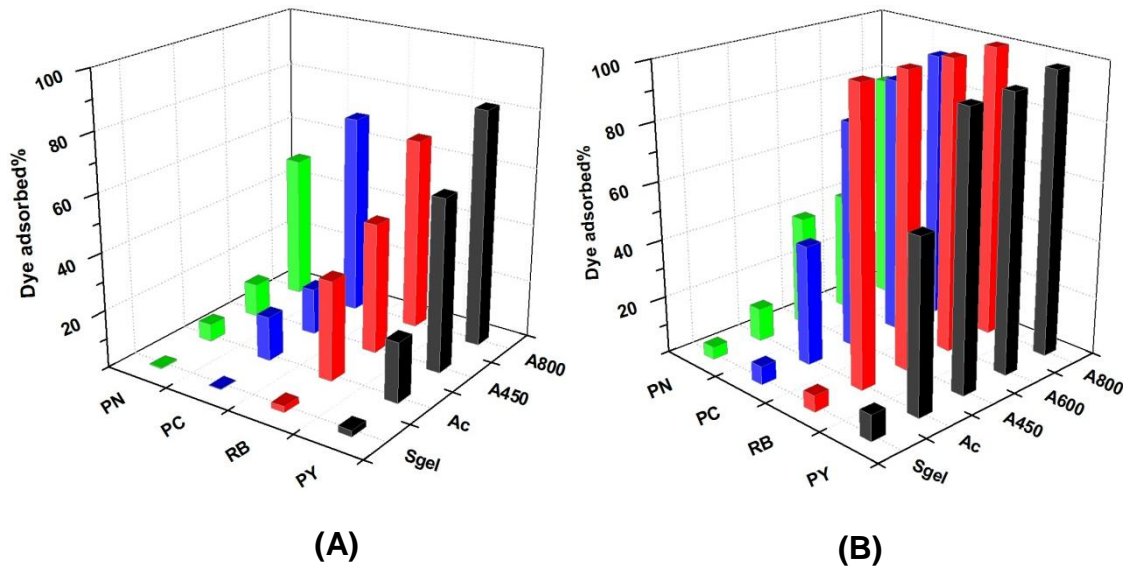
Fig.8.4.6: Dye removal percentage for the adsorbent materials employed when initial concentration of each dye corresponds to (A) 1.5 arbitrary unit of UV-VIS absorbance of dye solution (B) 0.2 arbitrary unit of UV-VIS absorbance of dye solution.
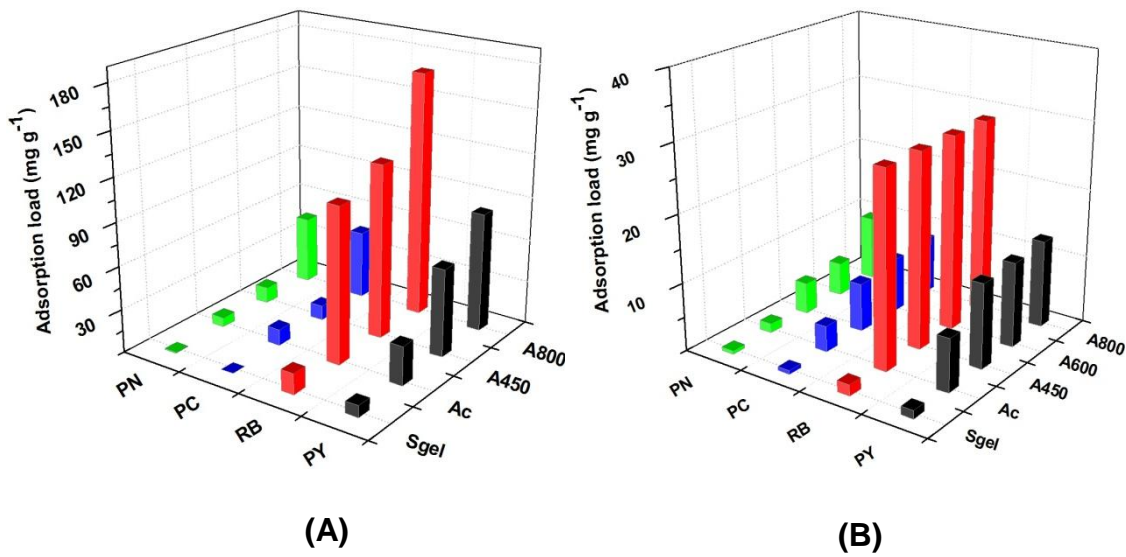
Fig.8.4.7: Dye adsorption load (mg g^{-1}) for the adsorbent materials employed when initial concentration of each dye corresponds to (A) 1.5 arbitrary unit of UV-VIS absorbance of dye solution (B) 0.2 arbitrary unit of UV-VIS absorbance of dye solution.
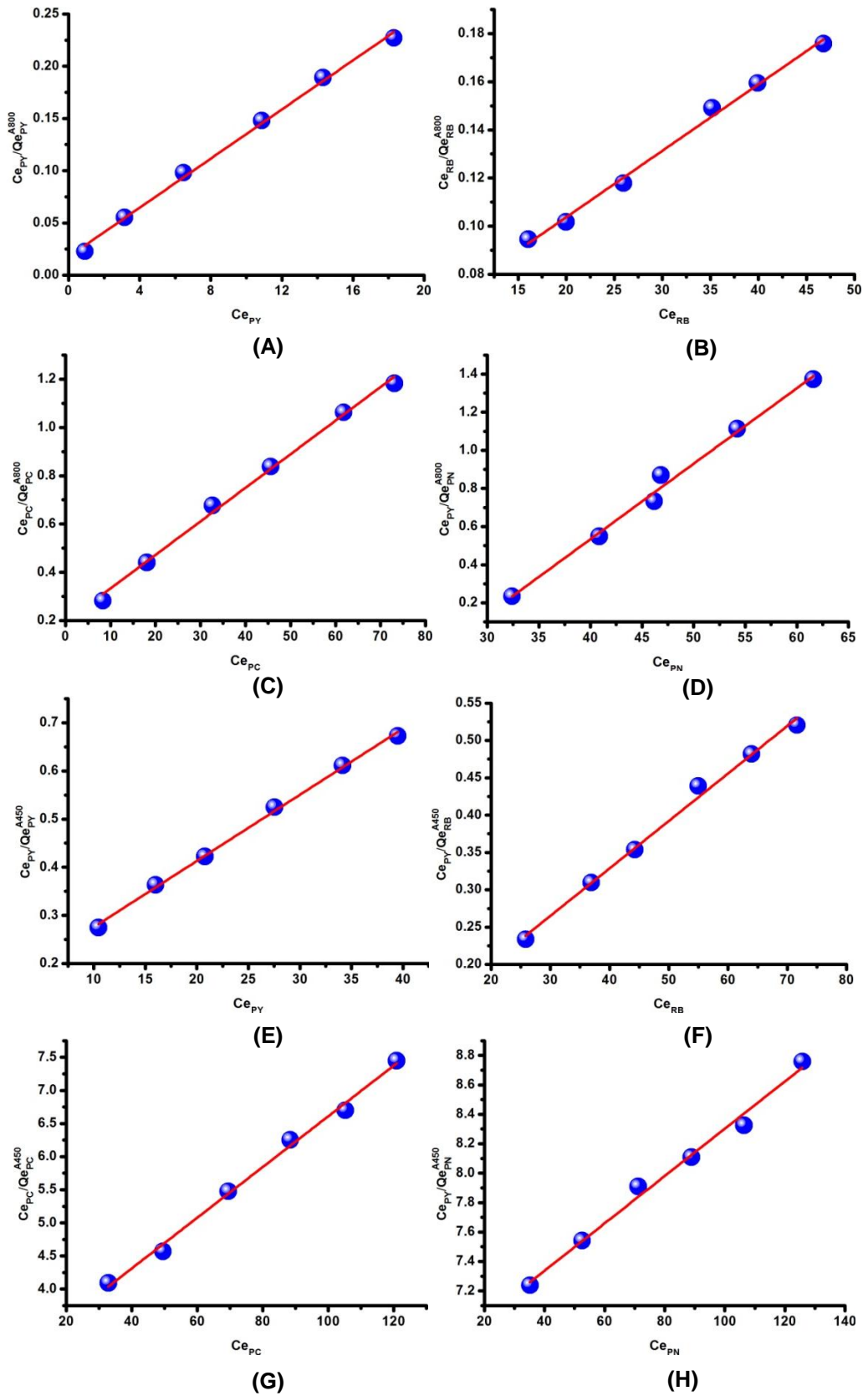
Fig.8.4.8: Employ A800 and apply Langmuir adsorption isotherm for (A) PY (B) RB, (C) PC and (D) PN; employ A450 and apply Langmuir adsorption isotherm for (E) PY, (F) RB, (G) PC and (H) PN.
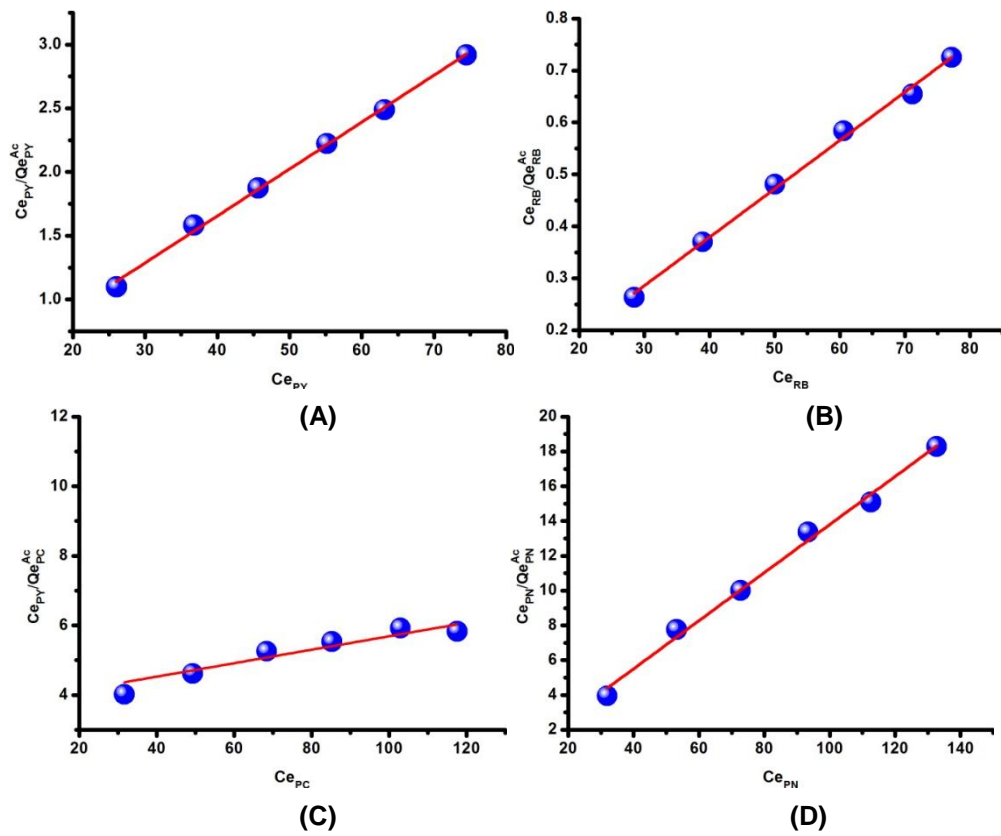
Fig.8.4.9: Employ AC and apply Langmuir adsorption isotherm for (A) PY (B) RB, (C) PC and (D) PN.
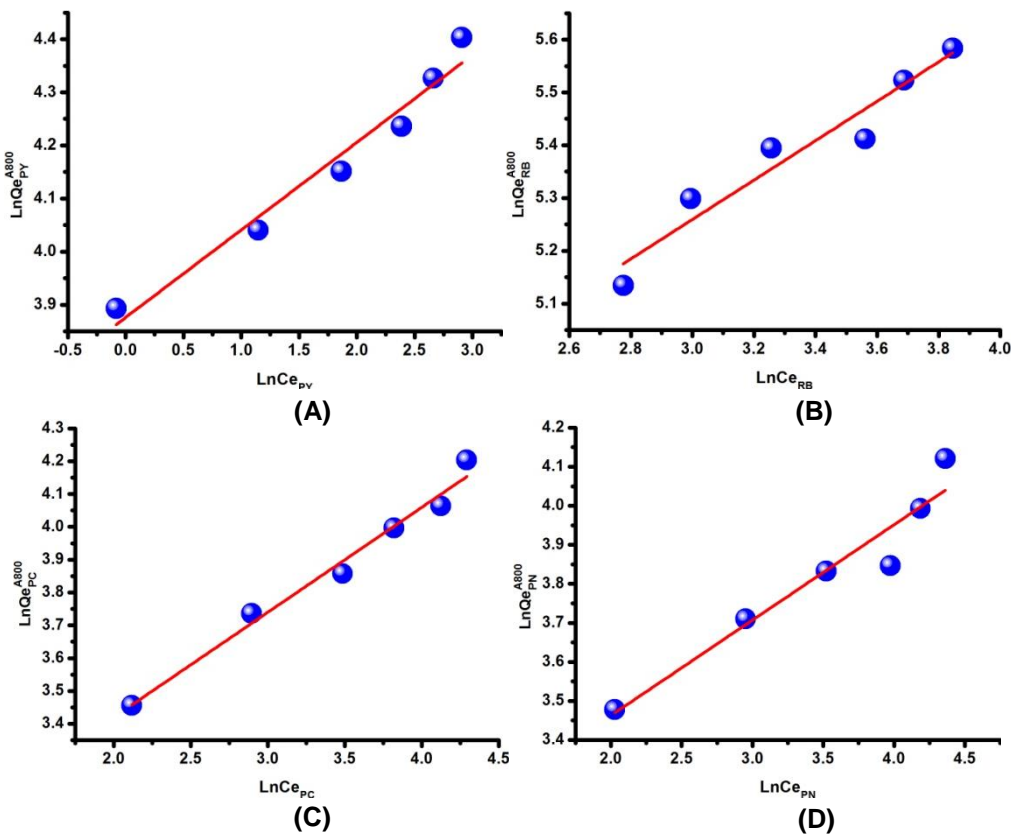
Fig.8.4.10: Employ A800 and apply Freundlich adsorption isotherm for (A) PY (B) RB, (C) PC and (D) PN.
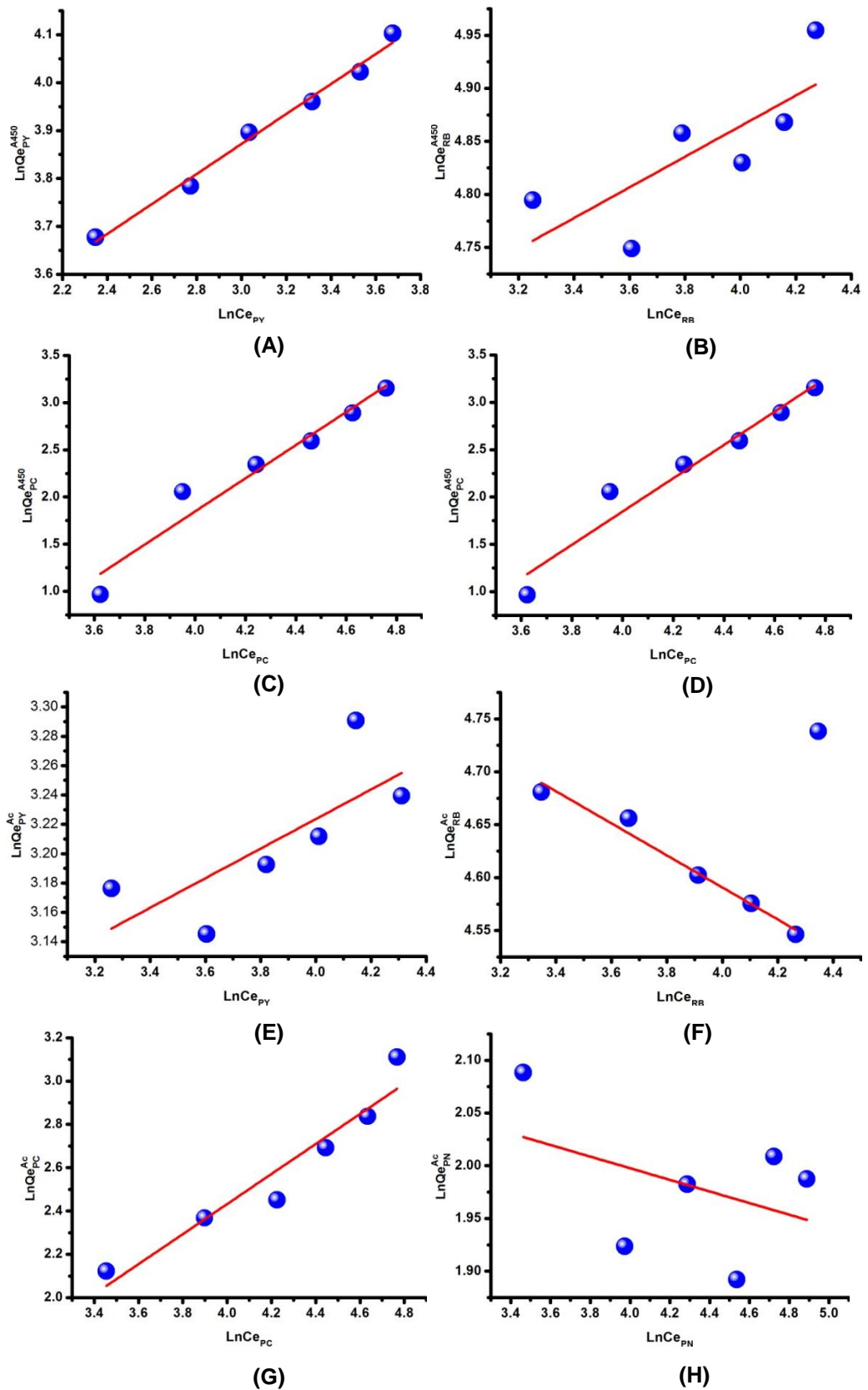
Fig.8.4.11: Employ A450 and apply Freundlich adsorption isotherm for (A) PY (B) RB, (C) PC and (D) PN; employ AC and apply Freundlich adsorption isotherm for (E) PY, (F) RB, (G) PC and (H) PN.
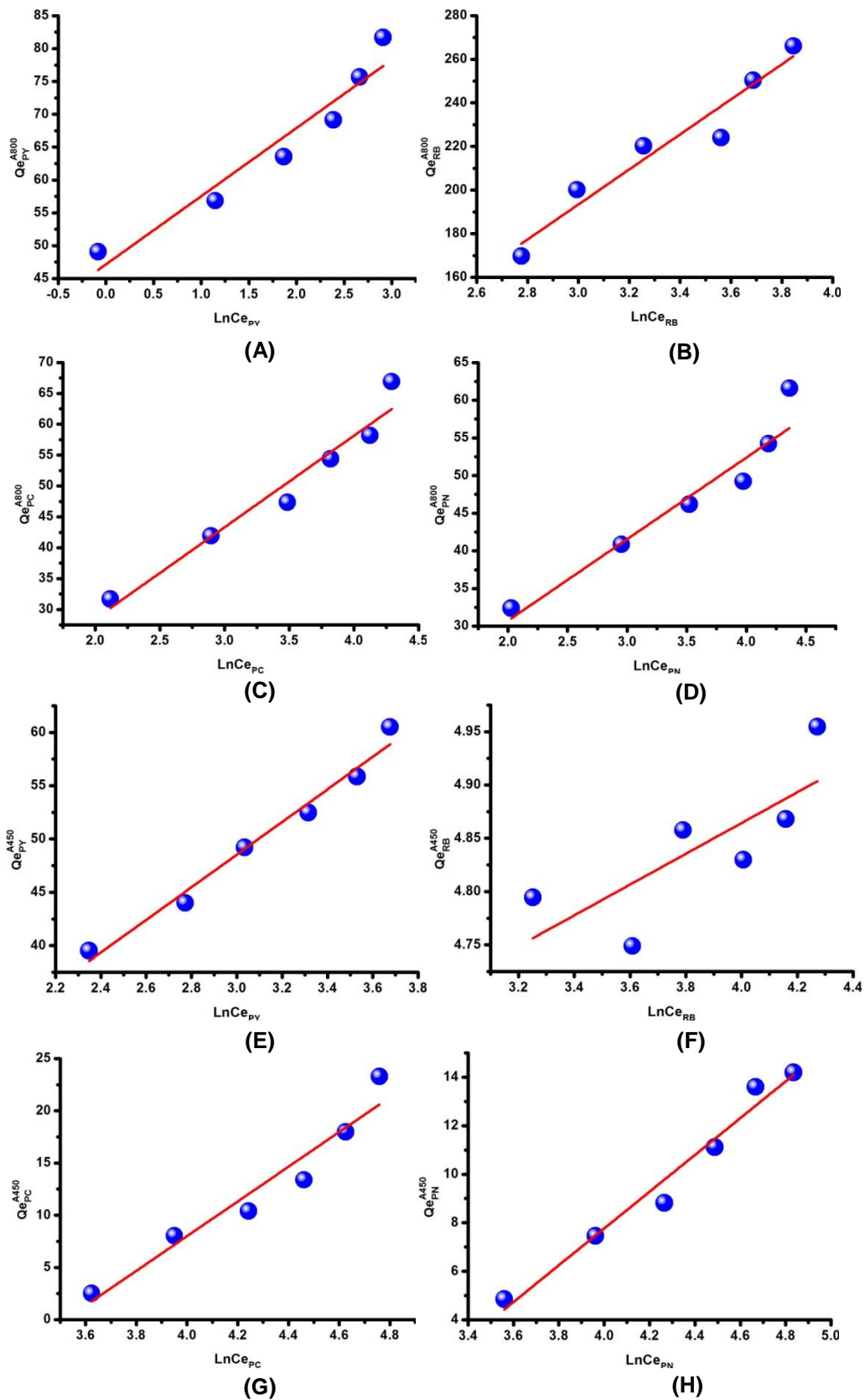
Fig.8.4.12: Employ A800 and apply Tempkin adsorption isotherm for (A) PY (B) RB, (C) PC and (D) PN; employ A450 and apply Tempkin adsorption isotherm for (E) PY, (F) RB, (G) PC and (H) PN.
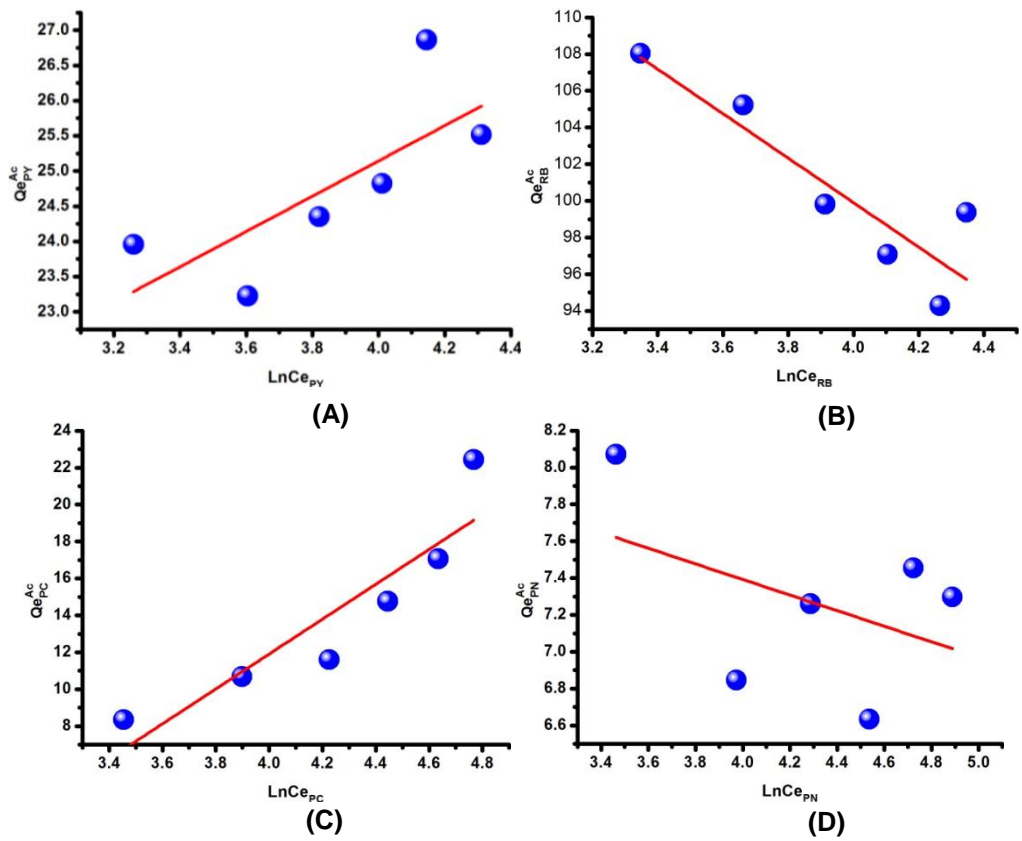
Fig.8.4.13: Employ AC and apply Tempkin adsorption isotherm for (A) PY (B) RB, (C) PC and (D) PN.
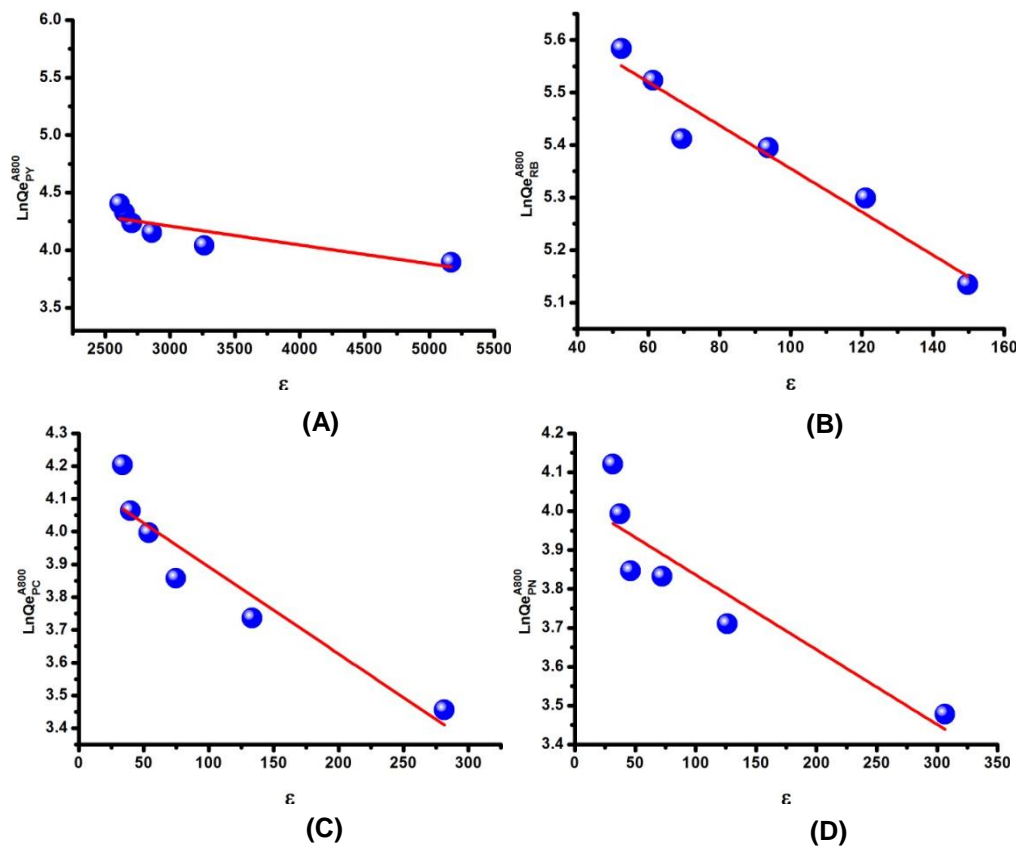
Fig.8.4.14: Employ A800 and apply Dubinin-Redushkevich adsorption isotherm for (A) PY (B) RB, (C) PC and (D) PN.
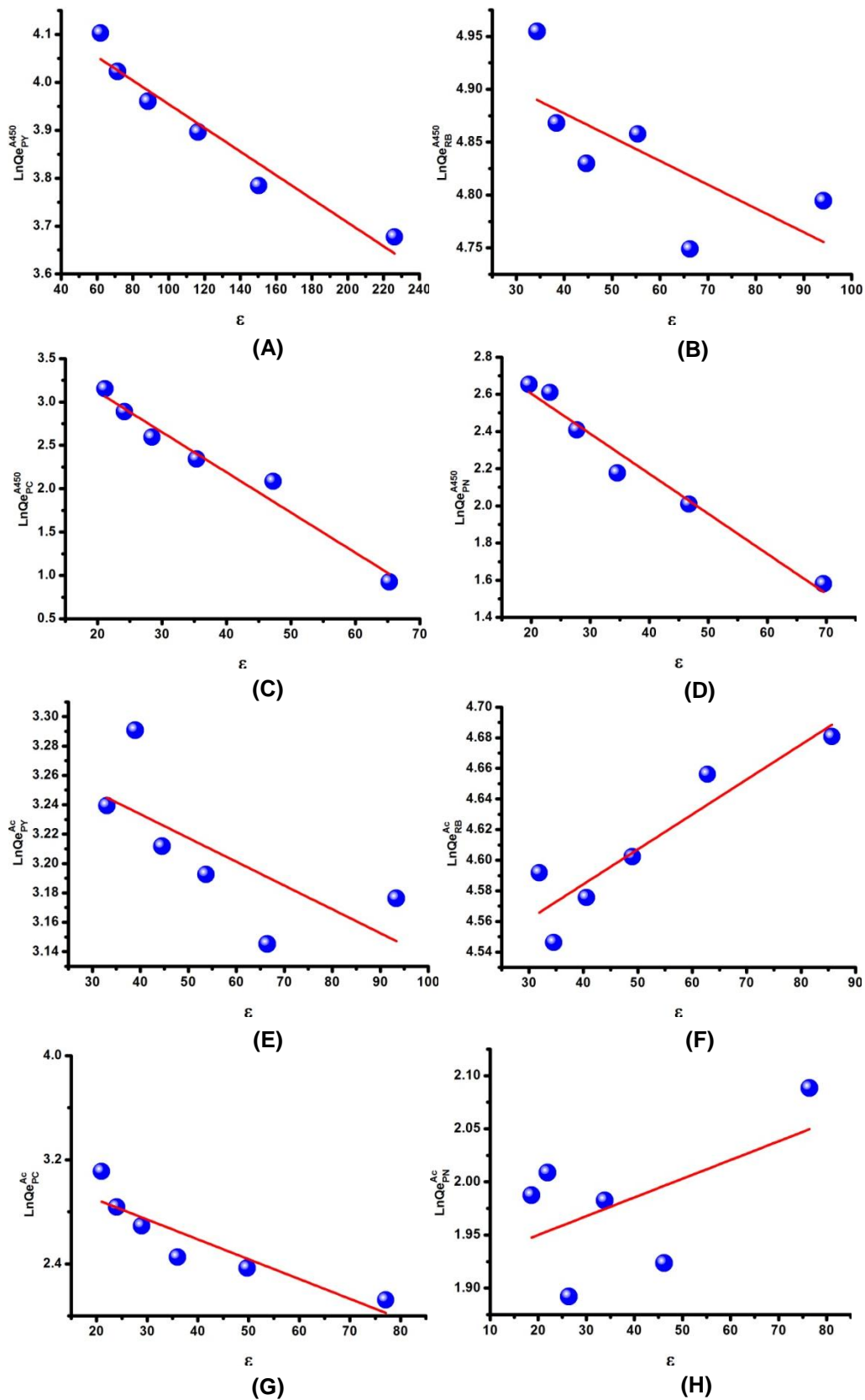
Fig.8.4.15: Employ A450 and apply Dubinin-Redushkevich adsorption isotherm for (A) PY (B) RB, (C) PC and (D) PN; employ AC and apply Dubinin-Redushkevich adsorption isotherm for (E) PY, (F) RB, (G) PC and (H) PN.
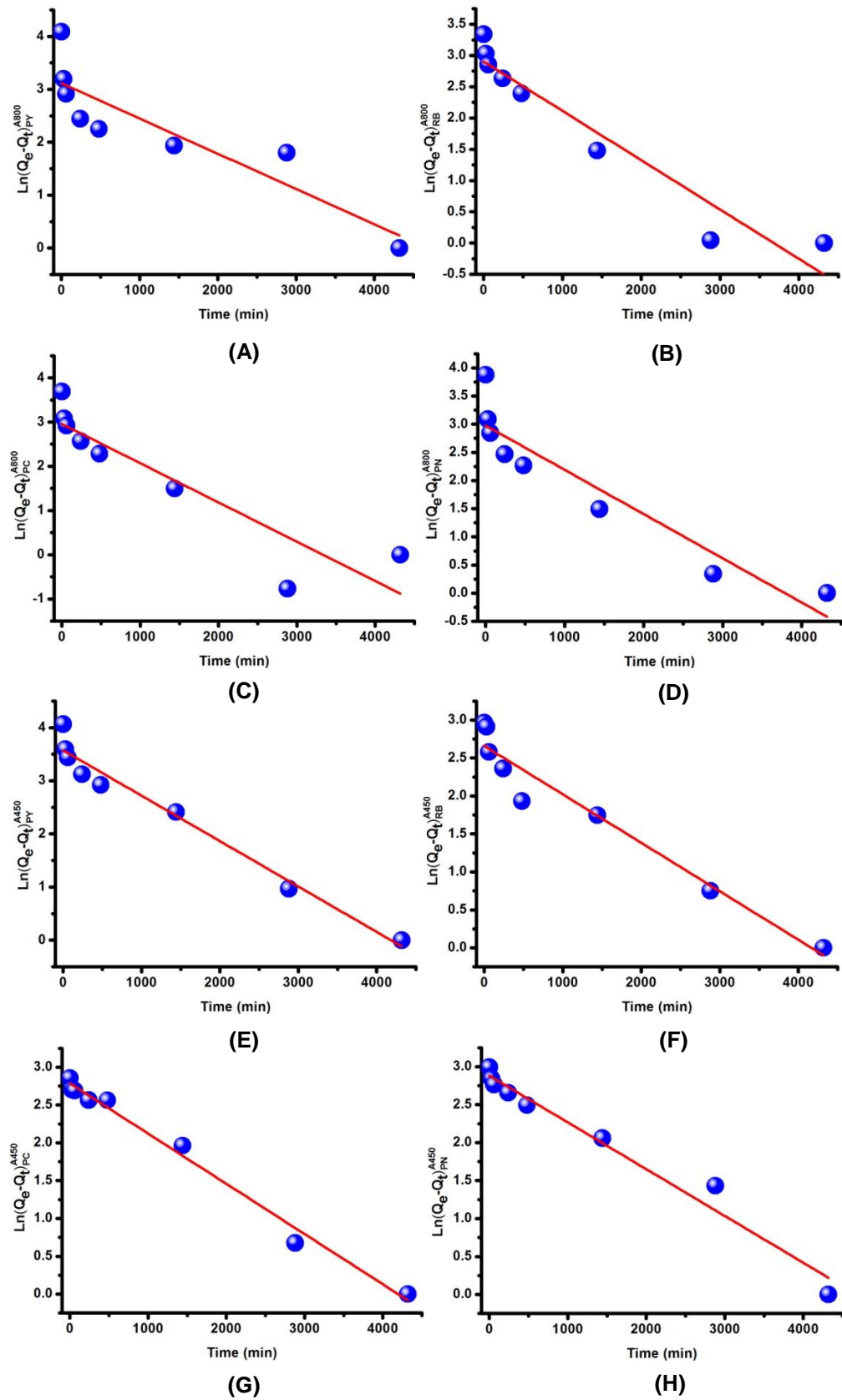
Fig.8.4.16: Employ A800 and apply Pseudo-first-order model for (A) PY, (B) RB, (C) PC and (PN); Employ A450 and apply Pseudo-first-order model for (A) PY, (B) RB, (C) PC and (PN).
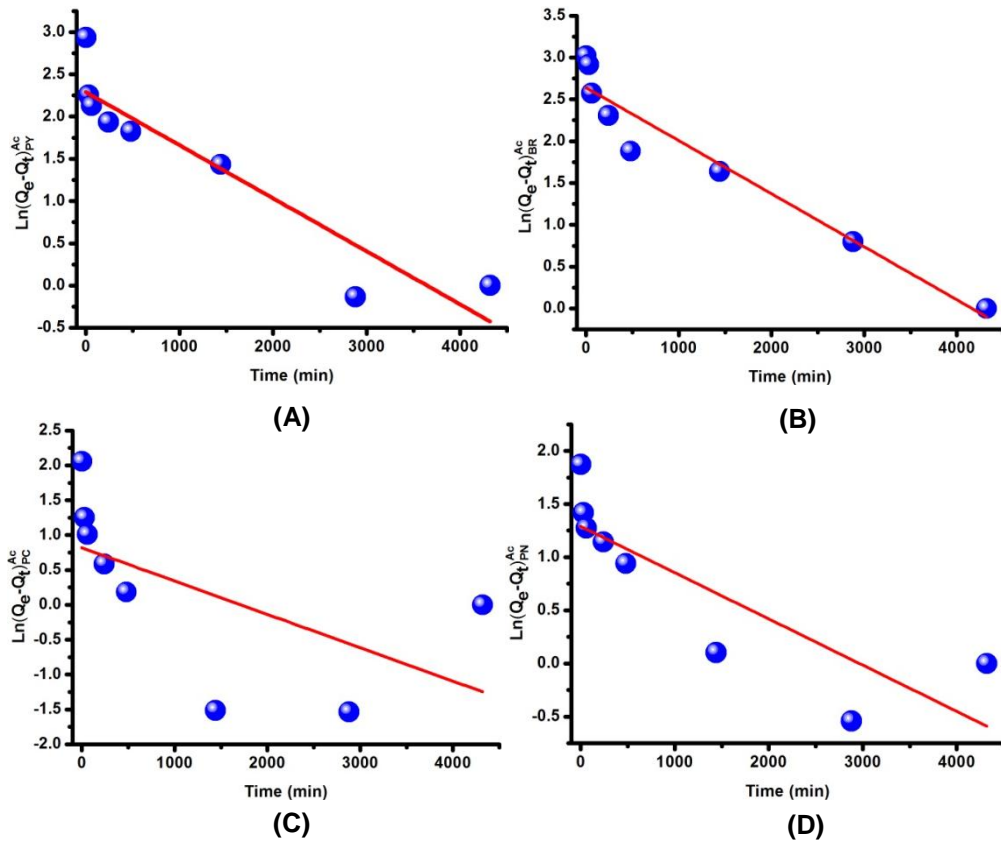
Fig.8.4.17: Employ AC and apply Pseudo-first-order model for (A) PY, (B) RB, (C) PC and (PN).
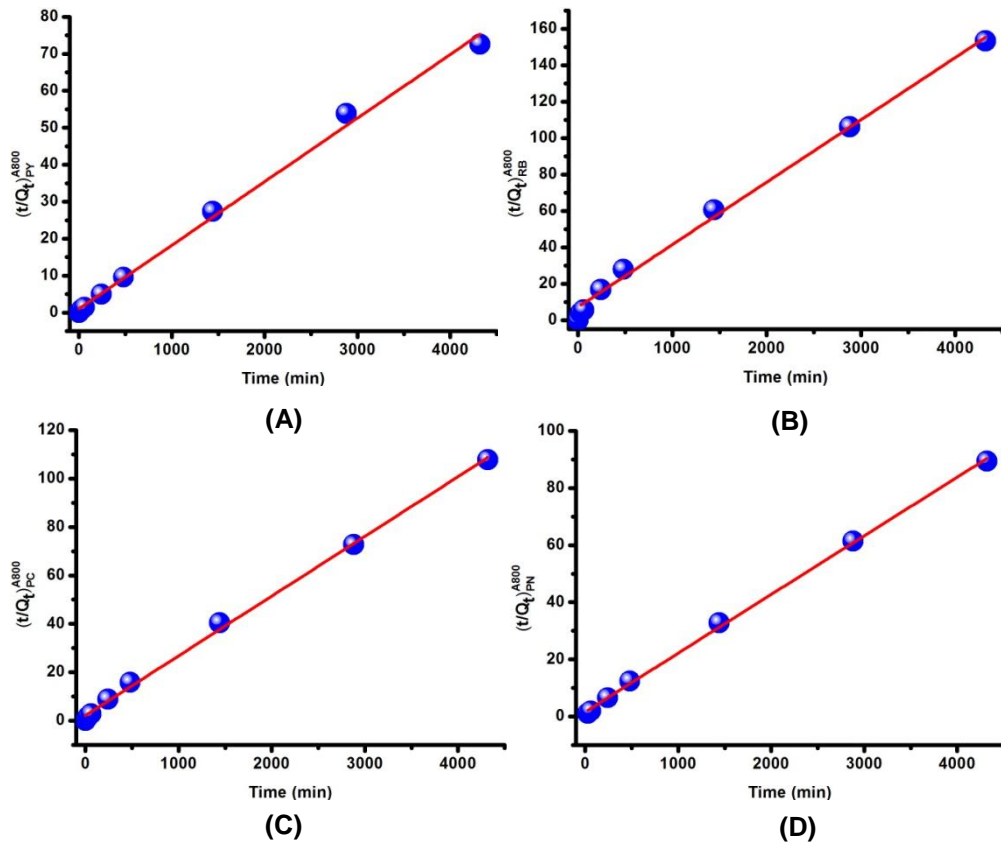
Fig.8.4.18: Employ A800 and apply Pseudo-second-order model for (A) PY, (B) RB, (C) PC and (PN).
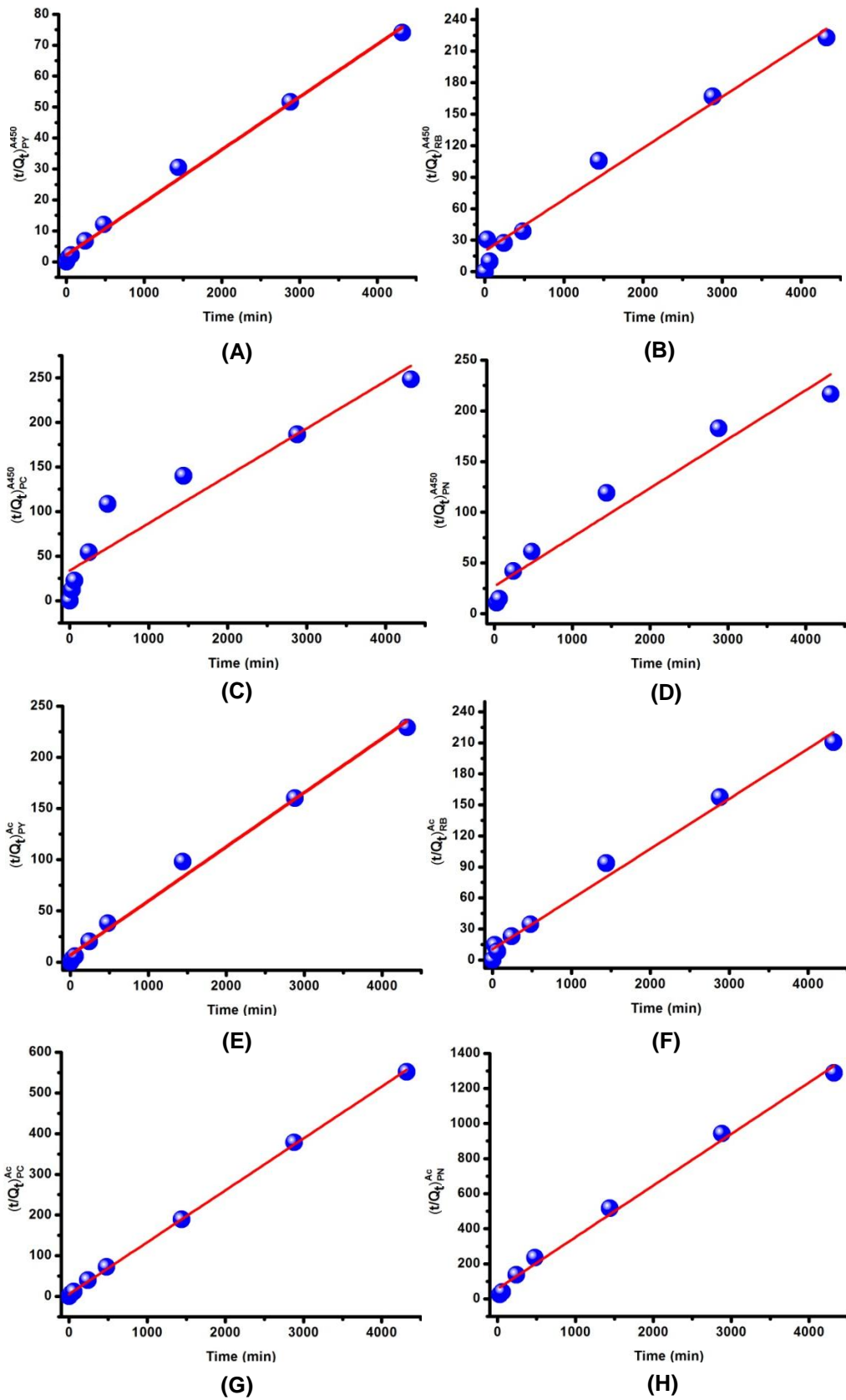
Fig.8.4.19: Employ A450 and apply Pseudo-second-order model for (A) PY, (B) RB, (C) PC and (PN); employ AC and apply Pseudo-second-order model for (A) PY, (B) RB, (C) PC and (PN).
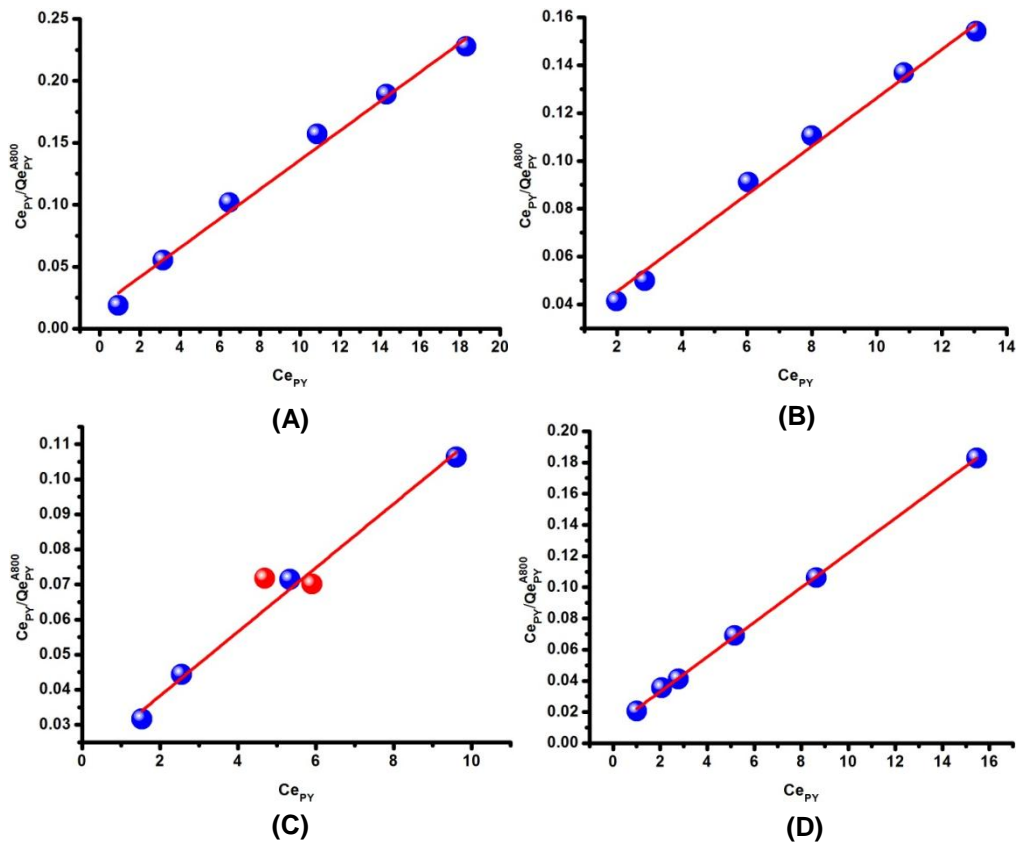
Fig.8.4.20: Employ A800 and apply Langmuir adsorption isotherm for PY adsorption at different temperatures: (A) 25 ^{o}C, (B) 35 ^{o}C, (C) 45 ^{o}C and (D) 55 ^{o}C.
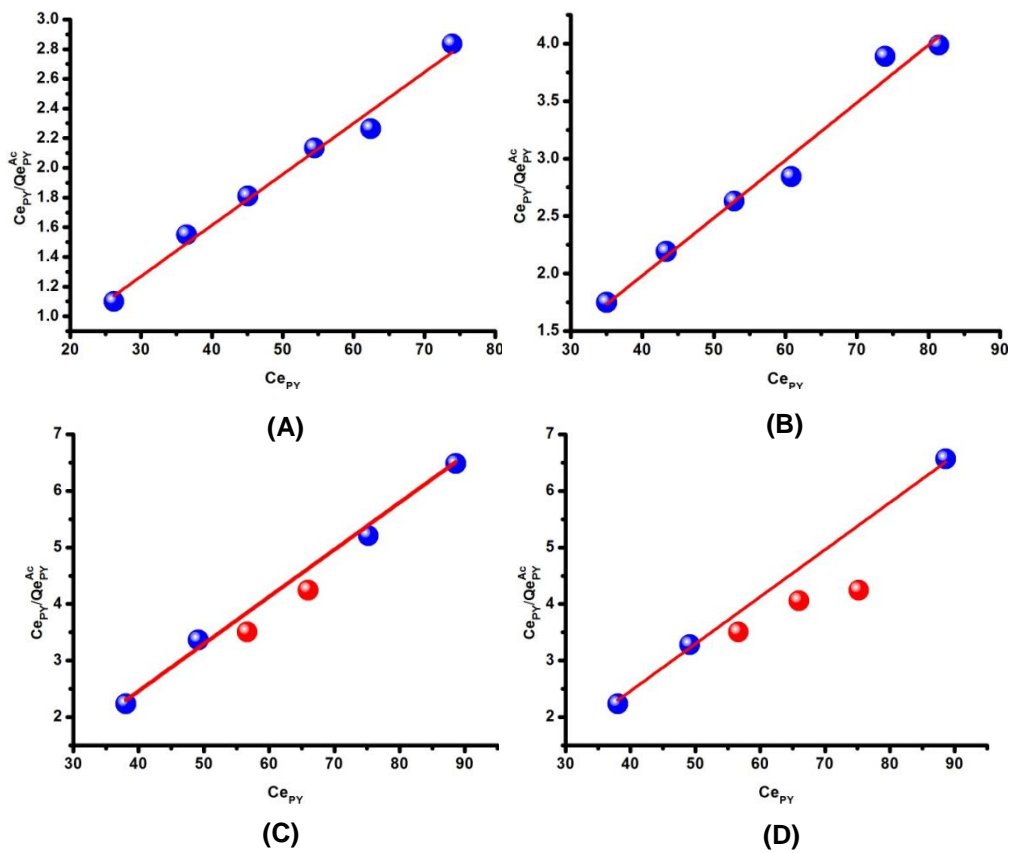
Fig.8.4.21: Employ AC and apply Langmuir adsorption isotherm for PY adsorption at different temperatures: (A) 25 ^{o}C, (B) 35 ^{o}C, (C) 45 ^{o}C and (D) 55 ^{o}C.
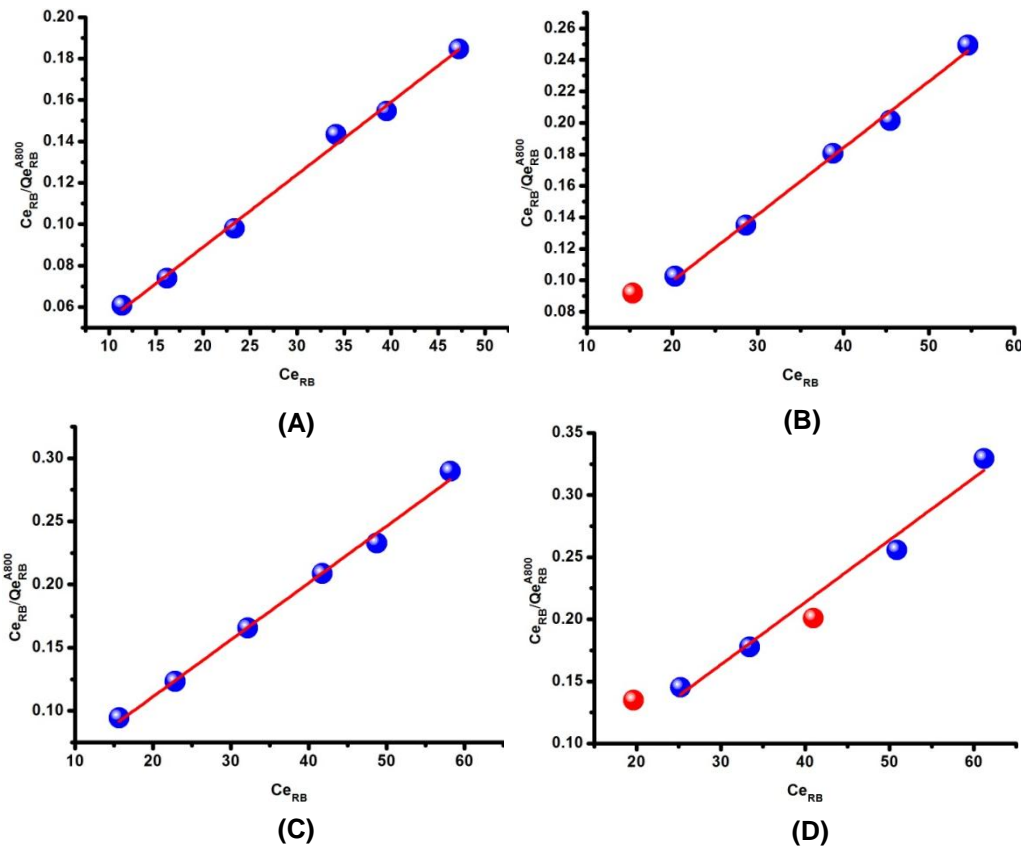
Fig.8.4.22: Employ A800 and apply Langmuir adsorption isotherm for RB adsorption at different temperatures: (A) 25 $^{\circ}$C, (B) 35 $^{\circ}$C, (C) 45 $^{\circ}$C and (D) 55 $^{\circ}$C.
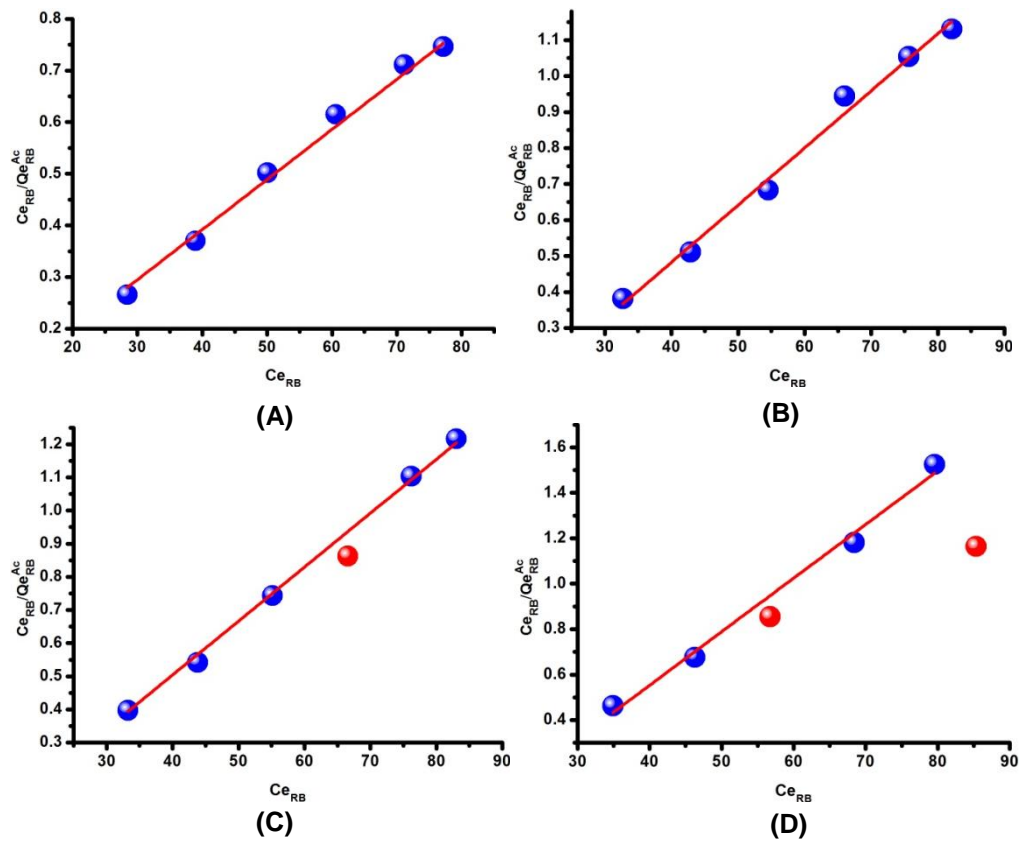
Fig.8.4.23: Employ AC and apply Langmuir adsorption isotherm for RB adsorption at different temperatures: (A) 25 $^{\circ}$C, (B) 35 $^{\circ}$C, (C) 45 $^{\circ}$C and (D) 55 $^{\circ}$C.
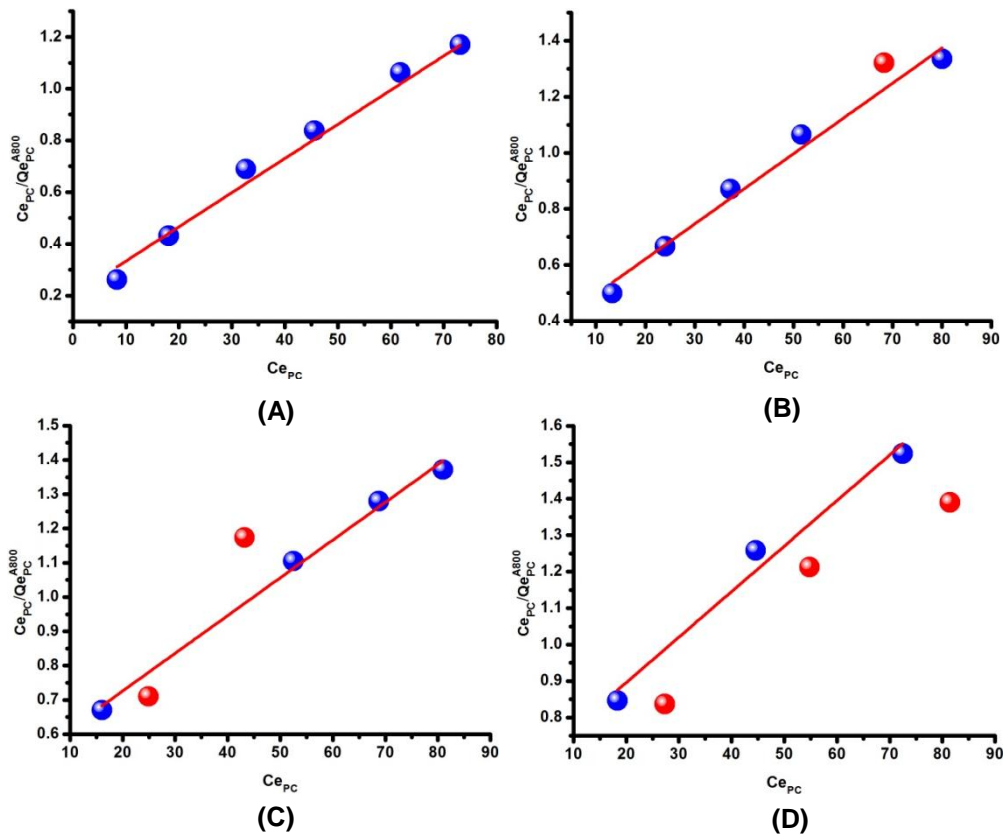
Fig.8.4.24: Employ A800 and apply Langmuir adsorption isotherm for PC adsorption at different temperatures: (A) 25 ^{o}C, (B) 35 ^{o}C, (C) 45 ^{o}C and (D) 55 ^{o}C.
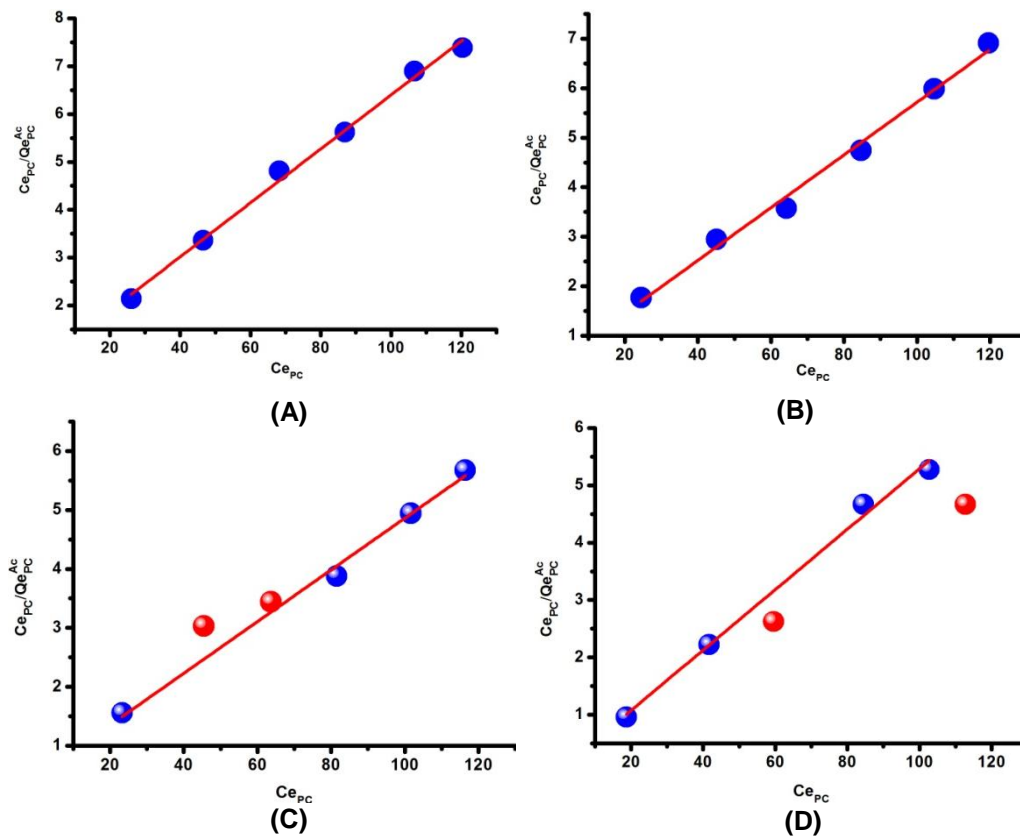
Fig.8.4.25: Employ AC and apply Langmuir adsorption isotherm for PC adsorption at different temperatures: (A) 25 ^{o}C, (B) 35 ^{o}C, (C) 45 ^{o}C and (D) 55 ^{o}C.
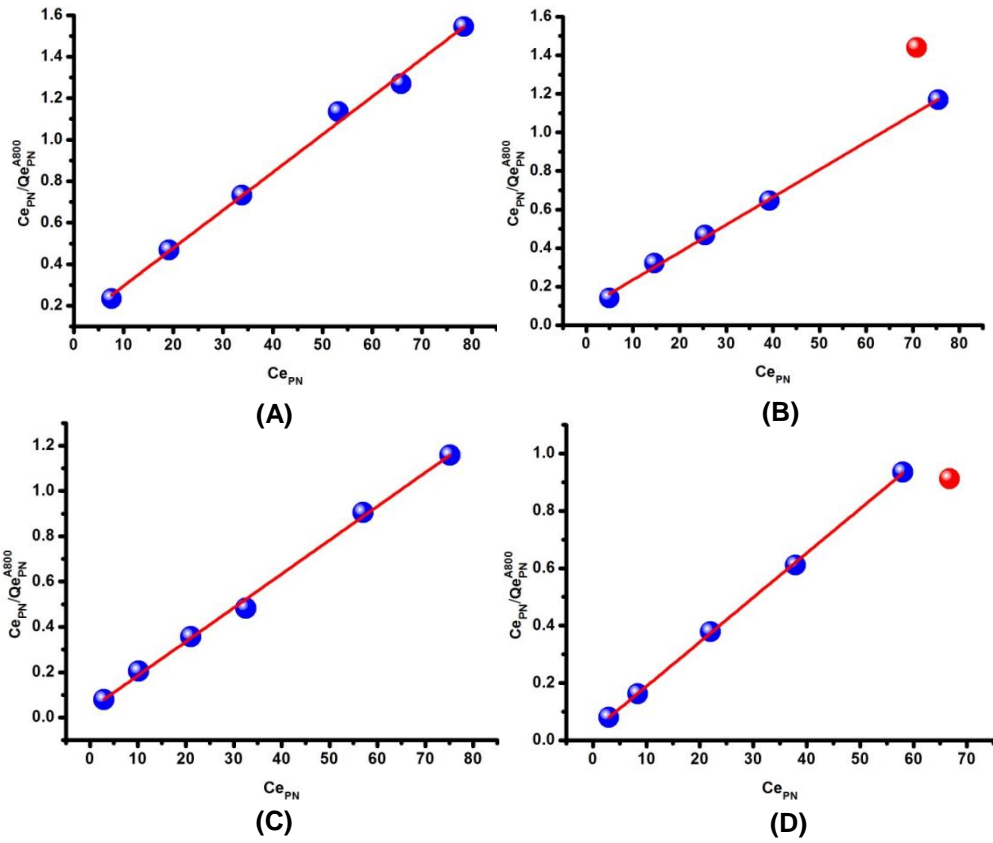
Fig.8.4.26: Employ A800 and apply Langmuir adsorption isotherm for PN adsorption at different temperatures: (A) 25 ^{o}C, (B) 35 ^{o}C, (C) 45 ^{o}C and (D) 55 ^{o}C.
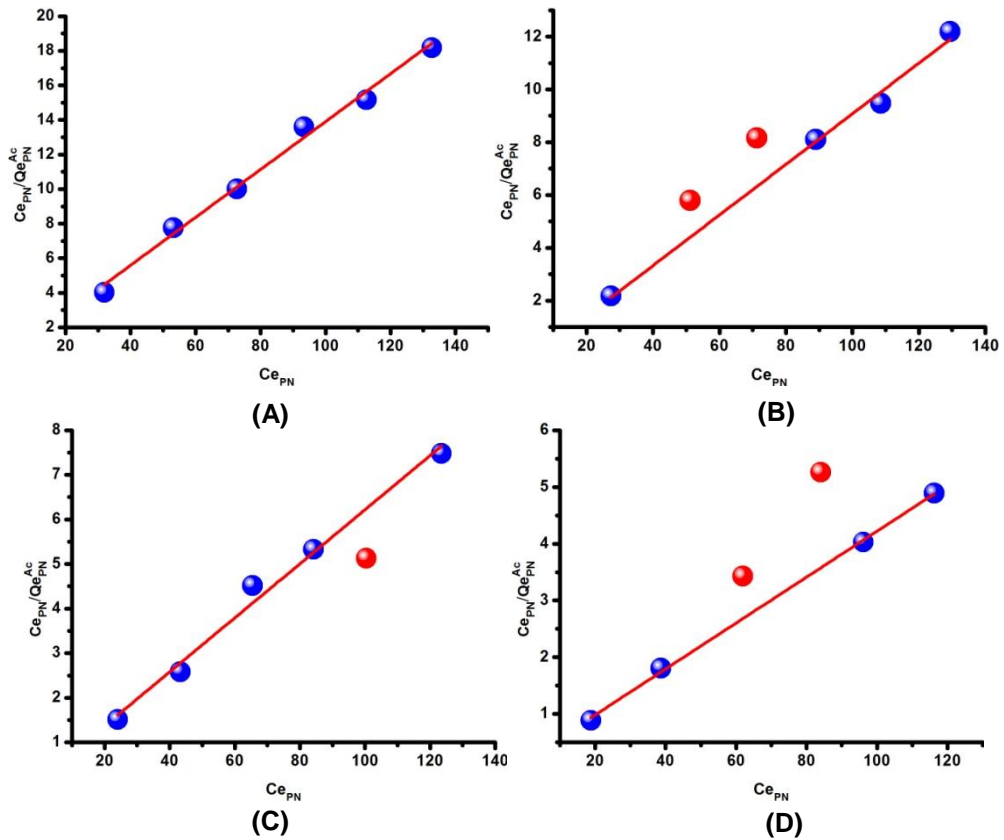
Fig.8.4.27: Employ AC and apply Langmuir adsorption isotherm for PN adsorption at different temperatures: (A) 25 ^{o}C, (B) 35 ^{o}C, (C) 45 ^{o}C and (D) 55 ^{o}C.
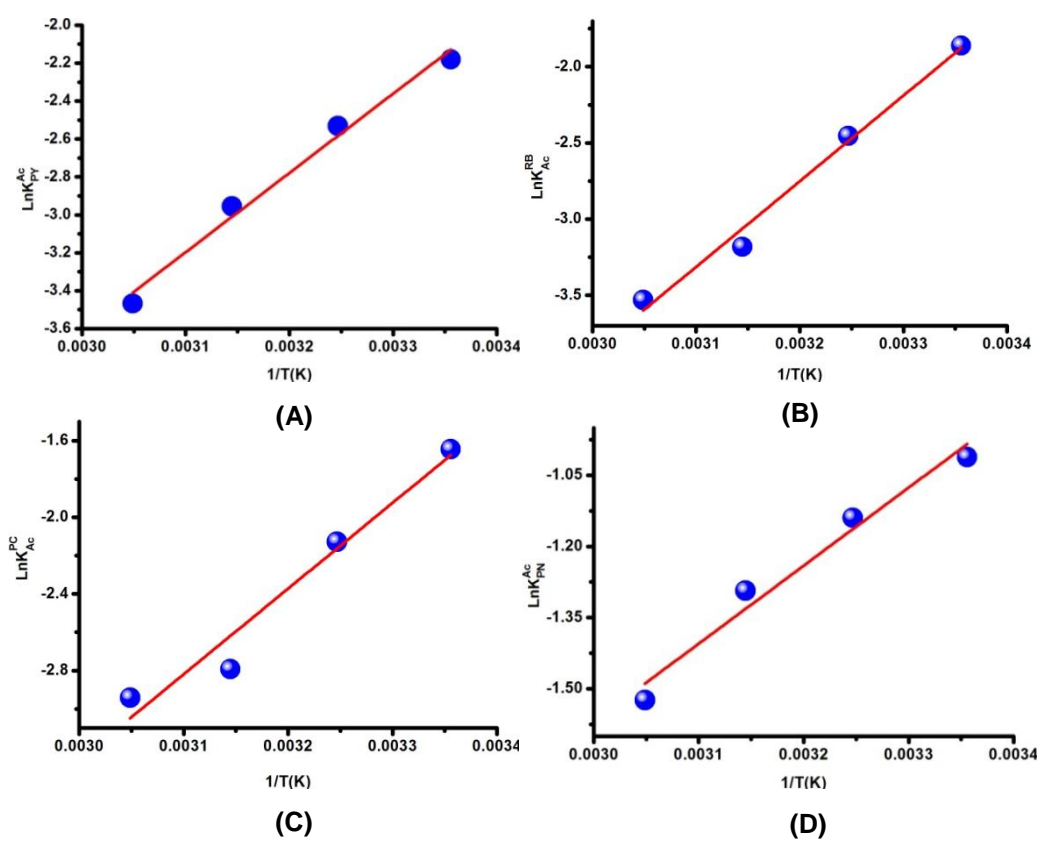
Fig.8.4.28: Plots of Lnk versus 1/T(K) for using AC for adsorption of (A) PY, (B) RB, (C) PC and (D) PN dyes.
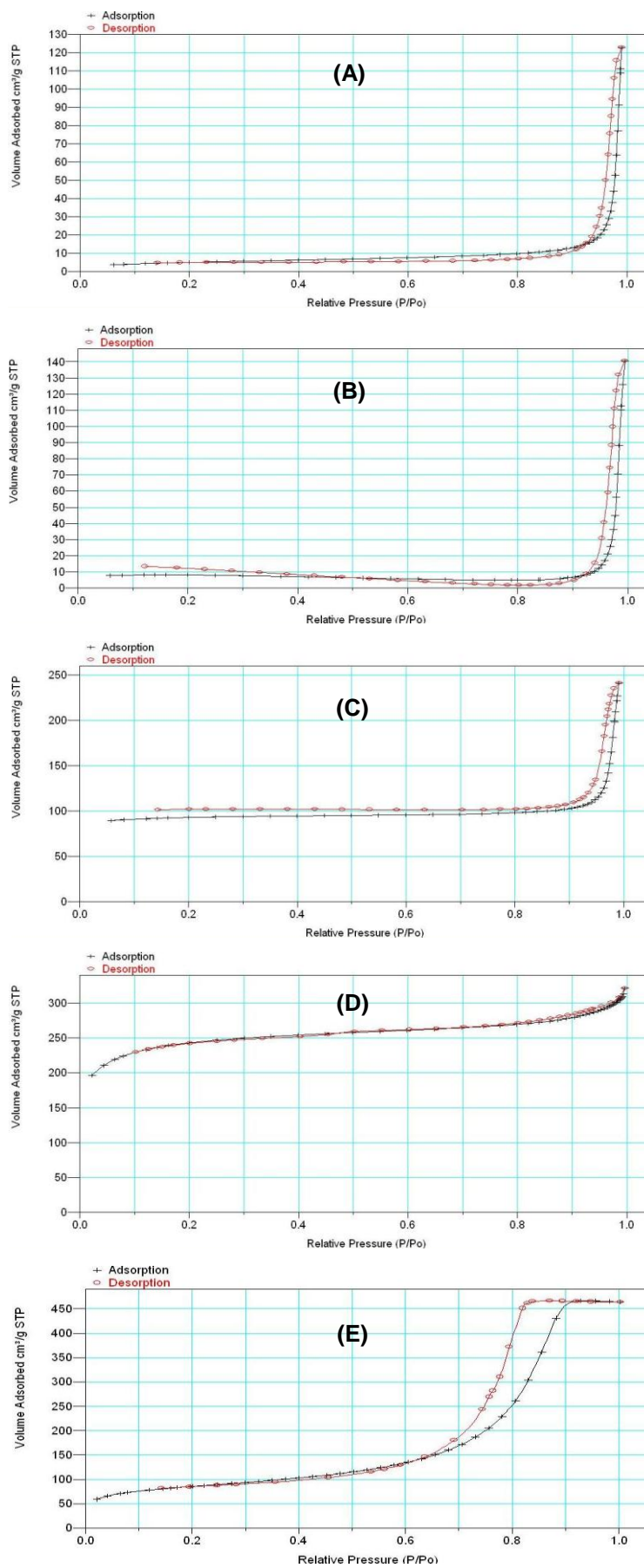
Fig.8.4.29: Adsorption isotherm plots for (A) S300, (B) S450, (C) S800, (D) AC and (E) Sgel
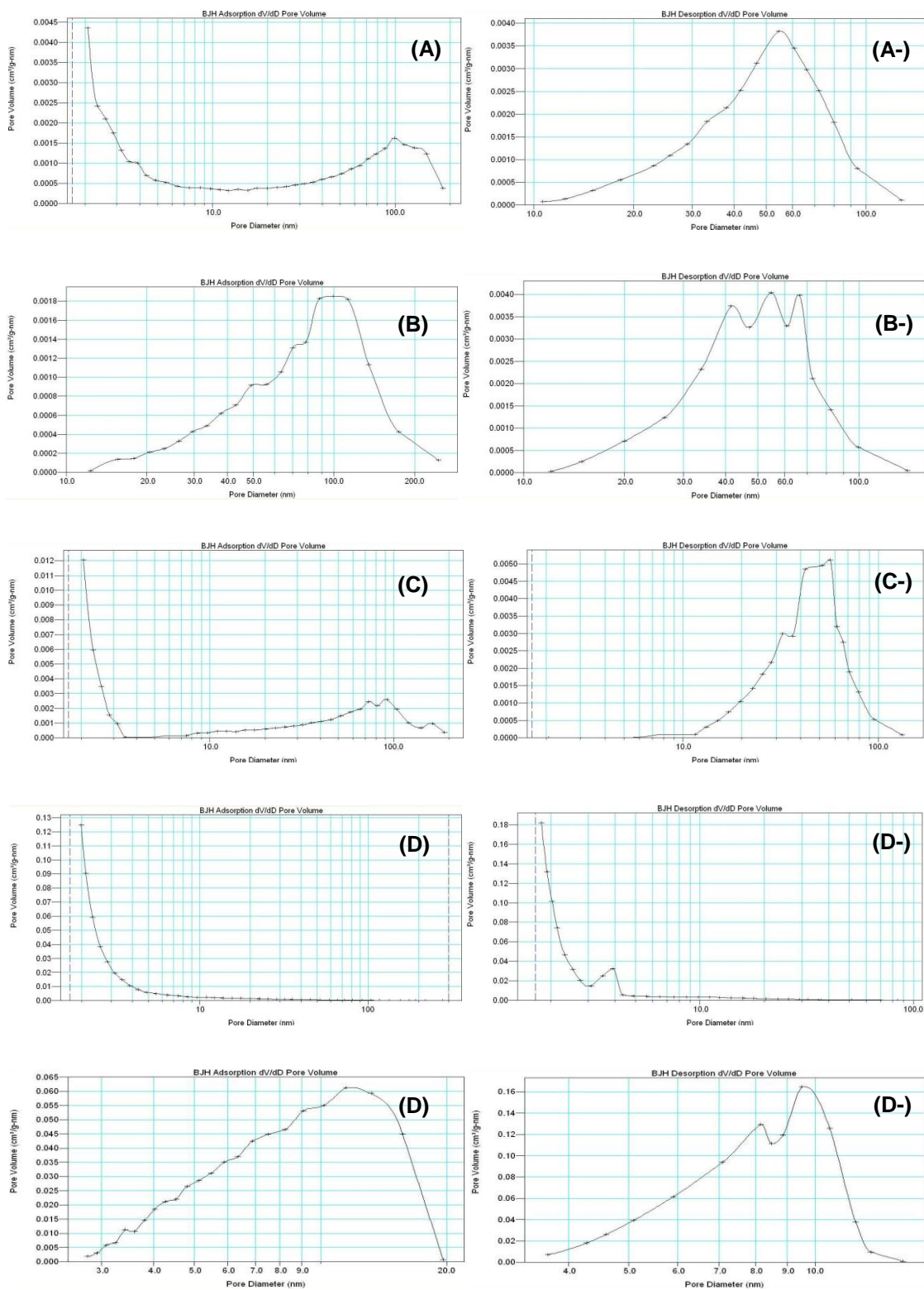
Fig.8.4.30: dV/dD pore size distribution versus pore diameter for (A) S300 (adsorption pore size distribution), (A-) S300 (desorption pore size distribution); (B) S450 (adsorption), (B-) S450 (desorption); (C) S800 (adsorption), (C-) S800 (desoption) and (D) AC (adsorption), (D-) AC (desorption), (E) Sgel (Adsorption), (E-) Sgel (desorption).
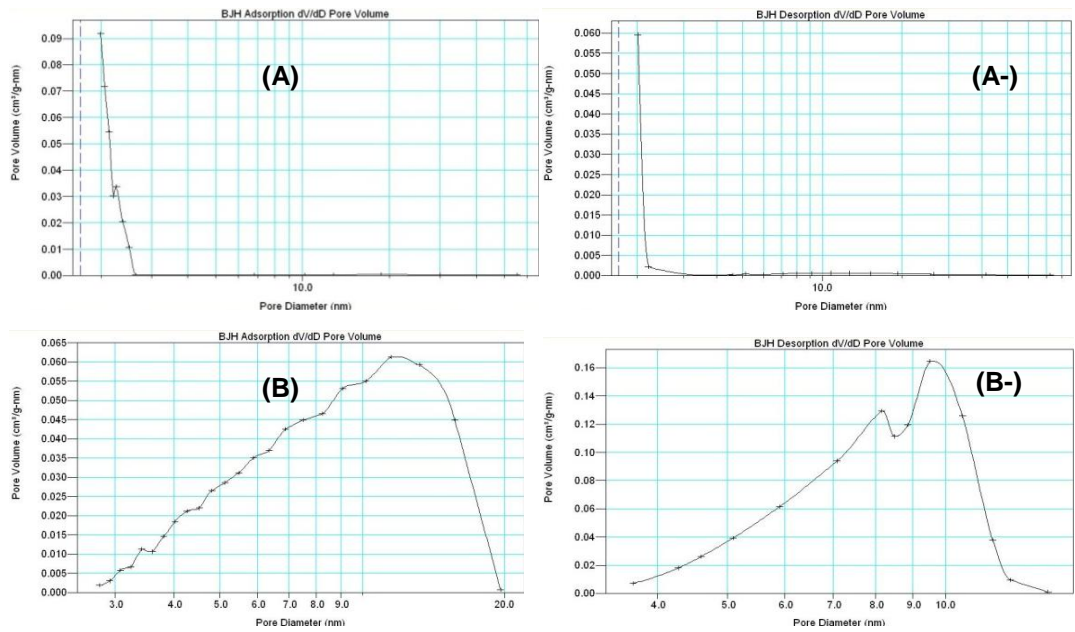
Fig.8.4.31: dV/dD pore size distribution for (A) AC (adsorption pore size distribution (Apsd)), (A-) AC (desorption pore size distribution (Dpsd)); (B) Sgel(Apsd), (B-) Sgel (Dpsd).
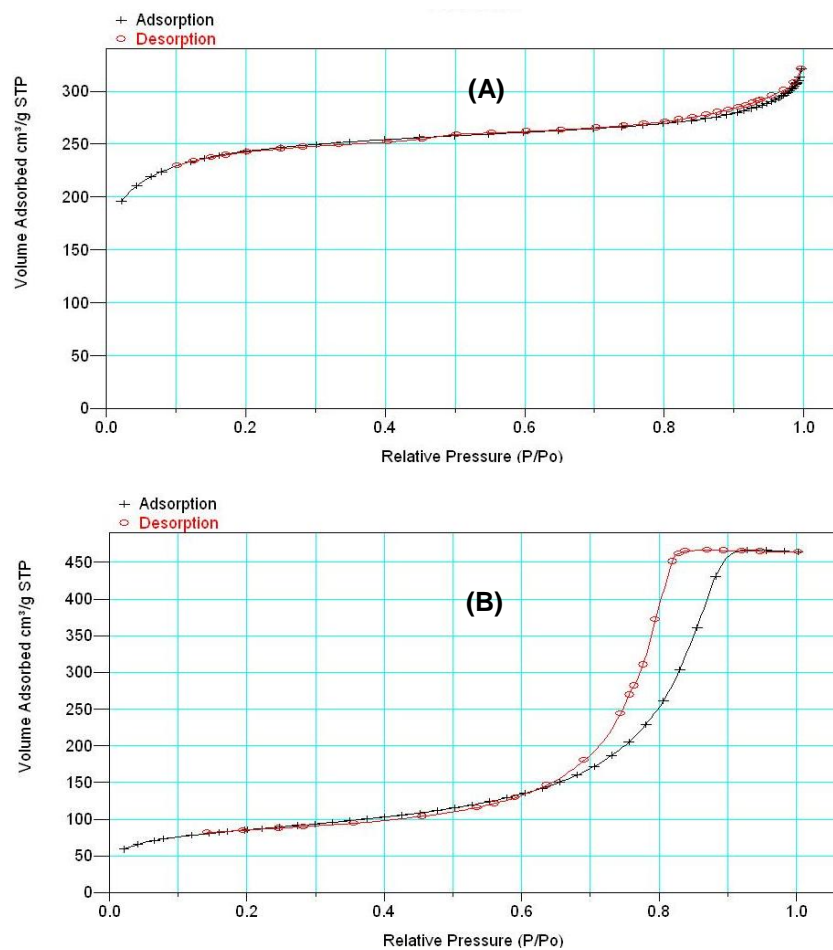
Fig.8.4.32: Linear isotherm plot for (A) AC and (B) Sgel.
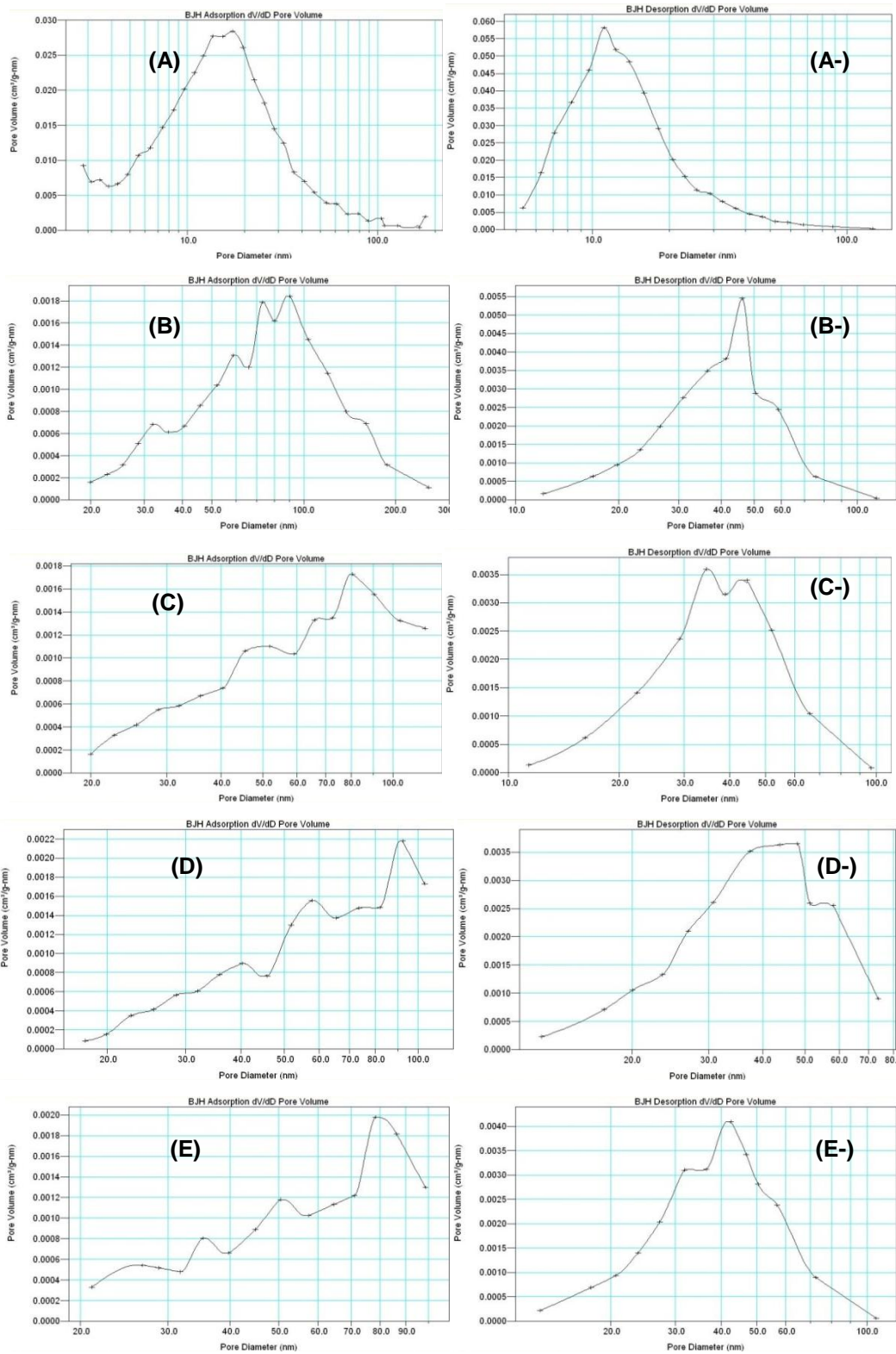
Fig.8.4.33: dV/dD pore size distribution for (A) A800 initial (adsorption pore size distribution (Apsd)), (A-) A800 initial (desorption pore size distribution (Dpsd)); (B) A800 loaded with PY (Apsd), (B-) A800 loaded with PY (Dpsd), (C) A800 loaded with RB (Apsd), (C-) A800 loaded with RB (Dpsd), (D) A800 loaded with PC (Apsd), (D-) A800 loaded with PC (Dpsd), (E) A800 loaded with PN (Apsd) and (E-) A800 loaded with PN (Dpsd).
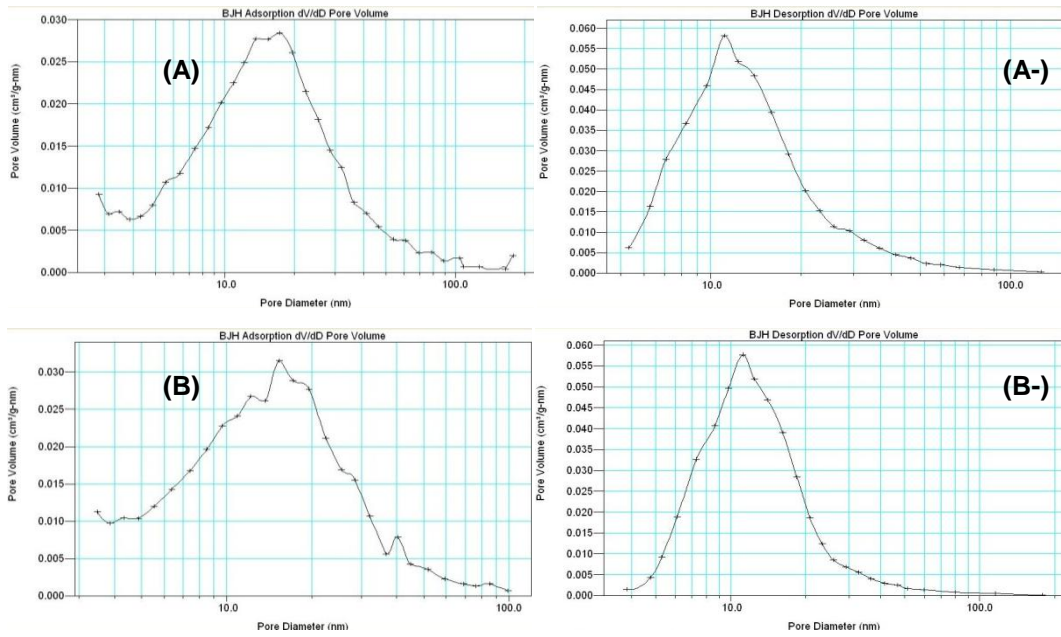
Fig.8.4.34: dV/dD pore size distribution for (A) A800 initial (adsorption pore size distribution (Apsd)), (A-) A800 initial (desorption pore size distribution (Dpsd)); (B) Thermally regenerated A800 loaded with PC (Apsd), (B-) thermally regenerated A800 loaded with PC (Dpsd).
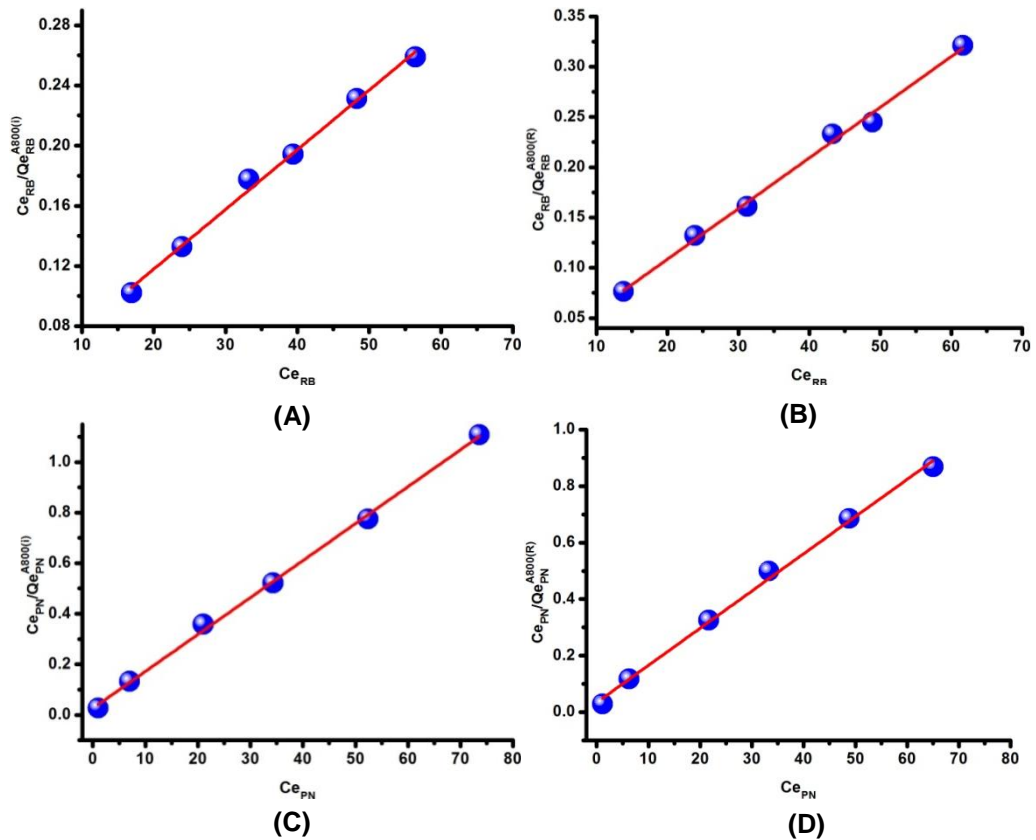
Fig.8.4.35: Employ A800 initial and apply Langmuir adsorption isotherm for (A) RB and (B) PN; employ thermally regenerated A800 and apply Langmuir adsorption isotherm for (A) RB and (B) PN.

Appendix five

(A)

(B)

(C)

(D)
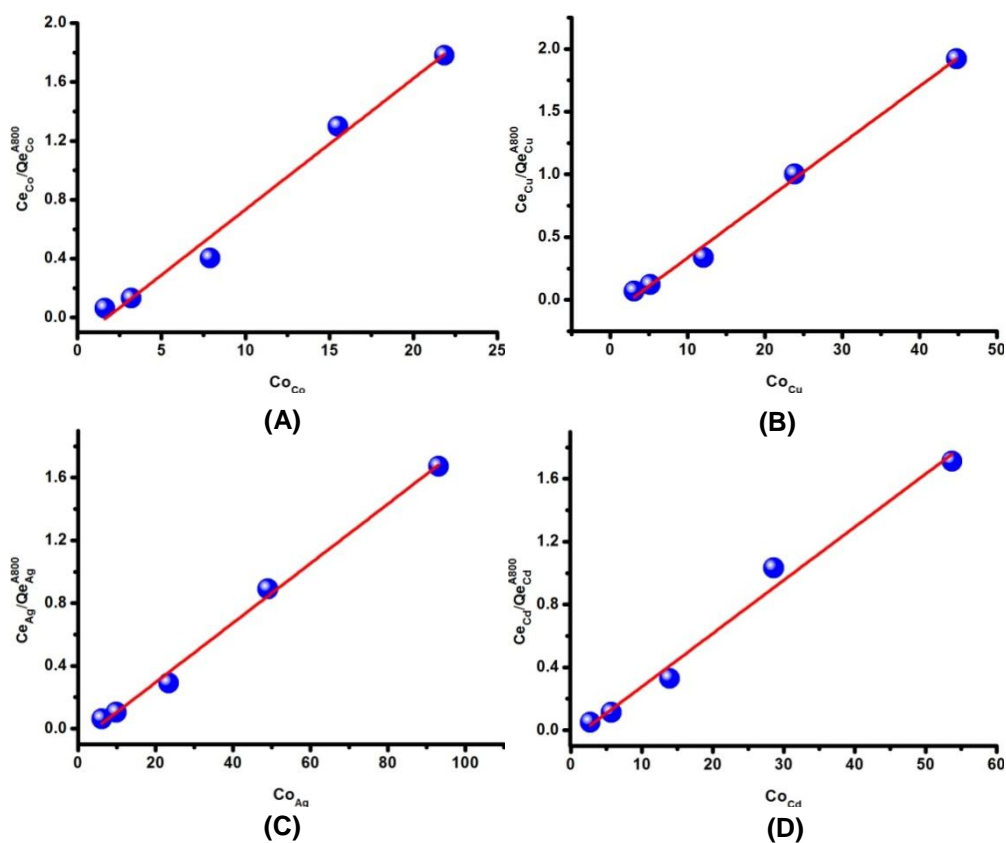
Fig.8.5.1: Employ A800 and apply Langmuir adsorption isotherm for (A) Co (B) Cu, (C) Ag and (D) Cd.

(A)

(B)

(C)

(D)
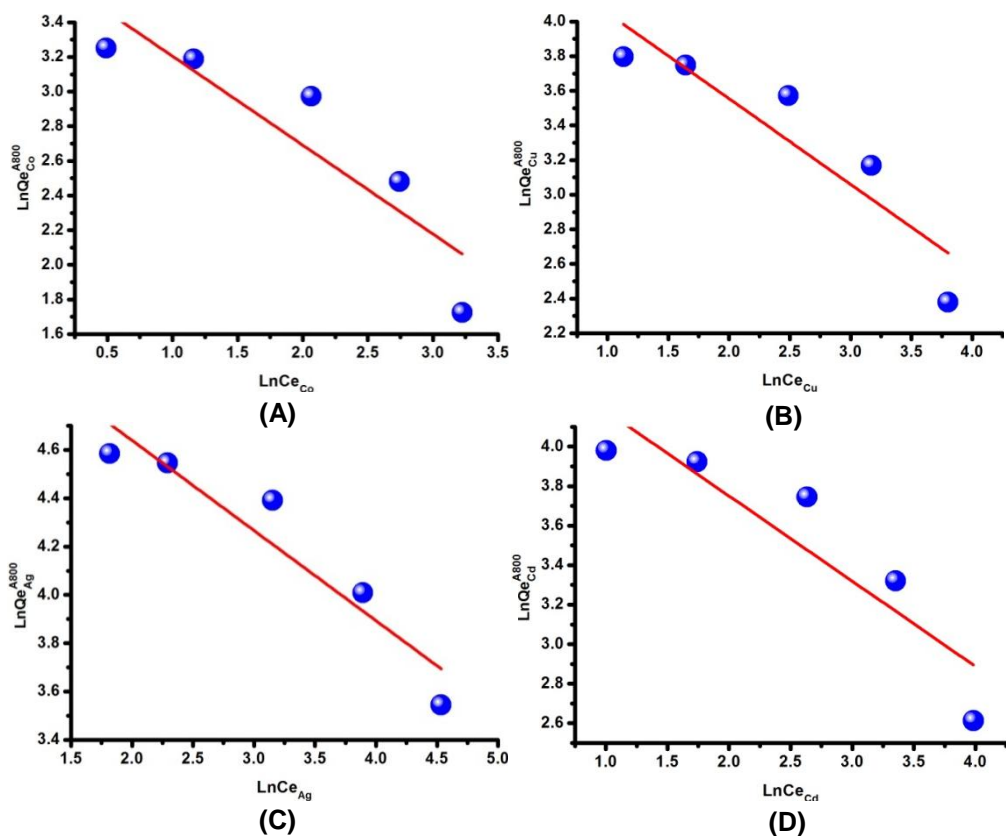
Fig.8.5.2: Employ A800 and apply Freundlich adsorption isotherm for (A) Co (B) Cu, (C) Ag and (D) Cd.
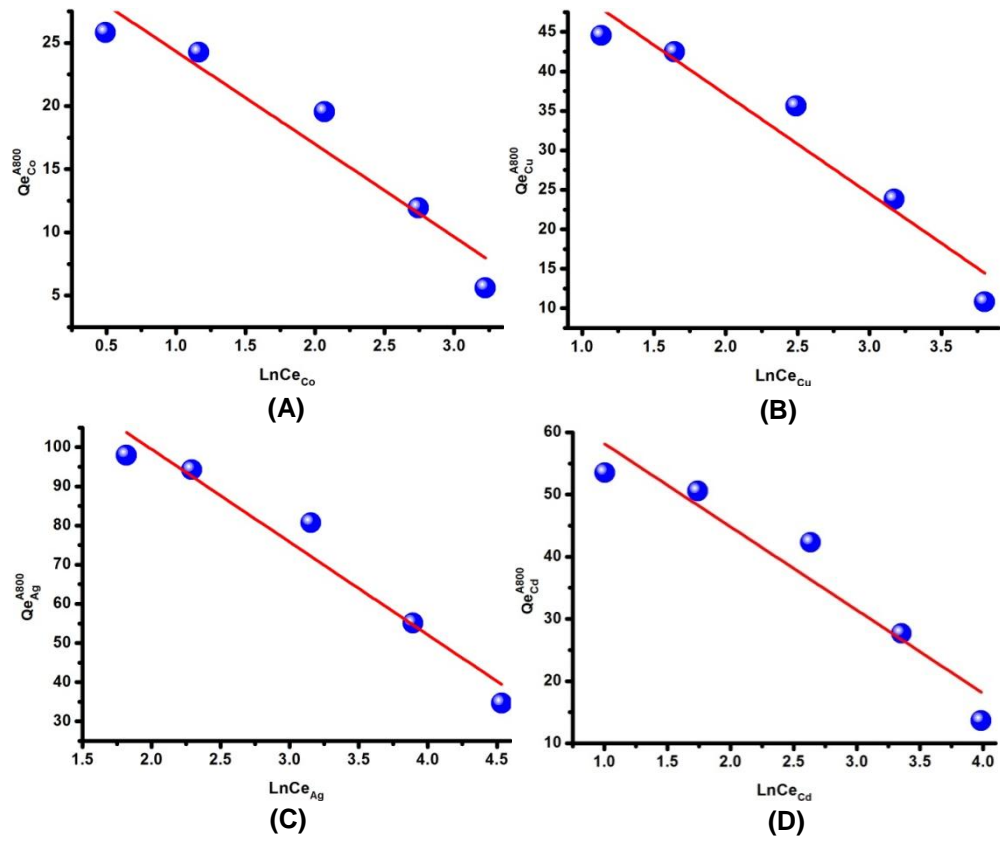
Fig.8.5.3: Employ A800 and apply Tempkin adsorption isotherm for (A) Co (B) Cu, (C) Ag and (D) Cd.
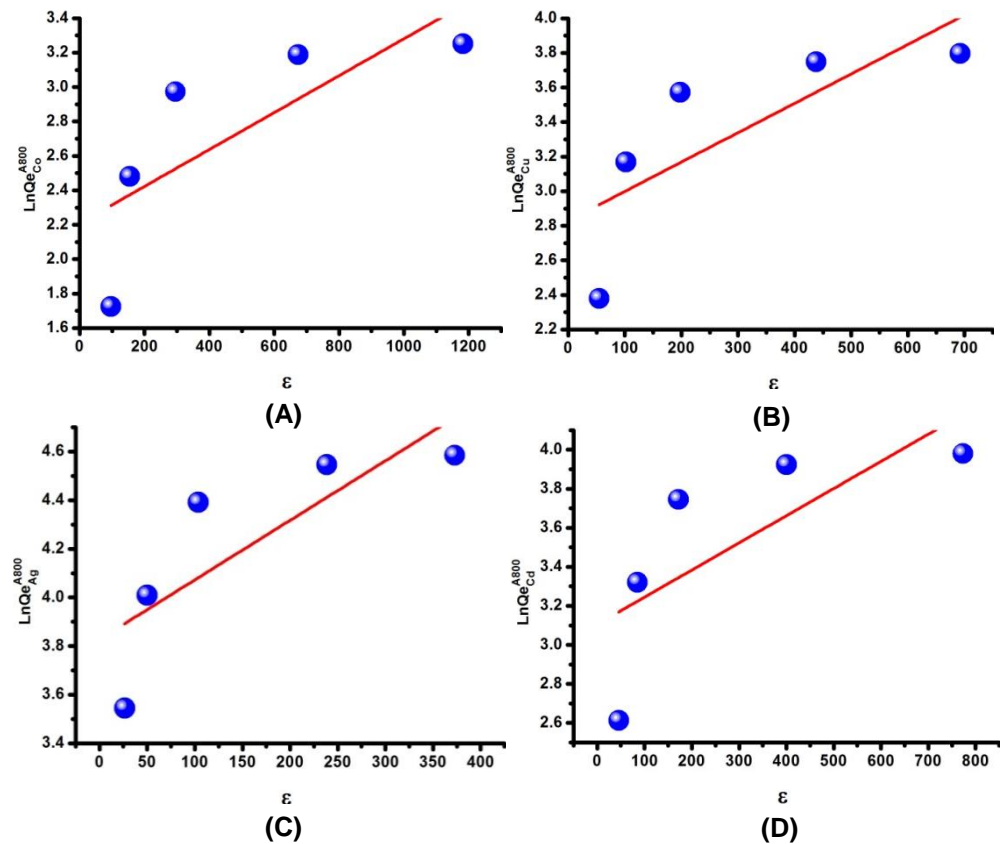
Fig.8.5.4: Employ A800 and apply Dubinin-Radushkevich adsorption isotherm for (A) Co (B) Cu, (C) Ag and (D) Cd.
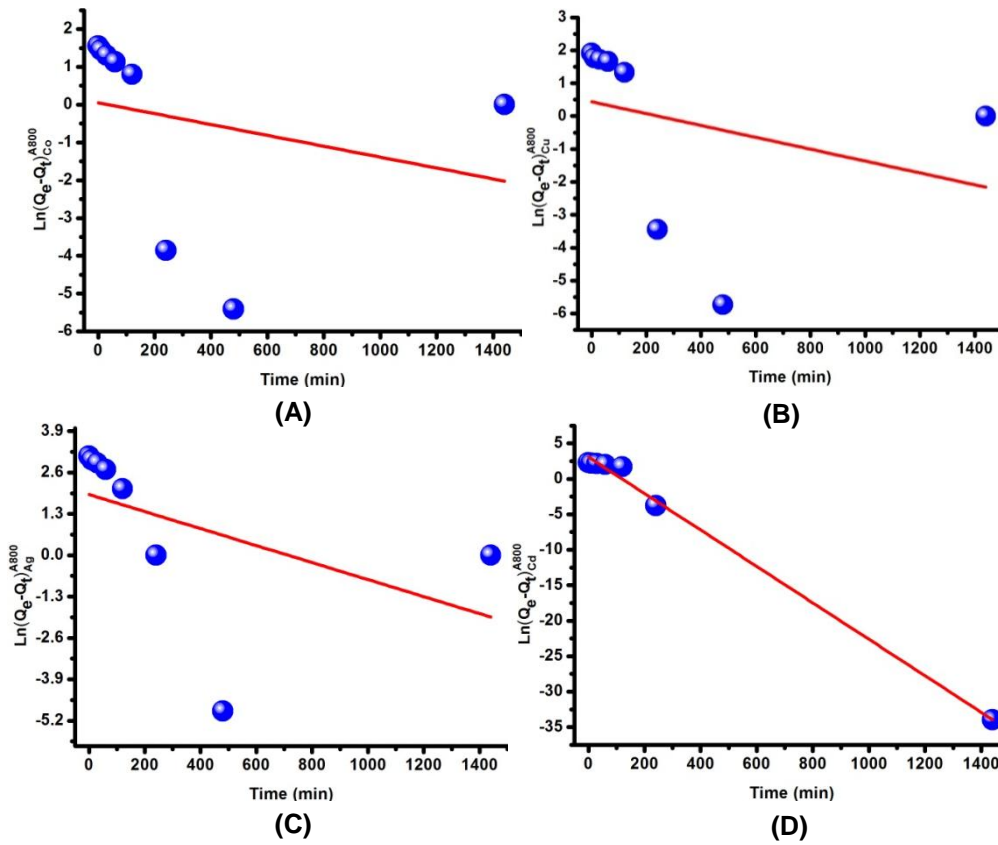
Fig.8.5.5: Employ A800 and apply Pseudo-first-order model for (A) Co, (B) Cu, (C) Ag and (D) Cd.
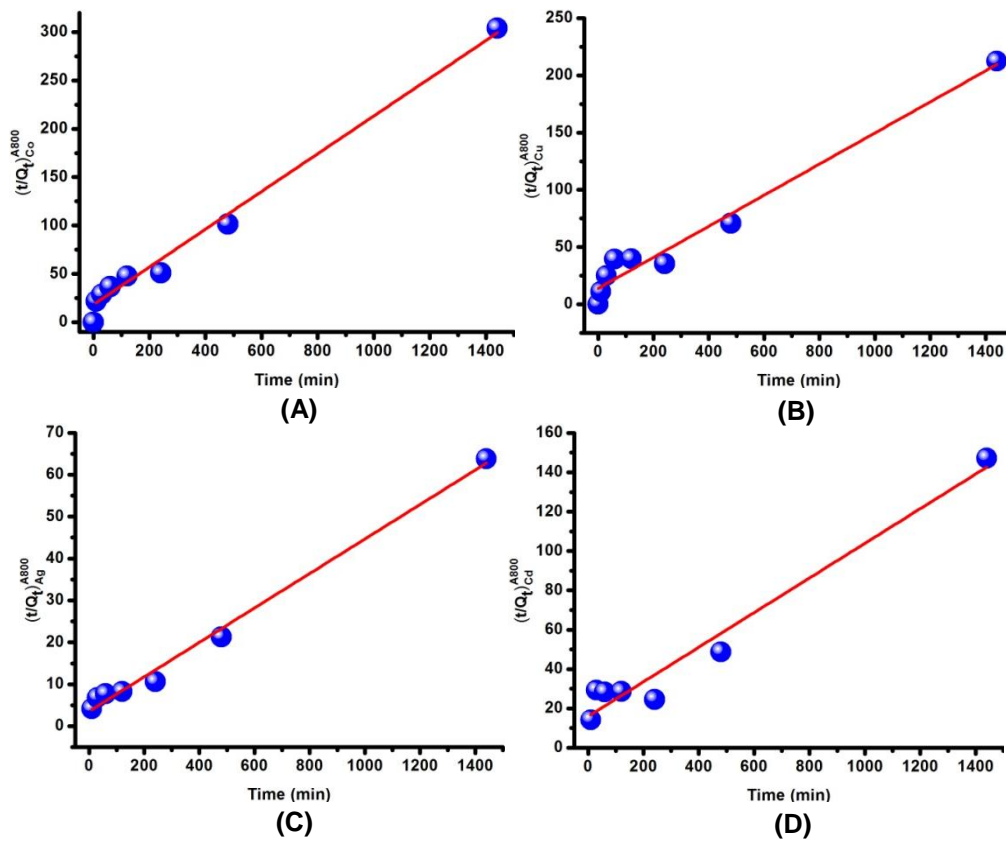
Fig.8.5.6: Employ A800 and apply Pseudo-second-order model for (A) Co, (B) Cu, (C) Ag and (D) Cd.

264

Abbreviations

A1	Expanded alginic acid oven dried
A2	Expanded alginic acid super critical CO_2 dried
AC	Powder activated carbon
A300	Algibon300
A450	Algibon450
A600	Algibon600
A800	Algibon800
BET	Brunauer Emmett and Teller
BOD	Biological oxygen demand
C_o	Initial solution concentration (mg/L)
C_e	Equilibrium solution concentration (mg/L)
COD	Chemical oxygen demand
DRIFT IR	Diffuse reflectance infrared fourier transform
D-R	Dubinin-Radushkevich
IUPAC	International Union of Pure and Applied Chemistry
ICP-OES	Inductively coupled plasma optical emission spectroscopy
K_L	Langmuir isotherm constant
K	Constant of equilibrium (L/mg)
K_F	Freundlich constant
M	Mass of adsorbent material used (mg and g)
NMR	Nuclear magnetic resonance
PSTA	Para toluene sulphonic acid
Q_e	Equilibrium concentration in solid phase (mg/g)
Q_t	Equilibrium concentration in solid phase at time (mg/g)
Q_m	Maximum adsorption capacity (mg/g)
R^2	Correlation coefficient
rpm	Rotation per minute
RF	Radio frequency
S800	Starbon800
S450	Starbon450
S300	Starbon300
Sgel	Silica gel
SEM	Scanning electron micrograph
$scCO_2$	Supercritical carbon dioxide

STA	Simultaneous thermal analysis
TG	Thermogravimetric analysis
UV-Vis	Ultraviolet-visible
V	Volume of the solution (mL and L)
WWTP	Wastewater treatment plant

References

[1] N. Ahalya, T. Ramachandra and R. Kanamadi, Biosorption of heavy metals, *Research Journal of Chemistry and Environment,* 2003, **4**, 71-79.

[2] R. Gong, Y. Sun, J. Chen, H. Liu and C. Yang, Effect of chemical modification on dye adsorption capacity of peanut hull, *Dyes and Pigments*, 2005, **67**, 175-181.

[3] G. Arabaci and A. Usluoglu, The enzymatic decolorization of textile dyes by the immobilized polyphenol oxidase from quince leaves, *The Scientific World Journal*, 2014, **1**, 1-5.

[4] W. Ngah, L. Teong and M. Hanafiah, Adsorption of dyes and heavy metal ions by chitosan composites: a review, *Carbohydrate Polymers*, 2011, **83**, 1446-1456.

[5] K. Kadirvelu, M. Kavipriya, C. Karthikab, M. Radhika, N. Vennilamani and S. Pattabhi, Utilization of various agricultural wastes for activated carbon preparation and application for the removal of dyes and metal ions from aqueous solutions, *Bioresource Technology*, 2003, **87**, 129-132.

[6] B. Tastan and G. Donmez, Single and binary biosorption of heavy metal ions and reactive dye by aspergillus versicolor, *Communications Faculty of Science University of Ankara Series B*, 2010, **56**,13-25.

[7] I. Ali, Advances in water treatment by adsorption technology, *Nature Protocols*, 2007, **6**, 2661-2667.

[8] S. Alvarez, J. Sotelo, G. Ovejero, A. Rodríguez and J. Garcia, Low-cost adsorbent for emerging contaminant removal in fixed-bed columns, *Chemical Engineering Transaction*, 2013, **32**, 61-66.

[9] V. Budarin, J. Clark, R. Luque and D. Macquarrie, Versatile mesoporous carbonaceous materials for acid catalysis, *Chemical Communications*, 2007, **1**, 634-636.

[10] P. Dapsens, C. Mondelli and J. Perez-Ramirez, Biobased chemicals from conception toward industrial reality: lessons learned and to be learned, *American Chemical Society Catalysis*, 2012, **2**,1487-1499.

[11] Q. Huo, J. Feng, F. Schuth and G. Stucky, Preparation of hard mesoporous silica spheres, *Chemistry of Materials*, 1997, **9**, 14-17.

[12] V. Budarin, J. Clark, R. Luque, D. Macquarrie, A. Koutinas and C. Webb, Tunable mesoporous materials optimised for aqueous phase esterifications, *Green Chemistry*, 2007, **9**, 992-995.

[13] H. Parker, V. Budarin, J. Clark and A. Hunt, Use of Starbon for the Adsorption and Desorption of Phenols, *ACS Sustainable Chemistry and Engineering*, 2013, **1**, 1311-1318.

[14] M. Salgota, E. Huertasa, S. Weberb, W. Dottb and J. Hollenderb, Wastewater reuse and risk: definition of key objectives, *Elservier Desalination*, 2006, **187**, 29-40.

[15] Guidelines for drinking-water quality, water quality requirement, Third edition, World Health Organization WHO, Geneva 2004.

[16] M. Shannon, P. Bohn, M. Elimelech, J. Georgiadis, B. Marin and A. Mayes, Science and technology for water purification in the coming decades, *Nature publishing Group*, 2008, **20**, 301-310.

[17] C. Binne, M. Kimber and G. Smethu, Basic water treatment, Third edition, Royal Society of Chemistry, London, 2003.

[18] B. Bolto and J. Gregory, Review: organic polyelectrolytes in water treatment, *Water Research*, 2007, **41**,2301-2324.

[19] Z. Aksu, Application of biosorption for the removal of organic pollutants: a review, *Process Biochemistry*, 2005, **40**, 997-1026.

[20] S. Batool, S. Akib, M. Ahmad, K. Balkhair and M. Ashraf, Study of modern nano enhanced techniques for removal of dyes and metals, *Journal of Nanomateials*, 2014, **2014**, 1-20.

[21] H. Zollinger, Color chemistry: synthesis, properties and applications of organic dyes and pigment, Third edition, Wiley-VCH, Zurich, Weinheim, 2003.

[22] A. Baban, A. Yediler and K. Ciliz, Integrated water management and CP implementation for wool and textile blend processes, *Clean*, 2010, **1**, 84-90.

[23] P. Anastas and J. Warner, Green chemistry: theory and practice, University Press, New York, Oxford, 2000.

[24] P. Anastas and N. Eghbali, Green chemistry: principles and practice, *Chemical Society Reviews*, 2010, **39**, 301-312.

[25] I. Bisschops and H. Spanjers, Literature review on textile wastewater characterisation, *Environmental Technology*, 2003, **24**,1399-1411.

[26] G. Mekala, B. Davidson, M. Samad and A. Boland, Wastewater reuse and recycling system: a perspective into India and Australia, International Water Management Institute IWMI, Australia, 2008.

[27] M. Libhaber and A. Orozco-Jaramillo, Sustainable treatment and reuse of municipal wastewater, First edition, International Water Association, London, 2012.

[28] A. Kumar, V. Joshi, B. Bisht and A. Singh, Determination of physicochemical pollutant indicators in solid and liquid waste, *International Journal of Research in Environmental Science and technology*, 2011, **1**, 1-6.

[29] F. Spellman, Handbook of water and wastewater treatment plant operations, CRC Press LLC, Florida, 2003.

[30] S. Kaul, T. Nandy, L. Szpyrkowicz, A. Gautam and D. Khanna, Wastewater management with special reference to tannaries, Discovery Publishing House, New Delhi, 2005.

[31] W. Grabow, World water congress: industrial wastewater and environmental contaminants: selected proceedings of the 1st Iwa world water congress, International Water Association, Paris, 2001.

[32] K. Grasshoff, K. Kremling and M. Ehrhardt, Methods of seawater analysis, Third edition, Wiley-VCH Publishers, Weinheim, New York, Chiester, Brisbane, Singapore, Toronto, 1999.

[33] T. Wintgens, T. Melin, A. Schafer, M. Muston, D. Bixio and C. Thoeye, The role of membrane processes in municipal wastewater reclamation and reuse, *Desalination*, 2005, **178**, 1-11.

[34] R. Mujeriego and T. Asano, The role of advanced treatment in wastewater reclamation and reuse, *Water Science and Technology*, 1999, **40**, 1-9.

[35] K. Raunkjar, T. Hvitved-Jacobsen and P. Nielsen, Measurement of pools of protein, carbohydrate and lipid in domestic wastewater, *Water Research*, 1994, **2**, 251-262.

[36] I. Mantis, D. Voutsa and C. Samara, Assessment of the environmental hazard from municipal and industrial wastewater treatment sludge by employing chemical and biological methods, *Ecotoxicology and Environmental Safety*, 2005, **3**, 397-407.

[37] Recommended standards for wastewater facilities 2004 edition, policies for the design, review, and approval of plans and specifications for wastewater collection and treatment facilities, Health Research Inc., Health Education Services Division, 2004, New York, accessed on 10/01/2015.

[38] M. Krzemieniewski, M. Debowski, A. Dobrzynska and M. Zielinski, Chemical oxygen demand reduction of various wastewater types using magnetic field-assisted fenton reaction, *Water Environment Research*, 2004, **1**, 301-309.

[39] P. Armenante, Characterization of industrial wastewaters, New Jersey Institute of Technology (NJIT), 1999, accessed on 10/1/2015.

[40] R. Droste, Theory and practice of water and wastewater treatment, John Wiley and Sons, New York, 1996.

[41] K. Oliveira-Esquerre, M. Mori and R. Bruns, Simulation of an industrial wastewater treatment plants using artificial neutral networks and principal components analysis, *Brazilian Journal of Chemical Engineering*, 2002, **4**, 365-370.

[42] E. Eriksson, K. Auffarth, M. Henze and A. Ledin, Characteristics of wastewater, *Urban Water*, 2002, **4**, 85-104.

[43] F. Raposo, M. de la Rubia, R. Borja and M. Alaiz, Assessment of a modified and optimised method for determining chemical oxygen demand of solid substrates and solutions with high suspended solid content, *Talanta*, 2008, **76**, 448-453.

[44] S. Qasim, Wastewater treatment plants: planning, design and operation, CRS press, Washington DC, 1998.

[45] J. Sokolowska-Gajda, H. Freeman and A. Reife, Synthetic dyes based on environmental considerations. Part 2: Iron complexed formazan dyes, *Dyes and Pigments*, 1996, **30**, 1-20.

[46] O. Tunay, L. Kabdasli, D. Ohron and G. Cansever, Use and minimalization of water in leather tanning processes, *Water Science Technology*, 1999, **1**, 237-244.

[47] R. Juang, R. Tseng, F. Wu and S. Lin, Use of chitin and chitosan in lobster shell wastes for colour removal from aqueous solutions, *Journal of Environmental Science and Health, part A*, 1996, **31**, 325-338.

[48] R. Bhat and P. Mathur, Changing scenario of food colours in India, *Current Science*, 1998, **74**, 198-202.

[49] S. Cook and D. Linden, Use of rhodamine WT to facilitate dilution and analysis of atrazine samples in short-term transport studies, *Journal of Environmental Quality*, 1997, **26**, 1438-1441.

[50] R. Wagner and J. Lindsey, Boron-dipyrromethane dyes for incorporation in synthetic multi-pigment light-harvesting arrays, *Pure and Applied Chemistry*, 1996, **68**, 1373-1380.

[51] D. Wrobel, A. Boguta and R. Ion, Mixtures of synthetic organic dyes in a photoelectronic cell, *Journal of Photochemistry and Photobiology A: Chemistry,* 2001, **138**, 7-22.

[52] C. Scarpi, F. Ninci, M. Centini and C. Anselmi, High-performance liquid chromatography determination of dir Schuler, C.A., Anthony R.G., and Ohlendorf, *Archives of environmental contamination and toxicology*, 1998, **29**, 845-853.

[53] P. Vankar, Chemistry of natural dyes, *SpringerLink Journals*, 2000,**10**, 73-80.

[54] C. Pearce, J. Lloyd and J. Guthrie, The removal of colour from textile wastewater using whole bacterial cells: a review, *dyes and Pigments*, 2003, **58**, 179-196.

[55] D. Knittel and E. Schollmeyer, Prevention of water pollution in dyeing processes of synthetic textiles, *European Water Pollution Control*, 1996, **6**, 6-10.

[56] J. Petek and P. Glavic, An integral approach to waste minimization in process industries, *Resources, Conservation and Recycling*, 1996, **17**,169-188.

[57] V. Rostovtsev, G. Luke, V. Fokin and K. Sharpless, A tepwise huisgen cycloaddition process: copper(I)-catalyzed regioselective "ligation" of azides and terminal alkynes, *Angewandte Chemie*, 2002, **14**, 2708-2711.

[58] N. Srivastava and C. Majumder, Novel biofiltration methods for the treatment of heavy metals from industrial wastewater, *Journal of Hazardous Materials*, 2008, **151**, 1-8.

[59] S. Ahluwalia and D. Goyal, Microbial and plant derived biomass for removal of heavy metals from wastewater, *Bioresource Technology*, 2007, **98**, 2243-2257.

[60] S. Kumar and S. Kochher, Screening for potential textile dye decolorizing bacteria, *International Journal for Science and Emerging Technologies with Latest Trends*, 2012, **1**, 36-48.

[61] T. Robinson, B. Chandran and P. Nigam, Removal of dyes from an artificial textile dye effluent by two agricultural waste residues, corncob and barley husk, *Environment International,* 2002, **28**, 29-33.

[62] K. Chung and C. Cerniglia, Mutagenicity of azo dyes: Structure-activity relationships, *Mutation Research*, 1992, **277**, 201-220.

[63] G. Costan, N. Bermingham, C. Blaise and J. Ferard, Potential ecotoxic effect probe (PEEP): a novel index to assess and compare the toxic potential of

industrial effluents, *Environmental Toxicology and Water Quality*, 1993, **8**, 115-140.

[64] N. Kress, B. Herut and B. Galil, Sewage sludge impact on sediment quality and benthic assemblages off the Mediterranean coast of Israel a long-term study, *Marine Environmental Research*, 2004, **57**, 213-233.

[65] T. Sato, B. Xing and S. Tao, Health risks of heavy metals to the general public in Tianjin, China via consumption of vegetables and fish, *Science of the Total Environment*, 2005, **350**, 28-37.

[66] T. Chen, Y. Zheng, M. Lei, Z. Huang, H. Wu, H. Chen, K. Fan, K. Yu, X. Wu and Q. Tian, Assessment of heavy metal pollution in surface soils of urban parks in Beijing, China, *chemosphere*, 2005, **60**, 542-551.

[67] V. Sarin and K. Pant, Removal of chromium from industrial waste by using eucalyptus bark, *Bioresource Technology*, 2006, **97**, 15-20.

[68] L. Khezami and R. Capart, Removal of chromium(VI) from aqueous solution by activated carbons: kinetic and equilibrium studies, J*ournal of Hazardous Materials*, 2005, **123**, 223-231.

[69] R. Lokhande, P. Singare and D. Pimple, Pollution in water of Kasardi river flowing along Taloja industrial area of Mumbai, *India, World Environment*, 2011, **1**, 6-13.

[70] D. Manohar, K. Krishnan and T. Anirudhan, Removal of mercury(II) from aqueous solutions and chlor-alkali industry wastewater using 2-mercaptobenzimidazole-clay, *Water Research*, 2002, **36**, 1609-1619.

[71] P. Daniszewski and R. Konieczny, Heavy metal content in water of Starzyc Lake (North-West Poland), *International Letters of Chemistry, Physics and Astronomy*, 2013, **3**, 269-278.

[72] V. Gupta, C. Jainb, I. Ali, M. Sharma and V. Saini, Removal of cadmium and nickel from wastewater using bagasse fly ash-a sugar industry waste, *Water Research*, 2003, **37**, 4038-4044.

[73] C. Borba, R. Guirardello, E. Silva, M. Veit and C. Tavares, Removal of nickel(II) ions from aqueous solution by biosorption in a fixed bed column: experimental and theoretical breakthrough curves, *Biochemical Engineering Journal*, 2006, **30**, 184-191.

[74] R. Ning, Arsenic removal by reverse osmosis, *Desalination*, 2002, **143**, 237-241.

[75] D. Mohan and C. Pittman, Arsenic removal from water/wastewater using adsorbents-a critical review, *Journal of Hazardous Materials*, 2007, **142**, 1-53.

[76] S. Obiri, Determination of heavy metals in water from Boreholes in Dumasi in the Wassa west district of western region of Republic of Ghana, *Environmental Monitoring and Assessment*, 2007, **130**, 455-463.

[77] M. Kazemipour, M. Ansari, S. Tajrobehkar, M. Majdzadeh and H. Kermani, Removal of lead, cadmium, zinc, and copper from industrial wastewater by carbon developed from walnut, hazelnut, almond, pistachio shell, and apricot stone, *Journal of Hazardous Materials*, 2008, **150**, 322-327.

[78] I. Jarup, Hazards of heavy metal contamination, *British Medical Bulletin*, 2003, **68**, 167-182.

[79] A. Gunay, E. Arslankaya and I. Tosun, Lead removal from aqueous solution by natural and pretreated clinoptilolite: adsorption equilibrium and kinetics, *Journal of Hazardous Materials*, 2007, **2**, 362-371.

[80] A. Okoye, P. Ejikeme and O. Onukwuli, Lead removal from wastewater using fluted pumpkin seed shell activated carbon: adsorption modeling and kinetics, *International Journal of Environment Science and Technology*, 2010, **4**, 793-800.

[81] D. Mohan and K. Singh, Single- and multi-component adsorption of cadmium and zinc using activated carbon derived from bagasse-an agricultural waste, *Water Research*, 2003, **36**, 2304-2318.

[82] H. Aluri, S. Runda, V. Settaluri, J. Bondili, V. Suryanarayana and P. Venkateshwar, Biosorption: an ecofriendly alternative for heavy metal removal, *African Journal of Biotechnology*, 2007, **25**, 2924-2931.

[83] K. Tsekova, D. Todorova, V. Dencheva and S. Ganeva, Biosorption of copper(II) and cadmium(II) from aqueous solutions by free and immobilized biomass of Aspergillus niger*, Bioresource Technology*, 2010, **101**, 1727-1731.

[84] J. Uriu-Adams and C. Keen, Copper oxidative stress and human health, *Molecular Aspects of Medicine*, 2005, **26**, 268-298.

[85] Q. Zhou, J. Zhang, J. Fu, J. Shi and G. Jiang, Biomonitoring: an appealing tool for assessment of metal pollution in the aquatic ecosystem, *Analytica Chimica Acta*, 2008, **2**, 135-150.

[86] D. Connell and G. Miller, Chemistry and ecotoxicology of pollution, John Wiley and Sons, New York, 1984.

[87] W. Liu, J. Zhao, Z. Ouyang, L. Soderlund and G. Liu, Impacts of sewage irrigation on heavy metals distribution and contamination in Beijing, China, *Environment International,*2005, **31**, 805-812.

[88] R. Rattan, S. Datta, P. Chhonkar, K. Suribabu and A. Singh, Long-term impact of irrigation with sewage effluents on heavy metal content in soils, crops and groundwater-a case study, Agriculture, *Ecosystem and Environment*, 2005, **109** 310-322.

[89] S. Rothenberg, X. Du, Y. Zhu and J. Jay, The impact of sewage irrigation on the uptake of mercury in corn plants (Zea mays) from suburban Beijing, *Environmental Pollution*, 2007, **149**, 246-251.

[90] M. Muchuweti, J. Birkett, E. Chinyanga, R. Zvauya, M. Scrimshaw and J. Lester, Heavy metal content of vegetables irrigated with mixture of wastewater and sewage sludge in Zimbabwe: implications for human health, Agriculture, *Ecosystem and Environment*, 2006, **112**, 41-48.

[91] S. Khan, Q. Cao, Y. Zheng, Y. Huang and Y. Zhu, Health risks of heavy metals in contaminated soils and food crops irrigated with wastewater in Beijing, China, *Environmental Pollution*, 2008, **152**, 686-692.

[92] Y. Wei, Minimization of excess sludge production for biological wastewater treatment, *Water research* ,2003,**18**, 4453-4462.

[93] U. Wiesmann, I. Choi and E. Dombrowski, Fundamentals of biological wastewater treatment, Wiley-VCH, Berlin, 2007.

[94] Y. Kim, S. Sasaki, K. Yano, K. Ikebukuro, K. Hashimoto and I. Karube, Photocatalytic sensor for the determination of chemical oxygen demand using flow injection analysis, *Analytica Chimica Acta*, 2001, **432**, 59-66.

[95] J. Appleton and J. Tyson, The rapid determination of chemical oxygen demand in wastewaters and effluents by flow injection analysis, *Analytica Chimica Acta*, 1986, **179**, 269-278.

[96] G. Tchobanoglous, F. Burton and H. Stensel, Wastewater engineering: treatment disposal and reuse, Metcalf and Eddy Inc., New York, 1991.

[97] V. Lazarova, P. Savoye, M. Janex, E. Blatchley and M. Pommepuy, Advanced wastewater disinfection technologies: state of the art and perspectives, *Water Science and Technology*, 1999, **40**, 203-213.

[98] E. El-Ashtoukhy, N. Amin and M. Abdel-Aziz, Decolorization of acid brown and reactive blue dyes by anodic oxidation in a batch recycle electrochemical reactor, *International Journal of Electrochemical Science,* 2012, **7**, 11137-11148.

[99] A. Pala and E. Tokat, Color removal from cotton textile industry wastewater in an activated sludge system with various additives, *Water Research*, 2002, **36**, 2920-2925.

[100] S. Raghuvanshi, R. Ingh and C. Kaushik, Kinetic study of methyelene blue dye bioadsorption on baggase, *Applied Ecology and Environmental Research*, 2004, **2**, 35-43.

[101] A. Ozcan, Y.Sahin, A. Koparal and M. Oturan, Electro-fento removal of the cationic dye basic blue 3 by using carbon flet cathode, *Journal of Environmental Engineering and Landscape Management,* 2009, **5**, 267-275.

[102] I. Slavova, M. Stoyanova, S. Christoskova and V. Ivanova, Study on the catalytic activity of cobalt and iron for the oxidation of acid organic 7 in aqueous solution, *Journal of international scientific publication: Ecology and safety,* 2012, **8**, 469-478.

[103] A. Pala and E. Tokat, Color removal from cotton textile industry wastewater in an activated sludge system with various additives, *Water Resource*, 2002, **36**, 2920-2925.

[104] J. Kapdan and F. Kargi, Simultaneous biodegradation and adsorption of textile dyestuff in an activated sludge unit, *Process Biochemistry*, 2002, **37**, 973-981.

[105] M. Marquez and C. Costa, Biomass concentration in pact process, *Water Research*, 1996, **30**, 2079-2085.

[106] V. Speccia and A. Gianetto, Powdered activated carbon in an activated sludge treatment, *Water Research*, 1984, **18**, 133-137.

[107] S. Ledakowicz, M. Solecka and R. Zylla, Biodegradation, decolourisation and detoxification of textile wastewater enhanced by advanced oxidation processes, *Journal of Biotechnology*, 2001, **89**, 175-184.

[108] B. Gao, H. Hahn and E. Hoffmann, Evaluation of aluminum-silicate polymer composite as a coagulant for water treatment, *Water Research*, 2002, **36**, 3573-3581.

[109] S. Papic, N. Koprivanac, A. Bozic and A. Metes, Removal of some reactive dyes from synthetic wastewater by combined Al(III) coagulation/carbon adsorption process, *Dyes and Pigments*, 2004, **62**, 291-298.

[110] S. Lin and C. Peng, Treatment of textile wastewater by electrochemical method, *Water Research*, 1994, **28**, 277-282.

[111] S. Lin and M. Chen, Treatment of textile wastewater by chemical methods for reuse, *Water Research*, 1997, **31**, 868-876.

[112] B. Langlais, D. Reckhow and D. Brink, Ozone in water treatment, application and engineering, Lewis Publishers, London, New York, Washington DC, 1991.

[113] C. Adams, W. Fusco and T. Kanzelmeyer, Ozone, hydrogen peroxide/ozone and UV/ozone treatment of chromium and copper complex dyes: decolorization and metal release, *Ozone Science and Engineering*,1995, **17**, 149-161.

[114] J. Scott and D. Ollis, Integrated chemical and biological oxidation processes for water treatment, review and recommendations, *Environmental Progress*, 1995, **14**, 88-103.

[115] I. Machenbach, Membrane technology for dyehouse effluent treatment, *Membrane Technology*, 1998, **98**, 7-10.

[116] K. Treffry-Goatley, C. Buckley and G. Groves, Reverse osmosis treatment and reuse of textile dye house effluents, *Desalination*, 1983, **47**,313-320.

[117] L. Tinghui, T. Matsuura and S. Sourirajan, Effect of membrane materials and average pore sizes on reverse osmosis separation of dyes, *Industrial and Engineering Chemistry*, 1983, **22**, 77-85.

[118] J. Radjenovic, M. Petrovic, F. Ventura and D. Barcelo, Rejection of pharmaceuticals in nanofiltration and reverse osmosis membrane drinking water treatment, *water research*, 2008, **42**, 3601-3610.

[119] A. Erswell, C. Brouchaert and C. Buckley, The reuse of reactive dye liquors using charged ultrafiltration membrane technology, *Desalination*, 1998, **70**, 157-167.

[120] Y. Xu, R. Lebrun, P. Gallo and P. Blond, Treatment of textile dye plant effluent by nanofiltration membrane, *Separation and Science Technology*, 1999, **34**, 2501-2519.

[121] A. Akbari, J. Remigy and P. Aptel, Treatment of textile dye effluent using a polyamide-based nanofiltration membrane, *Chemical Engineering Process*, 2002, **41**, 601-609.

[122] V. Freger, T. Arnot and J. Howell, Separation of concentrated organic/inorganic salt mixtures by nanofiltration, *Journal of Membrane Science*, 2000, **178**, 185-193.

[123] J. Kelly and P. Kelly, Nanofiltration of whey: quality, environmental and economic aspects, *Journal Society Dairy Technology*, 1995, **48**, 20-25.

[124] J. Watters, E. Biagtan and O. Senler, Ultrafiltration of a textile plant effluent, *Separation Science Technology*, 1991, **26**, 1295-1313.

[125] G. Ciardelli and N. Ranieri, The treatment and reuse of wastewater in the textile industry by means of ozonation and electroflocculation, *Water Research*, 2001, **35**, 567-572.

[126] M. Mignani, G. Nosenzo and A. Gualdi, Innovative ultrafiltration for wastewater reuse, *Desalination*, 1999, **124**, 287-292.

[127] M. Al-Malack and G. Anderson, Use of cross flow microfiltration in wastewater treatment, *Water Research*, 1997, **31**, 3064-3072.

[128] K. Choy, G. McKay and J. Porter, Sorption of acid dyes, from effluents using activated carbon, *Resources, Conservation and Recycling*, 1999, **27**, 57-71.

[129] Y. Slokar and A. Le Marechal, Methods of decoloration of textile wastewaters, *Dyes and Pigments*, 1997, **37**, 335-356.

[130] M. Kumar, T. Sridhari, K. Bhavani and P. Dutta, Trends in color removal from textile mill effluents, *Colorage*, 1998, **40**, 25-34.

[131] C. Raghavacharya, Colour removal from industrial eluents- a comparative review of available technologies, *Chemical Engineering World*, 1997, **32**, 53-54.

[132] K. Rao, K. Krishnaiah and K. Ashutush, Colour removal from a dye stuff industry effluent using activated carbon, *Indian Journal of Chemical Technology*, 1994, **1**, 13-19.

[133] F. Carrasco-Marin, M. Alvarez-Merino and C. Moreno-Castilla, Microporous activated carbons from a bituminous coal, *Fuel*, 1996, **75**, 966-970.

[134] V. Budarin, J. Clark, F. Deswarte, J. Hardy, A. Hunt and F. Kerton, Delicious not siliceous: expanded carbohydrates as renewable separation media for column chromatography, *Chemical Communications*, 2005, **23**, 2903-2905.

[135] M. Sala, V. Lopez-Grimau and C. Gutirrrez-Bouzan, Photo-electrochemical treatment of reactive dyes in wastewater and reuse of the effluent: method optimization, Materials, 2014, 7, 7349-7365.

[136] G. Oliveira, E. Ferraz, F. Chequer, M. Grando, J. Angeli, M. Tsuboy, J. Marcarini, M. Mantovani, M. Osugi, T. Lizier, M. Zanoni and D. Oliveira, Chlorination treatment of aqueous samples reduces, but does not eliminate, the mutagenic effect of the azo dyes disperse red 1, disperse red 13 and disperse orange 1, *Mutation Research/Genetic Toxicology and Environmental Mutagenesis*, 2010, **703**, 200-208.

[137] P. Carneiro, G. Umbuzeiro, D. Oliveira and M. Zanoni, Assessment of water contamination caused by a mutagenic textile effluent/dyehouse effluent bearing disperse dyes, *Journal of Hazardous Materials*, 2010, **174**, 694-699.

[138] H. Zollinger, Color chemistry-synthesis, properties and applications of organic dyes and pigments, Second edition, V.C.H Publishers, New York, 1991.

[139] M. Sala, A. Del Rio, J. Molina, F. Cases and M. Gutierrez-Bouzan, Influence of cell design and electrode materials on the decolouration of dyeing effluents, *International Journal of Electrochemical Science*, 2012, **7**, 12470-12488.

[140] DyStar®, Safety data sheet, Confidential, in accordance with regulation (EC) No. 1907/2006, Version 1.0/D/EN generated on 05/11/2012.

[141] V. Gupta, S. Khamparia, I. Tyagi, D. Jaspal, A. Malviya, Decolorization of mixture of dyes: a critical review, *Global Journal of Environmental Science and Management*, 2015, **1**, 71-94.

[142] Y. Ku and I. Jung, Photocatalytic reduction of Cr(VI) in aqueous solutions by UV irradiation with the presence of titanium dioxide, *Water Research*, 2001, **35**, 135-142.

[143] J. Huisman, G. Schouten and C. Schultz, Biologically produced sulphide for purification of process streams, effluent treatment and recovery of metals in the metal and mining industry, *Hydrometallurgy*, 2006, **83**, 106-113.

[144] K. Baltpurvins, R. Burns, G. Lawrance and A. Stuart, Effect of electrolyte composition on zinc hydroxide precipitation by lime, *Water Research*, 1997, **31**, 973-980.

[145] N. Kongsricharoern and C. Polprasert, Electrochemical precipitation of chromium (Cr^{6+}) from an electroplating wastewater, *Water Science Technology*, 1995, **31**, 109-117.

[146] A. Ozverdi and M. Erdem, Cu^{2+}, Cd^{2+} and Pb^{2+} adsorption from aqueous solutions by pyrite and synthetic iron sulphide, *Journal of Hazardous Materials*, 2006, **137**, 626-632.

[147] S. Islamoglu, L. Yilmaz and H. Ozbelge, Development of a precipitation based separation scheme for selective removal and recovery of heavy metals from cadmium rich electroplating industry effluents, Separation Science and Technology, 2006, **41**, 3367-3385.

[148] M. Gonzalez-Munoz, M. Rodriguez, S. Luquea and J. Alvareza, Recovery of heavy metals from metal industry waste waters by chemical precipitation and nanofiltration, *Desalination*, 2006, **200**, 742-744.

[149] S. Kang, J. Lee, S. Moon and K. Kim, Competitive adsorption characteristics of Co^{2+}, Ni^{2+}, and Cr^{3+} by IRN-77 cation exchange resin in synthesized wastewater, *Chemosphere*, 2004, **56**, 141-147.

[150] B. Alyuz and S. Veli, Kinetics and equilibrium studies for the removal of nickel and zinc from aqueous solutions by ion exchange resins, *Journal of Hazardous Materials*, 2009, **167**, 482-488.

[151] I. Gaballah and G. Kilbertus, Recovery of heavy metal ions through decontamination of synthetic solutions and industrial effluents using modified barks, *Journal of Geochemical Exploration*, 1998, **62**, 241-286.

[152] T. Kurniawan, G. Chan, W. Lo and S. Babel, Physico-chemical treatment techniques for wastewater laden with heavy metals, *Chemical Engineering Journal*, 2006, **118**, 83-98.

[153] J. Landaburu-Aguirre, V. Garcia, E. Pongracz and R. Keiski, The removal of zinc from synthetic wastewaters by micellar-enhanced ultrafiltration: statistical design of experiments, *Desalination*, 2009, **240**, 262-269.

[154] A. Shahalam, A. Al-Harthy and A. Al-Zawhry, Feed water pretreatment in RO systems in the Middle East, *Desalination*, 2002, **150**, 235-245.

[155] M. Muthukrishnan and B. Guha, Effect of pH on rejection of hexavalent chromium by nanofiltration, *Desalination*, 2008, **219**, 171-178.

[156] L. Cifuentes, I. Garcia, P. Arriagada and J. Casas, The use of electrodialysis for metal separation and water recovery from $CuSO_4$-H_2SO_4-Fe solutions, *Separation and Purification Technology*, 2009, **68**, 105-108.

[157] A. El-Samrani, B. Lartiges and F. Villieras, Chemical coagulation of combined sewer overflow: heavy metal removal and treatment optimization, *Water Research*, 2008, **42**, 951-960.

[158] Q. Chang and G. Wang, Study on the macromolecular coagulant PEX which traps heavy metals, *Chemical Engineering Science*, 2007, **62**, 4636-4643.

[159] Q. Chang, M. Zhang and J. Wang, Removal of Cu^{2+} and turbidity from wastewater by mercaptoacetyl chitosan, *Journal of Hazardous Materials*, 2009, **169**, 621-625.

[160] J. Duan, Q. Lu, R. Chen, Y. Duan, L. Wang, L. Gao and S. Pan, Synthesis of a novel flocculant on the basis of crosslinked Konjac glucomannan-graft polyacrylamide-co-sodium xanthate and its application in removal of Cu^{2+} ion, *Carbohydrate Polymers*, 2010, **80**, 436-441.

[161] S. Bratskaya, A. Pestov, Y. Yatluk and V. Avramenko, Heavy metals removal by flocculation/precipitation using N-(2-carboxyethyl)chitosans, *Colloids and Surfaces*, 2009, **339**, 140-144.

[162] L. Wang, Y. Hung and N. Shammas, Advanced physicochemical treatment, Springer, New Jersey, 2007.

[163] I. Heidmann and W. Calmano, Removal of Zn(II), Cu(II), Ni(II), Ag(I) and Cr(VI) present in aqueous solutions by aluminium electrocoagulation, *Journal of Hazardous Materials*, 2008, **152**, 934-941.

[164] A. Jusoh, L. Shiung, N. Ali and M. Noor, A simulation study of the removal efficiency of granular activated carbon on cadmium and lead, *Desalination*, 2007, **206**, 9-16.

[165] P. Chingombe, B. Saha and R. Wakeman, Surface modification and characterisation of a coal-based activated carbon, *Carbon*, 2005, **43**, 3132-3143.

[166] S. Iijima, Helical microtubules of graphitic carbon, *Nature*, 1991, **354**, 56-58.

[167] N. Kabbashi, M. Atieh, A. Al-Mamun, M. Mirghami, M. Alam and N. Yahya, Kinetic adsorption of application of carbon nanotubes for Pb(II) removal from aqueous solution, *Journal of Environmental Science*, 2009, **21**, 539-544.

[168] Y. Li, F. Liu, B. Xia, Q. Du, P. Zhang, D. Wang, Z. Wang and Y. Xia, Removal of copper from aqueous solution by carbon nanotube/calcium alginate composites, *Journal of Hazardous Materials*, 2010, **177**, 876-880.

[169] M. Acheampong, R. Meulepas and P. Lens, Removal of heavy metals and cyanide from gold mine wastewater, *Journal of Chemical Technology and Biotechnology*, 2010, **85**, 590-613.

[170] I. Gaballah and G. Kilbertus, Recovery of heavy metal ions through decontamination of synthetic solutions and industrial effluents using modified barks, *Journal of Geochemical Exploration*, 1998, **62**, 241-286.

[171] J. Rouquerol, F. Rouquerol and K. Sing, Adsorption by powders and porous solids: principles, methodology and applications, Academic press, San Diego, 1999.

[172] T. Hill, Relations between different definitions of physical adsorption, *The Journal of Physical Chemistry*, 1959, **4**, 456-460.

[173] N. Srivastava, A review of adsorbents and adsorbates in solid-vapour adsorption heat pump systems, *Applied thermal engineering*, 1998, **9**, 707-714.

[174] M. Al-Anber, Thermodynamics approach in the adsorption of heavy metals, InTech, Jordan, 2011.

[175] S. Greg and K. Sing, Adsorption, surface area and porosity, Academic press, London, New York, Paris, Tokio, 1982.

[176] I. Berend, J. Cases, M. Francois, L. Michot, A. Mason and F. Thomas, Mechanism of adsorption and desorption of water vapor by homonic montmorillonites: 2. the Li^+, Na^+, K^+, Rb^+ and Cs^+-exchange form, *Clays and Clay Minerals*,1995, **3**, 324-336.

[177] R. Wang and Q. Wang, Adsorption mechanism and improvements of the adsorption equation for adsorption refrigeration pairs, *International journal of energy research*, 1999, **10**, 887-898.

[178] A. Adamson and A. Gast, Physical chemistry of surfaces, Six edition, Wiley-Interscience, New York, 1997.

[179] A. Fahmi and C. Minot, A theoretical investigation of water adsorption on titanium dioxide surfaces, *Surface science*, 1994,**3**, 343-359.

[180] R. Tseng, Physical and chemical properties and adsorption type of activated carbon prepared from plum kernels by NaOH activation, *Journal of hazardous materials*, 2007, **3**, 1020-1027.

[181] J. Lennard, process of adsorption and diffusion on solid surface, *Transactions of the Faraday Society*, 1932, **28**, 333-359.

[182] P. Webb, Introduction to chemical adsorption analytical techniques and their applications to catalysis, *Micromeritics Instrument Corporation (MIC) Technical Publications*, 2003, **1**, 1-12.

[183] H. Erbil, Surface chemistry of solid and liquid interfaces, Blackwell Publishing, Oxford, Malden, Victoria, 2006.

[184] I. Langmuir, Chemical reactions at low pressures, *Journal of the American Chemical Society*, 1915, **37**, 1139-1167.

[185] H. Freundlich, Over the adsorption in-solutions: uber die adsorption in losungen, *Physical Chemistry*, 1906, **57**, 385-470.

[186] S. Brunauer, P. Emmett and E. Teller, Adsorption of gases in multi molecular layers, *Journal of the American Chemical Society*, 1938, **60**, 309-319.

[187] K. Birdi, Handbook of surface and colloid chemistry, Third edition, CRC press, London, New York, 2009.

[188] B. Zdravkov, J. Cermak, M. Sefara and J. Janku, Pore classification in the characterization of porous materials: a perspective, *Central European Journal of Chemistry*, 2007, **2**, 385-395.

[189] J. Choi, D. Do and H. Do, Surface diffusion of adsorbed molecules in porous media: Monolayer, multilayer, and capillary condensation regimes, *Industrial and Engineering Chemistry Research*, 2001, **19**, 2001.

[190] T. Allen, Particle size measurement, Fifth edition, Chaman and Hall, London, Weinheim, New York, Tokyo, Melbourne, Madras, 1997.

[191] K. Sing, D. Everett, R. Haul, L. Moscou, R. pierotti, J. Rouquerol and T. Siemieniewska, Reporting physisorption data for gas/solid systems with special reference to the determination of surface area and porosity, *Pure and Applied Chemistry*, 1985, **4**, 603-619.

[192] R. White, V. Budarin, R. Luque, J. Clark and D. Macquarrie, Tuneable porous carbonaceous materials from renewable resources, *Chemical Society Reviews*, 2009, **38**, 3401-3418.

[193] F. Rodriguez-Reinoso, The role of carbon materials in heterogeneous calatysis, *Science Direct*, 1998, **3**, 159-175.

[194] M. Ersoz and L. Barrott, Best practice guide on metals removal from drinking water by treatment, adsorption process, First edition, International Water Association Publishing, London, 2012.

[195] G. McKay, Types of adsorbent materials, use of adsorbents for the removal of pollutants from wastewaters, CRC Press, Boca Raton, Florida, 1996.

[196] S. Nomanbhay and K. Palanisamy, Removal of heavy metal from industrial wastewater using chitosan coated oil palm shell charcoal, *Electronic Journal of Biotechnology*, 2005, **1**,1635-1642.

[197] H. Genc, J. Tjell, D. Mcconchie and O. Schuiling, Adsorption of arsenate from water using neutralized red mud, *Journal of Colloid and interface Science*, 2003, **264**, 327-334.

[198] USGS, Bauxite and alumina, US Geological Survey Mineral Commodity Summaries, 1996.

[199] USGS, Bauxite and alumina, US Geological Survey Mineral Commodity Summaries, 2012.

[200] M. Rafatullah, O. Sulaiman, R. Hashim and A. Ahmad, Adsorption of methylene blue on low-cost adsorbents: a review, *Journal of Hazardous Materials*, 2010, **177**, 70-80.

[201] G. Grini, Non-conventional low-cost adsorbents for dye removal: a review, *Bioresource Technology*, 2006, **97**,1061-1085.

[202] F. Carrasco-Martin, M. Alvarez-Merino and C. Moreno-Castilla, Microporous activated carbons from a bituminous coal, *Fuel*, 1996, **75**, 966-970.

[203] S. Babel and T. Kurniawan, Low-cost adsorbents for heavy metals uptake from contaminated water: a review, *Journal of Hazardous Materials*, 2003, **B97**, 219-243.

[204] Y. Sun, J. Zhang , G. Yang and Z. Li, Removal of pollutants with activated carbon produced from K_2CO_3 activation of lignin from reed black liquors, *Chemical and Biochemical Engineering Quarterly*, 2006, **4**, 429-435.

[205] F. Rodrıiguez-Reinoso, M. Molina-Sabio and J. Gonzalez, Preparation of activated carbon-sepiolite pellets, *Carbon*, 2001, **39**, 776-779.

[206] B. Tryba, A. Morawski and M. Inagaki, Application of activated carbon, *Applied Catalysis, B: Environmental*, 2003, **4**, 427-433.

[207] J. Hayashi, A. Kazehaya, K. Muroyama and A. Watkinson, Preparation of activated *carbon* from lignin by chemical activation, *Carbon*, 2000, **13**, 1873-1878.

[208] J. Garrido, A. Linares-Solano, J. Martin-Martinez, M. Molina-Sabio, F. Rodriguez-Reinoso and R. Torregrosa, Electron microscopy of carbon structure, *Journal of Chemical Society, Faraday Transactions*, 1987, **3**, 1081-1088.

[209] S. Kanawade and R. Gaikwad, Removal of methylene blue from effluent by using activated carbon and water hyacinth as adsorbent, *International Journal of Chemical Engineering and Applications*, 2011, **5**, 317-319.

[210] M. Davis, Ordered porous materials for emerging applications, *Nature*, 2002, **417**, 813-821.

[211] U. Ciesla and F. Shuth, Ordered mesoporous materials, *microporous and mesoporous materials*, 1999, **27**, 131-149.

[212] C. Liang, Z. Li and S. Dai, Mesoporous carbon materials: synthesis and modification, *Angewandte Chemie International Edition,*2008, **47**, 3696-3717.

[213] C. Kresge, M. Leonowicz, W. Roth, J. Vartuli and J. Beck, Ordered mesoporous molecular sieves synthesized by a liquid-crystal template mechanism, *Nature*, 1992, **359**, 710-712.

[214] R. Ryoo, S. Joo and S. Jun, Synthesis of highly ordered carbon molecular sieves via template-mediated structural transformation, *Journal of Physical Chemistry B*, 1999, **103**, 7743-7746.

[215] S. Joo, J. Ghoi, I. Oh, J. Kwak, Z. Liu, O. Terasaki and R. Ryoo, Ordered nanoporous arrays of carbon supporting high dispersions of platinum nanoparticles, *Nature*, 2001, **412**, 169-172.

[216] M. Kruk, M. Jaroniec, T. Kim and R. Ryoo, Synthesis and characterization of hexagonally ordered carbon nanopipes, C*hemistry of Materials*, 2003, **15**, 2815-2823.

[217] S. Jun, S. Joo, R. Ryoo, M. Mruk, M. Jaroniec, Z. Liu, T. Ohsuna and O. Terasaki, Synthesis of new, nanoporous carbon with hexagonally ordered mesostructure, *Journal of the American Chemical Society*, 2000, **122**, 10712-10713.

[218] N. Atkin, R. Abeysekera, S. Cheng and A. Robards, An experimentally-based predictive model for the separation of amylopectin subunits during starch gelatinization, *Carbohydrate Polymers*, 1998, **36**, 173-192.

[219] R. Luque, D. Macquarrie, V. Budarin, J. Clark, K. Milkowski and R. White, Carbonaceous materials, US 2009/0078913 A1.

[220] R. White, C. Antonio, V. Budarin, E. Bergstrom, J. Thomas-Oates and J. Clark, Polysaccharide-derived carbons for polar Analyte separations, *Advanced Functional Materials*, 2010, **20**, 1834-1841.

[221] N. Atkin, R. Abeysekera and A. Robards, The events leading to the formation of ghost remnants from the starch granule surface and the contribution of the granule surface to the gelatinization endo therm, *Carbohydrate Polymers*, 1998, **36**, 193-204.

[222] R. White, Porous polysaccharide-derived materials, PhD thesis, University of York, 2008.

[223] M-M. Titirici, R. White, N. Brun, V. Budarin, D. Su, F. del Monte, J.. Clark, and M. MacLachlan, Sustainable carbon materials, *Chemical Society Reviews*, 2015, **44**, 250-290.

[224] A. Haug, 1968, United State patent 3, 396, 158.

[225] R. Ellis and M. Cochrane, Starch production and industrial use, *Journal of the Science of Food and Agriculture,* 1998, **77**, 289-311.

[226] R. Tester, J. Karkalas and X. Oi, Starch structure and digestibility enzyme-substrate relationship, *World's poultry science journal* ,2004, **2**, 186-195.

[227] R. Dodson, V. Budarin, A. Hunt, P. Shuttleworthab and J. Clark, Shaped mesoporous materials from fresh macroalgae, *Journal of Materials Chemistry A*, 2013, **1**, 5203-5207.

[228] J. Clark, D. Macquarrie and K. Milkowski, New materials based on renewable resources: chemically modified expanded corn starches as catalysts for liquid phase organic reactions*, Chemical Communications*, 2002, **1**, 2632-2633.

[229] R. White, V. Budarin and J. Clark, Tuneable mesoporous materials from α-D-Polysaccharides*, ChemSusChem*, 2008, **1**, 408-411.

[230] A. Hunt, A. Matharu and J. Clark, Education in chemistry, Waste or resource? Giving LCDs a new lease of life, *Royal Society of Chemistry*, 2010, **6**, 175-179.

[231] A. Lua and T. Yang, Effect of activation temperature on the textural and chemical properties of potassium hydroxide activated carbon prepared from pistachio-nut shell, *Journal of Colloid and Interface Science,* 2004, **274**, 594-601.

[232] V. Budarin, J. Clark, R. Luque, K. Milkowski, S. Tavener and A. Wilson, Starbons: new starch-derived mesoporous carbonaceous materials with tunable properties, *Angewandte Chemie International Edition*, 2006, **45**, 3782-3786.

[233] H. Parker, A. Hunt, V. Budarin, P. Shuttleworth, K. Millerb and J. Clark, The importance of being porous: polysaccharide-derived mesoporous materials for use in dye adsorption, *Royal Society of Chemistry Advances*, 2012, **2**, 8992-8997.

[234] A. Haug, B. Larsen and O. Smidsrod, A study of the constitution of alginic acid by partial acid hydrolysis, *Acta Chemica Scandinavica*, 1966, **20**, 183-190.

[235] D. Kaplan, Biopolymers from renewable resources, Springer-Verlag Publishing, Heidelberg, 1998.

[236] E. Atkins, I. Nieduszynski, W. Mackie, K. Parker and E. Smolko, Structural components of alginic acid, *biopolymers*, 1973, **12**, 1879-1887.

[237] A. Bhattacharjee, Hydrogel as novel drug delivery system: an insight to their types, properties and formulation approaches, *International Journal of Innovative Pharmaceutical Sciences and Research*, **2**, 2014, 1244-1259.

[238] A. Marriott, E. Bergstrom, A. Hunt, J. Thomas-Oates and J. Clark, A natural template approach to mesoporous carbon spheres for use as green

chromatographic, stationary phases, *Royal Society of Chemistry Advances*, 2014, **4**, 222-228.

[239] R. Einde, A. Goot and R. Boom, Understanding molecular weight reduction of starch during heating-shearing processes, *Journal of Food and Science*, 2003, **68**, 2396-2404.

[240] H. Jie and C. Wei, Optimization of extraction process of crude polysaccharides from wild edible BaChu mushroom by response surface methodology, *Carbohydrate Polymers*, 2008, **72**, 67-74.

[241] P. Shuttleworth, V. Budarin and J. Clark, Green power-"molten" starch adhesives, *Journal of Materials Chemistry*, 2009, **19**, 8589-8593.

[242] C. Garcia-Gonzalez, M. Jin, J. Gerth, C. Alvarez-Lorenzo and I. Smirnova, Polysaccharide-based aerogel microspheres for oral drug delivery, *Carbohydrate Polymers*, 2015, **117**, 797-806.

[243] R. Lloyd, J. Provis, K. Smeaton and J. van Deventer, Spatial distribution of pores in fly ash-based inorganic polymer gels visualised by Wood's metal intrusion, *Microporous and Mesoporous Materials*, 2009, **126**, 32-39.

[244] M. Juenger and H. Jennings, The use of nitrogen adsorption to assess the microstructure of cement paste, *Cement Concrete Research*, 2001, **31**, 883-892.

[245] P. Sepulveda, F. Ortega, M. Innocentini and V. Pandolfelli, Properties of highly porous hydroxyapatite obtained by the gelcasting of foams, *Journal of the American Ceramic Society*, 2000, **83**, 3021-3024.

[246] M. Yoshimura, T. Takaya and K. Nishinari, Effects of xyloglucan on the gelatinization and retrogradation of corn starch as studied by rheology and differential scanning calorimetry*, Food Hydrocolloids*, 1999, **13**, 101-111.

[247] M. Miles, V. Morris, P. Orford and S. Ring, The roles of amylose and amylopectin in the gelation and retrogradation of starch, *Carbohydrate Research*, 1985,**135**, 271-280.

[248] J. Clark, V. Budarin, T. Dugmore, R. Luque, D. Macquarrie and V. Strelko, Catalytic performance of carbonaceous materials in the esterification of succinic acid, *Catalysis Communications*, 2008, **9**, 1709-1714.

[249] Surface tension values of some common test liquids for surface energy analysis, http://www.surface-tension.de, accessed on 3/01/2015.

[250] Boiling points of some common fluids and gases, www.engineeringtoolbox .com/boiling-points-fluids-gases-d_155.html, accessed on 3/01/2015.

[251] Y. Hu, R. Liu, Y. Zhang and G. Li, Improvement of extraction capability of magnetic molecularly imprinted polymer beads in aqueous media via dual-phase solvent system, *Talanta*, 2009, **79**, 576-582.

[252] S. Choi, T. Kwon, S. Chung and TH. Kim, Surgical smoke may be a biohazard to surgeons performing laparoscopic surgery, *Surgical Endoscopy*, 2014, **28**, 2374-2380.

[253] P. Spencer and H. Schumburg, Neurotoxic properties of certain aliphatic hexacarbons, *Proceedings of the Royal Society of Medicine*, 1977, **70**, 37-38.

[254] H. Schumburg and P. Spencer, Neurobehavioral methods and effects in occupational and environmental health, *Brain*, 1976, **99**, 183-192.

[255] K. Taguchi, E. Fukusaki and T. Bamba, Determination of Niacin and its metabolites using supercritical fluid chromatography coupled to tandem mass spectrometry, *Mass Spectrom (Tokyo)*, 2014, **3**, 1-3.

[256] E. Sin, R. Marriott, A. Hunt and J. Clark, Identification, quantification and Chrastil modelling of wheat straw wax extraction using supercritical carbon dioxide, *Comptes Rendus Chimie*, 2014, **17**, 293-300.

[257] G. Vhquez, E. Alvarez and J. Navaza, Surface tension of alcohol + water from 20 to 50 ^{o}C, *Journal of Chemical and Engineering Data*, 1995, **40**, 611-614.

[258] F. Rouquerol, J. Rouquerol, K. Sing, P. Llewellyn and G. Maurin, Adsorption by powders and porous solids: principles, methodology and applications, Second edition, Academic press, Oxford, Amsterdam, Waltham, 2014.

[259] P. Shuttleworth, V. Budarin, S. Breeden, D. Macquarrie, R. Luque, R. White and J. Clark, STARBONS[®]: preparation, applications and transition from laboratory curiosity to scalable product, Nanotechnology 2011: bio sensors, instruments, medical, environment and energy, 2011, **3**, 766 -769.

[260] A. Marriott, A. Hunt, E. Bergstrom, K. Wilson, V. Budarin, J. Thomas-Oates, J. Clark and R. Brydson, Investigating the structure of biomass-derived non-graphitizing mesoporous carbons by electron energy loss spectroscopy in the transmission electron microscope and X-ray photoelectron spectroscopy, *Carbon*, 2014, **67**, 514-524.

[261] E. Atkins, I. Nieduszynski and H. Wills, Structural components of alginic acid. The crystalline structure of poly-α-L-guluronic acid. Results of X-Ray diffraction and polarized infrared studies, *Biopolymer*, 1973, **12**, 1879-1887.

[262] K. Draget, G. Braek and O. Smidsrod, Alginic acid gels: the effect of alginate chemical composition and molecular weight, *Carbohydrate Polymers*, 1994, **25**, 31-38.

[263] H. Chen, D. Musaev and M. Lin, Adsorption and dissociation of CO_x (x= 1, 2) on W(111) surface : a computational study, *The Journal of Physical Chemistry C*, 2008, **12**, 3341-3348.

[264] Infrared spectroscopy absorption table, www.ochemonline.com/Infrared_spectroscopy_absorption_table, accessed on 4/01/2015.

[265] B. Zelent, N. Nucci and J. Vanderkooi, Liquid and ice water and glycerol/water glasses compared by infrared spectroscopy from 295 to 12 K, The *Journal of Physical Chemistry A*, 2004, **108**, 11141-11150.

[266] R. Hielscher and P. Hellwig, The temperature-dependent hydrogen-bonding signature of lipids monitored in the far-infrared domain, *ChemPhysChem*, 2010, **11**, 435-441.

[267] N. Nikonenko, D. Buslov, N. Sushko and R. Zhbankov, Investigation of stretching vibrations of glycosidic linkages in disaccharides and polysaccharides with use of IR spectra deconvolution, *Biopolymers*, 2000, **57**, 257-262.

[268] J. Max and C. Chapados, Infrared spectroscopy of aqueous carboxylic acids: comparison between different acids and their salts, *The Journal of Physical Chemistry A*, 2004, **108**, 3324-3337.

[269] R. Brudler, R. Rammelsberg, T. Woo, E. Getzoff and K. Gerwert, Structure of the I_1 early intermediate of photoactive yellow protein by FTIR spectroscopy, *Nature Structural Biology*, 2001, **8**, 265-270.

[270] J. Pastor-Villegas, C. Valenzuela-Calahorro, A. Bernalte-Garcia and V. Gomez-Serrano, Characterisation study of char and activated carbon prepared from raw and extracted rockrose, *Carbon*, 1993, **7**, 1061-1069.

[271] A. Lua and T. Yang, Effect of activation temperature on the textural and chemical properties of potassium hydroxide activated carbon prepared from pistachio-nut shell, *Journal of Colloid and Interface Science,* 2004, **274**, 594-601.

[272] J. Blanchard, C. Brewer, S. Englard and G. Avigad, Solution structure of 5-Keto-D-fructose relevance to the specificity of hexose kinases, *Biochemistry*, 1982, **21**, 75-81.

[273] D. Savova, E. Apak, E. Ekinci, F. Yardim, N. Petrov, T. Budinova, M. Razvigorova and V. Minkova, Biomass conversion to carbon adsorbents and gas, *Biomass and Bioenergy*, 2001, **21**, 133-142.

[274] D. Hoebbel, T. Reinter and H. Schmidt, On the hydrolytic stability of organic ligands in Al-, Ti- and Zr-Alkoxide complexes, *Journal of Sol-Gel Science and Technology*, 1997, **10**, 115-126.

[275] R. Duarte, A. Silva and A. Duarte, Two-dimensional NMR studies of water-soluble organic matter in atmospheric aerosols, *Environmental Science Technology*, 2008, **42**, 8224-8230.

[276] M. Nazeeruddin*,* S. Zakeeruddin, J. Lagref, P. Liska, P. Comte, C. Barolo, G. Viscardi, K. Schenk and M. Graetzel, Stepwise assembly of amphiphilic ruthenium sensitizers and their applications in dye-sensitized solar cell, *Coordination Chemistry Reviews*, 2004, **248**, 1317-1328.

[277] I. Duarte, A. Barros, P. Belton, R. Righelato, M. Spraul, E. Humper and A. Gil, High-resolution nuclear magnetic resonance spectroscopy and multivariate analysis for the characterization of beer, *Journal of Agricultural and Food Chemistry*, 2002, **50**, 2475-2481.

[278] I. Wawer, M. Wolniak and K. Paradowska, Solid state NMR study of dietary fiber powders from aronia, bilberry, black currant and apple, *Solid State Nuclear Magnetic Resonance*, 2006, **30**, 106-113.

[279] F. Rodriguez-Reinoso, The role of carbon materials in heterogeneous catalysis, *Carbon*, 1998, **36**, 159-175.

[280] C. Moreno-Castilla, Adsorption of organic molecules from aqueous solutions on carbon materials, *Carbon*, 2004, **42**, 83-94.

[281] P. Shuttleworth, V. Budarin, R. White, V. Gunko, R. Luque and J. Clark, Molecular-level understanding of the carbonisation of polysaccharides, *Chemistry - A European Journal*, 2013, **28**, 9351-9357.

[282] M. Sala, V. Lopez-Grimau and C. Gutirrrez-Bouzan, Photo-electrochemical treatment of reactive dyes in wastewater and reuse of the effluent: method optimization, *Materials*, 2014, **7**, 7349-7365.

[283] M. Sala and M. Gutierrez-Bouzan, Electrochemical treatment of industrial wastewater and effluent reuse at laboratory and semi-industrial scale, *Journal of Cleaner Production*, 2014, **65**, 458-464.

[284] H. Lee and S. Pavlostathis, Decolorization and toxicity of reactive anthraquinone textile dyes under methanogenic conditions, *Water Research*, 2004, **38**, 1838-1852.

[285] E. Grima, F. Carnacho, J. Perez, J. Sevilla, F. Fernandez and A. Gomez, A mathematical model of microalgal growth in light-limited chemostat culture, *Journal of Chemical Technology and Biotechnology*, 1994, **61**, 167-173.

[286] H. Schulten, The three-dimensional structure of humic substances and soil organic matter studied by computational analytical chemistry, *Fresenius Journal of Analytical Chemistry*, 1995, **351**, 62-73.

[287] H. Schulten and P. Leinweber, New insights into organic-mineral particles: composition, properties and models of molecular structure, *Biology and Fertility of Soils*, 2000, **30**, 399-432.

[288] B. Puri and P.L. Walker, Surface complexes on carbons, chemistry and physics of carbon**,** Marcel Dekker Publisher, New York, 1970.

[289] M. Dubinin, E. Zaverina and V. Serpinsky, The sorption of water vapor by active carbon, *Journal of the American Chemical Society*, 1955, **77**, 1760-1766.

[290] S. Barton, M. Evans, J. Holland and J. Koresh, Water and cyclohexane vapour adsorption on oxidized porous carbon, *Carbon*, 1984, **3**, 265-272.

[291] E. Muller, L. Rull, L. Vega and K. Gubbins, Adsorption of water on activated carbons: a molecular simulation study, *The journal of physical chemistry*, 1996, **100**, 1189-1196.

[292] E. Muller and K. Gubbins, Molecular simulation study of hydrophilic and hydrophobic behavior of activated carbon surfaces, *Carbon*, 1998, **36**, 10, 1433-1438.

[293] C. McCallum, T. Bandosz, S. McGrother, E. Muller and K. Gubbins, A molecular model for adsorption of water on activated carbon: comparison of simulation and experiment, *Langmuir*, 1999, **15**, 533-544.

[294] Y. Kaneko, M. Abe and K. Ogino, Adsorption characteristics of organic compounds dissolved in water on surface-improved activated carbon fibers, *Colloids and Surfaces*, 1989, **37**, 211-222.

[295] P. Pendleton, S. Wong, R. Schumann, G. Levay, R. Denoyel and J. Rouquerol, Properties of activated carbon controlling 2-methylisoborneol adsorption, *Carbon*, 1997, **35**, 1141-1149.

[296] M. Franz, H. Arafat and N. Pinto, Effect of chemical surface heterogeneity on the adsorption mechanism of dissolved aromatics on activated carbon, *Carbon*, 2000, **38**, 1807-1819.

[297] R. Considine, R. Denoyel, P. Pendleton, R. Schumann and S. Wong, The influence of surface chemistry on activated carbon adsorption of 2-methylisoborneol from aqueous solution, *Colloids and Surfaces A,* 2001, **179**, 271-280.

[298] R. Coughlin and F. Ezra, Role of surface acidity in the adsorption of organic pollutants on the surface of carbon, *Environmental Science and Technology*, 1968, **2**, 291-297.

[299] E. Muller, F. Hung and K. Gubbins, Adsorption of water vapor-methane mixtures on activated carbons, *Langmuir*, 2000, **16**, 5418-5424.

[300] O. Mahajan, C. Moreno-Castilla and P. Walker, Surface-treated activated carbon for removal of phenol from water, *Separation Science Technology*, 1980, **15**, 1733-1752.

[301] Y. Qiu, Z. Zheng, Z. Zhou and G. Sheng, Effectiveness and mechanisms of dye adsorption on a straw-based biochar, *Bioresource Technology*, 2009, **100**, 5348-5351.

[302] S. Langergren and B. Svenska, Zur theorie der sogenannten adsorption geloester stoffe, *Veternskapsakad Handlingar*, 1898, **24**, 1-39.

[303] Q. Li, J. Zhai , W. Zhang, M. Wang and J. Zhou, Kinetic studies of adsorption of Pb(II), Cr(III) and Cu(II) from aqueous solution by sawdust and modified peanut husk, *Journal of Hazardous Materials*, 2007, **141**, 163-167.

[304] C. Namasivayam and D. Kavitha, Adsorptive removal of 2-chlorophenol by low-cost coirpitch, *Journal of Hazardous Materials B*, 2003, **98**, 257-274.

[305] Y. Ho and G. McKay, The kinetics of sorption of basic dyes from aqueous solution by sphagnum moss peat, *The Canadian Journal of Chemical Engineering*, 1998, **76**, 822-827.

[306] M. Otero, F. Rozada, L. Calvo, A. Garcia and A. Moran, Kinetic and equilibrium modelling of the methylene blue removal from solution by adsorbent materials produced from sewage sludges, *Biochemical Engineering Journal*, 2003, **15**, 59-68.

[307] F. Wu, R. Tseng and R. Juang, Kinetic modelling of liquid-phase adsorption of reactive dyes and metal ions on chitosan, *Water Research*, 2001, **35**, 613-618.

[308] S. Allen, G. Mckayb and J. Porter, Adsorption isotherm models for basic dye adsorption by peat in single and binary component systems, *Journal of Colloid and Interface Science*, 2004, **280**, 322-333.

[309] B. Hameed, A. Din and A. Ahmad, Adsorption of methylene blue onto bamboo-based activated carbon: kinetics and equilibrium studies, *Journal of hazardous materials*, 2007,**141**, 819-825.

[310] K. Fytianos, E. Voudrias and E. Kokkalis, Sorption-desorption behavior of 2,4-dichlorophenol by marine sediments, *Chemosphere*, 2000, **40**, 3-6.

[311] M. Tempkin and V. Pyzhev, Kinetics of ammonia synthesis on promoted iron catalyst, *Acta Physico-Chimica Sinica USSR*, 1940, **12**, 327-356.

[312] K. Foo and B. Hameed, Preparation of activated carbon from date stones by microwave induced chemical activation: application for methylene blue adsorption, *Chemical Engineering Journal*, 2011, **170**, 338-341.

[313] M. Dubinin and L. Radushkevich, The equation of the characteristic curve of the activated charcoal, *Proceedings Academy of Sciences USSR Physical Chemistry Section*, 1947, **55**, 331-337.

[314] K. Foo and B. Hameed, Factors affecting the carbon yield and adsorption capability of the mangosteen peel activated carbon prepared by microwave assisted K_2CO_3 activation, *Chemical Engineering Journal*, 2012, **180**, 66-74.

[315] K. Foo and B. Hameed, Insights into the modelling of adsorption isotherm systems, *Chemical Engineering Journal*, 2010, **156**, 2-10.

[316] V. Vadivelan and K. Kumar, Equilibrium, kinetics, mechanism, and process design for the sorption of methylene blue onto rice husk, *Journal of Colloid and Interface Science*, 2005, **286**, 90-100.

[317] S. Umoren, U. Etim and A. Israel, Adsorption of methylene blue from industrial effluent using poly (vinyl alcohol), *Journal of Materials and Environmental Science*, 2013, **4**, 75-86.

[318] Bodner research web, Chemical thermodynamics, Gibbs free energy, http://chemed.chem.purdue.edu/genchem/topicreview/bp/ch21/gibbs.php, accessed on 7/01/2015.

[319] A. Zarrouk, H. Zarrok, R. Salghi, N. Bouroumane, B. Hammouti, S. Al-Deyab and R. Touzani, The adsorption and corrosion inhibition of 2-[Bis-(3,5-dimethyl-pyrazol-1-ylmethyl)-amino]-pentanedioic acid on carbon steel corrosion in 1.0 m HCl, *International Journal of Electrochemical Science,* 2012, **7**, 10215-10232.

[320] B. Evbuomwan and M. Atuka, Kinetics and thermodynamic studies of biosorption of cadmium (ii) from aqueous solution onto garden grass (GAG), *Journal of Chemistry and Materials Research*, 2014, **1**, 12-22.

[321] M. Dogan, M. Alkan, O. Demirbas, Y. Ozdemir and C. Ozmetin, Adsorption kinetics of maxilon blue GRL onto sepiolite from aqueous solutions, *Chemical Engineering Journal*, 2006, **124**, 89-101.

[322] M. Salleh, D. Mahmoud, W. Abdul-Karim and A. Idris, Cationic and anionic dye adsorption by agricultural solid wastes: a comprehensive review, *Desalination*, 2011, **280**, 1-13.

[323] R. White, V. Budarin and J. Clark, Colloidal construction of porous polysaccharide-supported cadmium sulphide, *Colloids and Surfaces A: Physicochemical and Engineering Aspects*, 2014, **444**, 69-75.

[324] S. Massari and M. Ruberti, Rare earth elements as critical raw materials: focus on international markets and future strategies, *Resources Policy*, 2013, **38**, 36-43.

[325] European commission enterprise and industry, Critical raw materials for the EU, Report of the Ad-hoc working group on defining critical raw materials, 2010,http://ec.europa.eu/enterprise/policies/raw-materials/files/docs/report-b_en.pdf, accessed on 9/01/2015.

[326] APS panel on public affairs and the materials research society, energy critical elements: securing materials for emerging technologies, 2011, accessed on 20/01/15.

[327] R. Moss, E. Tzimas, H. Kara, P. Willis and J. Kooroshy, Critical metals in strategic energy technologies, European commission, Joint research centre, assessing rare metals as supply-chain bottlenecks in low-carbon energy technologies, 2011, accessed on 20/1/2015.

[328] A. Hunt, T. Farmer and J. Clark, Elemental sustainability and the importance of scarce element recovery, *Royal Society of Chemistry*, 2013, **22**, 1-28.

[329] K. Salazar, Mineral commodity summaries 2013: US Geological Survey (USGS), US Geological Survey, 2013.

[330] T. Brown, R. Shaw, T. Bide, E. Petavratzi, E. Raycraft and A. Walters, World mineral production 2007-11, British Geological Survey, 2013.

[331] J. Dodson, A. Hunt, H. Parker, Y. Yang and J. Clark, Elemental sustainability: towards the total recovery of scarce metals, *Chemical Engineering and Processing*, 2012, **51**, 69-78.

[332] V. Gupta, I. Ali, T. Saleh, A. Nayak and S. Agarwal, Chemical treatment technologies for waste-water recycling-an overview, *Royal Society of Chemistry Advances*, 2012, **2**, 6380-6388.

[333] S. Vigneswaran, H. Ngo, D. Chaudhary and Y. Hung, Physicochemical treatment processes for water reuse, *Minerals Engineering, 2004*, **7**, 165-1177.

[334] A. Hunt, C. Anderson, N. Bruce, A. Garcia, T. Graedel, M. Hodson, J. Meech, N. Nassar, H. Parker, E. Rylott, K. Sotiriou, Q. Zhang and J. Clark, Phytoextraction as a tool for green chemistry, *Green Processing and Synthesis*, 2014, **3**, 3-22.

[335] F. Glasser, Coal combustion wastes: characterization, reuse and disposal, Geological Society London Special publications, 2004, **236**, 211-222.

[336] L. Morf, R. Gloor, O. Haag, M. Haupt, S. Skutan, F. Lorenzo and D. Boni, Precious metals and rare earth elements in municipal solid waste-sources and fate in a Swiss incineration plant, *Waste Management*, 2013, **33**, 634-644.

[337] M. Rao, D. Ramana, K. Seshaiah, M. Wang and S. Chien, Removal of some metal ions by activated carbon prepared from Phaseolus aureus hulls, *Journal of Hazardous Materials*, 2009, **166**, 1006-1013.

[338] A. Lima, L. Ottosen, A. Pedersen and A. Ribeiro, Characterization of fly ash from bio and municipal waste, *Biomass and Bioenergy*, 2008, **32**, 277-282.

[339] Z. Shi, F. Li and S. Yao, Adsorption behaviors of lead ion onto acetate modified activated carbon fiber, *Desalination and Water Treatment*, 2011, **36**, 164-170.

[340] R. Bansal and M. Goyal, Activated carbon adsorption, CRC Press, Boca Raton, London, New York, Singapore, 2005.

[341] R. Cesuniene, A. Gefeniene, D. Kauspediene, J. Vaiciuniene and A. Selskiene, Kinetics of copper(II) and metal complex dye adsorption on activated carbon in the single and binary systems, *Chemija*, 2013, **2**, 88-96.

[342] D. Venkataraman, Y. Du, S. Wilson, K. Hirsch, P. Zhang and J. Moore, A coordination geometry table of the d-block elements and their ions, *Journal of Chemical Education*, 1997, **74**, 915-918.

[343] R. Shannon, Revised effective ionic radii and systematic studies of interatomic distances in halides and chalcogenides, *Acta Crystallographica*, 1976, **A32**, 751-767.

[344] K. Singh, S. Pande, S. Anwane and S. Bhoga, A study of iso- and alio-valent cation doped Ag_2SO_4 solid electrolyte, *Journal of Applied Physics*, 1998, **A 66**, 205-215.

[345] C. Moynihan and C. Angell, Mass transport in ionic melts at low temperatures, Chronopotentiometric diffusion coefficients of silver (I), cadmium (II) and Thallium (I) in calcium nitrate tetrahydrate, *The Journal of Physical Chemistry*, 1970, **74**, 736-742.

[346] M. Khan and G. Bouet, Formation of cobalt(II), nickel(II) and copper(II) chloro complexes in alcohols and the Irving-Williams order of stabilities, *Transition Metal Chemistry*, 1996, **21**, 231-234.

[347] Environmental chemistry, chemistry and hazardous materials news, Careers and resources, Periodic table of elements, http://environmentalchemistry.com/yogi/periodic/, accessed on 13/01/2015.

[348] Z. Aksu and J. Yener, A comparative adsorption/biosorption study of mono-chlorinated phenols onto various sorbents, *Waste Management*, 2001, **21**, 695-702.

[349] Y. Ho, Review of second-order models for adsorption systems, *Journal of Hazardous Materials,* 2006, **B136**, 681-689.